MODELLING AND ANALYSIS OF TURBOGENERATORS IN SINGLE MACHINE AND MULTI-MACHINE SUBSYNCHRONOUS RESONANCE STUDIES

by

Glenn Douglas Jennings
B.Sc.Eng.

Submitted in partial fulfilment of the requirements of the degree of Doctor of Philosophy, in the Department of Electrical Engineering, University of Natal, Durban, South Africa.

October 1987

I hereby declare that all the material incorporated in this thesis is my own original unaided work except where specific acknowledgement is made by name or in the form of a numbered reference. The work contained herein has not been submitted for a degree at any other university.

Signed: 

ABSTRACT

Subsynchronous Resonance (SSR) is a condition which occurs when turbogenerators are connected to series capacitively compensated transmission systems and it can cause large scale damage to the turbogenerators. The accuracy of predictions of this phenomenon are limited by the accuracy of the mathematical models used for the various system elements.

The modal method of modelling a turbogenerator shaft, in which parameters are associated with each natural torsional mode of the shaft, is investigated in detail and the sensitivity of SSR predictions (both small-signal and transient) to uncertainties in the mode parameters is evaluated. The modal model is then used to obtain reduced order shaft models and the accuracy of these reduced order modal models in SSR predictions is ascertained.

The determination of mode parameters from generator transient response waveforms is investigated. A continuing problem in this field is the separation of damping values obtained from measurements on a synchronized generator, into their mechanical and electrical components. A method is proposed in this thesis which uses eigenvalue scanning techniques together with FFT analysis to achieve this separation.

The SSR stability of, and the torsional interaction between two adjacent generators at a power station is studied. The analysis covers identical generators, nominally identical generators with small differences between their mode parameters and different generators with a coincident torsional mode. In addition, the torsional interaction between generators at different power stations which are remote from each other is investigated. This entire analysis is greatly assisted by modelling the turbogenerator shafts in modal form.

Finally the damping of SSR oscillations in two non-identical adjacent turbogenerators with a single controlled shunt reactor, which uses the sum of the generator speed signals as an input to the controller, is investigated.

ACKNOWLEDGEMENTS

The work presented in this thesis was carried out under the supervision of Professor R G Harley of the Department of Electrical Engineering, University of Natal, Durban. I wish to thank Professor Harley for his constant support, encouragement and patient guidance.

In addition I should like to thank:

my family for their support and encouragement;

my colleagues Dr J C Balda and Mr G Diana for their assistance and co-operation, and also Dr M A Lahoud for his guidance in the initial period;

Messrs A P Barrett, D C Levy and R C S Peplow for their help in the Digital Processes Laboratory of the Department of Electronic Engineering at the University of Natal;

Mr P J Facoline for drawing all the diagrams in the CAD work-station of the Department of Electronic Engineering at the University of Natal;

the University of Natal and the Council for Scientific and Industrial Research for their financial support.

TABLE OF CONTENTS

CHAPTER THREE : MODAL ANALYSIS REPRESENTATION OF A MULTI-INERTIA TURBOGENERATOR

CHAPTER FOUR : REDUCED ORDER MODAL MODELS

CHAPTER FIVE : DETERMINATION OF MODE PARAMETERS

CHAPTER SIX : SUBSYNCHRONOUS RESONANCE OF THE KOEBERG POWER STATION WITH TWO IDENTICAL GENERATING UNITS

CHAPTER SEVEN : TORSIONAL INTERACTION BETWEEN NON-IDENTICAL GENERATING UNITS

List of Symbols

The commonly used symbols and notations are given below. Other symbols used in the text are explained where they first occur.

ac	=	alternating current
b	=	voltage source for generator equivalent circuit
CCL	=	Critical Compensation Level
CWR	=	conventionally wound rotor
d,q	=	direct and quadrature axes in a rotor reference frame
D,Q	=	direct and quadrature axes in a synchronous reference frame
D	=	total mechanical damping of single inertia shaft
[D]	=	diagonal matrix of physical dashpot damping values
FFT	=	Fast Fourier Transform
f_{mi}	=	frequency of mechanical mode 'i' (Hz)
f_o	=	power system synchronous frequency (Hz)
f_r	=	resonant frequency of the transmission system (Hz)
f_s	=	frequency of subsynchronous electrical mode (Hz)
f_{si}	=	frequency mode 'i' when the generator is synchronized (Hz)
[I]	=	identity matrix
i_d, i_q	=	d,q axis components of generator stator current
J	=	total inertia of single inertia shaft
[J]	=	diagonal matrix of physical moments of inertia
J_{Mi}	=	mode inertia of mode 'i'
[K]	=	symmetrical matrix of physical shaft stiffnesses
L_g^*	=	inductance in generator equivalent circuit
L_a	=	armature leakage inductance
L_d, L_q	=	d,q axis stator self inductances
L_{md}, L_{mq}	=	d,q axis mutual inductances
L_{ffd}	=	field winding self inductance
L_{kkd}	=	d-axis damper self inductance
L_{kkq1}	=	first q-axis damper self inductance
L_{kkq2}	=	second q-axis damper self inductance
L_s	=	variable value of shunt reactor inductance
L_{sn}	=	nominal value of shunt reactor inductance

mmf = magnetomotive force

MTS = Mode Torque Susceptibility

N = level of series capacitor compensation (%)

p = derivative operator d/dt

P_b = real power at the infinite busbar

P_m = total output power to shaft from all turbine stages

P_t = real power at the terminals of the generator

$[P_\theta]$ = Park's transformation matrix

q_i = mode angle 'i' (angle of mode inertia 'i')

Q_b = reactive power at the infinite busbar

Q_t = reactive power at the terminals of the generator

$\underline{Q}_i$ = mode shape of mode 'i' (same as $\underline{Q}_{mi}$)

$\underline{Q}_{mi}$ = mode shape of mode 'i' (same as $\underline{Q}_i$)

$\underline{Q}_{si}$ = mode shape of mode 'i' when generator is synchronized

$\underline{Q}'_i$ = row 'i' of the modal transformation matrix

Q_{ij} = mode transfer factor at location 'i' for mode 'j'

$[Q]$ = modal transformation matrix

R_a = generator armature resistance

R_e = total external resistance between generator terminals and the infinite bus

s = slip

S_i = torsional interaction susceptibility of mode 'i'

SCR = silicon controlled rectifier

SSR = subsynchronous resonance

t = time

T'_{do}, T'_{qo} = d,q axis open circuit transient time constants

T''_{do}, T''_{qo} = d,q axis open circuit subtransient time constants

T'_d, T'_q = d,q axis short circuit transient time constants

T''_d, T''_q = d,q axis short circuit subtransient time constants

T_e = electrical torque

TIS = Torsional Interaction Susceptibility

T_m = mechanical torque

$\underline{T}_M$ = mode torque vector

V_b = voltage at the infinite busbar

V_t = voltage at the terminals of the generator

v_d, v_q = d,q axis components of generator stator voltages

v'_d, v'_q = d,q axis voltages behind transient reactance

v''_d, v''_q = d,q axis voltages behind subtransient reactance

X'_d, X'_q = d,q transient reactances

X''_d, X''_q = d,q subtransient reactances

X_e = total external inductive reactance between generator terminals and the infinite bus

$\underline{x}$ = state vector

$\underline{z}$ = state vector of shunt reactor controller

Δ = small change operator

δ = generator load angle

δ_i = angular position of inertia stage 'i'

σ_{mi} = decrement factor (damping) of mode 'i' (s^{-1})

σ_{si} = decrement factor of mode 'i' when generator is synchronized

ξ = damping factor (%)

ψ_d, ψ_q = d,q axis stator flux linkages

ν_i = natural frequency of mechanical mode 'i' (rad^m/s)

ω_o = system synchronous frequency (rad^e/s)

ω_i = angular velocity of inertia stage 'i'

ω_r = angular velocity of generator rotor

$[0]$ = null matrix

$\underline{0}$ = null vector

$\underline{X}$ = signifies a column vector X

$\underline{X}^T$ = transpose of a vector $\underline{X}$

$[X]$ = signifies a matrix X

$[X]^{-1}$ = inverse of a matrix X

$[X]^T$ = transpose of a matrix

X_o = steady-state value of variable X

CHAPTER ONE

INTRODUCTION

1.1 General

The operation of a synchronous turbogenerator in a power system is limited by considerations of stability at leading power factors. The problem has been further increased in later years by the design of modern turbogenerators with lower inertia constants and smaller short circuit ratios as well as the tendency to transmit more power at higher voltages over longer distances. The introduction of long distance power transmission saw the advent of series capacitors to compensate for the high inductance of long transmission lines. Series capacitor compensation is now in use world wide as it is the most economical way of increasing the power transfer capability between two points. In South Africa, since the introduction of the 400 kV system there has been long distance power transmission from the Eastern Transvaal coal fields to the coastal cities. Prior to this the power for the coastal cities was generated locally and no great stability problems existed. In order to increase the power transmission to the more distant coastal cities, series capacitors were introduced in the transmission line. More lately, the Koeberg nuclear power station in the Western Cape has been constructed and its two turbogenerators are connected to the main industrial centre of the country in the Transvaal, some 1400 km away through a 400 kV series capacitor compensated transmission system.

Although series capacitance increases the power transfer capabilities of a power system, together with the system inductance and resistance it forms a

circuit which resonates at its natural electrical frequency after a change in system variables, and this may lead to a type of instability called Subsynchronous Resonance (SSR). There are two mechanisms through which SSR can manifest itself depending upon the level of series compensation (ratio of capacitive to inductive reactance). At high compensation levels, an induction generator effect takes place and is predominantly an electrical resonance which arises if the effective system resistance is too low. The second mechanism is called torsional interaction and it occurs due to the interaction between the electrical and mechanical system. The turbogenerator shaft system can be modelled as a simple, single-lumped inertia, but a more accurate model would represent each turbine stage and its interconnecting torsional shaft. Such a more detailed mechanical model has a number of natural torsional oscillatory modes. The electrical and mechanical systems will interact when the series compensated transmission line possesses an electrical resonance (f_r) which induces airgap fluxes at complementary frequencies (of $f_o \pm f_r$) that are close to a mechanical resonant mode. This interaction may result in oscillations which are self-excited.

A further effect of SSR due to series capacitors is to induce torques in a turbogenerator shaft following a system disturbance which are much larger than those developed as a result of a three-phase fault in an uncompensated system. This phenomenon, known as shaft torque amplification, is due to the resonance effect and the fact that the damping of torsional modes in turbogenerators is extremely low.

This SSR phenomenon lead to two incidents of generator shaft failure at Mohave Power Station in Nevada, U.S.A. These incidents caused concern amongst the power generation industry, even more so since the conventional stability analysis programs had not predicted the large oscillatory torques which had preceeded the shaft failures. The ensuing years saw a great deal of research effort put into the analysis of SSR and the finding of possible countermeasures against its destructive action. From this effort a sound understanding of this phenomenon was advanced and numerous possible countermeasures were suggested and are still being done so today.

Around this time of intense interest in SSR the Koeberg power station was under construction. A single machine study of the Koeberg system showed that at modest levels of series compensation a Koeberg turbogenerator could be susceptible to damage from SSR. These findings prompted much local research interest into the Koeberg SSR problem and many publications followed dealing with system modelling, multi-machine SSR and SSR countermeasures. The work in this thesis further investigates the SSR phenomenon in relation to the Koeberg system, with particular emphasis being placed on system modelling and the multi-machine representation of the system.

Chapter Two investigates the sophistication of the electrical and mechanical models required for the analysis of multi-inertia turbogenerators in an SSR environment and considers some of the limitations and advantages of the more commonly used simplified turbogenerator models. This analysis considers three electrical models of the generator, two mechanical models of the generator, two electrical systems and five changes in the steady state conditions.

Although much research has gone into solutions to the SSR problem, an important question which remains difficult to answer, is the exact level of compensation at which the system can operate stably, and the uncertainty associated with this CRITICAL COMPENSATION LEVEL (CCL). This stability limit depends greatly on both the electromagnetic and, in particular, the mechanical damping present in the system. In most conventional stability programs the mechanical system is represented by an interconnected spring mass model with viscous dampers associated with each inertia. However, these dashpot values can be neither calculated nor measured and values have mostly been estimated subject to a large degree of uncertainty. This problem can be overcome by transforming the shaft equations into the frequency domain where these equations become decoupled and all the shaft parameters, including the damping are measurable. With this model of the shaft, called the modal model, mechanical parameters are associated with each natural torsional mode of vibration of the shaft. By using measured mode parameters the stability limits can be determined more accurately.

Nevertheless, errors will be incurred in the measurement of mode parameters and Chapter Three investigates the sensitivity of CCL predictions and shaft torque amplification predictions to these errors.

In any SSR study, but particularly in a multi-machine study, the number of mechanical states is normally large and the resultant computer execution time can become excessive. It is thus advantageous to be able to reduce the order of a system without losing accuracy. This aspect is evaluated in Chapter Four where the modal analysis technique is used to obtain reduced order modal models for the mechanical system. CCL calculations and transient shaft torque calculations following a system disturbance are performed with the reduced order models in order to ascertain their accuracy and hence determine the feasibility of their use in SSR studies.

One of the major advantages of the modal model is that it is possible to determine all the mode parameters from measurements taken on the system. This measurement of mode parameters is investigated in Chapter Five where mode parameters are determined from analytically generated transient response data. In practice, a variety of tests are performed to determine mode parameters for a turbogenerator; some test are performed with the generator at standstill while others are performed with the generator synchronized to the network. Due to the effect of the electrical network, especially the electrical damping, the parameters obtained from measurement on a synchronized generator are different to those obtained from measurements on an unsynchronized generator. The mode parameters required to be used in the modal model are those related to the unsynchronized generator, however, it is easier to determine mode parameters for a synchronized generator. Thus it is necessary to be able to determine the unsynchronized generator parameters from those obtained from measurements on a synchronized generator. In particular this requires the separation of measured damping values into mechanical and electrical components. This is easily done if the generator electrical torque is accurately known however the accurate determination of the electrical torque is difficult to achieve. A method is illustrated in Chapter Five for determining the mode parameters related to an unsynchronized generator from measurements on a

synchronized generator which does not require any knowledge of the electrical torque.

Mostly all of the research on the Koeberg SSR problem dealt with the first phase of the Koeberg project in which a single turbogenerator was to be commissioned; these studies thus considered only a single turbogenerator at the power station. At a later stage, a second nominally identical turbogenerator was commissioned and this necessitated the extension of the earlier single machine studies to consider the effect of the second unit. This aspect is investigated in Chapter Six which firstly considers the effect of the increase in the generating capacity at Koeberg on the stations SSR stability; for this study the two generators at Koeberg are considered as a single equivalent generator. Secondly, the torsional characteristics of the power station are investigated with the two generators modelled as separate units in a multi-machine study and are compared with those for the single equivalent generator representation.

The analysis in Chapter Six considers only truly identical generators whereas in practice, there are likely to be small differences in the generator parameters even for nominally identical units. Moreover, it is possible that two different generators at a power station may have one of their torsional modes at the same frequency. Chapter Seven therefore investigates the torsional interaction between non-identical neighbouring units and considers the effect of disparities between the mechanical parameters of these units on the SSR stability of the system. This investigation also considers the possible torsional interaction between remote generators at different power stations and considers the possibility of SSR with torsional energy being exchanged between the two generators.

Up till now the most technically and economically viable SSR countermeasure appears to be the shunt reactor stabilizer (or dynamic stabilizer) which acts as an electric torque modulator by using an SCR bridge to vary the inductance of a shunt reactor at the generator terminals. Lately, systems have been considered with two interacting neighbouring turbogenerators both susceptible to SSR and it has been proposed to damp out SSR oscillations in

these units by means of a single shunt reactor stabilizer controlled by the sum of the two turbogenerators' speed signals. These studies only considered truly identical generators at the same operating point. Chapter Seven concludes by extending these studies to include non-identical units and investigates the effect of phase differences in the generators' speed signals due to dissimilarities in their parameters on the operation of the controller.

Finally the conclusions of this thesis and suggestions for further work are contained in Chapter Eight.

1.2 Contributions to Power Systems Analysis

The work presented in this thesis contributes to the analysis of power systems as summarized below :

(a) The modal analysis technique for modelling turbogenerator shafts is presented and it's usefulness in SSR studies is investigated in detail.

(b) The use of modal analysis to obtain reduced order models and the accuracy of these low order models in eigenvalue and transient calculations is evaluated.

(c) A method for obtaining mode parameters for a turbogenerator that is synchronized without requiring any knowledge of the generator electrical torque is presented.

(d) The modal analysis representation of turbogenerators in a multi-machine system is used to extensively investigate the torsional interaction between turbogenerators with similar modes in a power system.

(e) The operation of a single shunt reactor stabilized in damping out SSR oscillations in two similar but non-identical neighbouring turbogenerators is investigated.

A number of computer programs have been developed in order to produce the results in this thesis :

(A) Transient simulation programs for the various system models presented in Chapter Two.

(B) A single machine transient program which represents the turbogenerator shaft in modal form.

(C) A small-signal analysis program for a single machine system with the turbogenerator shaft represented in modal form.

(D) Two single machine eigenvalue scanning programs; one which calculates the CCL as a function of a scanned parameter, the other identifies generator mode parameters from measured system modes.

(E) An existing multi-machine program has been modified to enable the modelling of turbogenerator shafts in modal form as well as the inclusion of shunt reactor stabilizers. This program calculates the transient response of the system as well as the small-signal stability.

1.3 Research Publications

Many of the findings of this thesis have already been published in a number of papers on system modelling [1-3] and multi-machine systems [4,5].

CHAPTER TWO

MATHEMATICAL MODELS OF A TURBOGENERATOR SYSTEM

2.1 Introduction

The study of power system stability is a complex one which requires accurate mathematical modelling of the various components of the system. In order to perform a meaningful stability study it is important to understand thoroughly the phenomenon which is being investigated as well as the limitations and abilities of the various models used. The use of too simple a model will lead to inaccurate results whereas too much detail results in excessive computation time and wasted money. This thesis deals primarily with the subject of Subsynchronous Resonance (SSR) and in this chapter a few models of the three main interacting subsystems involved in SSR are reviewed, namely the transmission system, the generator electrical circuits and the turbogenerator shaft mechanical system. Although the work in this chapter is not new, it provides a useful basis for the rest of the thesis.

A few decades ago when high speed digital computers were not readily available stability calculations for a large power system containing many lines, loads and generators, were extremely cumbersome and time consuming. They were carried out on analogue computers, and before that on network analysers and mechanical integrating devices. Consequently the number of differential equations per generator had to be kept to a minimum; moreover the network equations could be simplified if the generator was represented by an AC voltage phasor and an impedance.

In the early days, stability calculations were carried out for generators with fixed excitation, assuming the field flux linkages to be constant [6] (neglecting transformer action terms) and having a second order non-linear differential equation for the mechanical motion (the well known "equal area criterion"); such a mathematical model did not represent the electrical transients in the machine's windings. Damping could be allowed for by a constant damping coefficient.

Later methods [7,8] were developed to allow for changing field flux linkage in order to represent the effects of voltage regulators and from this grew the need to not only represent the transient field current, but also the transients in the stator or armature three phase windings ABC. However, the non-linear differential equations describing the ABC phase currents contain the products of variables as well as time-varying inductances which are a function of the rotor position. However, Park [9] showed that the ABC equations can be transformed into so-called two-axis or d,q equations with constant inductances; moreover, if the speed is assumed constant, the d,q equations are linear and analytical solutions are possible.

Although computing power is becoming cheaper and more readily available and the detailed representation of generators is readily programmed, many existing computer stability programs [10] still use the simplified models which represent the generator by an AC phasor voltage and an impedance as elements of the AC power network. The degree of inaccuracy associated with each of the simplified models depends on such factors as the type and duration of the disturbance applied to the system, the peculiar combination of system parameter values, and whether any series capacitors are present in the vicinity of a particular generator. The larger turbogenerators have multiple separate turbine stages, and in certain cases, the mechanical resonance of the entire shaft system may need to be represented more accurately than only by a single equivalent lumped inertia. It therefore became necessary to establish the limitations of using the existing simplified computer stability programs.

This chapter therefore considers

- three electrical models of the generator in Fig 2.1
  - . an accurate model
  - . a simpler model derived by neglecting the stator $p\psi$ terms
  - . an even simpler model derived by neglecting damper windings
- two mechanical models of the generator
  - . an accurate model representing the inertia of each major rotating mass and the interconnecting shafts
  - . a simpler model which represents the shaft system as a single inertia
- two models of the transmission system
  - . one with the transmission system represented by a resistor, inductor and capacitor in series
  - . the other with the transmission system represented only by a resistor with an inductor in series
- five changes in the steady state conditions
  - . change in shaft torque
  - . change in generator field voltage
  - . change in transmission system impedance
  - . change in infinite busbar voltage
  - . application of a three phase short circuit

Only balanced operating conditions are considered. The results show that for certain disturbances the simplified models yield perfectly acceptable results, but that there exists a combination of operating conditions and system parameters when the simplified results are completely wrong.

2.2 The Generator Electrical System

The conventionally wound rotor (CWR) synchronous generator is mathematically represented by the well-known [11] two-axis model under the following assumptions:

(a) the synchronous machine is ideal with a sinusoidal air-gap mmf (for a cylindrical rotor machine) and a linear magnetic circuit;

(b) iron and stray losses are negligible;

(c) the system is balanced;

The complexity of the model is determined by the number of rotor circuits chosen to represent the damping effects of currents induced in damper bars, the solid rotor body, teeth and slot wedges [12,13] and seldom results in more than three rotor circuits on each axis [14]. The turbogenerator considered in this thesis (Appendix I) represents the electrical damping by one damper on the d-axis and two on the q-axis [15] as illustrated in Fig 2.2. Based upon the sign conventions and per-unit system described in Appendix A, the voltage equations for the six coils in Fig 2.2 can be expressed as follows in terms of d and q variables when the d- and q- axes are attached to the minor and major reluctance axes of the rotor respectively:

$$v_d = R_a i_d + p\psi_d + \omega\psi_q \tag{2.1}$$

$$v_q = R_a i_q + p\psi_q - \omega\psi_d \tag{2.2}$$

$$v_{fd} = R_{fd} i_{fd} + p\psi_{fd} \tag{2.3}$$

$$v_{kd} = R_{kd} i_{kd} + p\psi_{kd} \tag{2.4}$$

$$v_{kq1} = R_{kq1} i_{kq1} + p\psi_{kq1} \tag{2.5}$$

$$v_{kq2} = R_{kq2} i_{kq2} + p\psi_{kq2} \tag{2.6}$$

The six flux linkages are given by:

$$\begin{bmatrix} \psi_d \\ \psi_{fd} \\ \psi_{kd} \\ \psi_q \\ \psi_{kq1} \\ \psi_{kq2} \end{bmatrix} = \left[\begin{array}{ccc|ccc} L_d & L_{md} & L_{md} & & & \\ L_{md} & L_{ffd} & L_{md} & & [0] & \\ L_{md} & L_{md} & L_{kkd} & & & \\ \hline & & & L_q & L_{mq} & L_{mq} \\ & [0] & & L_{mq} & L_{kkq1} & L_{mq} \\ & & & L_{mq} & L_{mq} & L_{kkq2} \end{array}\right] \begin{bmatrix} i_d \\ i_{fd} \\ i_{kd} \\ i_q \\ i_{kq1} \\ i_{kq2} \end{bmatrix} \tag{2.7}$$

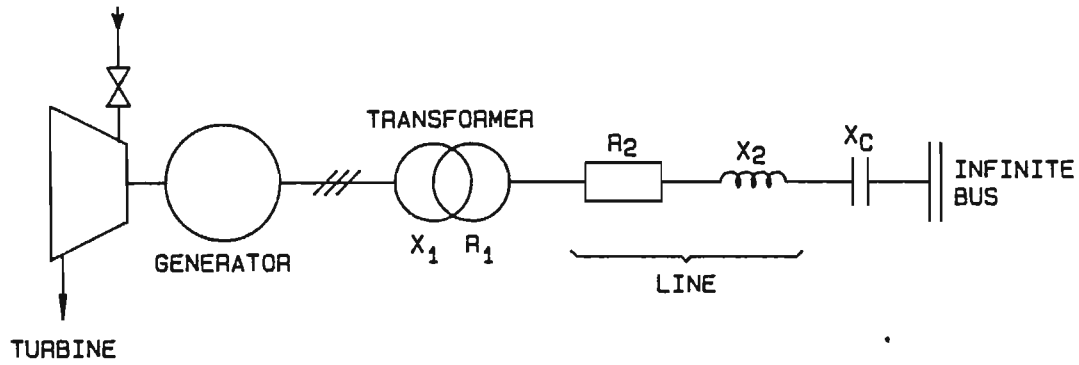

Fig 2.1 Turbogenerator synchronized to an infinite busbar.

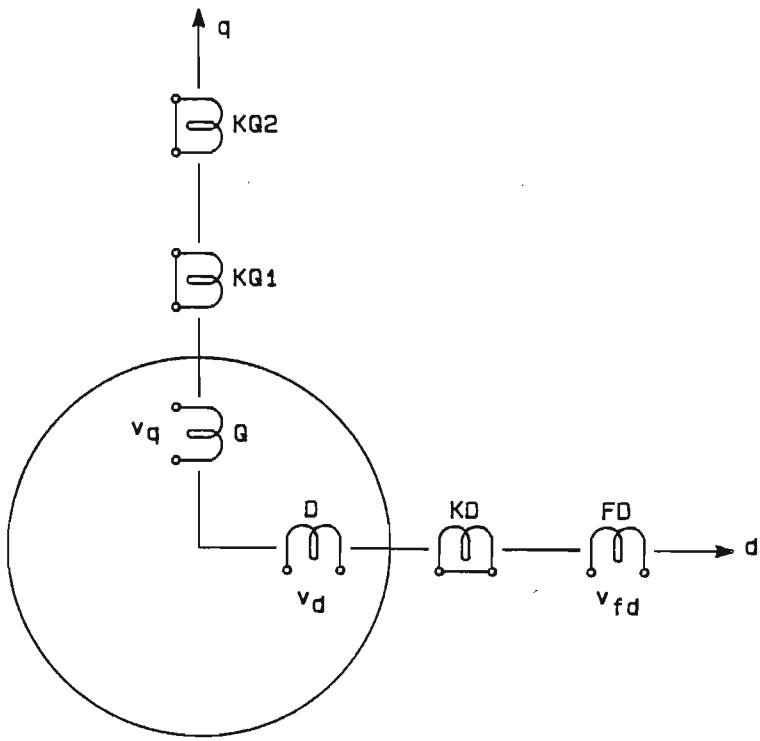

Fig 2.2 Two-axis representation of a three phase synchronous machine.

The electrical torque is defined by:

$$T_e = \omega_o(\psi_d i_q - \psi_q i_d)/2 \qquad (2.8)$$

Equations (2.1) to (2.8) therefore describe the machine's electrical behaviour in terms of d,q variables instead of in terms of ABC phase variables. The speed ω is a variable and is obtained from the equations describing the mechanical system as presented in Sect 2.3. This electrical model requires six first order differential equations to be solved, some of which are non-linear and can only be solved by analogue computer, or a step-by-step integration method on a digital computer.

The above model is just one of the many different possible ways [16] of representing a generator in stability studies. In order to save computer time, the mathematical models currently in use usually make one or more of the following simplifying assumptions to the above fundamental sixth order electrical model, especially in multi-machine studies:

(a) The $p\psi_d$ and $p\psi_q$ or "stator transient" terms in the armature voltage equations (2.1) and (2.2) are often neglected; this is the most significant time saving simplification since it eliminates the 50 Hz transient component in the d,q variables and relieves the pressure to have an integration time step which is sufficiently small in comparison to the period of a 50 Hz wave. This simplification leads to a fourth order electrical model.

(b) Additional simplification is possible by the omission of some or all of the damper circuits. Even if all damper circuits are omitted, their action can still be represented approximately by a damping torque proportional to slip, instead of it being calculated as an inherent part of the electrical torque. The omission of damper circuits in the above model results in an electrical model of order one, two or three depending on the number of damper circuits omitted.

(c) Although (a) and (b) are the major simplifications, it is often assumed further that armature and tie-line resistances are negligible, but this does not reduce the order of the model. In the following development of the different models, resistance effects and speed variations are included in the voltage equations for the sake of completeness.

The rest of this section summarizes the equations of the above simplified models; the accuracy of their predicted results compared to the results without any simplifying assumptions are evaluated in Sections 2.4 to 2.7.

2.2.1 Model 1 - The accurate model

Model 1 which uses eqns (2.1) to (2.8) to describe the machine without any of the simplifying assumptions stated above, will be referred to as the "Accurate Model" although it does not allow for saturation [17] or slot harmonic effects. The d,q equations (2.1) to (2.6) can be rearranged into the following matrix form if their flux linkages are replaced by currents with the aid of eqn (2.7):

$$\underline{v} = \{[R] + \omega[G] + p[L]\}\underline{i} \tag{2.9}$$

where ω represents the angular velocity of the rotor, and the vectors of axis coil voltages and currents, $\underline{v}$ and $\underline{i}$, and matrices [R], [G] and [L] are defined in Appendix C.1.

Now eqn (2.9) may be rearranged into the following state-space form which contains the current as state variables:

$$p\underline{i} = [L]^{-1}\{\underline{v} - ([R] + \omega[G])\underline{i}\} \tag{2.10}$$

Moreover, eqn (2.8) can be combined with eqn (2.7) in order to express the electrical torque as follows in terms of currents only:

$$T_e = -\underline{i}^T[G]\underline{i}\omega_o/2 \tag{2.11}$$

The solution of the currents by numerical integration of eqn (2.10) is used to calculate the electrical torque in eqn (2.11).

The voltage expressions for the interconnecting R-L-C tie-line are (Appendix C.2):

$$v_d = \sqrt{2}V_b \sin\delta - Ri_d - Lpi_d - \omega Li_q + i_q/\omega C - pv_q^C/\omega \quad (2.12)$$

$$v_q = -\sqrt{2}V_b \cos\delta - Ri_q - Lpi_q + \omega Li_q - i_d/\omega C + pv_d^C/\omega \quad (2.13)$$

where the series capacitor voltage drops v_d^C and v_q^C are chosen as state variables.

2.2.2 Model 2 - Voltage behind subtransient reactance

This model differs from the Accurate Model mainly because it neglects the stator transient terms $p\psi_d$ and $p\psi_q$ in eqns (2.1) and (2.2). However, it will also be shown that if the q-axis subtransient reactance X_q'' is assumed to be equal to the d-axis subtransient reactance X_d'', the machine may be treated as a network component and analysed in terms of phasors representing phase values.

Omitting the $p\psi_d$ and $p\psi_q$ terms is often a valid simplification when the transient disturbance experienced by the machine is only a mild one, such that the flux linkages ψ_d and ψ_q change relatively slowly with respect to the supply frequency. On this basis, eqns (2.1) and (2.2) become:

$$v_d = R_a i_d + \omega\psi_q \quad (2.14)$$

$$v_q = R_a i_q - \omega\psi_d \quad (2.15)$$

which can be rewritten (using the expressions for $\omega_o\psi_d$ and $\omega_o\psi_q$ from eqns B.10 and B.11) as:

$$v_d = R_a i_d + (1 - s)\omega_o\psi_q \quad (2.16)$$

$$= R_a i_d + X_q'' i_q + v_d'' \quad (2.17)$$

$$v_q = R_a i_q - (1 - s)\omega_o \psi_d \tag{2.18}$$

$$= R_a i_q - X''_d i_d + v''_q \tag{2.19}$$

where

$$\omega = (1-s)\omega_o$$

$$v''_d = -sX''_q i_q + \omega(X''_q - X_a)[\psi_{kq1}/X_{kq1} + \psi_{kq2}/X_{kq2}] \tag{2.20}$$

$$v''_q = sX''_d i_d - \omega(X''_d - X_a)[\psi_{fd}/X_{fd} + \psi_{kd}/X_{kd}] \tag{2.21}$$

The two voltages v''_d and v''_q are known [11,18] as the axes components of the voltage behind subtransient reactance.

The following set of equations are obtained for the time rate of change of rotor flux linkages by eliminating i_{fd}, i_{kd}, i_{kq1} and i_{kq2} from eqns (2.3) to (2.6) (using eqns (B.4) to (B.7)), and defining new parameters T'_{do}, T''_{do}, T'_{qo} and T''_{qo} (see Appendix B.2):

$$p\psi_{fd} = v_{fd} + \frac{1}{T'_{do}}\left\{\frac{(X''_d - X_a)}{(X'_d - X_a)}\left[\frac{X_{md} i_d}{\omega_o} + \frac{X_{md}\psi_{kd}}{X_{kd}}\right] - \psi_{fd}\left[1 + \frac{(X''_d - X_a)X_{md}}{X_{kd}X_{fd}}\right]\right\} \tag{2.22}$$

$$p\psi_{kd} = [(X'_d - X_a)i_d/\omega_o + (X'_d - X_a)\psi_{fd}/X_{fd} - \psi_{kd}]/T''_{do} \tag{2.23}$$

$$p\psi_{kq1} = \frac{1}{T'_{qo}}\left\{\frac{(X''_q - X_a)}{(X'_q - X_a)}\left[\frac{X_{mq} i_q}{\omega_o} + \frac{X_{mq}\psi_{kq2}}{X_{kq2}}\right] - \psi_{kq1}\left[1 + \frac{(X''_q - X_a)X_{mq}}{X_{kq1}X_{kq2}}\right]\right\} \tag{2.24}$$

$$p\psi_{kq2} = [(X'_q - X_a)i_q/\omega_o + (X'_q - X_a)\psi_{kq1}/X_{kq1} - \psi_{kq2}]/T''_{qo} \tag{2.25}$$

The equation for the electrical torque is obtained by substituting eqns (B.8) and (B.9) for ψ_d and ψ_q into eqn (2.8) to yield:

$$T_e = [(X''_d - X''_q)i_d i_q - v''_q i_q - v''_d i_d]/[2(1 - s)] \tag{2.26}$$

The voltage equations for the interconnecting tie-line are given by:

$$v_d = \sqrt{2}V_b \sin\delta - Ri_d - (\omega L - 1/\omega C)i_q \tag{2.27}$$

$$v_q = -\sqrt{2}V_b \cos\delta - Ri_q + (\omega L - 1/\omega C)i_d \tag{2.28}$$

In order to represent the machine as an element of an AC network and thereby avoid a d,q analysis of the network, it is customary [11] to assume at this stage that $X''_d = X''_q = X''$ (zero subtransient saliency; Appendix B.3). This allows the machine to be considered as a phasor voltage $\bar{V}''$ behind a subtransient reactance X", and the equations are redefined as follows:

$$v_d = R_a i_d + X'' i_q + v''_d \tag{2.29}$$

$$v_q = R_a i_q - X'' i_d + v''_q \tag{2.30}$$

$$v''_d = -sX'' i_q + \omega(X'' - X_a)[\psi_{kq1}/X_{kq1} + \psi_{kq2}/X_{kq2}] \tag{2.31}$$

$$v''_q = sX'' i_d - \omega(X'' - X_a)[\psi_{fd}/X_{fd} + \psi_{kd}/X_{kd}] \tag{2.32}$$

$$p\psi_{fd} = v_{fd} + \frac{1}{T'_{do}}\left\{\frac{(X'' - X_a)}{(X'_d - X_a)}\left[\frac{X_{md} i_d}{\omega_o} + \frac{X_{md}\psi_{kd}}{X_{kd}}\right] - \psi_{fd}\left[1 + \frac{(X'' - X_a)X_{md}}{X_{kd}X_{fd}}\right]\right\} \tag{2.33}$$

$$p\psi_{kd} = [(X'_d - X_a)i_d/\omega_o + (X'_d - X_a)\psi_{fd}/X_{fd} - \psi_{kd}]/T''_{do} \tag{2.34}$$

$$p\psi_{kq1} = \frac{1}{T'_{qo}}\left\{\frac{(X'' - X_a)}{(X'_q - X_a)}\left[\frac{X_{mq} i_q}{\omega_o} + \frac{X_{mq}\psi_{kq2}}{X_{kq2}}\right] - \psi_{kq1}\left[1 + \frac{(X'' - X_a)X_{mq}}{X_{kq1}X_{kq2}}\right]\right\} \tag{2.35}$$

$$p\psi_{kq2} = [(X'_q - X_a)i_q/\omega_o + (X'_q - X_a)\psi_{kq1}/X_{kq1} - \psi_{kq2}]/T''_{qo} \tag{2.36}$$

$$T_e = (-v''_q i_q - v''_d i_d)/2(1 - s) \tag{2.37}$$

Equations (2.29) and (2.30) can now be rewritten as a single phasor equation of the form:

$$\bar{V} = R_a \bar{I} + jX''\bar{I} + \bar{V}'' \tag{2.38}$$

where:

$$\bar{V}'' = V_d'' + jV_q'' = (v_d'' - jv_q'')/\sqrt{2} \tag{2.39}$$

$$\bar{I} = I_d + jI_q = (i_d - ji_q)/\sqrt{2} \tag{2.40}$$

This phasor representation is more clearly illustrated by the equivalent circuit and phasor diagram shown in Fig 2.3.

2.2.3 Model 3 - Voltage behind transient reactance

In addition to neglecting the $p\psi_d$ and $p\psi_q$ terms, Model 3 also omits two damper circuits (the d-axis damper and one q-axis damper). Quadrature axis damper circuits provide much of the damping torque so a single q-axis rotor circuit is retained to approximate these damping effects as suggested in Ref [19]. This results in a symmetrical machine with one rotor coil on each axis (Model 1.1 in Ref [19]). In addition, in a similar manner as X_d'' and X_q'' were set equal in Model 2, the transient reactances X_d' and X_q' are set equal in this model (Appendix B.3), thus again enabling the machine to be treated as a network component.

The equations describing this model are derived from those of Model 2 by setting $X'' = X'$ and letting X_{kd} and X_{kq2} tend to infinity in eqns (2.29) to (2.37). This results in the following equations:

$$v_d = R_a i_d + X' i_q + v_d' \tag{2.41}$$

$$v_q = R_a i_q - X' i_d + v_q' \tag{2.42}$$

$$v_d' = -sX' i_q + \omega(X' - X_a)\psi_{kq1}/X_{kq1} \tag{2.43}$$

$$v_q' = sX' i_d - \omega(X' - X_a)\psi_{fd}/X_{fd} \tag{2.44}$$

$$p\psi_{kq1} = [X_{mq} i_q/\omega_o - \psi_{kq1}]/T_{qo}' \tag{2.45}$$

$$p\psi_{fd} = v_{fd} + [X_{md} i_d/\omega_o - \psi_{fd}]/T_{do}' \tag{2.46}$$

$$T_e = (-v_q' i_q - v_d' i_d)/2(1 - s) \tag{2.47}$$

The voltage equations for the interconnecting tie-line are the same as eqns (2.27) and (2.28). Equations (2.41) and (2.42) can be combined into a single voltage phasor $\bar{V}'$ behind the transient reactance X', where

$$\bar{V} = R_a\bar{I} + jX'\bar{I} + \bar{V}' \tag{2.48}$$

and

$$\bar{V}' = V'_d + jV'_q = (v'_d - jv'_q)/\sqrt{2} \tag{2.49}$$

$$\bar{I} = I_d + jI_q = (i_d - ji_q)/\sqrt{2} \tag{2.50}$$

This is illustrated in the equivalent circuit and phasor diagram of Fig 2.4.

2.3 The Mechanical System

In many computer simulation programs the mechanical system is modelled as a single equivalent inertia representing the combined inertia of all the turbine stages, the generator and the exciter, in which case the transient behaviour of the generator load angle is described by the following second order differential equation:

$$Jp^2\delta + Dp\delta + T_e + T_m = 0 \tag{2.51}$$

where

$$T_m = P_m\omega_o/\omega_r \tag{2.52}$$

and δ = generator load angle
J = total equivalent inertia
D = mechanical damping
T_m = mechanical torque from turbine to generator
P_m = total output power on shaft from all turbine stages
ω_r = generator rotor speed

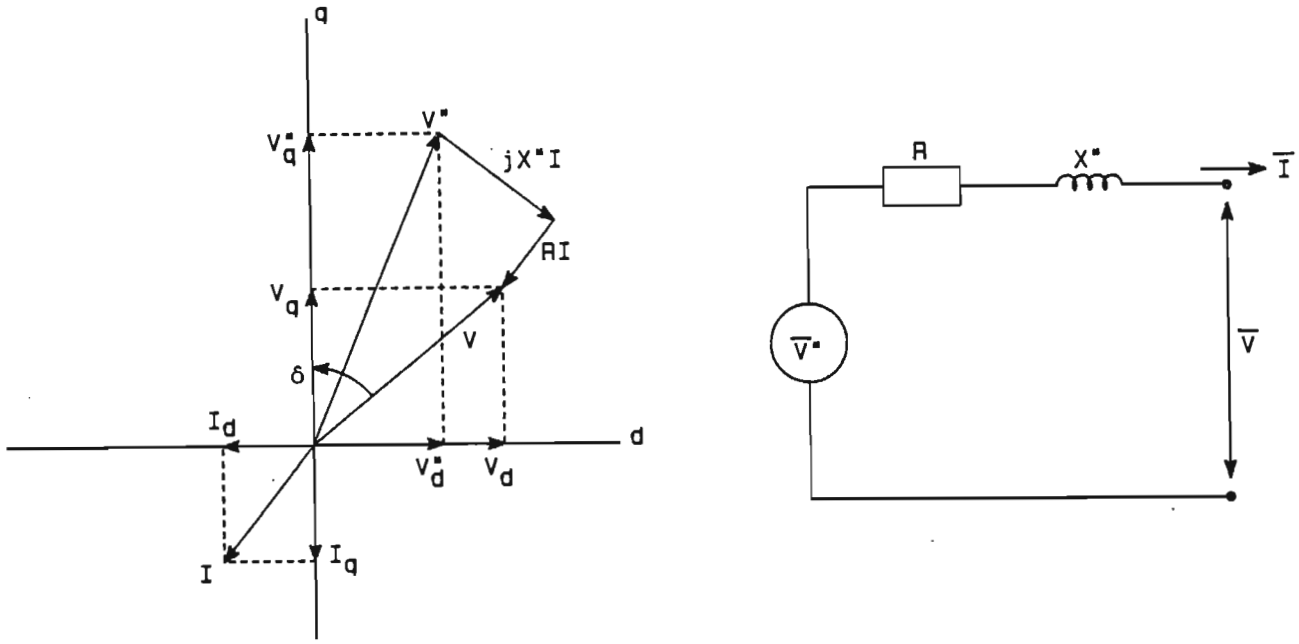

Fig 2.3 Model 2 phasor diagram and equivalent circuit.

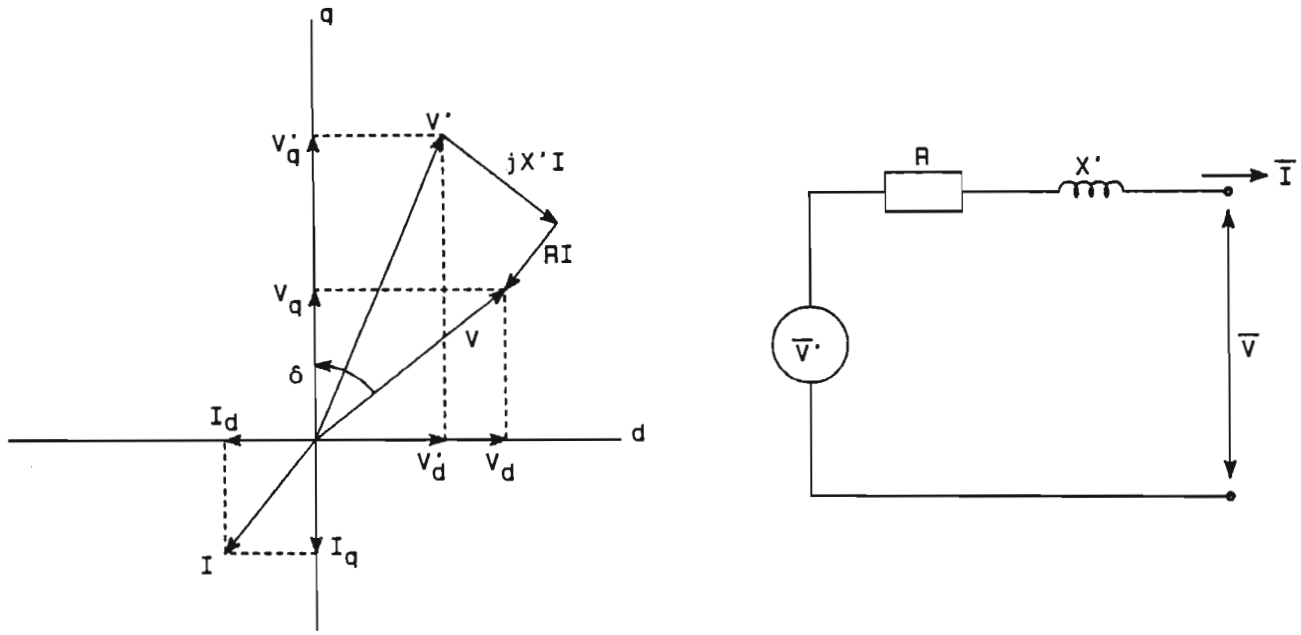

Fig 2.4 Model 3 phasor diagram and equivalent circuit.

In terms of the sign convention explained in Appendix A.1, T_m and P_m have negative numerical values for generator operation. In certain cases such a simplified mechanical representation can yield completely erroneous results, and it then becomes necessary to represent the inertias separately, but interconnected by torsionally flexible shafts as illustrated in Fig 2.5. Such a multi-inertia system can be described [15] by a set of second order differential equations of the form:

$$[J]p^2\underline{\delta} + [D]p\underline{\delta} + [K]\underline{\delta} + \underline{T}_e + \underline{T}_m = \underline{0} \tag{2.53}$$

where $\underline{\delta}$ = rotor angular position vector
$[J]$ = diagonal matrix of inertias
$[D]$ = diagonal matrix of damping coefficients
$[K]$ = symmetric matrix of shaft stiffnesses
$\underline{T}_e$ = electrical torque vector
$\underline{T}_m$ = mechanical torque input vector

The individual matrices and vectors of eqn (2.53) are given in Appendix C.3. The mechanical system equation (2.51) or (2.53) combined with the various electrical models in Sect 2.2 and the appropriate transmission system equations results in turbogenerator system models varying in complexity from fourth order to twentieth order.

Throughout this thesis the effect of any governor action is neglected, and it is assumed that the power developed by each turbine stage remains constant throughout the disturbance being considered. Previous studies [20,21] have shown that the relatively slow turbine and mechanical governor have no major influence on SSR stability.

2.4 Single Inertia Mechanical System with R-L Transmission System

The system equations for each model are used to calculate the transient response of a synchronous generator connected through a transmission line to an infinite bus (see Fig 2.1) when subjected to the following five

different disturbances or faults:

Fault 1 - 10% increase in prime mover torque.
Fault 2 - 10% reduction in the field voltage.
Fault 3 - 40% increase in the line impedance.
Fault 4 - 10% reduction in the infinite bus voltage.
Fault 5 - 3 phase short circuit at the machine terminals.

Unless otherwise stated, the initial steady operating point at the generator terminals prior to each fault is P_t = 0.5 p.u., Q_t = 0.2 p.u., V_t = 1.05 p.u. The system parameters appear in Appendix I.

The following series of results apply to a generator with a single lumped inertia and a transmission line represented by a series inductance and resistance.

2.4.1 Change in prime mover torque

This disturbance consists of a 10% step increase in the applied shaft torque (T_m in eqn (2.51)) from the prime mover. Fig 2.6 shows the subsequent behaviour of generator load angle, electrical torque, terminal voltage and phase current as predicted by the Accurate Model. The load angle swings at a frequency of about 0.7 Hz to a new larger steady state value where the increased electrical torque is once again equal to the applied shaft torque.

Instead of showing the corresponding set of four graphs for each of the other two models, only their load angle curve will be shown in order to conserve space. Fig 2.7 therefore illustrates the load angle behaviour for this 10% increase in applied shaft torque when predicted by all three models. The response predicted by Model 2 is practically identical to that predicted by the Accurate Model and the $p\psi$ terms thus appear to have no influence under these conditions. Even the omission of two damper windings in Model 3 does not seem to have much affect on the predicted result with the greatest difference between Model 3 and the Accurate Model

being only 0.15 degrees which is not of any practical significance.

The error is small because the electrical system experiences this type of disturbance as a mild one slowed down by the rotating inertia.

2.4.2 Change in applied field voltage

This disturbance consists of a 10% step reduction in the applied field voltage. Fig 2.8 depicts the three calculated load angles increasing slowly to a new steady state value, and the difference between the curves is still quite small and not of any practical significance. Once again the generator experiences this disturbance as a mild one due to the long field circuit time constant which smoothes out the change in field current and hence in electrical torque.

2.4.3 Change in tie-line impedance

This disturbance consists of a 40% step increase in the values of R_2 from 0.0845 p.u. to 0.1183 p.u. and in X_2 from 0.6897 p.u. to 0.9656 p.u. and could represent the switching out of one leg of a parallel section of transmission line. Fig 2.9 illustrates the familiar swing in the three predicted values of load angle to a higher steady state value. Although a 40% increase in X_2 is an extremely large change in system impedance, this increase in tie-line inductance actually slows down the rate of change of stator currents and reduces the effect of the $p\psi$ terms. Hence, since the current and air-gap flux do not change violently the three swing curves do not differ very much.

2.4.4 Change in infinite busbar voltage

This disturbance consists of a 10% step reduction in the value of the infinite busbar voltage V_b. The predicted swing curves in Fig 2.10 show that Model 2 again has no visible error whereas Model 3 predicts a less damped response. Although the error of 0.45 degrees at the first peak in

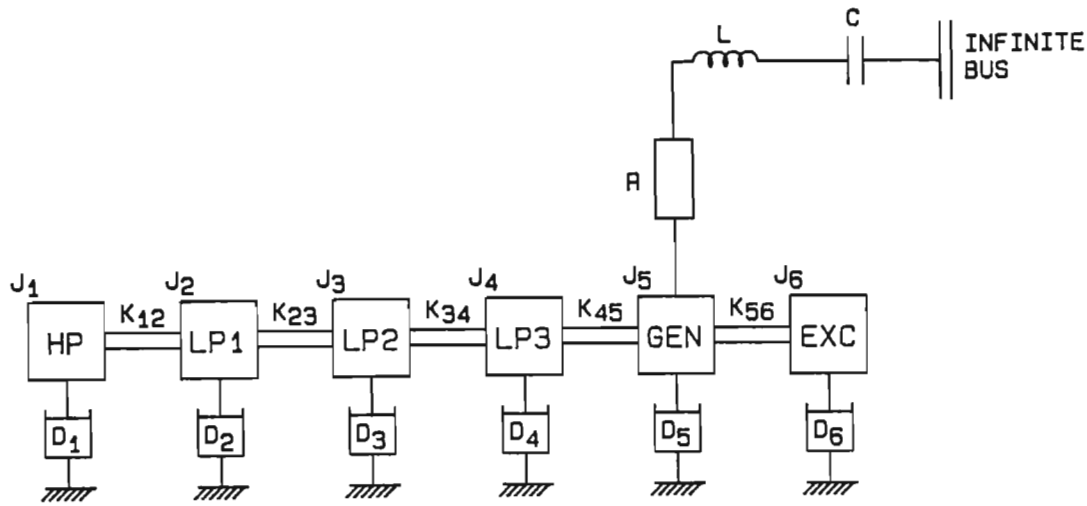

Fig 2.5 Multi-inertia representation of the turbogenerator system.

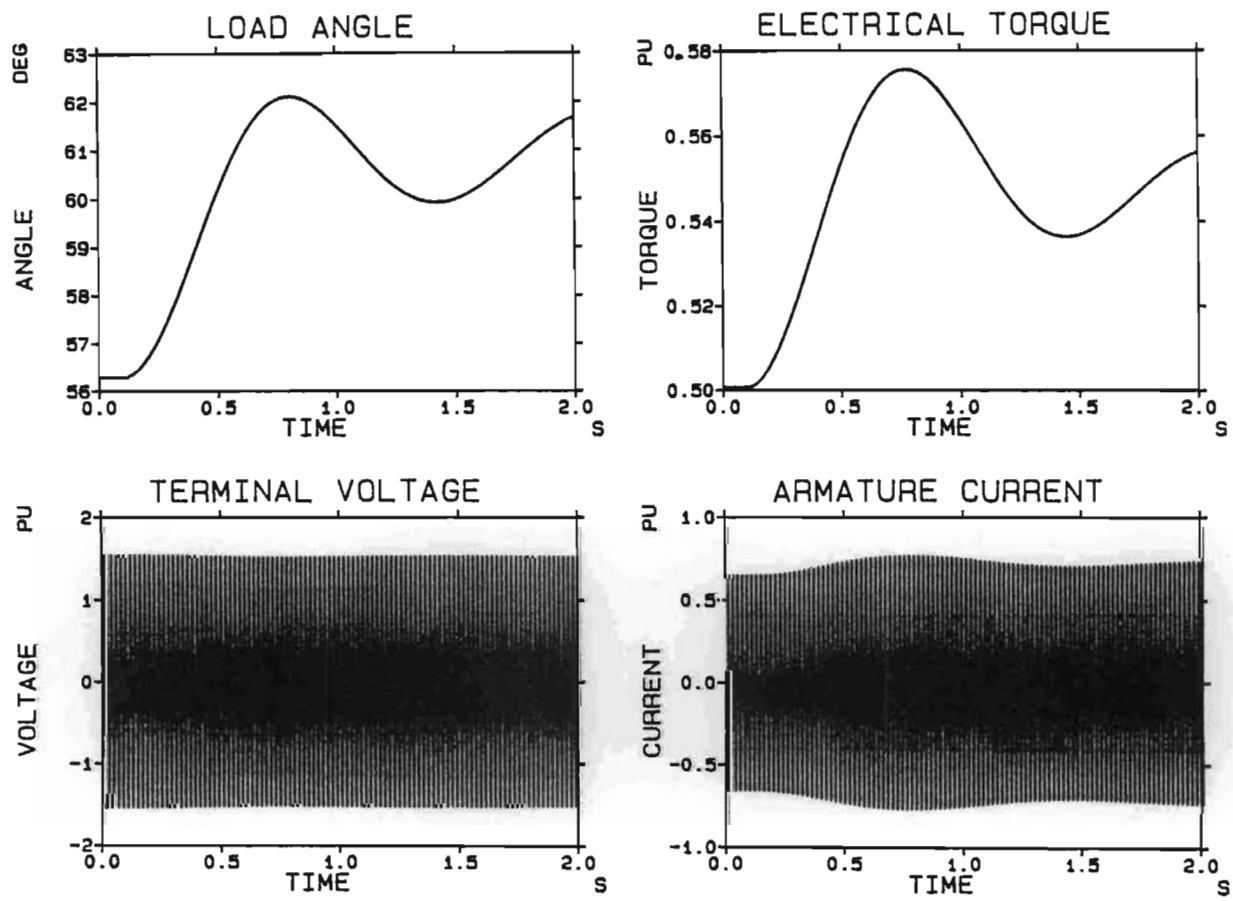

Fig 2.6 Transient response to a 10% step increase in applied shaft torque as predicted by the Accurate Model.

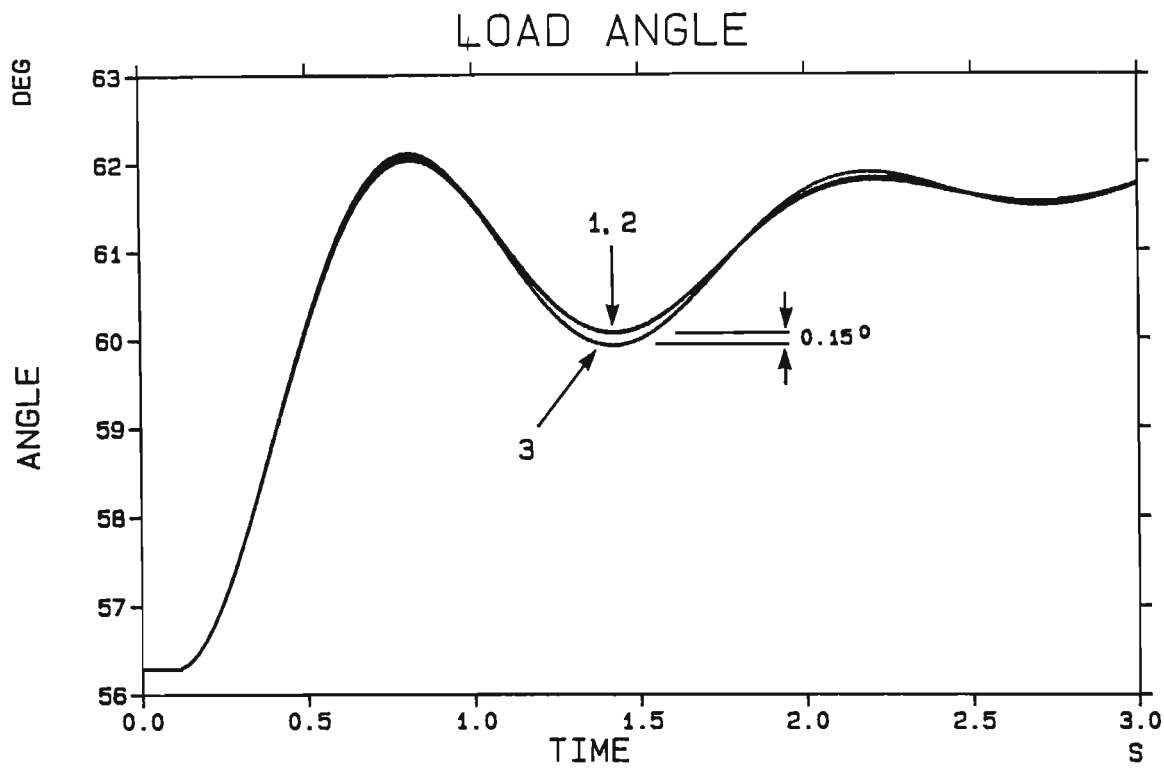

Fig 2.7 Load angle curves for a 10% step increase in applied shaft torque; Curves: 1 - Accurate Model; 2 - Model 2; 3 - Model 3.

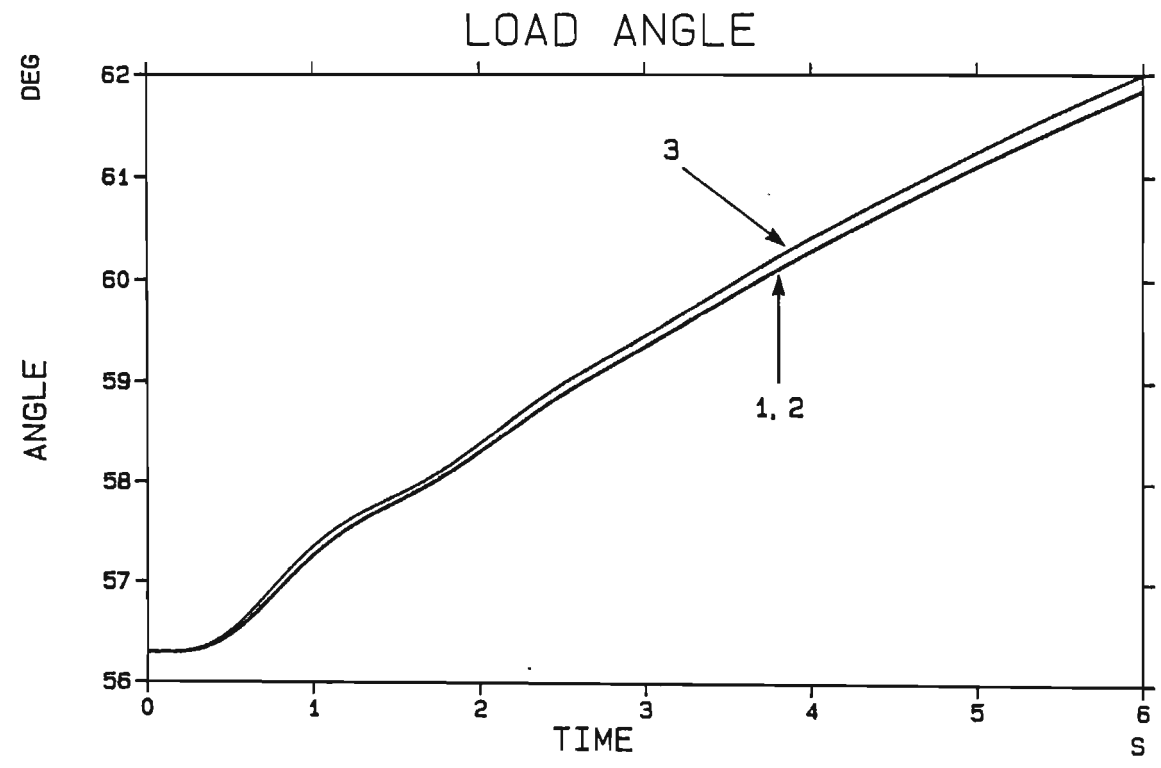

Fig 2.8 Load angle curves for a 10% step reduction in applied field voltage; Curves: 1 - Accurate Model; 2 - Model 2; 3 - Model 3.

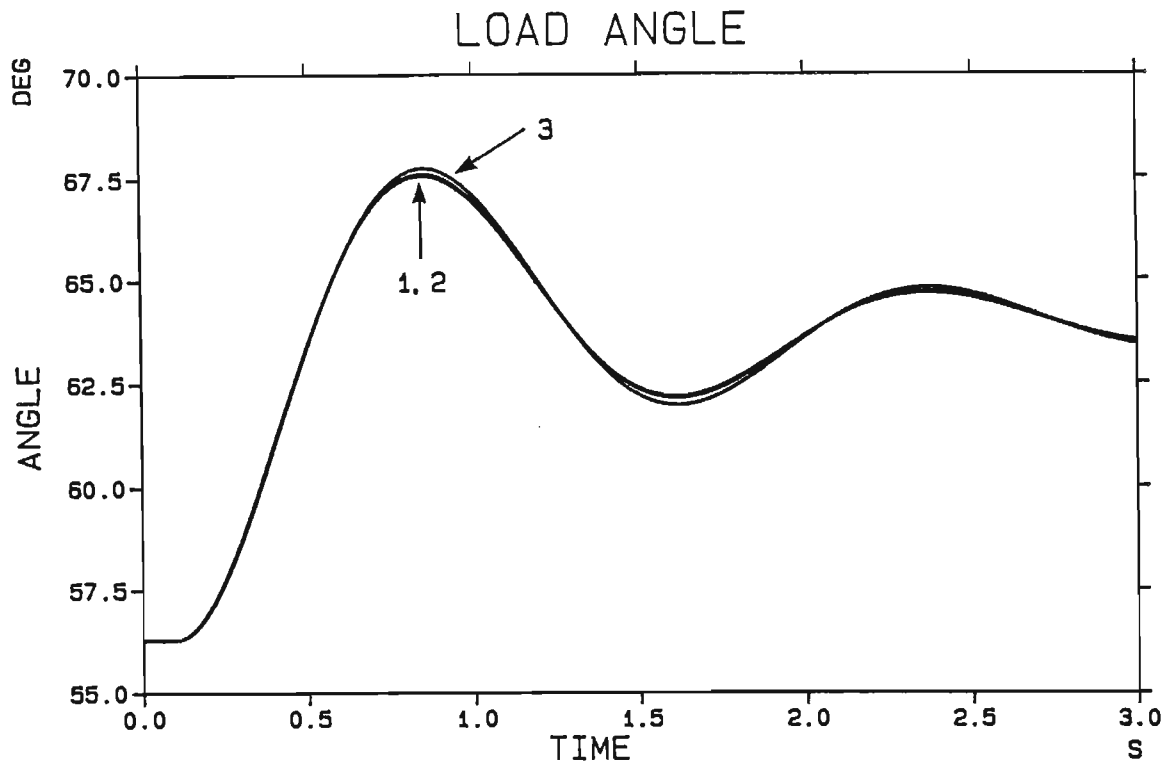

Fig 2.9 Load angle curves for a 40% step increase in tie-line impedance; Curves: 1 - Accurate Model; 2 - Model 2; 3 - Model 3.

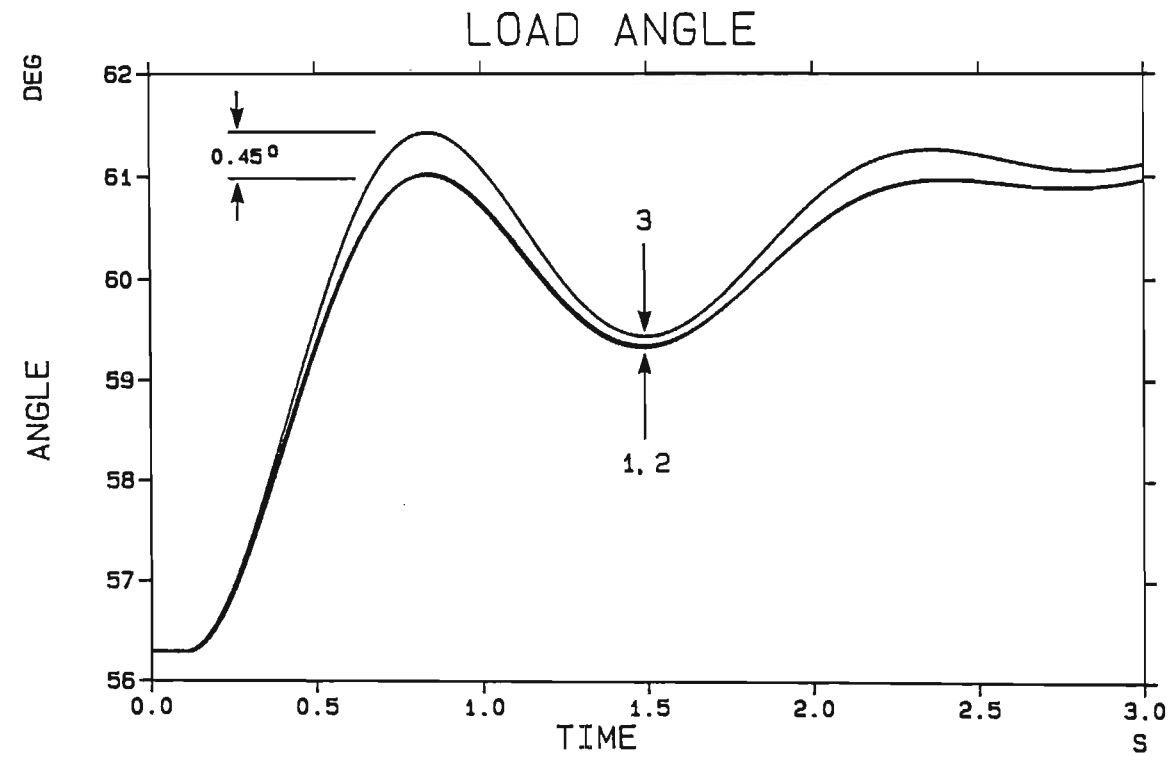

Fig 2.10 Load angle curves for a 10% step reduction in infinite busbar voltage; Curves: 1 - Accurate Model; 2 - Model 2; 3 - Model 3.

the Model 3 swing curve is greater than for the previous three faults it is still not of any practical significance. Even though this disturbance is on the electrical side, it is impedance-wise sufficiently remote from the generator (tie-line resistance R = 0.0855 p.u. and tie-line reactance X_L = 0.8397 p.u.) to create only mild changes in the phase currents and therefore in the stator flux and in the electrical torque.

The four disturbances described so far do not cause any violent reactions in the phase currents and therefore in the stator flux. As a result, the air-gap flux linkage components ψ_d and ψ_q change only gradually, so that their time derivatives $p\psi_d$ and $p\psi_q$, which appear as "transformer" voltages in eqns (2.1) and (2.2) are much smaller than the "rotational" voltages $\omega\psi_d$ and $\omega\psi_q$ in those same equations. As a result only a small error is incurred by neglecting $p\psi_d$ and $p\psi_q$ when using Models 2 and 3 for such disturbances.

2.4.5 Three phase short circuit

This disturbance consists of a temporary 100 ms duration symmetrical three phase short circuit on the generator terminals, and is considered to be the most severe fault from a transient stability point of view.

Previous studies [11,18] have shown that during this type of disturbance, the generator response is quite different from that during the other disturbances considered so far. The main reasons are firstly that the synchronizing connection to the infinite busbar is completely severed during the fault so that all the pre-fault applied shaft torque becomes accelerating torque, and secondly that the currents and flux levels change so rapidly that the $p\psi_d$ and $p\psi_q$ terms are no longer negligible with respect to $\omega\psi_d$ and $\omega\psi_q$ respectively in eqns (2.1) and (2.2).

Fig 2.11 compares the results predicted by Model 3 with those predicted by the Accurate Model. Since the results predicted by Model 2 are similar to those of Model 3, only those of Model 3 appear in Fig 2.11. However, all three predicted swing curves appear in Fig 2.12.

A comparison of the results in these two diagrams shows that the different generator models predict different load angle swings although all three models (Fig 2.12) predict that the generator remains stable. The first peak of the load angle swing predicted by the Accurate Model is considerably less (5 degrees) than that predicted by Models 2 and 3. This difference can be explained by the fact that the Accurate Model contains the $p\psi$ terms which give rise to a dc component in the phase current [18]. This dc current and its effect on the electrical torque can be seen in Fig 2.11; the 50 Hz component of electrical torque predicted by the Accurate Model has a peak eight times larger than the pre-fault torque. Thus the dc component of current has a large effect in the generator and causes losses in the generator rotor which for the situation studied are larger than the pre-fault power supplied by the turbine. This momentary power unbalance causes the generator to slow down and the load angle to decrease temporarily during the fault; this decrease is shown in Fig 2.11 as BS which is an abbreviation of backswing, the term generally used [11] to describe this phenomenon.

The value of the error in Fig 2.12 depends on a number of parameters including the pre-fault values of steady active power, excitation level, generator inertia and the tie-line impedance, as well as on the duration of the fault, and its electrical distance from the generator terminals. In order to illustrate the effect of some of these factors, the results of Fig 2.12 are repeated in Fig 2.13, but for a fault duration of 250 ms (instead of only 100 ms) and an initial operating point of P_t = 0.6 p.u., Q_t = 0.25 p.u. and V_t = 1.05 p.u.

Fig 2.13 shows that the two simplified models both erroneously predict instability when compared to the accurately calculated curve. There is no obvious backswinging of the accurate load angle, since the transient loss torque under these conditions is practically equal to the pre-fault steady shaft torque. If it were actually less than the pre-fault steady shaft torque it would not decelerate the rotor but only reduce the rate of acceleration.

Although these short circuit results clearly show some significant errors between the Accurate Model and Model 3 the errors between the simplified Models 2 and 3 are not all that significant. Anyway, all the errors are failing to safety.

This seems to indicate that not much additional accuracy would be gained by replacing a Model 3 by a Model 2 in an existing Power System Stability computer program, since Model 2 introduces two more differential equations per generator with the concomitant additional computer time and little extra accuracy. In fact, the amplitude of the errors between Models 2 and 3 are of the same order as that introduced by the incorrect representation of saturation in any of the three models [17].

2.5 Single Inertia Mechanical System with R-L-C Transmission System

This disturbance consists of the same three phase short circuit as for Fig 2.12, but the transmission line has now been lengthened (with a consequential increase in X_2 from 0.6897 p.u. to 1.0097 p.u.) and a series capacitor X_c = 0.32 p.u. has been added. This value of X_c ensures that under steady operating conditions the longer line has the same effective value of inductive reactance as the shorter line.

The omission of the $p\psi_d$, $p\psi_q$ terms by Models 2 and 3 also imply omission of pi_d, pi_q in the generator stator and the transmission line. This allows the voltage across the line reactance to be calculated (see eqns (2.27) and (2.38)) as:

$$(\omega L - 1/\omega C)i_q = (X_L - X_c)i_q = X_{LE}i_q \qquad (2.54)$$

$$(\omega L - 1/\omega C)i_d = (X_L - X_c)i_d = X_{LE}i_d \qquad (2.55)$$

where X_{LE} is defined as an effective inductive reactance, and for this test $X_{LE} = X_L - X_c = 1.1597 - 0.32 = 0.8397$ p.u. which is the same as the X_L used to calculate the results in Fig 2.12. The load angle swing curves predicted by Models 2 and 3 for this test are therefore identical to those

shown in Fig 2.12 and are repeated as curves 2 and 3 in Fig 2.14 for the purposes of comparison.

The Accurate Model represents the voltage across the tie-line by eqns (2.12) and (2.13) which consider X_L and X_c as separate elements. However, the accurately calculated swing curve with this transmission line configuration is identical to curve 1 from Fig 2.12 calculated for the short transmission line with no X_c and they appear superimposed as a single curve (curve 1) in Fig 2.14. The accurate curve calculated with the capacitor voltage states included does not display any subsynchronous oscillations since the turbine and generator inertia stages are at this point still represented as a single lumped inertia. However, these results change considerably if the mechanical system is represented by its separate inertias and shafts as shown by the curve in Fig 2.18; this will be discussed in more detail in Sects 2.6 and 2.7.

2.6 Multi-Inertia Mechanical System with R-L Transmission System

The three phase short circuit tests of Sect 2.4.5 are repeated but the mechanical system is now represented as separate inertias and shafts as illustrated in Fig 2.5 in order to correctly model the shaft dynamics according to eqn (2.53).

Fig 2.15 shows the variation in electrical torque, rotor position (rotor angle), phase current and terminal voltage, but when the shaft dynamics are included. A comparison of Figs 2.11 and 2.15 shows that the correct detailed modelling of the shaft dynamics does not seem to have much affect on the phase current, terminal voltage, electrical torque, and upon the 0.7 Hz fundamental load angle (now called the rotor angle) swing curves. However, the rotor angle curves in Fig 2.15 clearly contain ripple at subsynchronous frequency due to the torsional resonance of the shaft system. The comparisons made in Sect 2.4.5 between the Accurate Model results and the Model 2 and 3 results also apply here.

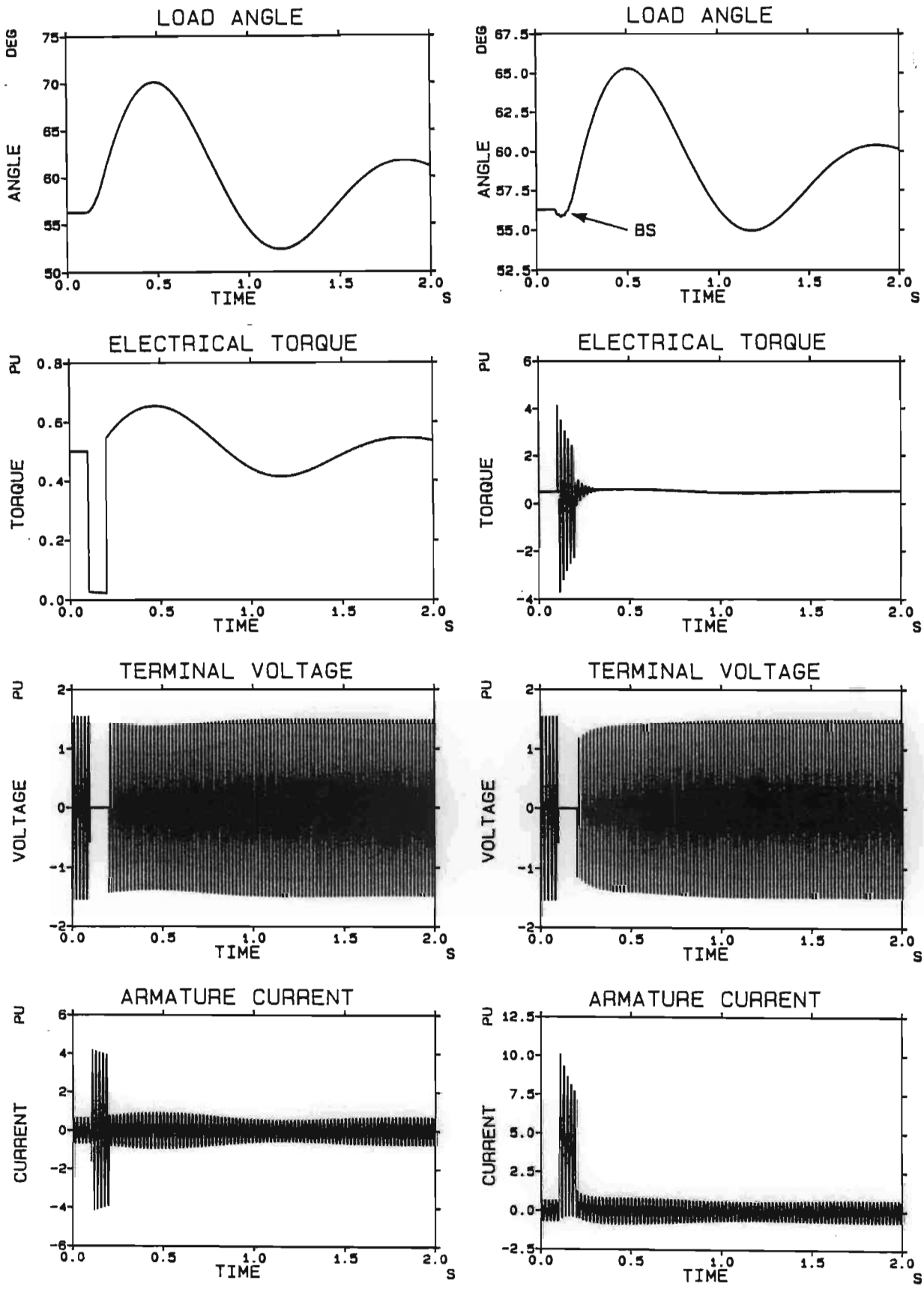

(a) Model 3 (similar to Model 2)

(b) Accurate Model

Fig 2.11 Transient response to a 100 ms three phase short circuit.

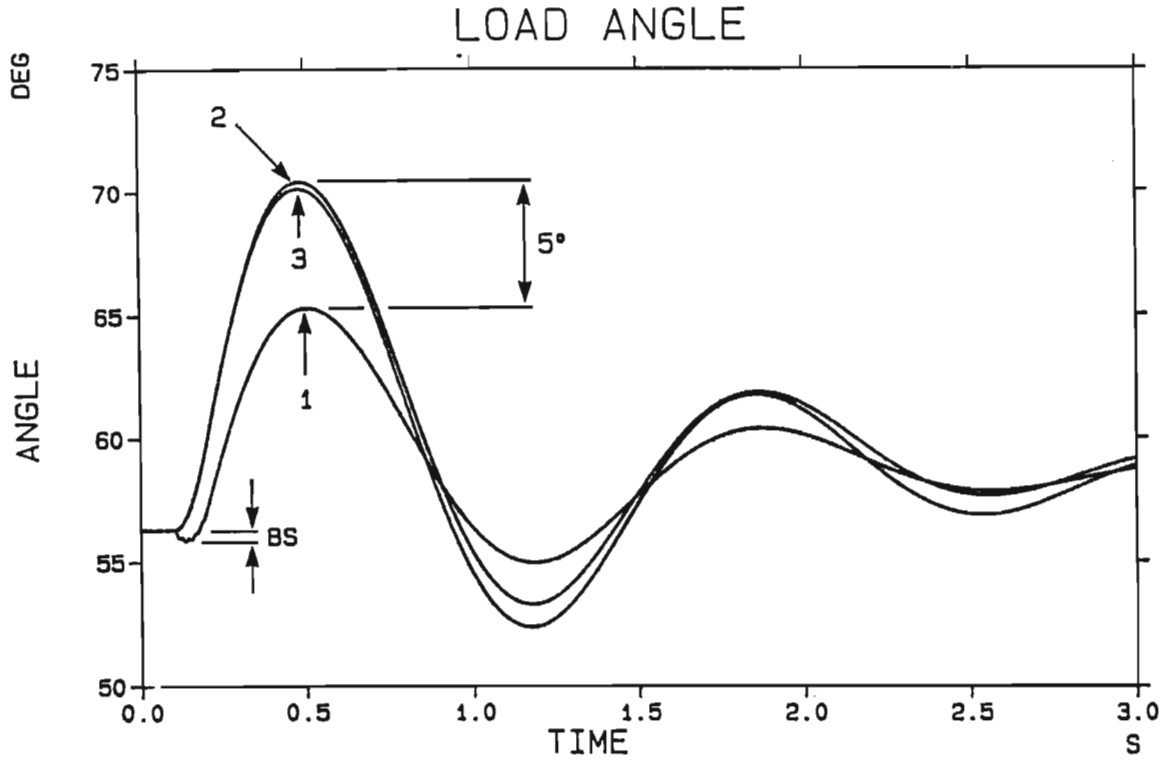

Fig 2.12 Load angle curves for a 100 ms three phase short circuit;
Curves: 1 - Accurate Model; 2 - Model 2; 3 - Model 3.

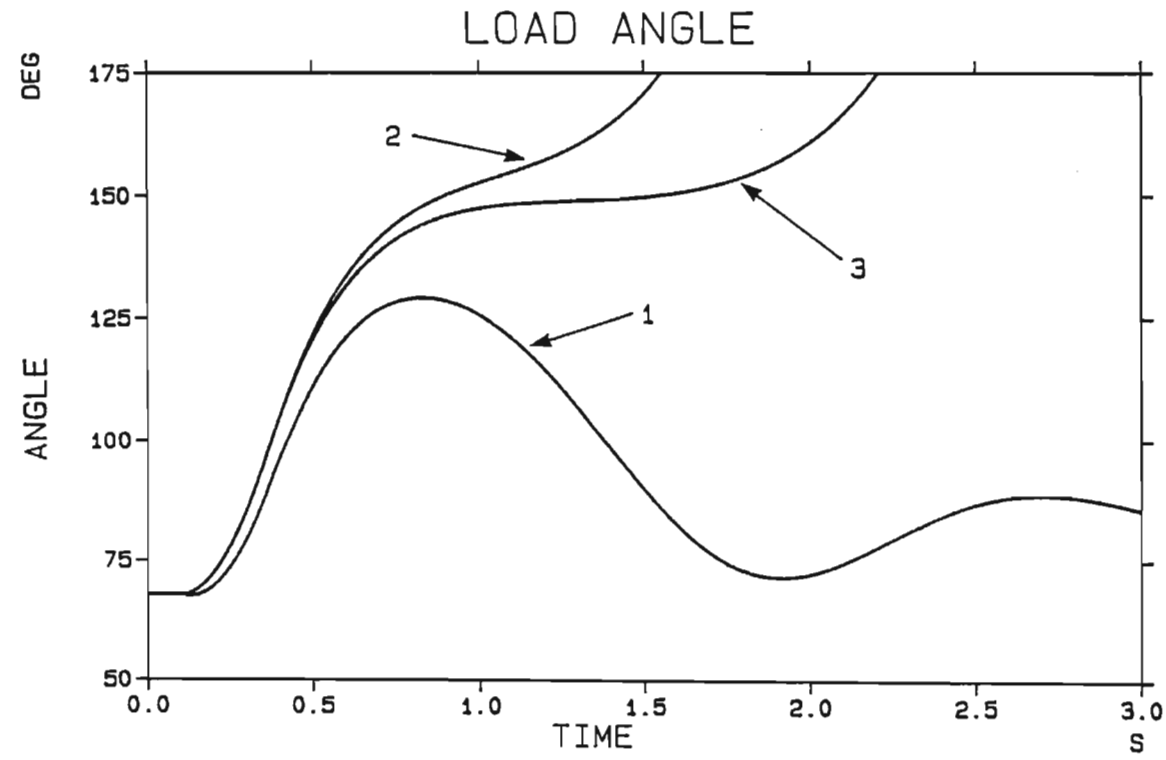

Fig 2.13 Load angle curves for a 250 ms three phase short circuit;
Curves: 1 - Accurate Model; 2 - Model 2; 3 - Model 3.

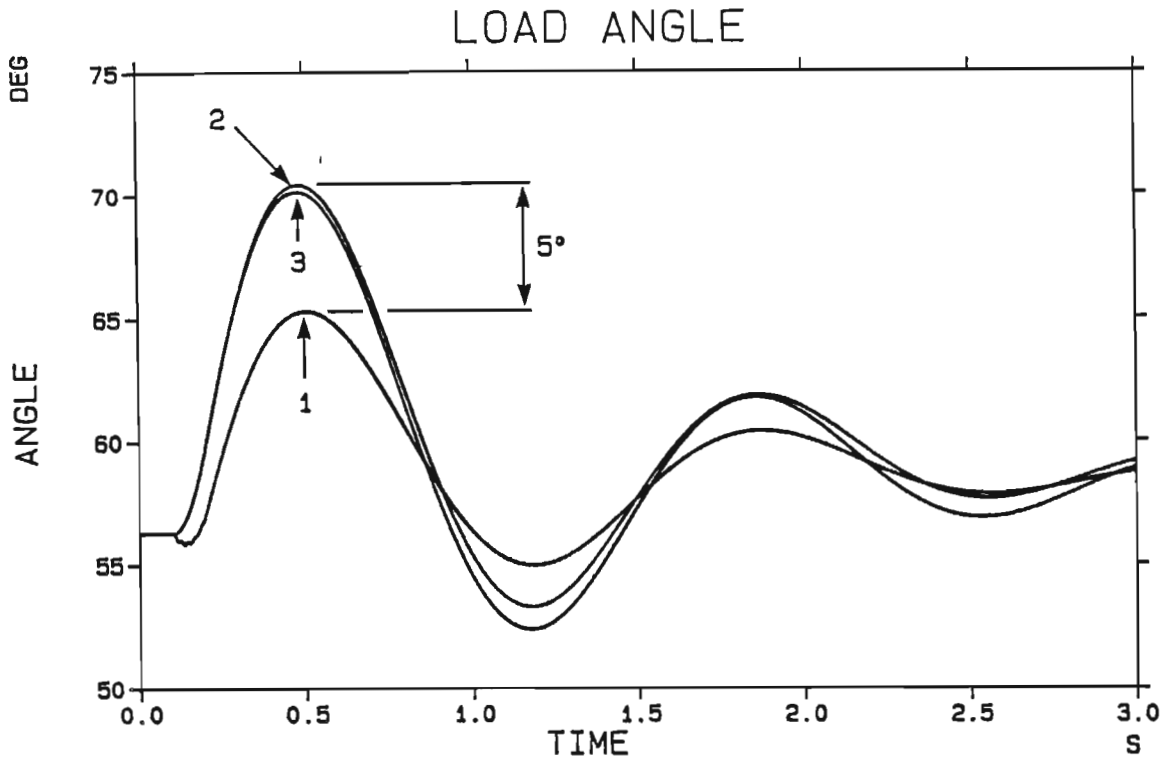

Fig 2.14 Load angle curves for a 100 ms three phase short circuit when the tie-line contains a series capacitor of 0.32 p.u.; Curves: 1 - Accurate Model; 2 - Model 2; 3 - Model 3.

The three predicted curves for rotor angle in Fig 2.16 illustrates the difference in the results, and should be compared with the three curves in Fig 2.12. The comparison shows that although the fundamental 0.7 Hz waves in Fig 2.16 again differ by about 5 degrees at the first peak, the superimposed ripple in the accurate result differs considerably from the simplified curves.

If the fault duration is increased to 250 ms and the initial operating point changed to P_t = 0.6 p.u., Q_t = 0.25 p.u. and V_t = 1.05 p.u. (as in the case of Fig 2.13) then Model 2 and 3 again yield a completely erroneous result in Fig 2.17, although (as in every other case so far) nevertheless failing to safety.

The general conclusion from this section of results is that the addition of shaft dynamics to each of the three mathematical models (by means of the extra mechanical twelve first order differential equations) does not significantly change the swing curves which have been calculated without shaft dynamics.

2.7 Multi-Inertia Mechanical System with R-L-C Transmission System

2.7.1 No build up of subsynchronous oscillations

The short circuit tests of Sect 2.6 are repeated with the exception however, that the series capacitor X_c = 0.32 p.u. of Sect 2.5 is again added to the line, and X_2 is increased from 0.6897 p.u. to 1.0097 p.u. as before. The rotor angle curves predicted by the three models appear in Fig 2.18. All three curves are identical to those in Fig 2.16 and curve 1 is in fact (as in Fig 2.14) the accurate curve from Fig 2.16 superimposed on the one calculated with X_c. It is significant to note that even with shaft dynamics included, the introduction of series capacitance has not altered the accurately calculated rotor angle at all.

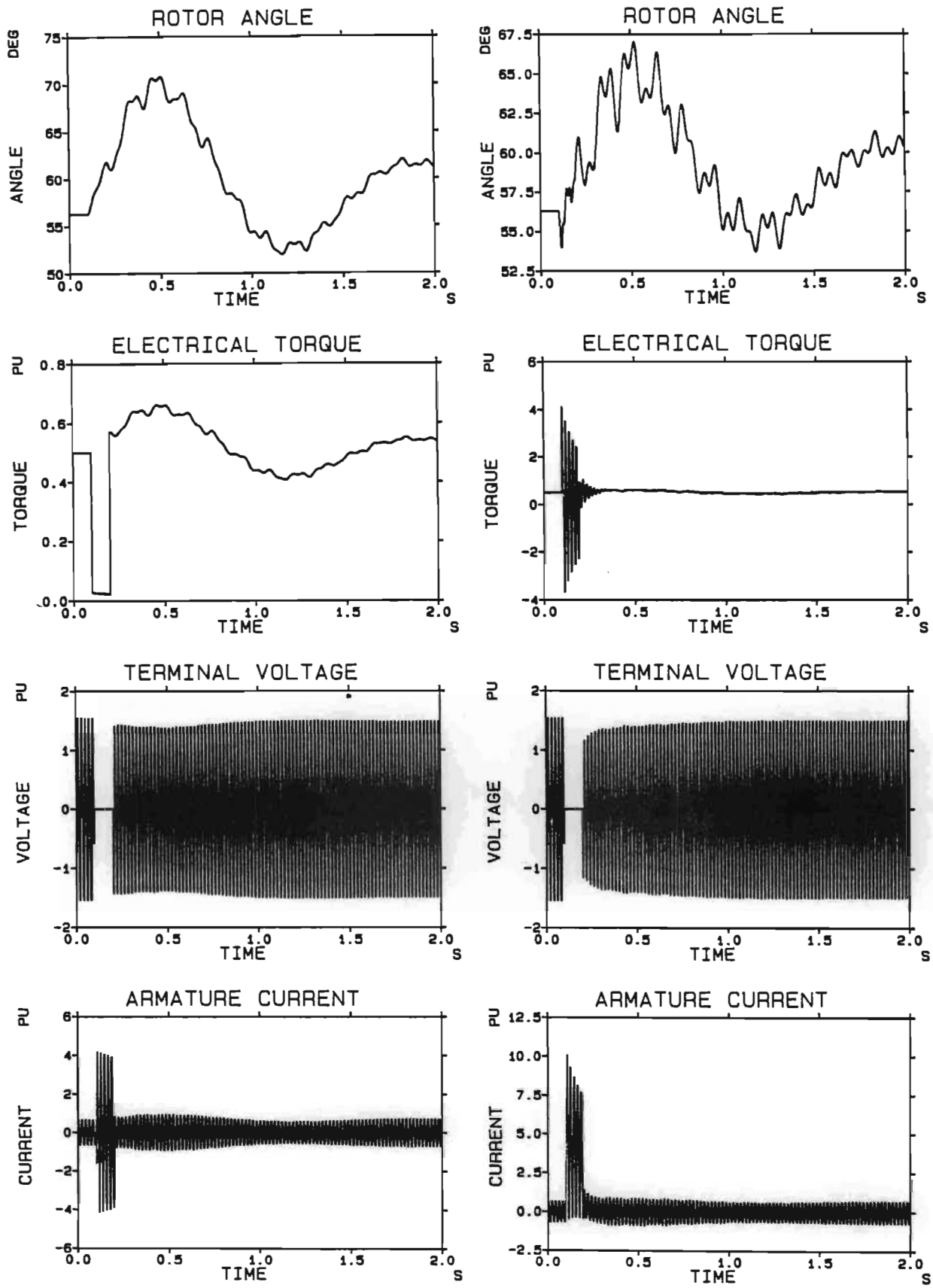

(a) Model 3 (similar to Model 2)

(b) Accurate Model

Fig 2.15 Transient response to a 100 ms three phase short circuit when shaft dynamics are included, but with no series capacitance.

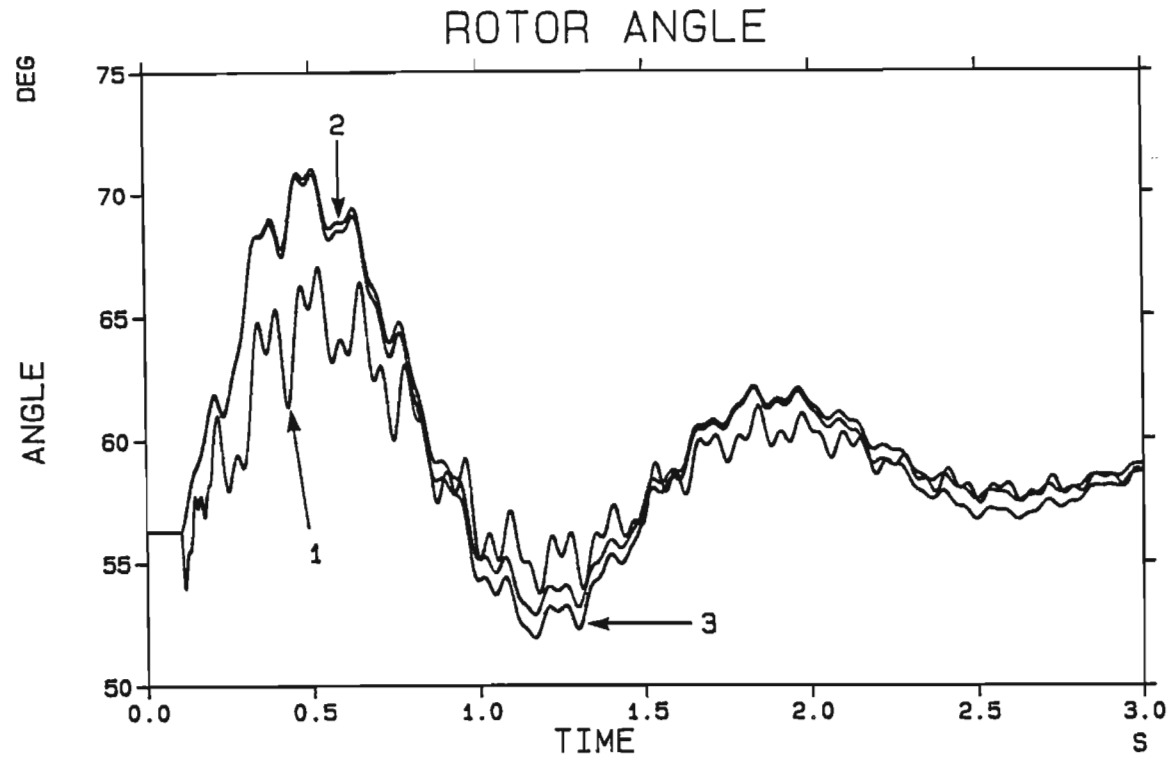

Fig 2.16 Rotor angle curves for a 100 ms three phase short circuit when shaft dynamics are included, but with no series capacitance; Curves: 1 - Accurate Model; 2 - Model 2; 3 - Model 3.

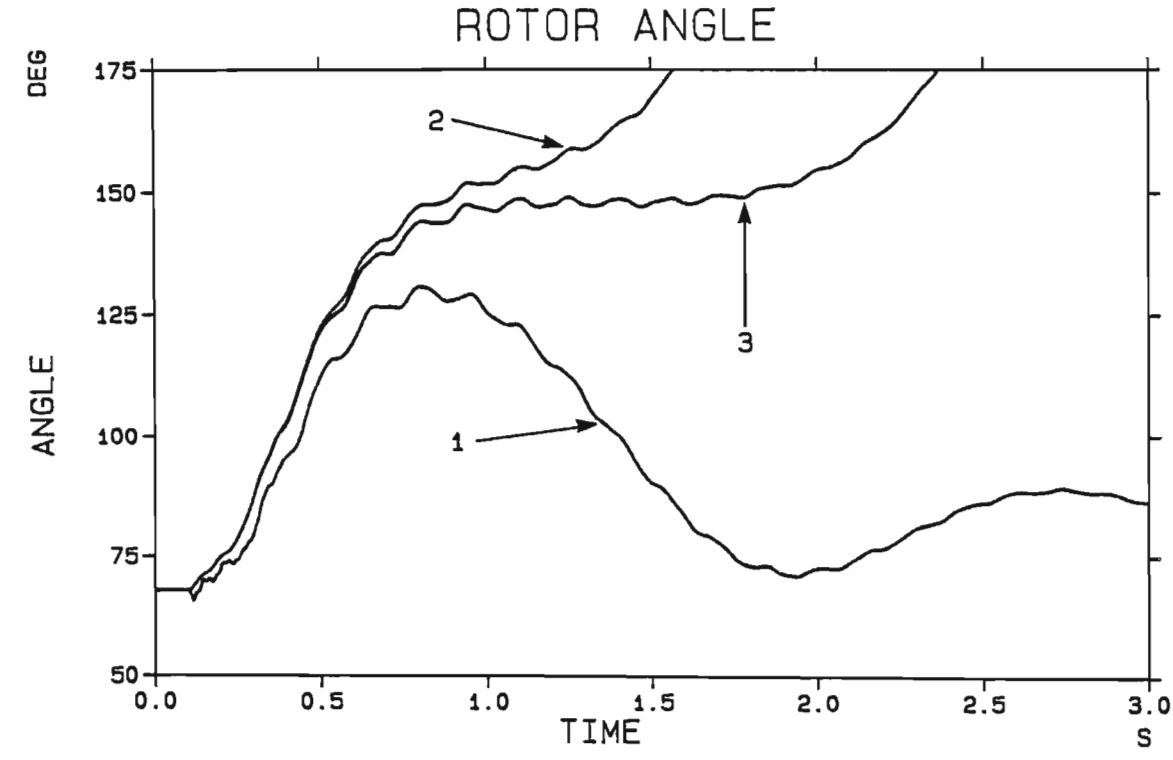

Fig 2.17 Rotor angle curves for a 250 ms three phase short circuit when shaft dynamics are included, but with no series capacitance; Curves: 1 - Accurate Model; 2 - Model 2; 3 - Model 3.

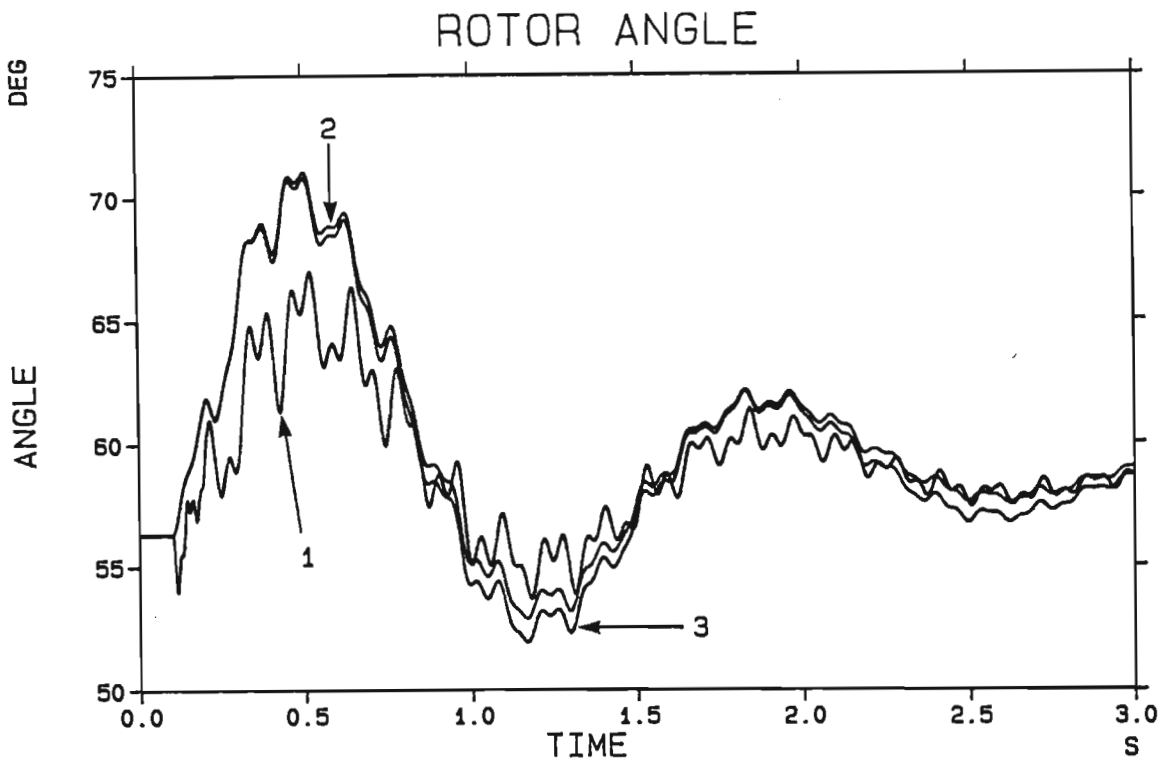

Fig 2.18 Stable rotor angle curves following a 100 ms three phase short circuit when shaft dynamics are included and a series capacitor of 0.32 p.u. is present; Curves: 1 - Accurate Model; 2 - Model 2; 3 - Model 3.

This value of X_c (=0.32 p.u.) was not sufficient to cause the growing unstable SSR oscillations of curve 1 in Fig 2.20. Such possible instabilities are examined in the next section where it is shown that the approximate models give completely wrong results which do not fail to safety.

2.7.2 Build up of subsynchronous oscillations

The short circuit tests of Sect 2.7.1 are repeated but the series capacitor is increased to X_c = 0.66 p.u. which yields an unstable dynamic response. The fault duration is 100 ms and the initial steady operating point is P_t = 0.5 p.u., Q_t = 0.2 p.u., V_t = 1.05 p.u.

The Accurate Model results are shown in Fig 2.19 (b), and these clearly show the familiar subsynchronous resonance (SSR) oscillations present in the rotor angle and the electrical torque. These SSR frequencies are also present in the voltage and current waveforms, but each time at frequencies equal to 50 Hz plus and minus the mechanical frequency.

When Model 3 is used to predict the response of this same system to the same fault, it yields a stable response as shown in Fig 2.19 (a). The results in Fig 2.19 prove that for this combination of system parameters the simplified Model 3 fails completely, but alas not to safety as it did in the sections considered so far.

The rotor angle curves of Model 2 are similar to those of Model 3 as illustrated in Fig 2.20. This diagram therefore shows that both simplified models predict a stable transient response while the Accurate Model predicts an unstable subsynchronous response. Of all the disturbances and system configurations considered so far, this disturbance to this particular generator and transmission line requires that only the Accurate Model be used to predict the system's behaviour.

Further calculations with the three models of the capacitively compensated system's behaviour revealed that the limitations of the two simpler models

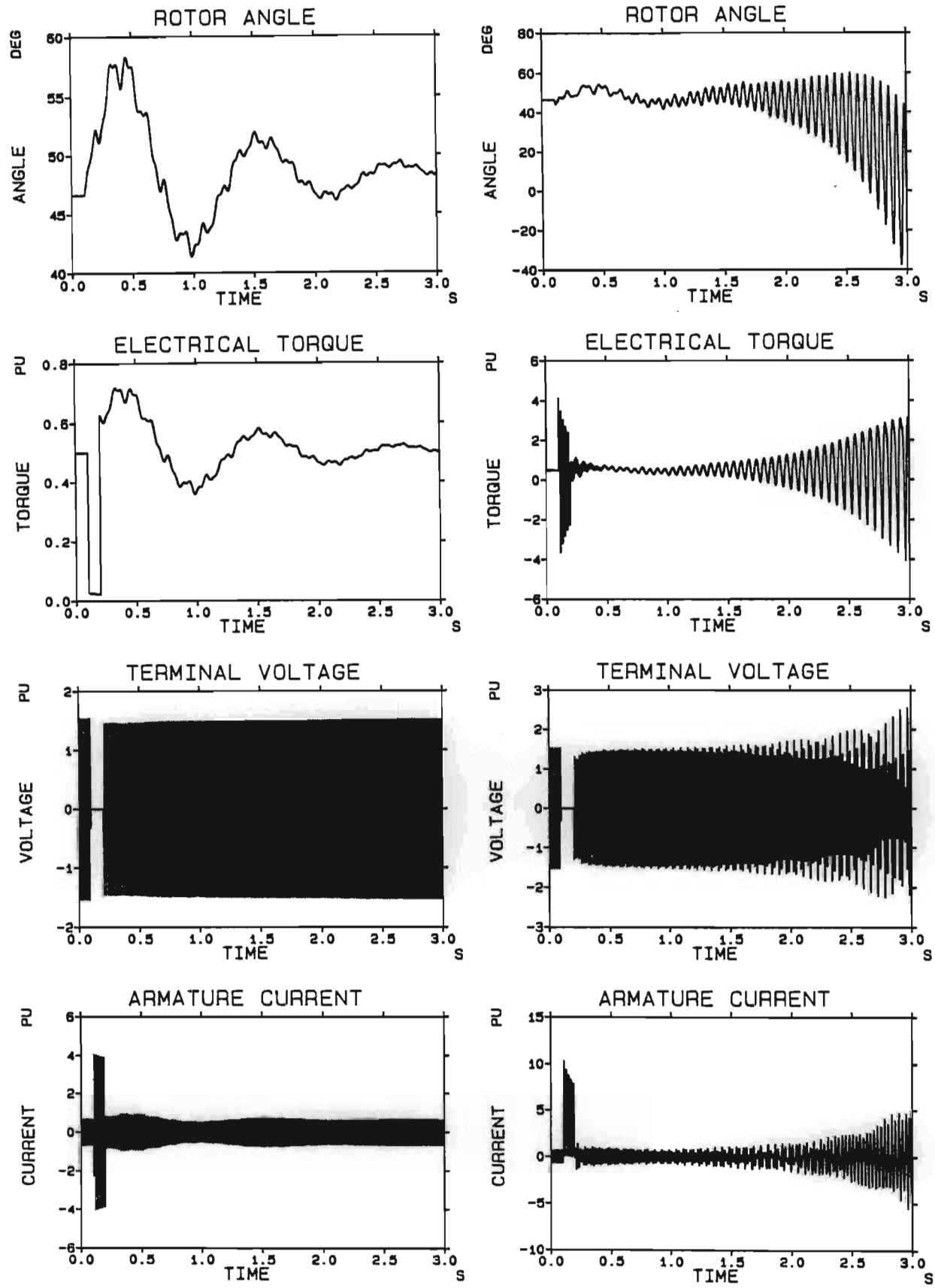

(a) Model 3 (similar to Model 2)

(b) Accurate Model

Fig 2.19 Transient response to a 100 ms three phase short circuit when shaft dynamics are included and a series capacitor of 0.66 p.u. is present.

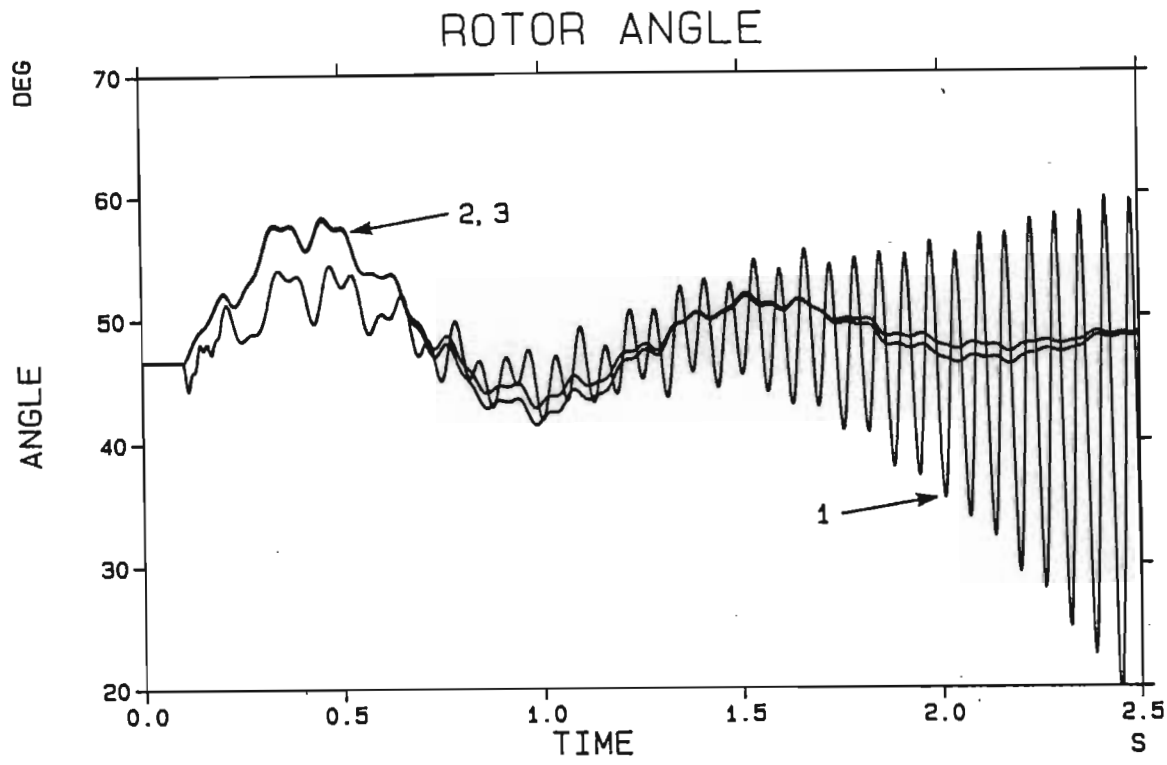

Fig 2.20 Rotor angle curves following a 100 ms three phase short circuit when shaft dynamics are included and a series capacitor of 0.66 p.u. is present; Curves: 1 - Accurate Model; 2 - Model 2; 3 - Model 3.

in Fig 2.20 were not due to the short circuit in particular, but because these models failed to accurately represent the interaction between the electrical and mechanical systems whenever the tie-line contained a capacitor.

In other words, whether subsynchronous instability is brought on by a short circuit or a change in any other system parameter, the simplified models will never be able to predict an unstable response unless the compensation level is so high that the SSR is caused by the so-called induction generator effect and the generator becomes self-excited. However, it is unlikely that a line will be operated at such high compensation levels so that this property of the simpler models has little practical value.

2.8 Conclusions

This chapter has revised the theory of three different mathematical models which can be used to predict the transient behaviour of a turbogenerator. The so-called Accurate Model is based on the two-axis theory, while the other two models are derived from the Accurate Model after various degrees of simplification. The two simplified models are Model 2 which neglects the stator transients $p\psi_d$ and $p\psi_q$, and Model 3 which in addition also neglects a damper winding from each axis.

Five different disturbances have been considered, with and without a series capacitor in the tie-line, and with the turbine and generator rotors represented either as a single equivalent inertia or as a multi-inertia system interconnected by torsionally flexible shafts. From all these investigations, the following main conclusions can be drawn:

(a) when there are no series capacitors present in the transmission system, it is not important to model the torsional characteristics of the turbogenerator shaft system;

(b) when there are series capacitors present in the transmission system and there is no likelihood of a build up of subsynchronous oscillations, it is not important to model the turbogenerator shaft system accurately;

(c) when there are series capacitors present in the transmission system and subsynchronous oscillations are expected to build up the shaft system and the electrical circuits of the turbogenerator must be modelled accurately;

(d) when the disturbance only results in small electrical changes in the generator, e.g. small changes in shaft torque, in generator field voltage, in infinite busbar voltage or in system impedance, a simple generator representation is adequate (provided there is no threat of SSR);

(e) when the disturbance results in large electrical changes in the generator, e.g. three phase short circuit on the generator terminals, then the accurate generator representation should be used.

CHAPTER THREE

MODAL ANALYSIS REPRESENTATION OF A MULTI-INERTIA TURBOGENERATOR

3.1 Introduction

In Chapter Two various turbogenerator system models were analysed and the ability of these models to represent different systems under fault conditions was determined. From the results it was seen that under conditions of series capacitor compensated power transmission a system could become unstable with growing sub-harmonic oscillations (see Fig 2.20). This fact is of great concern in the power industry since series capacitors are generally the most economical method of increasing the power transfer capability of an EHV transmission line and are in widespread use today. This instability associated with the use of series capacitors is due to electrical resonances at subsynchronous frequencies, introduced by the inclusion of capacitance in the transmission network, interacting with the turbogenerator mechanical system and its resonances and is known as Subsynchronous Resonance (SSR). Since the majority of this thesis is concerned with the subject of SSR it is useful at this stage to discuss this phenomenon in more detail.

SSR is an electrical power system condition where the electrical network and the mechanical system of a turbogenerator exchange energy, through the generator electrical torque, at one or more frequencies below the synchronous frequency of the system. This oscillatory energy interchange may be lightly damped, undamped or even negatively damped. Two separate mechanisms of SSR have been identified [22], namely the induction generator effect and the torsional interaction effect; in addition series capacitance

also causes the torque amplification effect which is sometimes considered as a third SSR condition.

Series capacitors cause subsynchronous line currents with frequency f_r to flow in each of the generator stator phase windings. These currents give rise to positive and negative sequence components of airgap flux which rotate at f_o-f_r and f_o+f_r respectively. These two frequencies are referred to as complementary electrical frequencies. The equivalent circuit representation of a synchronous machine at a non-synchronous frequency contains a term R/s, where R is the effective rotor resistance and s is the slip. However, the rotor circuits turn faster than the positive sequence flux component, thereby producing a negative slip component. This causes the resistance of the rotor to subsynchronous currents, when referred to the stator terminals, to be negative; when its value exceeds the positive network resistance, self-excitation occurs in the generator. This phenomenon, also referred to as the induction generator effect, is usually only a problem at compensation levels in excess of 80%, or in other words, when f_r is numerically close to f_o thereby giving rise to low values of negative slip and consequently large values of negative referred rotor resistances.

The torsional interaction effect, on the other hand, refers to the interaction between the rotating mechanical system and the electrical system. When the rotor field flux, which rotates at the speed of the rotor, overtakes the more slowly rotating positive sequence subsynchronous flux of the stator, a subsynchronous oscillatory component of electrical torque is produced whose frequency is the difference between f_o and f_r. If this torque frequency coincides with, or is close to, a rotational modal frequency f_{mi} of the shaft system, a regenerative feedback situation may arise. The enhanced subsynchronous electrical torque may exceed the inherent mechanical damping of the rotating system, thereby producing unstable oscillations [23].

The torque amplification effect occurs when electrical torques are close in frequency to one of the torsional natural modes; in this case torques may

be induced in the shaft following a system disturbance which are much larger than those developed as a result of a three-phase fault in an uncompensated system. Torsional interaction and torque amplification both occur simultaneously (as does the induction generator effect) however torsional interaction concerns the damping of shaft oscillations whereas torque amplification concerns the magnitude of these oscillations.

Since the two incidents of generator shaft failure at Mohave Power Station in Nevada, U.S.A. [23] the problem of SSR has received much attention. In South Africa the two turbogenerators at Koeberg nuclear power station in the Western Cape are connected through 1400 km of 400 kV series capacitor compensated transmission line to the larger Transvaal grid. An early investigation [15] showed that unless precautionary steps were taken, unstable SSR oscillations could occur on the Koeberg system if the transmission system was to be operated with high levels of series capacitor compensation.

This first investigation assumed Koeberg to be connected to the Transvaal grid (infinite bus) through a single R-L-C transmission line. Later studies [20,24,25] extended this to include the effects of other generating stations connected to the line, R-L and induction motor loads at various points along the line and a more accurate representation of the transmission system with separately compensated parallel lines. All these studies attempted to predict the stability characteristics of the system, in particular the maximum safe level of compensation at which the system could operate without inducing SSR. This CRITICAL COMPENSATION LEVEL (CCL) was calculated with the emphasis on the accurate modelling of the electrical system, but the results obtained were still only approximate due to a large degree of uncertainty in the modelling of the mechanical system and exact values of all the system parameters. Over the past six years these early investigations have continuously been extended and the rest of this thesis reports on some of these aspects although they do not necessarily apply to the Koeberg system only but to any SSR prone system in general.

Initial investigations into SSR soon showed that in order to analyse the torsional interaction and torque amplification phenomena it was necessary to model the torsional characteristics of the shaft [23,26]; this led to the representation of the mechanical system as a multi-inertia shaft with the inertias interconnected by torsionally flexible springs (the connecting shafts) as shown in Fig 2.5. This lumped parameter model, referred to as the 'physical model' or spring-mass model [22] has been used in all the CCL calculations for the Koeberg system to date [15,20,24,25] as well as in numerous SSR studies worldwide.

The accuracy of the predicted CCL depends in general on the mathematical model and the validity of parameters, but in particular on the electrical and mechanical damping; the latter in turn is due to such factors as lubrication oil, shaft metal hysteresis [27], windage and friction, steam forces on buckets, coupling slip and plastic deformation at high levels of strain. In the physical model of the mechanical system in Fig 2.5 the non-strain-related damping factors are represented by a viscous dashpot damper D_i associated with each inertia. (It is sometimes also assumed that viscous dampers exist between inertia elements in order to represent the effects of shaft material damping, but this form of damping is highly amplitude dependent and difficult to model [27]). These damping values D_i in the physical model can be neither calculated nor measured which therefore presents a major limitation of this method of shaft representation. It means that the D_i's must be assigned estimated values (which cannot be done with any degree of accuracy) and so the accuracy of the mechanical model, and thus of the whole stability analysis, is limited by the accuracy of the damping estimates. This inaccurate damping representation not only affects the torsional interaction studies (CCL calculations) but also influences the predictions of shaft fatigue life expenditure following system disturbances since it will incorrectly predict the duration for which damaging shaft torque levels persist. Moreover, the magnitude of these peak shaft torques (incurred due to the torque amplification phenomena) are dependent on the shaft torsional characteristics (including the damping) so inaccuracies in the modelling of the shaft which may result from the use of the physical model will

influence the prediction of the torque amplification effect. Furthermore, in the design of SSR countermeasures and controllers the amount of mechanical damping present is important since the cost of any countermeasure is generally linked to the amount of positive damping that has to be added to the system in order to maintain stability. This is directly dependent on the amount of mechanical damping present and so an uncertainty in the mechanical damping would result in a more expensive countermeasure due to the necessity to design the countermeasure to be effective at the lowest expectation of damping.

This problem of having to estimate the values of D_i can be overcome by transforming the shaft equations into the frequency domain where the equations are decoupled and all the shaft parameters, including the damping, are measurable [2,23,28]. With this model of the shaft, called the 'modal model' or modal spring-mass model [22], values of inertia, damping and stiffness (called mode or modal parameters) are associated with each natural mode of vibration of the shaft. This modal representation has shown itself to be useful in various studies to date [29-31]. By using measured values of mode (or modal) damping with the modal model, the CCL can be determined more accurately, and SSR countermeasures can be designed more economically. Furthermore, a more accurate representation of the torsional characteristics of the shaft with measured shaft parameters in the modal model enables better predictions of torque amplification and shaft fatigue life reduction.

This chapter firstly restates the modal theory and then uses it in small-signal and transient stability studies. Although the modal model allows a more accurate representation of the shaft than the physical model, measurement errors nevertheless also occur in the determination of mode parameters and this chapter investigates the sensitivity of CCL and torque amplification calculations to such mode parameter errors. Such a sensitivity study has not been reported on before.

3.2 The Modal Transformation

Although the theory of modal analysis is well known [22,32-35] it is useful to restate it here since the modal form of representing the shaft is used extensively throughout the thesis.

The modal transformation is performed by considering the unforced, undamped mechanical system of Fig 2.5 which is described by (from eqn (2.53))

$$[J]p^2\underline{\delta} + [K]\underline{\delta} = \underline{0} \tag{3.1}$$

Since [J] is non-singular, $[J]^{-1}$ exists and eqn (3.1) can be rewritten as

$$p^2\underline{\delta} = -[J]^{-1}[K]\underline{\delta} \tag{3.2}$$

where the symmetric matrix $[J]^{-1}[K]$ is the system dynamic matrix with real non-negative eigenvalues λ_i [34]. The eigenvalues are given by the solution of the scalar equation

$$\det\{[J]^{-1}[K] - \lambda[I]\} = 0 \tag{3.3}$$

where [I] is the identity matrix. The eigenvalues λ_i obtained from the solution to eqn (3.3) satisfy the following equation

$$[J]^{-1}[K]\underline{Q}_i = \lambda_i\underline{Q}_i \tag{3.4}$$

where $\underline{Q}_i$ is the eigenvector corresponding to λ_i. These eigenvalues and eigenvectors determine the torsional characteristics of the shaft as discussed in Sect 3.3. Equation (3.4) can be recast to take into account all the eigenvalues resulting in the following matrix equation

$$[J]^{-1}[K][Q] = [\Lambda][Q] \tag{3.5}$$

where [Q] is a matrix of column-wise eigenvectors and [Λ] is a diagonal matrix of eigenvalues.

Now choose the following change of co-ordinates from angular position vector $\underline{\delta}$ to mode angle vector $\underline{q}$ where the transformation matrix is the matrix of eigenvectors [Q], so that

$$\underline{\delta} = [Q]\underline{q} \tag{3.6}$$

Substitution of eqn (3.6) and its first two derivatives into eqn (2.53) and multiplying on the left by $[Q]^T$ gives rise to the following equation

$$[Q]^T[J][Q]p^2\underline{q} + [Q]^T[D][Q]p\underline{q} + [Q]^T[K][Q]\underline{q} + [Q]^T(\underline{T}_m + \underline{T}_e) = \underline{0} \tag{3.7}$$

which can be written as

$$[J_M]p^2\underline{q} + [D_M]p\underline{q} + [K_M]\underline{q} + \underline{T}_M = \underline{0} \tag{3.8}$$

where $[J_M]$, $[D_M]$, $[K_M]$ and $\underline{T}_M$ are the mode inertia matrix, mode damping matrix, mode stiffness matrix and the mode torque vector respectively and are defined as

$$\begin{aligned} [J_M] &= [Q]^T[J][Q] \\ [D_M] &= [Q]^T[D][Q] \\ [K_M] &= [Q]^T[K][Q] \\ \underline{T}_M &= [Q]^T(\underline{T}_m + \underline{T}_e) \end{aligned} \tag{3.9}$$

The elements of row 'j' and column 'i' of $[J_M]$ and $[K_M]$ are given by $\underline{Q}_j^T[J]\underline{Q}_i$ and $\underline{Q}_j^T[K]\underline{Q}_i$ respectively. These are related by eqn (3.4) which when multiplied by $\underline{Q}_j^T[J]$ gives

$$-\lambda_i\underline{Q}_j^T[J]\underline{Q}_i + \underline{Q}_j^T[K]\underline{Q}_i = 0 \tag{3.10}$$

Writing eqn (3.4) for mode 'j' and multiplying by $\underline{Q}_i^T[J]$ leads to

$$-\lambda_j\underline{Q}_i^T[J]\underline{Q}_j + \underline{Q}_i^T[K]\underline{Q}_j = 0 \tag{3.11}$$

Since [J] and [K] are symmetric, the transpose of eqn (3.11) is

$$-\lambda_j \underline{Q}_j^T[J]\underline{Q}_i + \underline{Q}_j^T[K]\underline{Q}_i = 0 \qquad (3.12)$$

Now eqn (3.10) subtracted from eqn (3.12) leads to

$$(\lambda_i - \lambda_j)\underline{Q}_j^T[J]\underline{Q}_i = 0 \qquad (3.13)$$

If $\lambda_i \neq \lambda_j$ then from eqn (3.10) and eqn (3.13)

$$\underline{Q}_j^T[J]\underline{Q}_i = 0 \quad i \neq j \qquad (3.14)$$

$$\underline{Q}_j^T[K]\underline{Q}_i = 0 \quad i \neq j \qquad (3.15)$$

If the damping is assumed to be proportional (i.e. $[D] = \alpha[J]+\beta[K]$), which is a reasonable assumption for turbogenerator shafts [23,32], then

$$\underline{Q}_j^T[D]\underline{Q}_i = 0 \quad i \neq j \qquad (3.16)$$

For the case where i = j :

$$\begin{aligned} \underline{Q}_i^T[J]\underline{Q}_i &= J_{Mi} \\ \underline{Q}_i^T[D]\underline{Q}_i &= D_{Mi} \\ \underline{Q}_i^T[K]\underline{Q}_i &= K_{Mi} \end{aligned} \qquad (3.17)$$

Equations (3.14) to (3.16) are called the orthogonality conditions and together with eqn (3.17) they show that the modal transformation matrix [Q] diagonalizes the physical parameter matrices. Hence eqn (3.8) is decoupled and represents the shaft as shown in Fig 3.1 where each shaft mode has mechanical parameters associated with it. The torque T_{Mi} applied to mode 'i' is a weighted sum of the mechanical and electrical torques applied at each of the physical inertias where the weighting vector is the eigenvector $\underline{Q}_i$ such that

$$T_{Mi} = \underline{Q}_i^T(\underline{T}_m + \underline{T}_e) \qquad (3.18)$$

3.3 Mode Diagrams of the Koeberg Turbogenerator

The mode diagrams describe the undamped oscillations of the mechanical system when oscillating at one of its natural modes. When the mechanical system is resonating at the i'th natural mode then eqn (3.1) has the following solution [34]

$$\underline{\delta}_i = \underline{x}_i \sin(\nu_i t + \theta_i) \tag{3.19}$$

Equation (3.19) infers that in a natural mode of oscillation all masses follow the same response function where ν_i is the natural frequency of the mode, θ_i is the phase angle of the mode and $\underline{x}_i$ is the vector of maximum rotor angular amplitudes or the mode shape of mode i. Substituting eqn (3.19) into eqn (3.2) yields

$$\nu_i^2 \underline{x}_i = [J]^{-1}[K]\underline{x}_i \tag{3.20}$$

for each natural mode of oscillation. This is just a repetition of the eigenvalue statement of eqn (3.4) where the natural frequency of mode i is related to the i'th eigenvalue by $\nu_i = \sqrt{\lambda_i}$ and the mode shape $\underline{x}_i$ of mode i is just the i'th eigenvector $\underline{Q}_i$. The mode diagrams and frequencies of the Koeberg turbogenerator determined by such an eigenvalue analysis of the physical equations are shown in Fig 3.2.

These mode diagrams give the relative displacements of the different shaft locations for the different modes. For example, if the shaft were excited at 17.49 Hz (mode 4) then all the masses, with the exception of the high pressure turbine stage, would experience little movement. On the other hand if mode 1 were excited then the ends of the shaft would twist up in opposite directions. Mode 0, referred to as the inertial mode of oscillation is a dc mode and describes all the masses rotating in unison with no twisting between any masses. The point where a mode shape crosses the zero displacement axis is called a nodal point and at such a point the shaft experiences no movement when excited in that mode. Furthermore, it is impossible to excite a mode if the applied force acts at a nodal point.

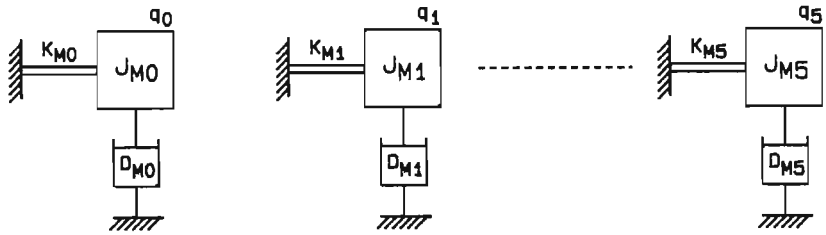

Fig 3.1 Modal model of the turbogenerator mechanical system.

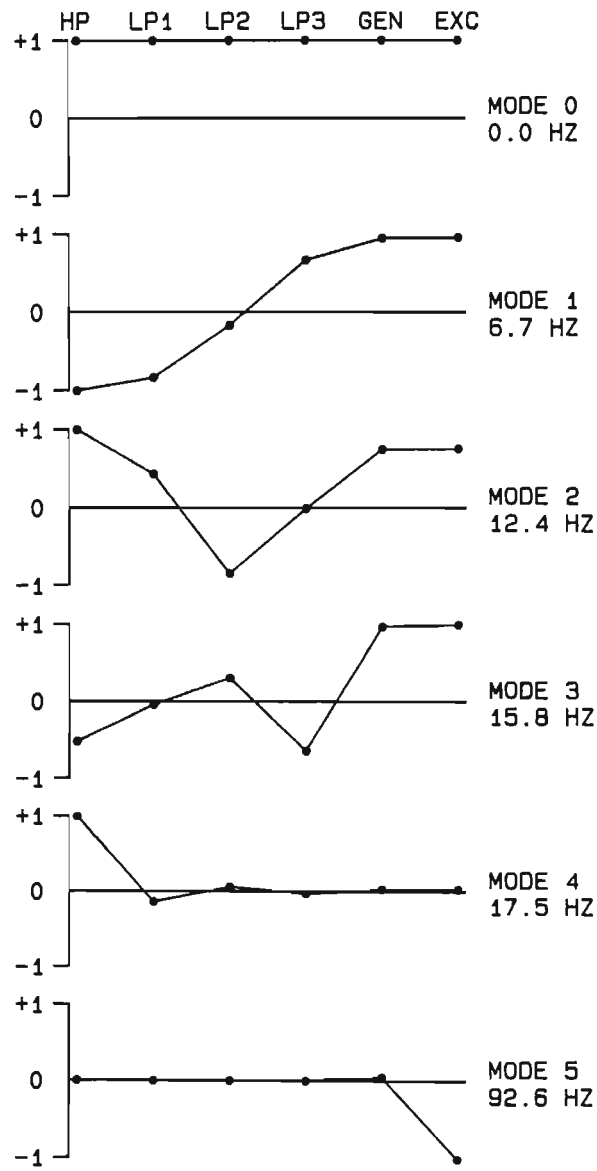

Fig 3.2 Mode diagrams of the Koeberg turbogenerator mechanical system.

From the mode diagrams it is seen that the generator location (where the electrical torque is applied to the shaft) is practically at a nodal point for modes 4 and 5 so it is expected that these modes will be weakly excited by electrical disturbances.

3.4 Uniqueness of the Mode Parameters

The modal transformation matrix [Q] contains as its columns the eigenvectors or mode shapes $\underline{Q}_i$ of each mode and these give the relative mode deflections at each inertia for that mode. Since a mode shape contains only relative deflections for that mode, it may have any scaling irrespective of the scaling of any other mode shape. Thus, the mode parameter matrices in eqn (3.8) are not unique but depend on the scaling of [Q] which can be scaled in numerous different acceptable ways. In this thesis [Q] is scaled so that the maximum deflection in each mode shape is unity.

The equation describing the motion of mode 'i' (following from eqns (3.8) and (3.18)) is

$$J_{Mi}p^2q_i + D_{Mi}pq_i + K_{Mi}q_i + T_{Mi} = 0 \qquad (3.21)$$

and this can be rewritten as eqn (3.22) below in terms of mode variables which have unique values :

$$p^2q_i + 2\xi_i\nu_i pq_i + \nu_i^2 q_i + T_{Mi}/J_{Mi} = 0 \qquad (3.22)$$

In this form each mode is characterized uniquely by its frequency ν_i and mechanical decrement factor [22] (or damping) σ_{mi} [22] given by

$$\nu_i = \sqrt{K_{Mi}/J_{Mi}} \qquad (3.23)$$

$$\sigma_{mi} = \xi_i\nu_i = D_{Mi}/(2J_{Mi}) \qquad (3.24)$$

The scaling of [Q], and hence each J_{Mi}, determines the amplitude of oscillation of each mode inertia, but does not affect the magnitude of modal oscillations expressed in physical rotor variables.

In a study to determine the mode parameters from transient data, a mode parameter identification algorithm would typically supply for each mode, ν_i, σ_i, $\underline{Q}_i$ and indirectly J_{Mi} (see Chapter Five). The mode damping D_{Mi} and mode stiffness K_{Mi} are then calculated from eqns (3.23) and (3.24) as

$$D_{Mi} = 2J_{Mi}\sigma_{mi} \tag{3.25}$$

$$K_{Mi} = \nu_i^2 J_{Mi} \tag{3.26}$$

The rest of this chapter investigates the use of the modal model in transient and small-signal stability studies. The system considered is the same single-machine-infinite-bus system (Fig 2.1) used in Chapter Two and the generator is represented by the accurate model of Sect 2.2.1. The modal model of the mechanical system is combined with this generator electrical model to obtain a 20th order model for the system. The non-linear and linear differential equations describing the turbogenerator system in physical form appear in Appendix C while those describing the system in modal form appear in Appendix D. The transmission system parameters and the generator electrical parameters are the same as those used in Chapter Two and appear in Appendix I. The mode parameters used in this chapter are derived from the physical shaft parameters and are given in Appendix I; in a practical case the mode parameters would be measured.

3.5 Eigenvalue Analysis with the Modal Model

The linearized system equations in modal form are used to calculate the system eigenvalues as a function of the percentage capacitor compensation expressed for the single-generator-infinite-bus system in Fig 2.1 as:

$$\% \text{ compensation} = N = 100.X_c/(X_1 + X_2 + X_d'') \tag{3.27}$$

For each calculation the initial conditions are V_b = 1.0 p.u., P_b = 0.8 p.u. and Q_b = 0.2 p.u. Fig 3.3(a) shows the eigenvalue loci in the direction of the arrows as N is varied from 5% to 90% representing a range of X_c from 0.07 p.u. to 1.31 p.u. Table 3.1 shows the numerical value of these eigenvalues at a particular compensation level of 25%. These eigenvalues have been presented elsewhere [15] and are repeated here since they are the focal point of much of the work to follow in this thesis.

Table 3.1 System eigenvalues calculated with the modal model for a compensation level of 25%.

Mode		Real	Imaginary
E1	Supersynchronous flux	-9.88	±470.8
E2	Subsynchronous flux	-9.10	±156.7
M5	Supersynchronous mechanical	-0.79	±581.8
M4	Subsynchronous mechanical	-1.16	±109.9
M3		-0.69	±100.4
M2		-0.81	±78.2
M1		-0.82	±42.8
M0	Inertial mode	-1.04	±5.4
M	Magnetic stability	-0.18	0.0
R1	Rotor circuits	-1.02	0.0
R2		-10.5	0.0
R3		-17.4	0.0

Although individual eigenvalues cannot be related to any particular part of the system, it is true that certain eigenvalues are influenced more by some system parameters than others so they can be separated into groups as shown in Table 3.1. E1 and E2 are related to the transmission system and are the super-synchronous and subsynchronous electrical modes respectively; M1 to M5 are related to the shaft torsional modes; M0 is the inertial mode or hunting mode usually analysed in a conventional stiff-shaft stability study; M is the magnetic stability mode and R1 to R3 are modes associated with the generator rotor circuits.

The loci in Fig 3.3(a) show that as the compensation is increased E1 increases in frequency while E2 decreases in frequency and that at certain values of X_c where the frequency of E2 is close to the subsynchronous mechanical modes, the torsional interaction effect causes some of these modes to go unstable. Modes M4 and M5 are seen to be practically unaffected by the electrical modes E1 and E2. This confirms the predictions from the mode shape diagrams in Sect 3.3 that these modes would be difficult to excite from the electrical network due to their mode transfer factors at the generator rotor, Q_{54} and Q_{55}, being small (0.03 and 0.05 respectively; see Appendix I).

The important part of Fig 3.3(a) is that part enclosed in the rectangle and expanded in Fig 3.3(b) showing the mechanical loci as they go unstable. As the compensation level is increased M3 moves towards the RHP and becomes unstable at N = 37.7%. A further increase in compensation causes M3 to move into the RHP and eventually back into the LHP where it becomes stable at N = 53.0%. Similarly, M2 and M1 become unstable between the limits indicated on the graph and at N = 89.2% the induction generator effect occurs with E2 going unstable. The CCL for each mode is that value of compensation at which the mode first goes unstable and for modes M1 to M3 this is 65.5%, 50.9% and 37.7% respectively. The overall CCL for the system is determined by the CCL for the mode which first goes unstable, M3 in this case. According to Ref [15] the South African system requires a N = 31% which lies on the stable side of the M3 locus, but the margin of safety depends on the uncertainty associated with the values assumed for mechanical parameters in Appendix I.

The stability limits of the mechanical modes can be more clearly seen in Fig 3.4 where the real parts (or inherently the negative of the damping) of M1 to M3 in Fig 3.3(b) have been plotted as a function of the series capacitance X_c. The stability limits given in Fig 3.3(b) are shown here as points A to F where the curves cross the zero real axis. The system is stable only where all three curves are negative, that is for a compensation below A, from D to E and above F (but below the value at which the induction generator effect takes place). The area below A is considered

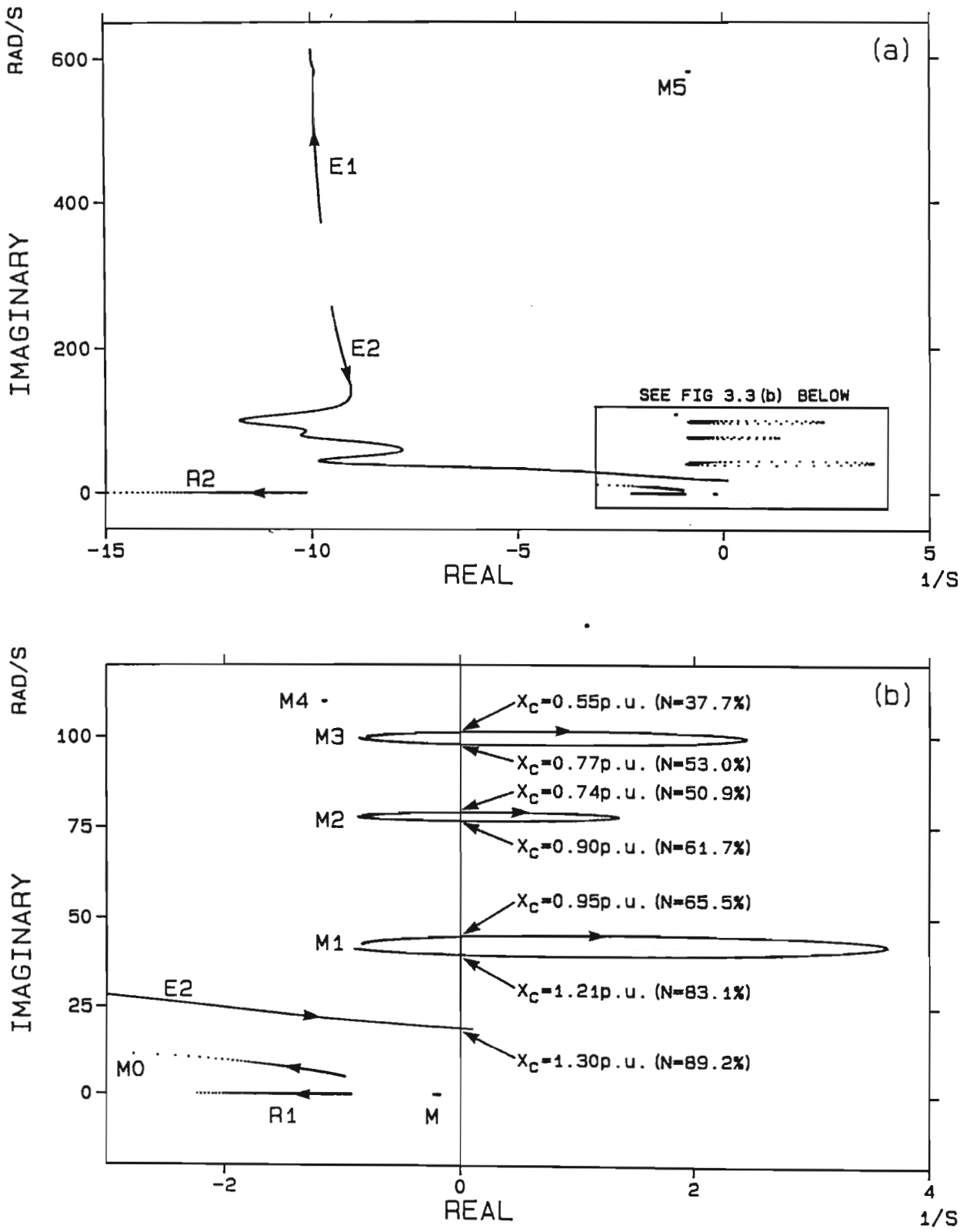

Fig 3.3 Eigenvalue loci calculated with the modal model as the compensation level N is varied from 5% (X_c = 0.07 p.u.) to 90% (X_c = 1.31 p.u.).

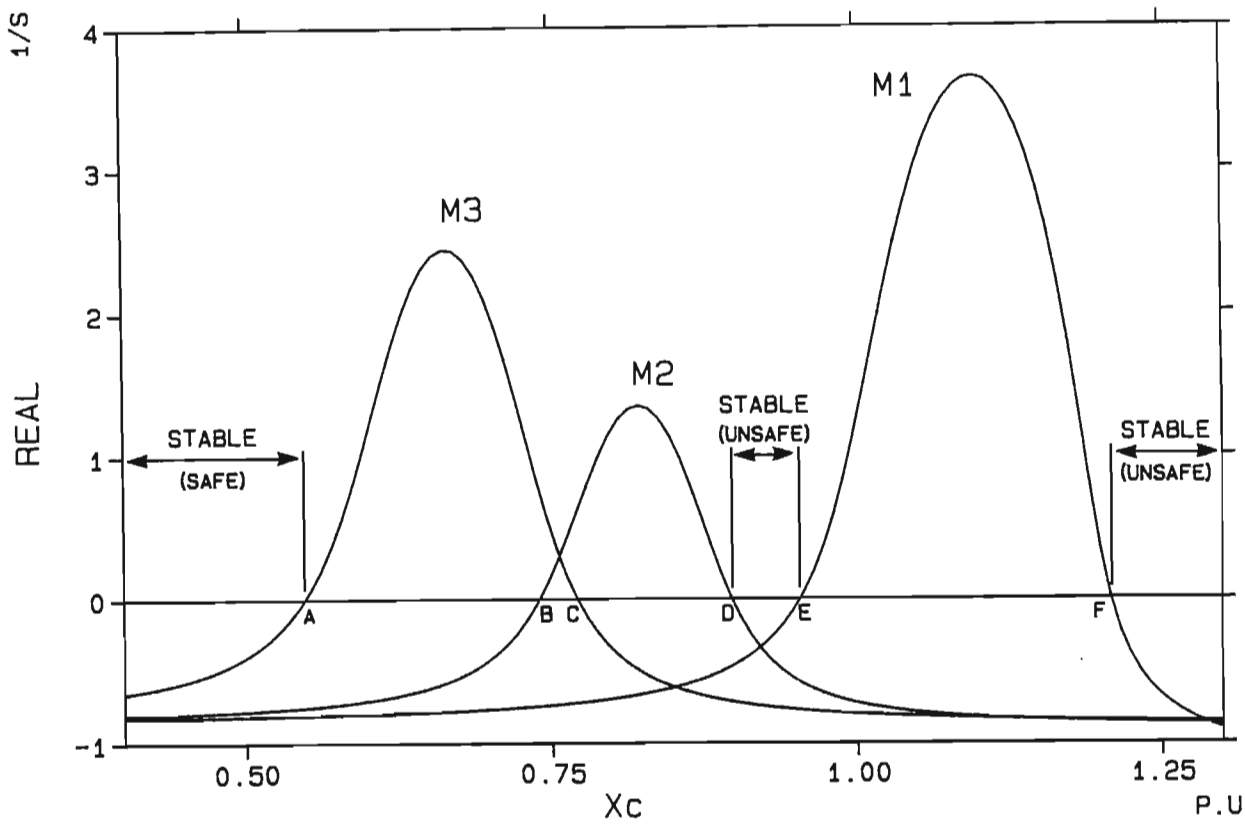

Fig 3.4 Real part of mechanical mode eigenvalues M1 to M3 as a function of the series capacitance X_c showing regions of stability.

to be a safe stable area and is the region of compensation in which the system should be operated without any SSR countermeasure; the regions from D to E and above F are unsafe stable areas since a reduction in the compensation level from a position inside one of these areas could cause the onset of SSR.

3.6 Sensitivity of the CCL to Mode Parameter Errors

The results shown in Figs 3.3 and 3.4 have been calculated with the modal model and are identical to those calculated with the physical model since the mode parameters are derived from the physical parameters. However,

one of the advantages of the modal model is that in a practical case the mode parameters would be measured and the torsional characteristics of the shaft would be modelled more accurately than in the case of a physical representation; this would result in a more accurate calculation of the CCL. Nevertheless, it must be accepted that while the modal model with measured parameters will be more accurate than the physical model, in any measuring process errors will occur although they will be smaller than the error incurred by using the physical model and estimating the damping. The following sections therefore investigate to what extent uncertainties in the mode parameters affect the CCL calculations. In each case the mode parameter values in Appendix I are assumed to be the true shaft parameters and are referred to as the NOMINAL VALUES and the CCL calculation (from diagrams such as Fig 3.4) is repeated for different values of the particular mode parameter around its nominal value. In order to compare the results for different modes the mode parameters are normalized around their nominal values and the CCL for each mode is normalized around the value calculated with the nominal mode parameters.

3.6.1 Mode transfer factor errors

The eigenvalue loci of Fig 3.3 showed that modes M4 and M5 did not interact with the electrical system due to the low value of modal response (or mode transfer factor) at the generator rotor for these modes. This leads one to expect the CCL to be affected by the value of the mode transfer factor at the generator rotor. Figure 3.5 shows how the CCLs for M1 (mode 1), M2 (mode 2) and M3 (mode 3) vary as the mode transfer factors Q_{51}, Q_{52} and Q_{53} are varied from 0.5 to 1.5 times their nominal values (of 0.95, 0.75 and 0.97 respectively). The normalized values of CCL = 1.0 for M1 to M3 correspond to a compensation level N of 37.7%, 50.9% and 65.5% respectively (see Fig 3.3).

The results show that for all three modes the CCL decreases as the mode transfer factor increases. This is because a higher value of mode transfer factor at the generator rotor means that the mode is more strongly coupled to the electrical system and a greater portion of mechanical

oscillations at the mode frequency are reflected into the electrical system. For a reduction of Q_{52} below about 58% of its nominal value (Q_{52}=0.43) M2 does not go unstable and the CCL for this mode does not exist as seen by the incomplete curve for M2.

The M3 curve is the important one since it determines the overall CCL for the system as explained in Sect 3.5 (Fig 3.4). Measurement of the mode transfer factor to within about 10% should be possible and an error of this magnitude in Q_{53} will result in an error of 2.7% in the CCL.

3.6.2 Mode inertia errors

The mode transfer factors at the generator rotor affect the CCLs since they determine to what extent the electrical torque excites the mechanical modes. This is also influenced by the values of the mode inertias as can be seen from eqn (3.22), hence errors in mode inertia will also affect the accuracy of the CCL.

Fig 3.6 shows how the CCLs for M1, M2 and M3 vary as the mode inertias J_{M1}, J_{M2} and J_{M3} are varied from 0.2 to 2.0 times their nominal values (of 0.0172 p.u., 0.0128 p.u. and 0.0097 p.u. respectively) while the mode frequencies and mode decrements are kept constant. The variation in CCL is seen to be more non-linear than was the case for the mode transfer factor with the greatest sensitivity being for lower values of mode inertia. The CCLs increase as the mode inertias increase due to the greater attenuation of the exciting torque as seen from eqn (3.22). Once again the M3 CCL is seen to be more sensitive to mode parameter variations than the M1 and M2 curves. Using a value of J_{M3} that is 10% less than the true value of mode 3 inertia results in an error of 1.7% in the CCL.

3.6.3 Mode decrement factor errors

Another factor which affects the CCLs is the real value of the eigenvalues M1 to M3 before any interaction with the subsynchronous electrical mode occurs. This value depends inter alia on the mechanical decrement factor

(or mode damping), hence errors in this parameter also influence the accuracy of the CCL.

Fig 3.7 shows the variation in the normalized values of CCL as the mode decrement factors σ_{m1} to σ_{m3} are varied from 0.2 to 2.0 times their nominal value (of 0.79 s^{-1}). The variation in the CCLs is seen to be very similar to that obtained in Sect 3.6.2 for the mode inertias with M3 again being the most sensitive one. As the decrement factors increase, the eigenvalues start further away from the imaginary axis and the CCL increases. For lower values of decrement factor the CCL is more sensitive to errors in the damping. A 10% error in the value of the mode 3 decrement factor results in an error of 1.2% in the CCL; this is the smallest error in the CCL for a 10% error in any of the mode 3 parameter considered so far.

The difference in the sensitivity of the mode 3 CCL to the different mode parameters is summarized in Fig 3.8 where the mode 3 curves from Figs 3.5 to 3.7 are plotted on the same axes over the same range of 0.5 to 1.5 times the nominal value of each particular mode parameter. This clearly indicates that the mode transfer factor has the greatest effect on the CCL and the mode decrement factor has the least effect. However, these results must be viewed in conjunction with the expected errors in the determination of the parameters; the mode transfer factor being the easiest to determine accurately and the decrement factor the most difficult one. In fact, whereas the mode transfer factor can be measured to within about 10% the decrement factor can be out by as much as 50% (still less than the error that can occur with estimated values of damping in the physical model) and in this light the decrement factor is the most important factor in determining the error in the CCL. Moreover, the nominal value of the mode 3 decrement factor in this analysis is 0.79 s^{-1} and measured values [28,36,37] on some machines are even smaller (0.1 s^{-1}); at these lower values the CCL is even more sensitive to damping errors.

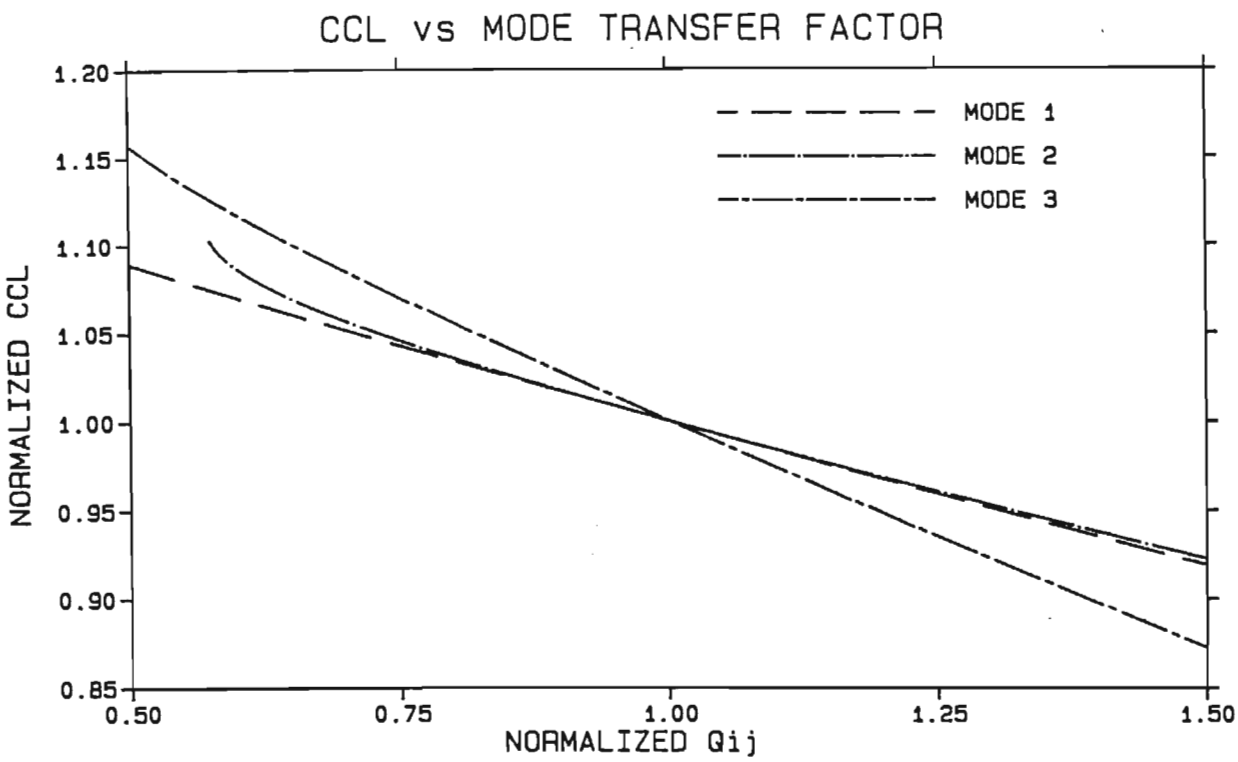

Fig 3.5 Sensitivity of the M1 (mode 1), M2 (mode 2) and M3 (mode 3) CCLs to the mode transfer factors Q_{51}, Q_{52} and Q_{53} respectively.

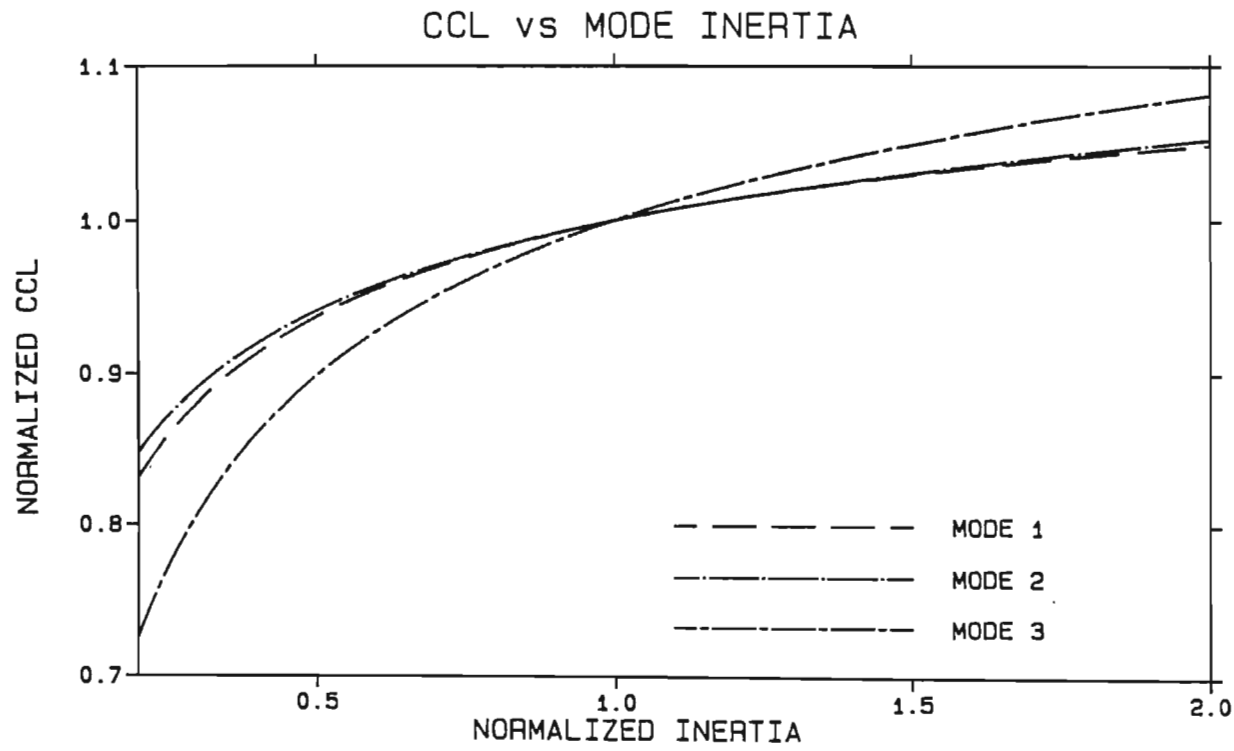

Fig 3.6 Sensitivity of the M1 (mode 1), M2 (mode 2) and M3 (mode 3) CCLs to the mode inertias J_{M1}, J_{M2} and J_{M3} respectively.

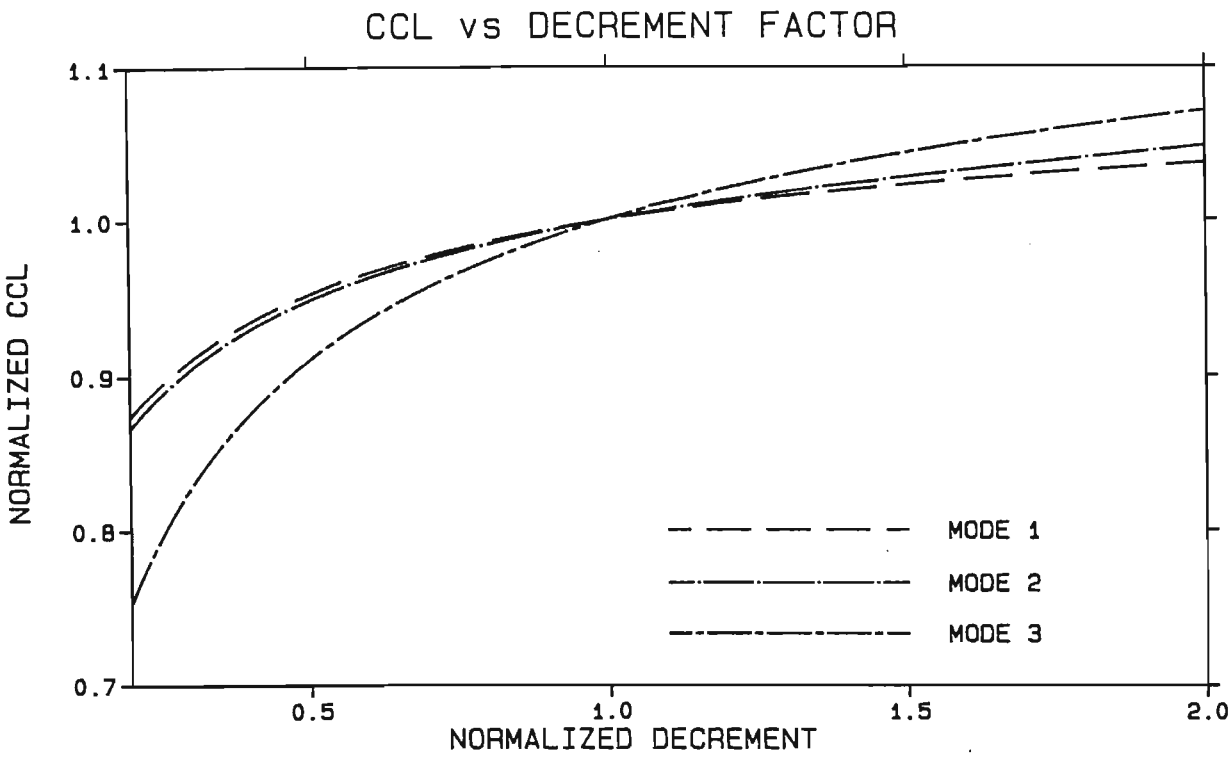

Fig 3.7 Sensitivity of the M1 (mode 1), M2 (mode 2) and M3 (mode 3) CCLs to the mode decrement factors σ_{m1}, σ_{m2} and σ_{m3} respectively.

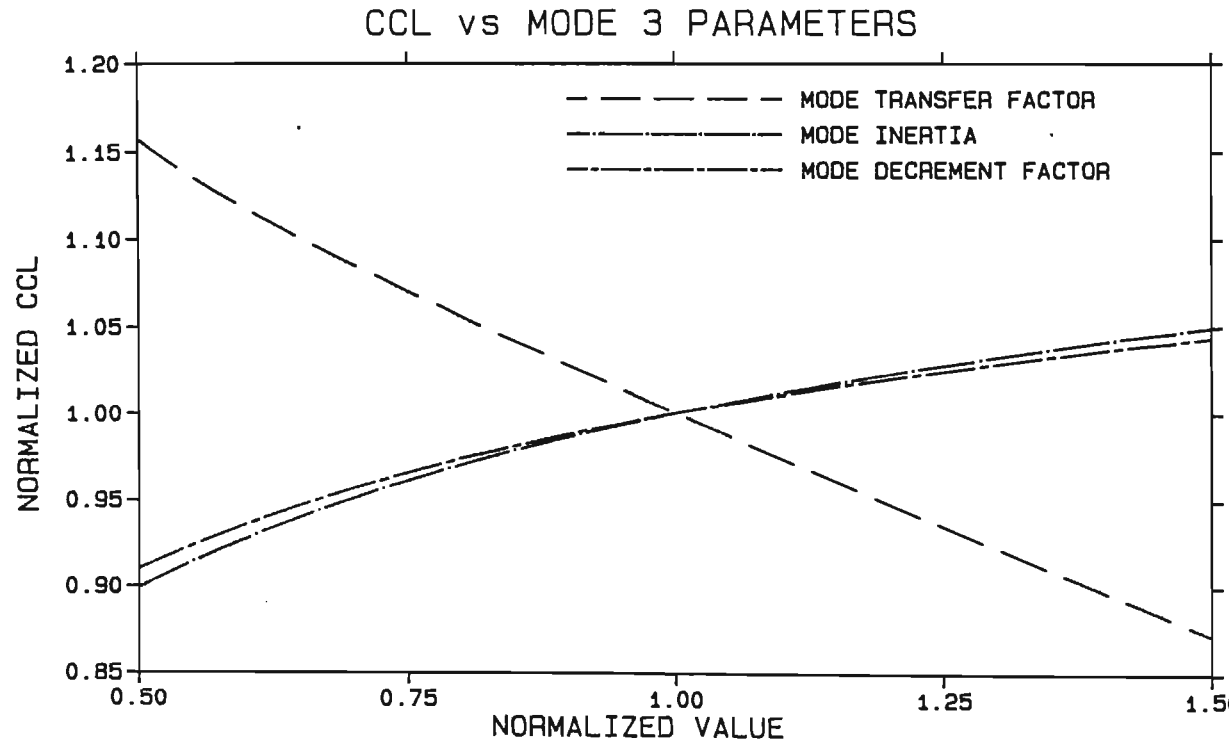

Fig 3.8 Comparison of the sensitivities of the M3 CCL to the mode 3 parameters.

3.7 Transient Response Calculated with the Modal Model

The disturbance considered in this section is a temporary 100 ms three phase short circuit on the high voltage side of the transformer in Fig 2.1 and the initial conditions prior to the fault are V_b = 1.0 p.u. , P_b = 0.8 p.u. and Q_b = 0.2 p.u. The system is assumed to be uncompensated (X_c = 0.0 p.u.).

Fig 3.9 shows the generator rotor angle and the electrical torque as well as the Fast Fourier Transform (FFT) of these variables calculated for this disturbance. The rotor angle for this disturbance was also calculated using the physical model of the mechanical system and the result can be seen as the dotted curve plotted on the same axes as the curve in Fig 3.9. As expected the two results are identical and this confirms that the modal model can be used instead of the physical model to generate the same results.

The rotor angle in Fig 3.9 calculated with the modal model is not found by directly integrating a differential equation, but is constructed as a weighted sum of the six modes of oscillation of the shaft which are shown in Fig 3.10(a) as follows :

$$\delta_k = \sum_{i=0}^{5} Q_{ki} q_i = \underline{Q}'_k \underline{q} \qquad (3.28)$$

where $\underline{Q}'_k$ is row 'k' of the transformation matrix [Q] and is a row vector containing the mode deflections at physical location 'k'. The FFTs of rotor angle and electrical torque show frequencies at 6.8, 12.4, 15.9 and 92.6 Hz corresponding to modes 1, 2, 3 and 5 respectively. The small amplitude at the mode 5 frequency and the non-appearance of the mode 4 frequency again confirm the prediction from the mode shape diagrams in Sect 3.3 and the eigenvalue calculations in Sect 3.5 that these two modes would be difficult to excite from the electrical network.

Fig 3.10(a) shows that the oscillation of each mode inertia is not a pure sinusoid at the particular mode frequency but that there is a contribution from other frequencies; this is particularly evident in the first few

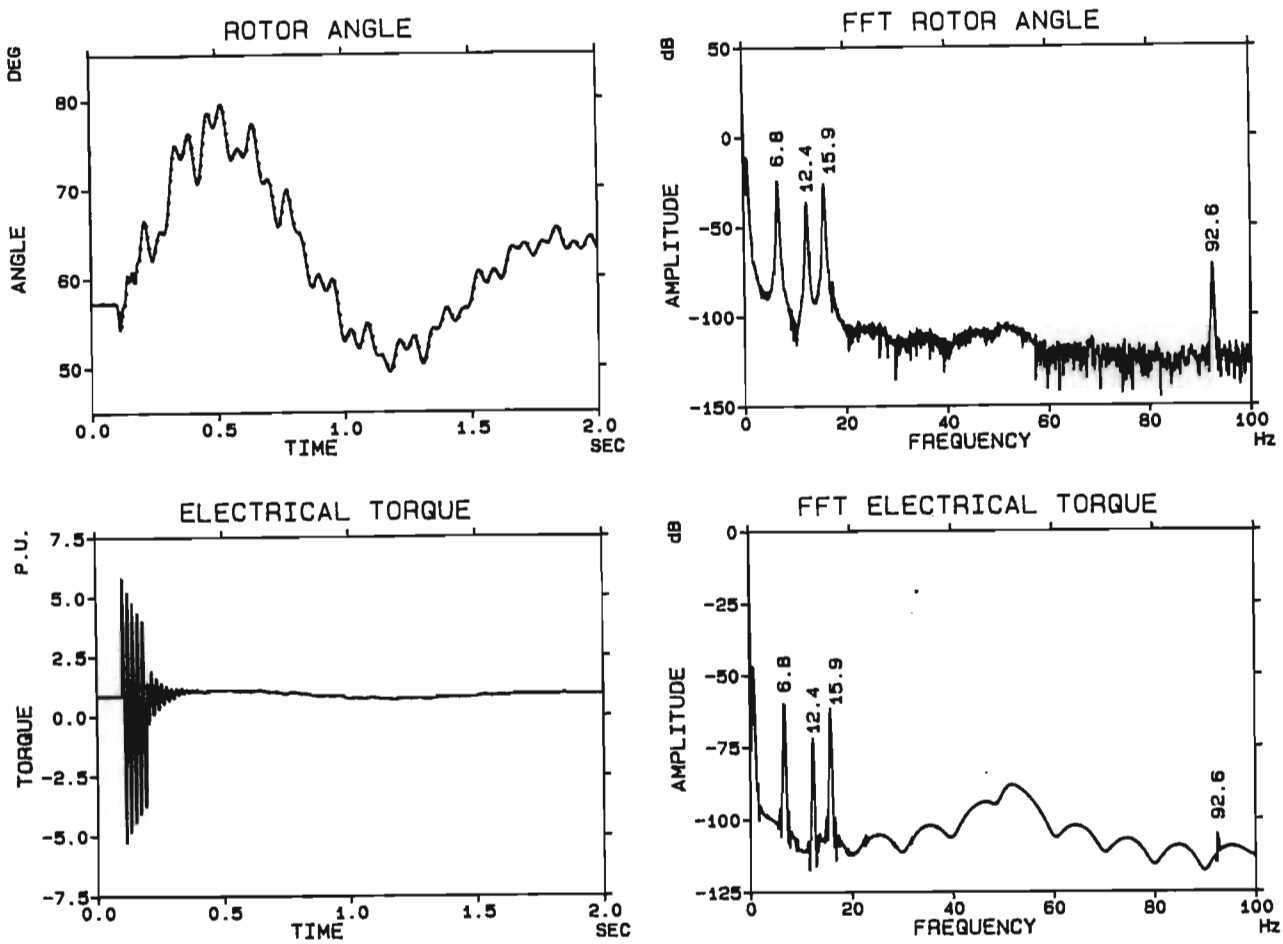

Fig 3.9 Transient response of the turbogenerator calculated with the modal model following a 100 ms three phase short circuit on the high voltage side of the generator transformer.

cycles. The FFT's of these mode angles are given in Fig 3.10(b) and they show clearly that although the oscillation of each mode inertia is dominated by its mode frequency, its oscillation nevertheless contains frequency components corresponding to the other modes. These frequencies appear due to the fact that the electrical torque in Fig 3.9, which forms part of the excitation torque for each mode inertia, contains oscillations at each of the mode frequencies as seen from its FFT. These results show that while the modal mechanical equations have been completely decoupled, the mechanical modes nevertheless become (weakly) coupled through the electrical system when the generator is synchronized and they may have an effect on each other. This weak coupling is investigated in more detail in Chapter Four.

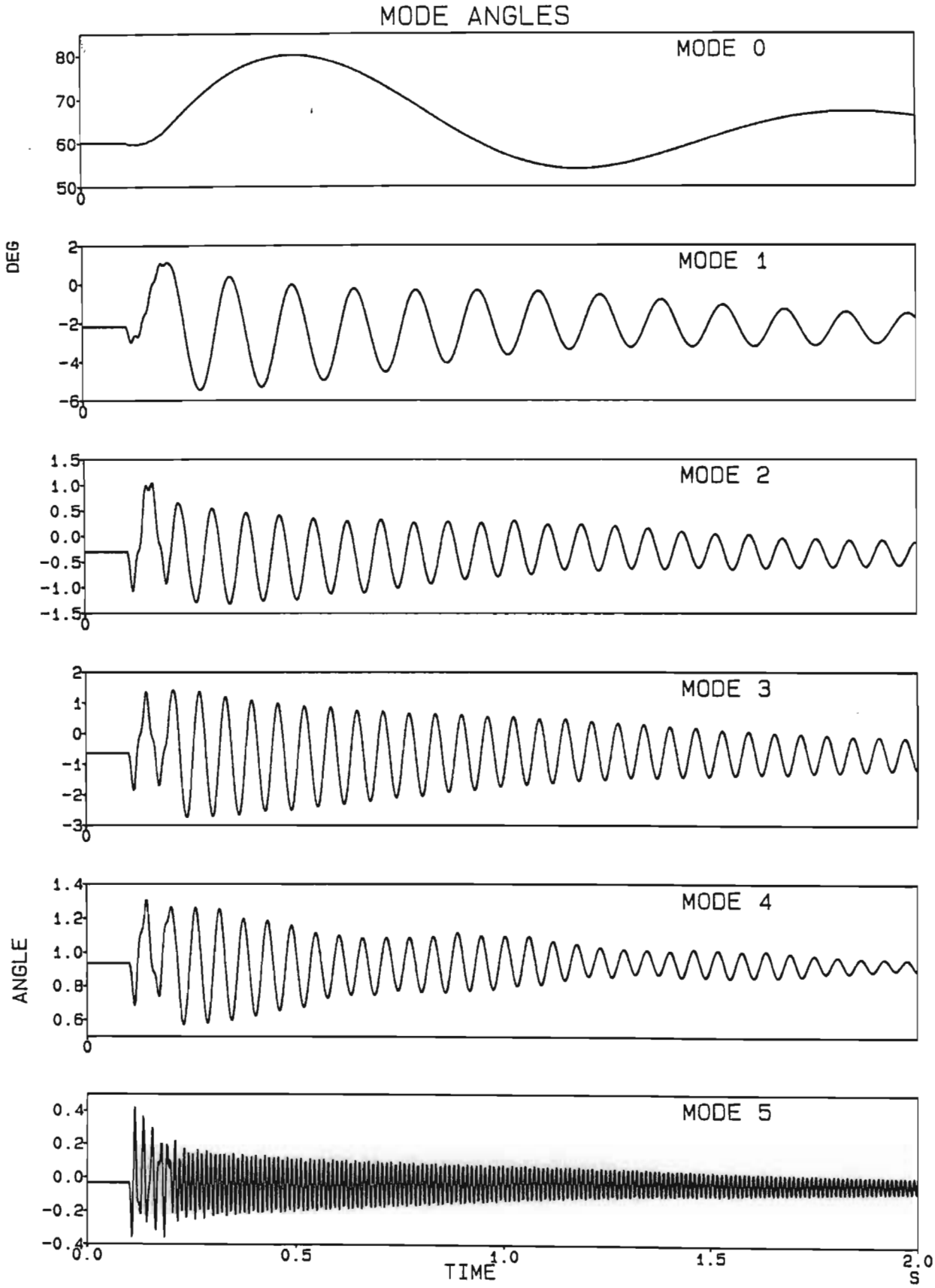

Fig 3.10 (a) Mode angles q_i (angular displacement of the mode inertias) following a 100 ms three phase short circuit on the high voltage side of the generator transformer.

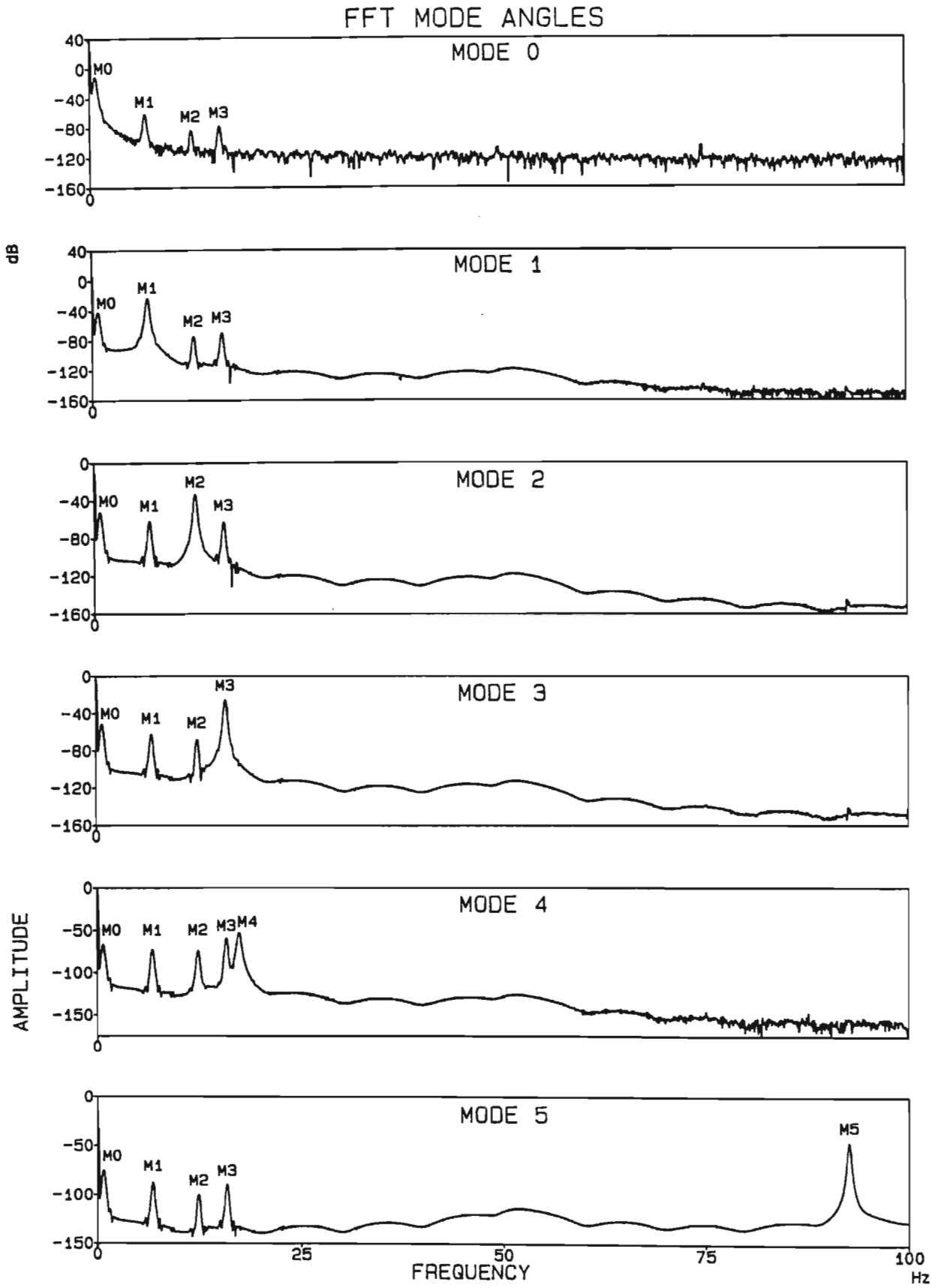

Fig 3.10 (b) FFTs of the mode angles in Fig 3.10(a).

3.8 Shaft Torque Amplification

The shaft torques of the various sections of the shaft are calculated by first determining the angular deflections of the various shaft locations using the modal model and then determining the torques from a knowledge of the shaft stiffnesses. The fault considered in this section is a three phase short circuit at the infinite bus and not at the generator transformer as in Sect 3.7 since for an infinite bus fault the percentage compensation during the fault is the same as before and after the fault; in the case of a fault at the generator transformer there is no capacitance in the generator stator circuit during the fault. Changing the transmission line natural frequency during the fault will merely add an additional variable to the analysis and detract from the real issue being investigated.

The shaft torques for a 100 ms fault on an uncompensated system are shown in Fig 3.11 and the mechanical mode eigenvalues for this case appear in Table 3.2. The shaft torques contain multi-modal responses with some modes contributing more than others along different shaft sections (i.e. mode 3 in the LP3-GEN section). The relative contribution by a mode to different shaft sections can be deduced from the mode shape diagram, however a comparison between the different mode contributions at a certain section also depends on the degree to which the mode is excited (discussed in Chapter Four); this in turn depends amongst other things on the fault duration. The effect of fault duration is shown in Fig 3.12 where the maximum shaft torques (given as half the maximum peak-to-peak value) are plotted as the fault duration is varied from 0.002 s to 0.250 s. Sections LP1-LP2, LP2-LP3 and LP3-GEN show an increase in peak torques of as much as 65% between the best and worst clearing times within the given time range. The GEN-EXC section clearly shows the cyclic variation in peak torque amplitude at the period of mode 5 (10.8 ms) which is its main contributor. This cyclic variation is also evident but less obvious in the LP3-GEN section for mode 3. The final graph shape will depend on the interference pattern of the various mode contributions.

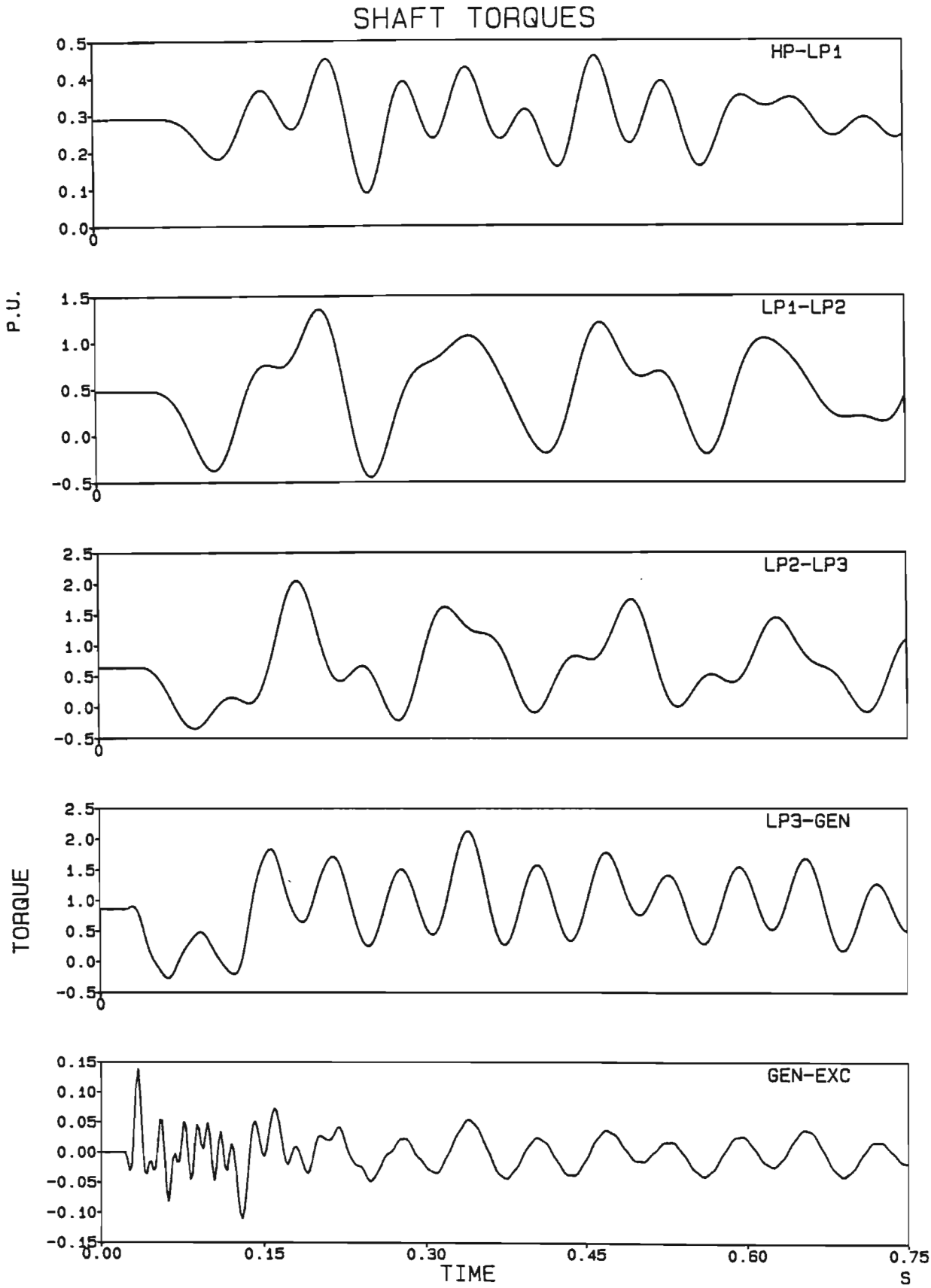

Fig 3.11 Shaft torques calculated with the modal model following a 100 ms three phase short circuit at the infinite bus with no series compensation.

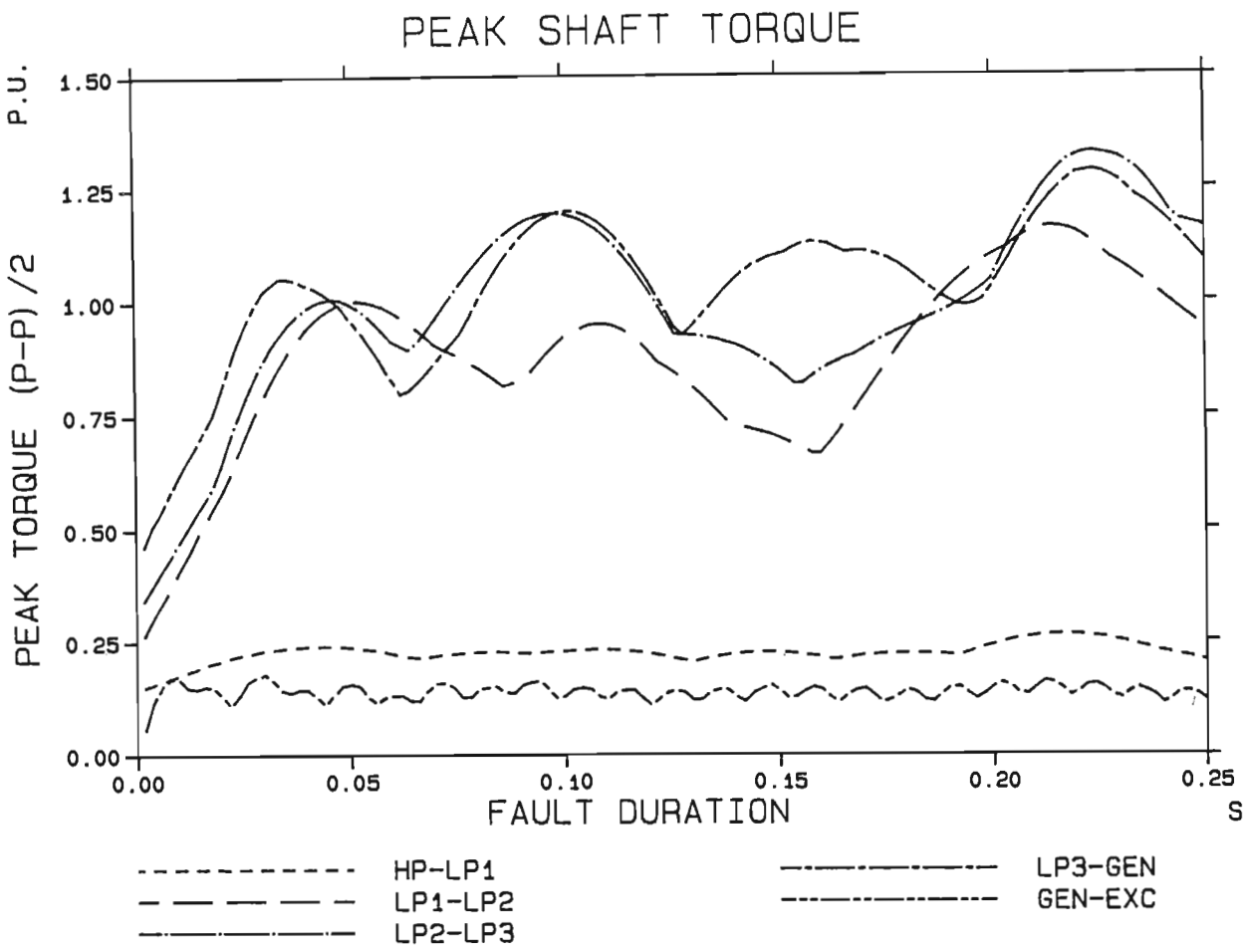

Fig 3.12 Effect of fault duration on the peak shaft torques in an uncompensated system following a temporary three phase short circuit at the infinite bus.

Table 3.2 Mechanical mode eigenvalues for an uncompensated system

Mode	Real	Imaginary
M0	-0.975	±4.90
M1	-0.836	±42.58
M2	-0.835	±78.01
M3	-0.797	±99.99
M4	-1.162	±109.90
M5	-0.789	±581.77

In order to investigate the shaft torque amplification effect the shaft torques of Fig 3.11 are recalculated with a series capacitor of 0.667 p.u. in the line. This value is chosen from Fig 3.4 to give the worst tuning for mode 3 (frequency of E2 equal to M3) and in order to separate the torque amplification and torsional interaction phenomena, the mode dampings σ_{mi} are adjusted with an eigenvalue scanning program so that the real parts of the mechanical mode eigenvalues (M0 to M5) are the same as for the uncompensated system (Table 3.2). The resulting shaft torques in Fig 3.13 are clearly larger than those of Fig 3.11 due to the torque amplification effect with the LP3-GEN section being the worst affected due to its large mode shape deflection for mode 3. The mode 3 oscillations are now clearly evident in all the sections although the constructive and destructive interference is still apparent in the LP1-LP2 and LP2-LP3 sections.

The effect of fault duration on the peak torques in the compensated system is shown in Fig 3.14. In this case the fault duration is seen to have an even larger effect on the peak torques than in the uncompensated system (Fig 3.12) with a 300% increase in the LP3-GEN peak torque between best and worst case clearing times. The characteristic cyclic variation in the peak torque at the mode 3 frequency is clearly evident in the LP3-GEN torque and the effect of destructive interference with the mode 3 torques is seen in the LP1-LP2 and LP2-LP3 curves at around 170 ms. The effect of torque amplification on each shaft section is shown in Fig 3.15 which compares the uncompensated and compensated system peak torques for all five shaft sections. Clearly, torque amplification results in large shaft torques which can cause considerable shaft damage. Prediction of these torques relies on the mechanical model and will be affected by any errors in the mechanical model parameters.

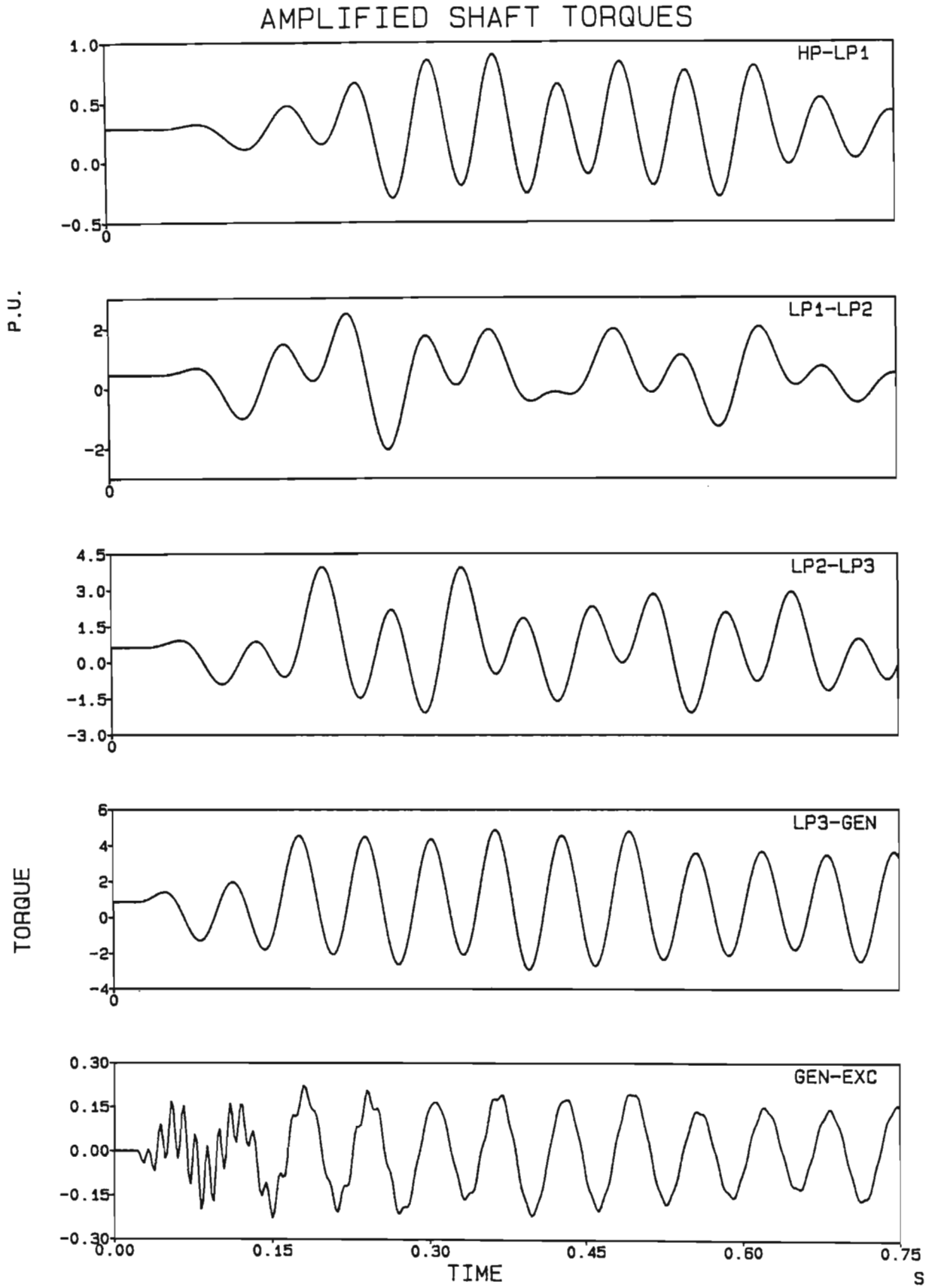

Fig 3.13 Shaft torques calculated with the modal model following a 100 ms three phase short circuit at the infinite bus when there is a series capacitor of 0.667 p.u. in the transmission line.

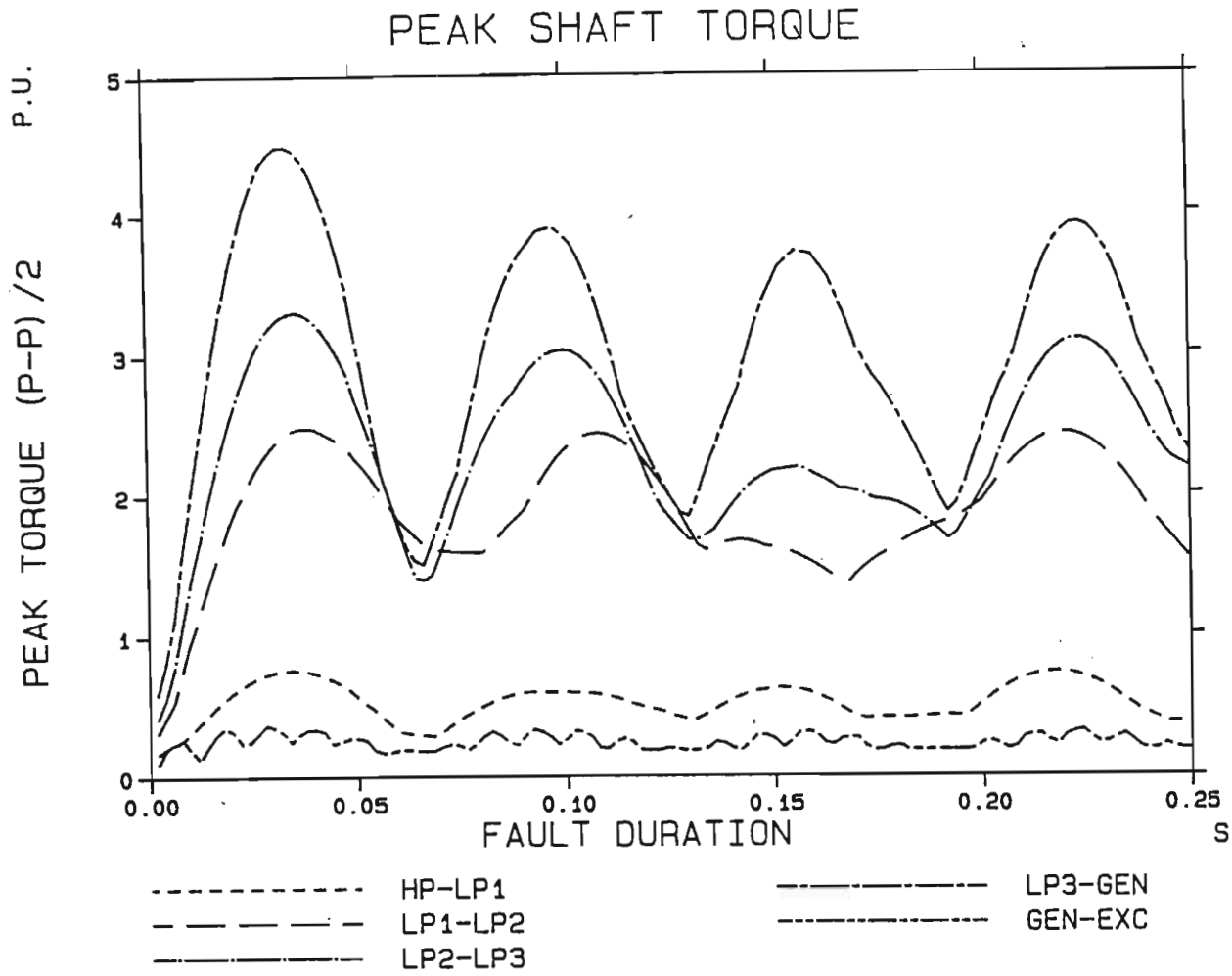

Fig 3.14 Effect of fault duration on the peak shaft torques following a temporary three phase short circuit at the infinite bus when there is a series capacitor of 0.667 p.u. in the transmission line.

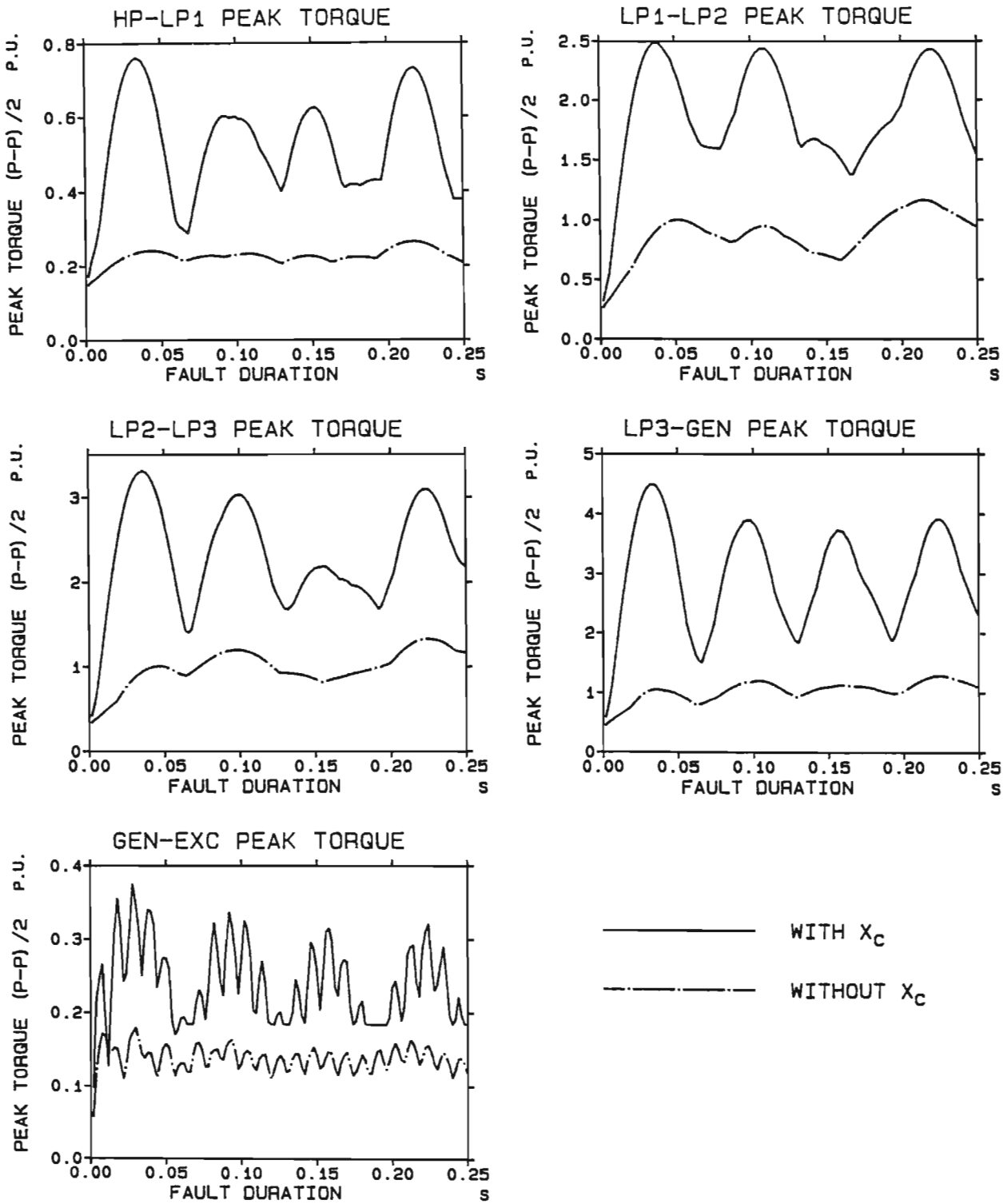

Fig 3.15 Comparison of peak shaft torques as a function of fault duration with and without series capacitance showing the torque amplification effect.

3.9 Sensitivity of Torque Amplification to Mode Parameter Errors

3.9.1 Mode decrement factor errors

This section investigates the effect of mechanical decrement factor on the torque amplification phenomenon. It is generally accepted that the magnitude of peak shaft torques following a disturbance is greatly affected by the material hysteretic damping which is highly amplitude dependent and limits the size of peak torques [27]. Mechanical viscous damping due to steam, windage etc represented by the mechanical decrement factors in the modal model is considered to be unimportant for peak torque calculations [29,31,38]. Reference [29] states "..., the peak mechanical response torques following brief electrical transients are practically independent of the damping level,..." and Ref [31] states, "The magnitude of the maximum torque is therefore only slightly dependent on the mechanical damping". Reference [38] talking about mechanical damping says "Fortunately, these parameters have very little influence on the peak torque values during transient disturbances". Mechanical viscous damping is considered important only in determining how long damaging levels of shaft torque persist.

Figure 3.16 shows normalized peak torques as a function of normalized mode 3 damping (decrement factor) for the compensated system where the normalized damping of 1.0 yields the same real value of the M3 eigenvalue in Table 3.2. The normalized peak torques of unity correspond to those per-unit values in Fig 3.14 for a fault duration of 0.098 s.

The peak torques increase with a decrease in damping and this variation can be quite large with a 24% increase in the LP3-GEN peak torque for a 20% decrease in the damping. (At this reduced value of mode 3 damping the real part of eigenvalue M3 is at $-0.09\ s^{-1}$ compared to the $-0.8\ s^{-1}$ with a normalized damping of 1.0). This variation in peak torque with damping does not appear to agree with the previously stated views of Refs [29,31,38] and is due to the multi-modal nature of the shaft torque response. Fig 3.17 shows the transient torque calculated for the three centre shaft sections based on using the two extreme values of damping from Fig 3.16. The shaft torques vary little with damping over the initial few cycles and the initial peak torques are practically the same for both

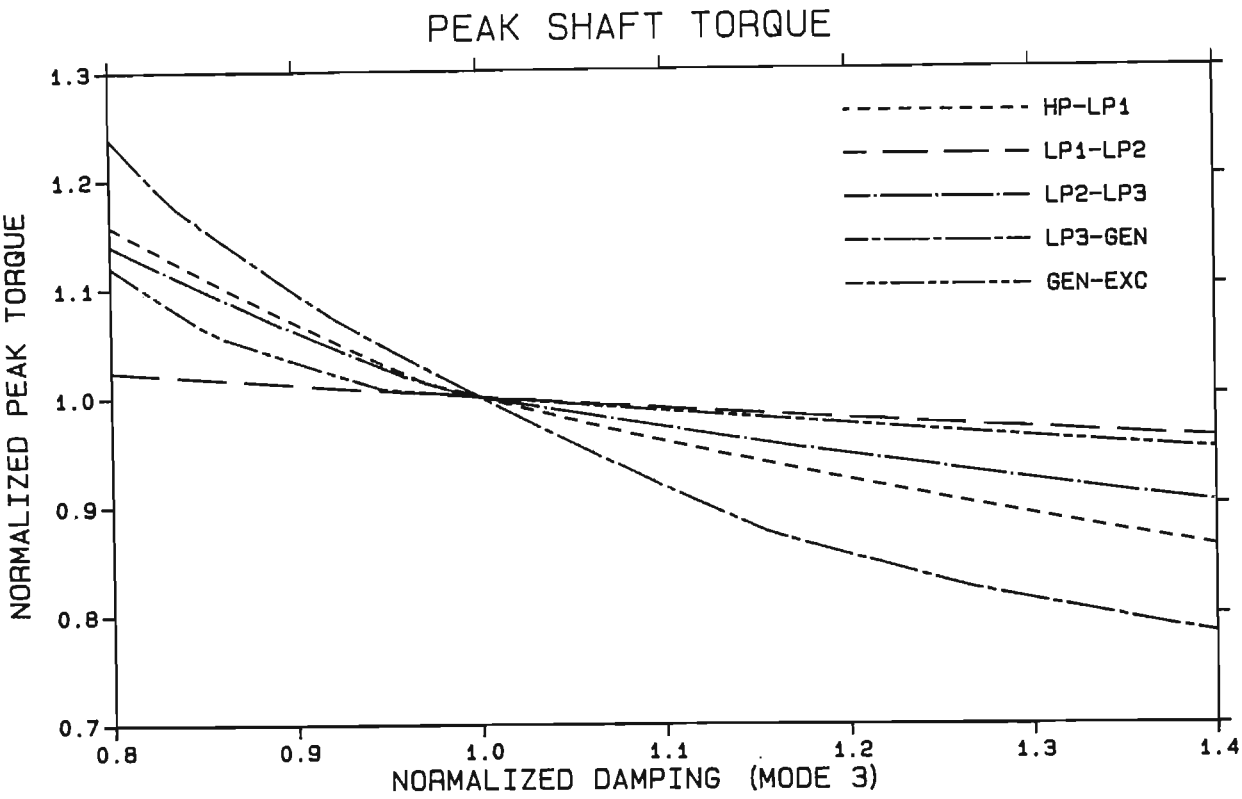

Fig 3.16 Sensitivity of the peak shaft torques following a 98 ms three phase short circuit at the infinite bus to the mode 3 damping (decrement factor); a series capacitor of 0.667 p.u. is present.

damping values. If the shaft response were a single frequency then the maximum torques would occur initially (at fault initiation or fault removal) and later peaks would be smaller (for a stable system). However, for a multi-modal response the envelopes of positive and negative torque peaks are not smooth but vary depending on the degree of constructive or destructive interference between the various modes at a particular instance of time. Hence, for the case of lower damping the maximum negative peak torque occurs at the 8th negative peak for the LP2-LP3 section and at the 11th negative peak for the LP3-GEN section. For the higher damping these peaks are so reduced that they no longer constitute the extreme values. These results show that the mechanical viscous damping as represented in the modal model not only affects shaft fatigue life reduction by determining how long shaft torques persist at a damaging level, but may also affect the magnitude of the maximum peak torque experienced by the shaft following a disturbance.

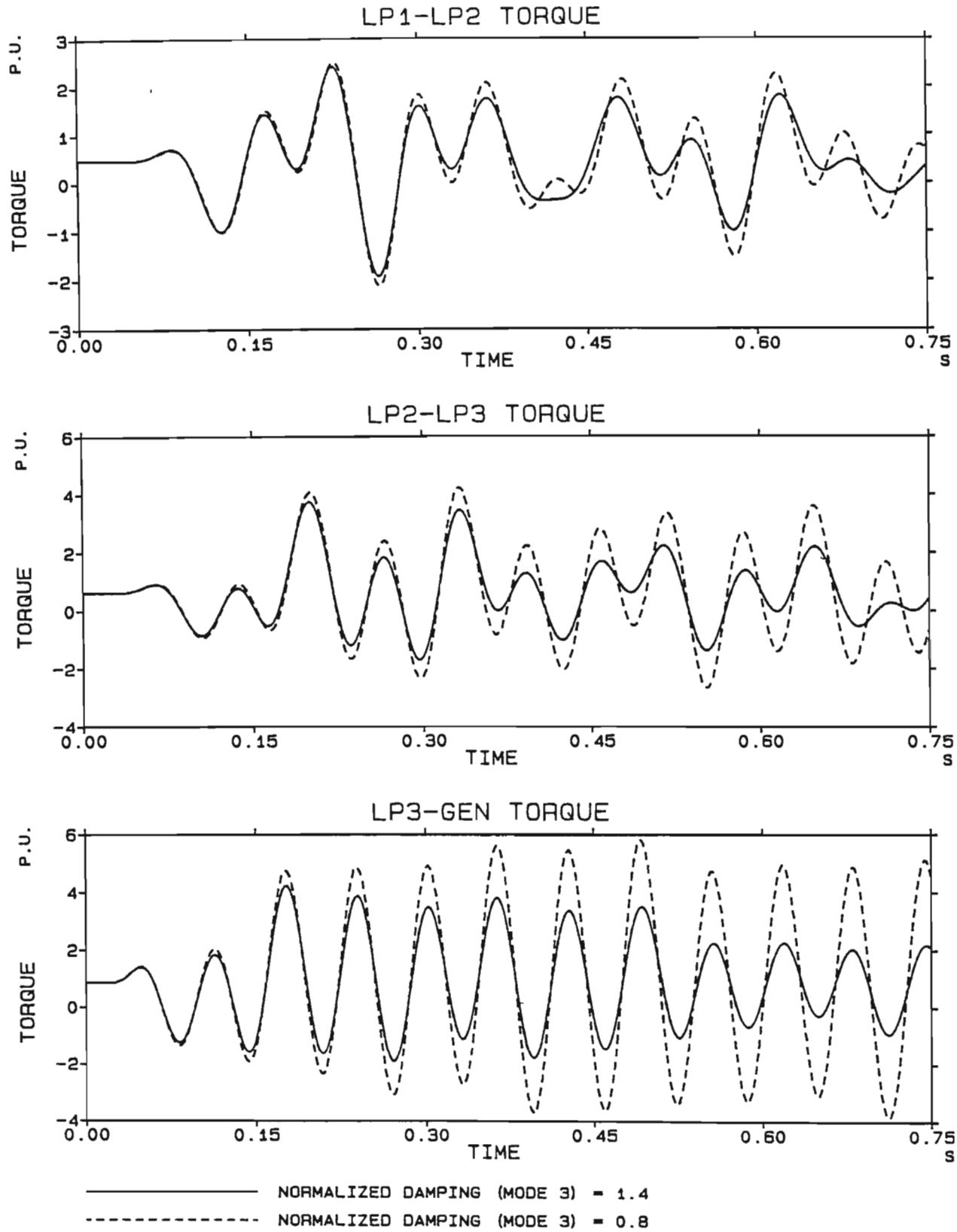

Fig 3.17 LP1-LP2, LP2-LP3 and LP3-GEN shaft torques following a 98 ms three phase short circuit at the infinite bus calculated for two different values of mode 3 damping.

3.9.2 Mode inertia errors

Fig 3.18(a) shows how the peak torques for the different shaft sections vary as the mode 3 inertia is varied from 0.8 to 1.4 times its nominal value. A normalized peak torque of 1.0 for a section corresponds to the per-unit values of torque in Fig 3.14 for a fault duration of 0.098 s. The shaft torques increase with a reduction in the mode 3 inertia due to the resultant stronger coupling of mode 3 to the electrical system.

These results are a bit misleading however, since as the mode inertia is changed the damping of the M3 eigenvalue also changes and below a normalized inertia of 0.8 M3 goes unstable. Thus, in Fig 3.18(a) the effects of inertia variation and damping variation are intermixed. In order to separate these two components, the calculations are repeated but at each new value of mode 3 inertia the system eigenvalues are scanned and the mode decrement factors are adjusted so that the real parts of the mechanical mode eigenvalues M0 to M5 remain the same as those in Table 3.2. The mode 3 inertia can now be varied from 0.5 to 1.5 times its nominal value with no problems of stability and the resulting peak shaft torques (showing only the effect of inertia variation) appear in Fig 3.18(b). The adjustment in the mode 2 and 3 dampings (decrement factors) required to ensure that the real parts of M0 to M5 do not change as the mode 3 inertia is varied are shown in Fig 3.19(a); the other mode dampings remained practically unchanged. The curves in Fig 3.18(b) show the same effect as those in Fig 3.18(a) except that the variation in peak torque is not as severe. This is more clearly seen in Fig 3.19(b) which compares the LP3-GEN peak torque with and without the damping adjustment.

These results show that the peak torque is not unduly affected by inaccuracies in the mode inertia alone with a 6% error in LP3-GEN peak torque for a 10% error in mode 3 inertia, however when the affect of mode inertia error on the damping is included the LP3-GEN peak torque error is 15% for a 10% inertia error and this is significant.

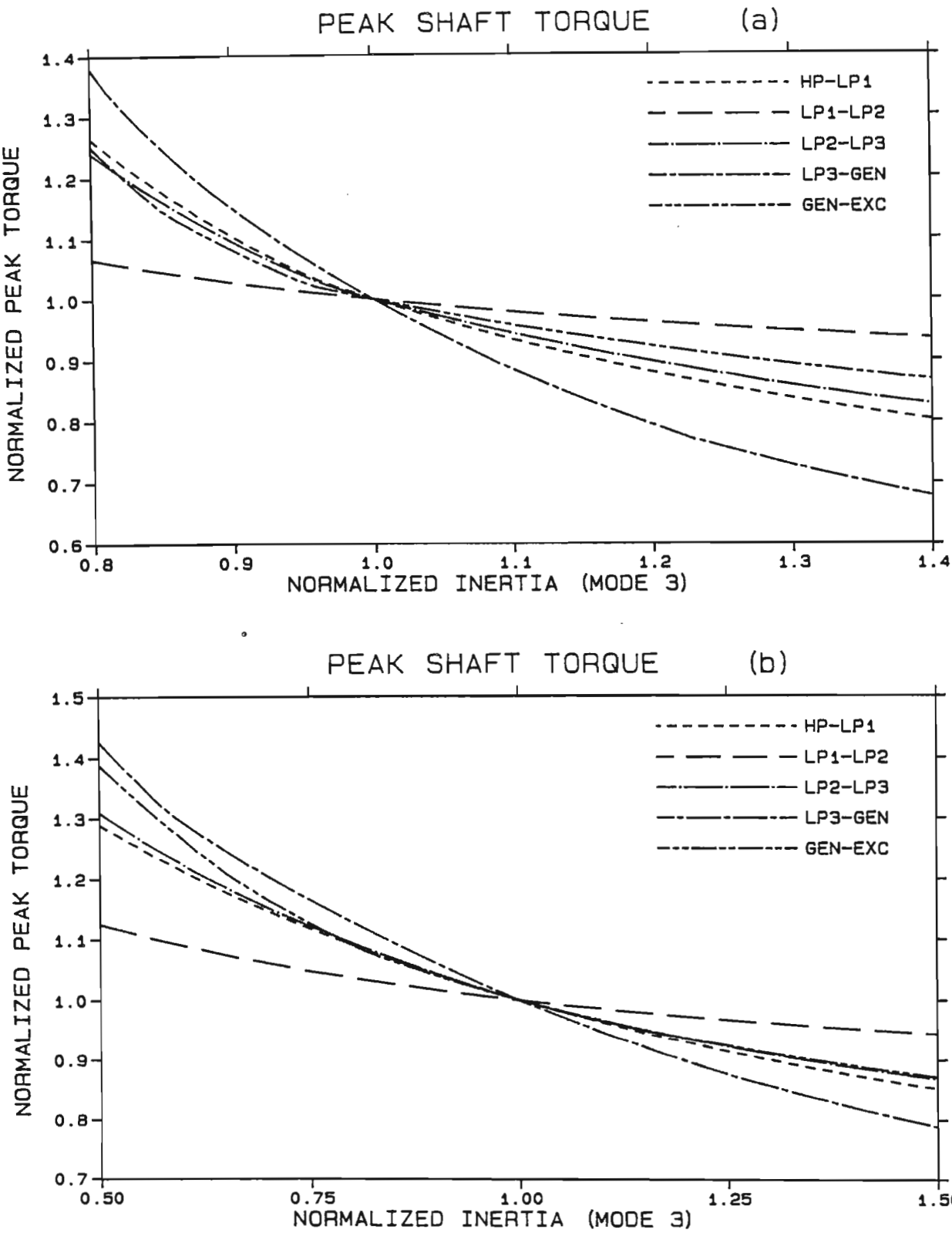

Fig 3.18 (a) Sensitivity of the peak shaft torques for the fault in Fig 3.16 to the mode 3 inertia.
(b) Same as (a) but with the mode dampings adjusted such that the real parts of M0-M5 remain constant as the inertia is varied.

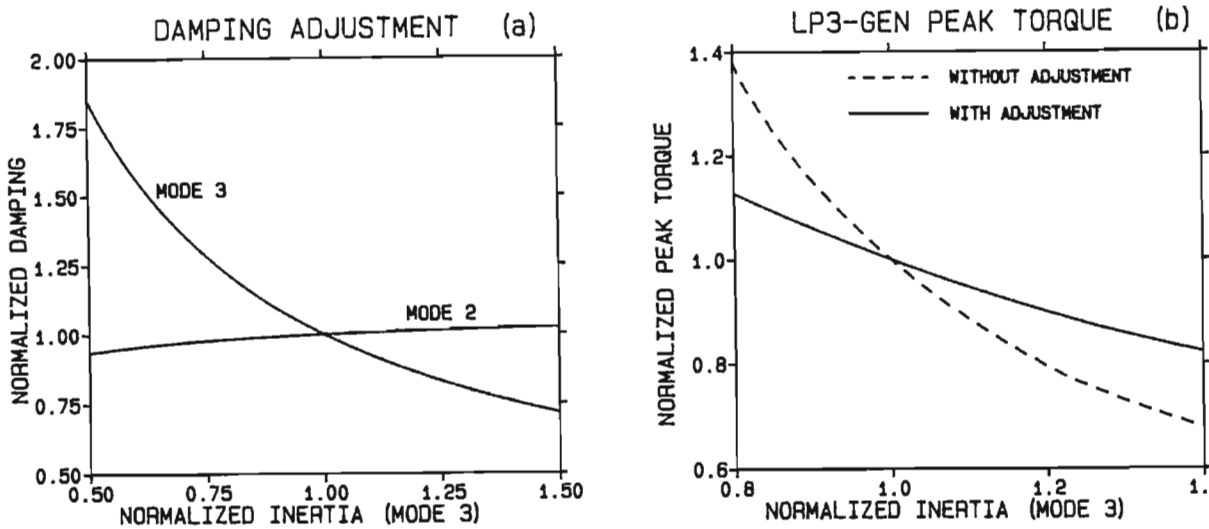

Fig 3.19 (a) Mode 2 and 3 damping adjustments to retain the same real parts of eigenvalues M0-M5 as the mode 3 inertia is varied.
(b) Comparison of LP3-GEN peak torque with and without damping adjustments.

3.9.3 Mode transfer factor errors

Fig 3.20(a) shows the variation in the peak torques for the first four shaft sections as the mode 3 transfer factor at the generator rotor Q_{53} is varied from 0.5 to 1.5 times its nominal value of 0.97. The mode dampings are adjusted as shown in Fig 3.20(b) to ensure the system mechanical mode eigenvalues M0 to M5 have the same real parts as in Table 3.2 for each value of Q_{53}. Only mode 2 and 3 are shown since the other mode dampings are hardly affected. The results show that the LP3-GEN section is greatly affected by the variations in transfer factor whereas the other sections, with the exception of the GEN-EXC section shown in Fig 3.20(c), are less affected.

The reason for the differences between the first three sections (see Fig 2.5 for section details) and the last two is that the change in transfer factor affects the first three sections by virtue of a change in coupling strength between mode 3 and the electrical system whereas the two shaft sections adjacent to the generator in addition have their mode shape deflections altered by the transfer factor change. Hence, the GEN-EXC

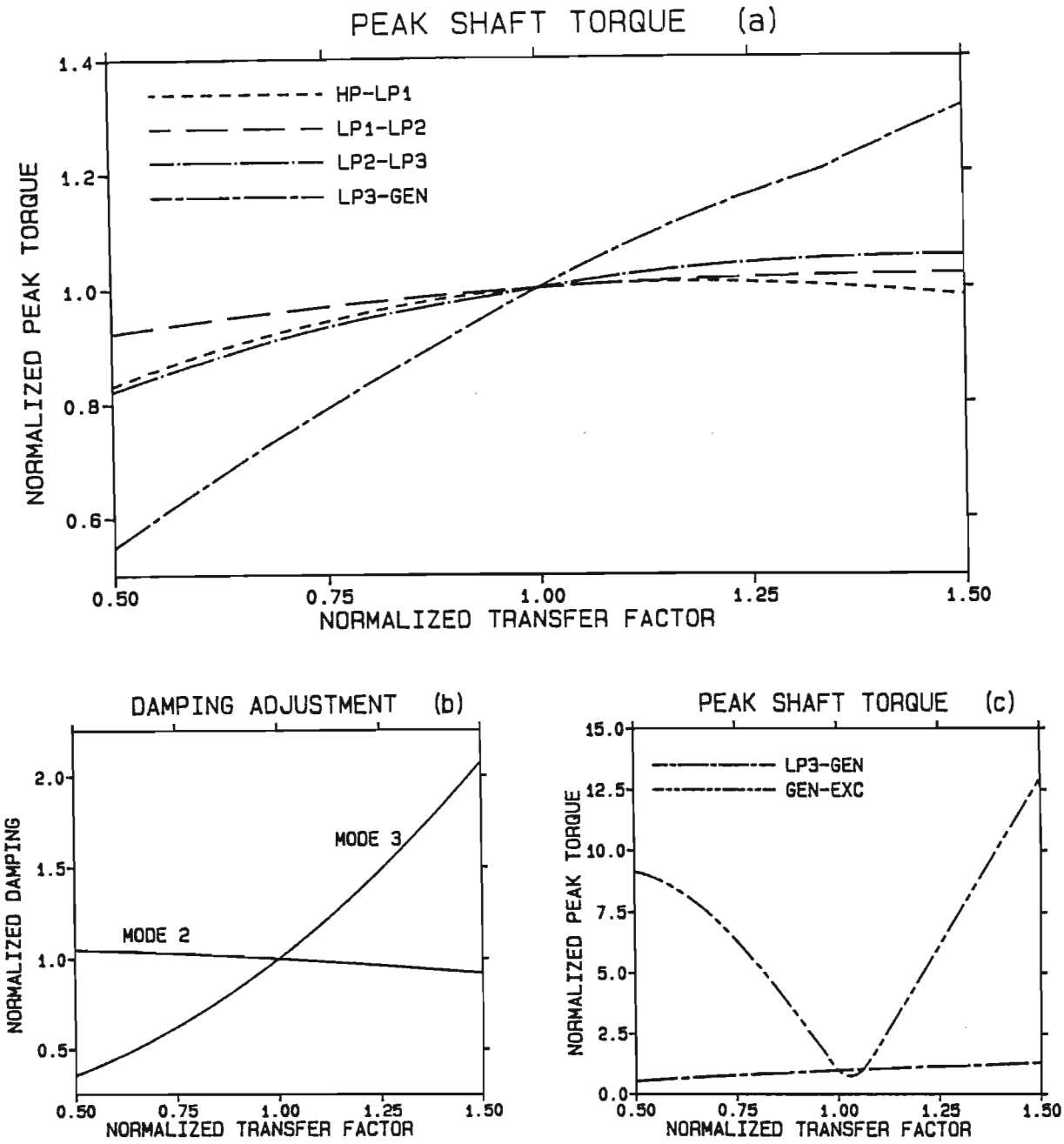

Fig 3.20 (a) Sensitivity of the peak shaft torques (excluding the GEN-EXC section) for the fault in Fig 3.16 to the mode 3 transfer factor at the generator rotor Q_{53}; the mode dampings are adjusted to retain the same real parts of eigenvalues M0-M5 as the transfer factor is varied.

(b) Mode 2 and 3 damping adjustments to retain the same real parts of eigenvalues M0-M5.

(c) Comparison of the sensitivities to Q_{53} of the LP3-GEN peak torque (from (a)) and the GEN-EXC peak torque.

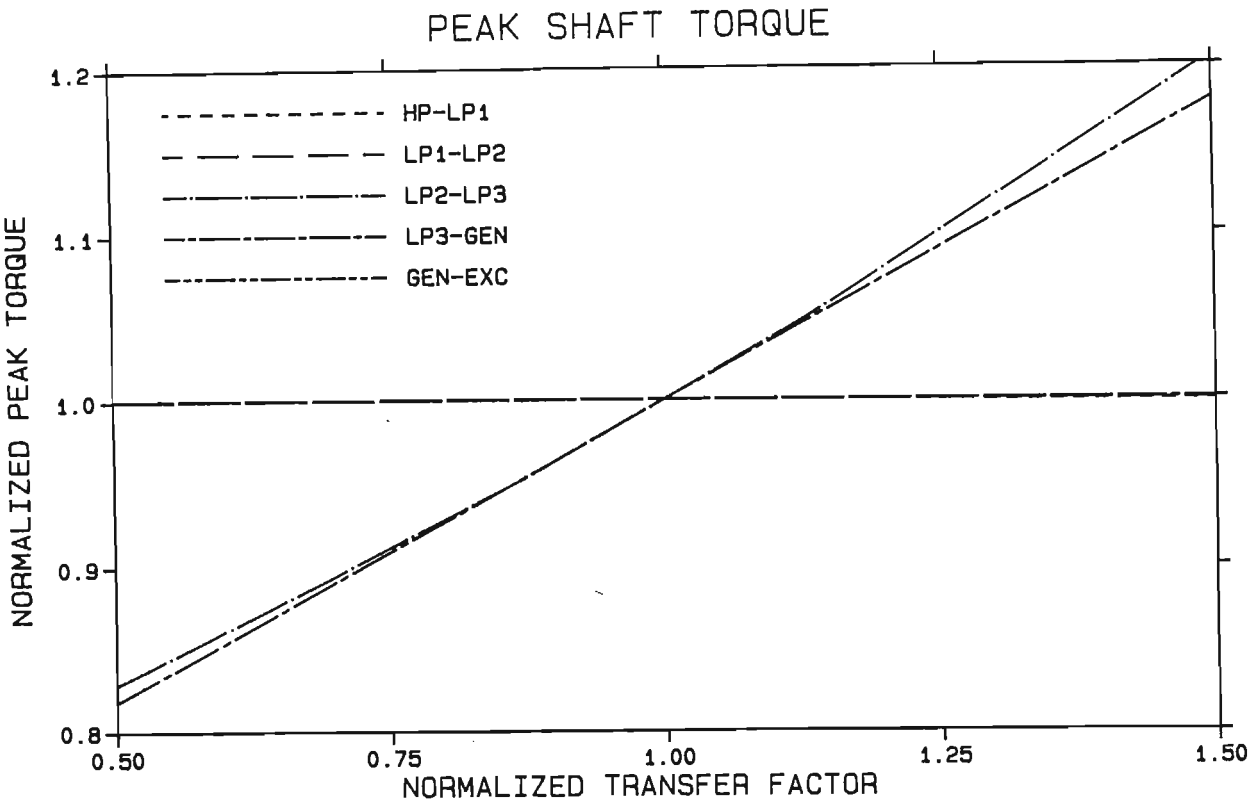

Fig 3.21 Sensitivity of the peak shaft torques for the fault in Fig 3.16 to the mode 3 transfer factor at the LP3 turbine Q_{43}.

section which has a small peak torque and little contribution from mode 3 experiences a large increase in its peak torque when it receives an increased contribution from mode 3. Although its peak torque increases by a factor of 12.5 for a 50% increase in Q_{53} this is still not a very large torque. However, for the LP3-GEN section the variation is more important although still not too severe (7% increase in peak torque for a 10% increase in Q_{53}). This error is worse though if the effects of mode transfer factor errors on the damping is considered.

The HP-LP1, LP1-LP2 and LP2-LP3 curves in Fig 3.20 have shown the effect of changed coupling strength and the LP3-GEN curve shows the effect of changed coupling strength together with changed mode shape deflection. Fig 3.21 shows the peak shaft torques as a function of the normalized mode 3

transfer factor at the LP3 turbine Q_{43} where the LP2-LP3 and LP3-GEN curves illustrates the effect of changed mode shape deflection on its own. The peak torques vary fairly linearly and a 10% change in the transfer factor results in a 3.7% change in the peak torque.

These sensitivity results have merely given an indication of the errors one might expect to incur in shaft torque predictions due to mode parameter errors. The results are however reasonably dependent on the torsional characteristics of the particular turbogenerator being studied.

3.10 Conclusions

This chapter has restated the modal analysis theory and investigated the use of the modal model in transient and small-signal stability studies. In particular, the sensitivity of Critical Compensation Level (CCL) and torque amplification predictions to mode parameter uncertainties have been evaluated.

Eigenvalue calculations showed that the CCL is most sensitive to errors in the mode transfer factor at the generator rotor and least sensitive to errors in the mechanical decrement factor. This result is interesting since the damping is generally accepted as being the parameter which most affects the accuracy of CCL calculations. However, although the CCL has been shown to be least sensitive to decrement factor errors this result must be assessed in conjunction with the expected accuracy in determining the various shaft parameters. The mode damping is the most difficult to obtain accurately and in this respect errors in the damping are likely to be the major cause of uncertainty in the predicted value of the CCL. Nevertheless, the results show that inaccurate modelling of the mode shapes and mode inertias can cause appreciable error in the calculated CCL.

Transient calculations performed in this chapter with the modal model demonstrated the extent to which torque amplification predictions can be affected by errors in the mode parameters. Results showed that viscous

forms of the mechanical damping as represented by mechanical decrement factors in the modal model can affect the values of peak shaft torques. This form of damping has been considered by some authors [29,31,38] to have little influence on the peak values of torque. Although this may be so in most cases, the results show that if the peak torque in a multi-modal response occurs only after a number of cycles and not during the initial post-fault period, then viscous damping terms can influence the value of the peak torque.

The results illustrate the magnitudes of errors one can expect in torque amplification predictions due to uncertainties in mode parameters and show that accurate modelling of torsional characteristics are important for transient torque studies.

CHAPTER FOUR

REDUCED ORDER MODAL MODELS

4.1 Introduction

The previous chapter has investigated the use of the modal analysis technique in representing the torsional characteristics of a turbogenerator shaft. A major advantage in using the modal representation of a shaft instead of the conventional physical representation is that the modal shaft parameters (especially the damping) can be measured and used directly in a stability study whereas the parameters of the physical model cannot all be measured and some have to be estimated (in the case of damping) with some uncertainty. This chapter investigates a further advantage of the modal model which allows one to retain certain modes and to neglect those which are of no interest or are not necessary for the particular study being done. This leads to reduced order shaft models which cannot be attained with the physical representation.

In an SSR stability study it is necessary to model network transients (RLC instead of RL), as well as the torsional characteristics of any SSR susceptible turbogenerators and the stator transformer voltage terms in these generator's electrical equations. Thus for the simplest single-machine-infinite-bus system shown in Fig 2.1 consisting of a six inertia shaft and an electrical model of the generator with four rotor circuits, a 20th order system model is required for an SSR study. This represents a large increase in system order compared to the six or so differential equations that would be used for this system in a conventional stability study [39]. The main reason for this large increase in system order is

the modelling of the shaft torsional characteristics which increases the order of the mechanical model from two to twelve. With the size and speed of modern day computers, a system of this magnitude is not excessive and the full order system is readily solved, but in multi-machine studies where the number of generators susceptible to SSR may be large, the full order model of the system may be excessive. Furthermore, many powerful techniques employed in the design of SSR controllers are severely hampered by large system orders and model reduction may be necessary to employ these techniques efficiently [40-42].

The modal model of the shaft enables the mechanical system order to be reduced thereby simplifying multi-machine studies and controller designs. This chapter therefore investigates the system order reduction capabilities of the modal model in both small-signal and transient stability studies and finds that system order reductions which still yield reasonably accurate results are possible with the modal model, especially in the case of small-signal stability studies.

4.2 Mode Excitability

As soon as the idea of reducing the number of modes is suggested, the problem arises of how to decide which modes should be included and which ones can be neglected. In some cases where the mode has a nodal point or near nodal point at the position of excitation (generator) the choice is obvious, but the validity of neglecting certain modes which have a substantial degree of interaction with the electrical network (active modes) is not so obvious.

The use of the mode shape matrix [Q] as the basis for retaining selected modes in a reduced order model is unreliable since the mode shapes are all scaled independently. Thus while it is possible to compare mode responses at different shaft locations for the same mode, it is not possible to make meaningful comparisons between responses due to different modes, nor for that matter can modes from different generators be easily compared. In

order to overcome this problem, it is useful to introduce parameters which allow comparisons between different modes, including those from different generators. Firstly, the mode excitability E_i is defined as the ability of the electrical torque of the generator to excite mode 'i'; E_i is determined from the transfer function between the electrical torque and the rotor angles (see eqn (E.11)) as

$$E_i = 50 \frac{Q_{gi}}{J_{Mi}\sqrt{(\nu_i^2 - \sigma_{mi}^2)}} \qquad (4.1)$$

where J_{Mi}, ν_i and σ_{mi} are the mode 'i' inertia, frequency and damping respectively; Q_{gi} is the mode shape deflection of mode 'i' at the generator, and the scaling factor of 50 is included to result in values of shaft parameters defined below to be between 0 and 100 in most cases. E_i is still dependent on the mode shape scaling, however when combined with the mode shape it provides information about a mode that is independent of scaling and which can be compared with other modes from the same shaft system or with modes from other turbogenerators. For instance, the phenomenon of torsional interaction involves the excitation of a mode from the electrical network as well as the reflection of the mode's mechanical oscillations back into the electrical system. Hence, define S_i, the susceptibility of mode 'i' to SSR instability due to torsional interaction, as the mode excitability multiplied by the mode transfer factor governing the reflection of oscillations back into the electrical system:

$$S_i = E_i Q_{gi} \qquad (4.2)$$

The mode excitability values and torsional interaction susceptibility (TIS) values for the Koeberg generator shaft system appear in Table 4.1. The TIS values are independent of mode shape scaling and can be compared with each other; clearly modes 4 and 5 are far less susceptible to torsional interaction than modes 1 to 3 and this agrees with the conclusions drawn from the mode shape diagrams (Fig 3.2) in Sect 3.3 and the eigenvalue loci in Fig 3.3. However, from the mode shapes alone it was not possible to

say which of modes 1, 2 and 3 would have the strongest interaction with the electrical system and which would have the weakest; this information is given by the TIS values which predict mode 1 to be the most susceptible to torsional interaction (S_1=63.1) and mode 2 the least (S_2=28.0). This result agrees with the eigenvalue loci in Fig 3.3(b) which show that M1 is destabilized the most and M2 the least.

Table 4.1 Excitability and torsional interaction susceptibility of the Koeberg turbogenerator shaft modes

MODE	1	2	3	4	5
E_i	66.2	37.6	50.2	9.8	19.4
S_i	63.1	28.0	48.6	0.3	1.0

The TIS values S_i also allow one to compare modes from different turbogenerator shafts. Thus, an idea of the torsional performance of a turbogenerator can be gained by a comparison of its mode's TIS values with those of a turbogenerator which one is familiar with. For instance, the 588 MVA turbogenerator considered by Hammons [43] has its first three torsional frequencies at 20.3 Hz, 31.6 Hz and 34.7 Hz and for these modes the TIS values are S_1=41.1, S_2=6.8 and S_3=12.3 respectively. This shaft's most active torsional mode (mode 1) is less susceptible to torsional interaction than modes 1 and 3 of the Koeberg shaft but more susceptible than mode 2 of Koeberg. The actual strength of torsional interaction of a particular mode will depend not only on the susceptibility of that mode to torsional interaction, but also on the electrical network with which it is interacting, including the generator electrical circuits, and the operating point of the generator. Thus in order to show the difference in the TIS values between the Koeberg shaft and the Hammons generator shaft, the two shafts are considered with the same generator electrical circuits and transmission system (those used in the calculation of Fig 3.3). The eigenvalue loci of Fig 3.3(b) are recalculated here (with zero mechanical damping) for both shafts and appear in Fig 4.1 where the Koeberg modes are labelled M1 to M3 and the Hammons generator modes H1 to H3. The strength of interaction of the modes are as predicted by the TIS values and the

comparisons made between the modes from different shafts are valid.

In using reduced order modal models to determine shaft torques due to transient disturbances it is necessary to have some idea of the expected contribution from the different modes to the various shaft torques. It is also advantageous to be able to identify which torques are likely to be the largest and hence will require monitoring. This information can to a large extent be obtained from the mode excitability values in conjunction with the mode shapes. If the mode torque susceptibility (MTS) A^i_{nm} of shaft section n-m from mode i is defined as the mode excitability multiplied by the mode shape deflection across the section, then

$$A^i_{nm} = E_i(Q_{ni} - Q_{mi}) \tag{4.3}$$

For the Koeberg turbogenerator shaft the MTS values for the various shaft sections appear below in Table 4.2.

Table 4.2 Mode Torque Susceptibility (MTS) values for the Koeberg Turbogenerator Shaft

	SHAFT SECTIONS				
MODE	HP-LP1	LP1-LP2	LP2-LP3	LP3-GEN	GEN-EXC
1	11.0	43.7	56.1	18.6	0.4
2	21.4	48.2	31.7	28.4	0.5
3	24.4	17.1	47.4	80.7	1.5
4	11.1	1.9	0.8	0.5	0.0
5	0.0	0.0	0.0	1.0	20.4

These values, which are independent of mode shape scaling, indicate the susceptibility of the different shaft sections to large torque contributions from the various modes and enable comparisons of torque susceptibility at various shaft sections as well as comparisons between different mode contributions at the same section. The largest torque susceptibility occurs at the LP3-GEN section for mode 3 and the second largest at the LP2-LP3 section for mode 1. Although the MTS values are a

useful guide to assessing the make-up of the various shaft torques, it must be remembered that they, like the TIS values, are only an indication of the susceptibility of the shaft to the various torques. The actual magnitude of the various torque components will depend on the degree to which the modes are excited or more specifically, the frequency spectrum of the exciting torque. This is determined by a number of different factors such as the transmission system (especially series capacitance which leads to torque amplification), operating point of the generator and the duration of external disturbances.

4.3 Eigenvalue Analysis with Reduced Order Models

In this section the accuracy of various reduced order models of the shaft in small-signal stability studies is investigated with particular emphasis on Critical Compensation Level (CCL) calculations. The system studied is the same single-machine-infinite-bus system considered in Chapters Two and Three (shown in Fig 2.1), the parameters for which are given in Appendix I.

4.3.1 Reduction to eighth order model

As a first step, modes 4 and 5 are neglected on the basis that their TIS values (0.3 and 1.0 respectively) are much smaller than those for modes 1 to 3; in addition mode 5 is a supersynchronous mode which does not interact unstably with the electrical network. The real part of the mechanical mode eigenvalues calculated in Fig 3.4 with the full order shaft model (as the series capacitance is scanned) are recalculated here but using the reduced 8th order shaft model; the results are plotted together with those from Fig 3.4 in Fig 4.2. The curves calculated with the 8th order model (plotted as the dotted lines) are practically identical to those calculated with the full 12th order model. Thus the CCLs (labelled as points A, B and E) can be determined with an 8th order shaft model equally as well as with the 12th order model.

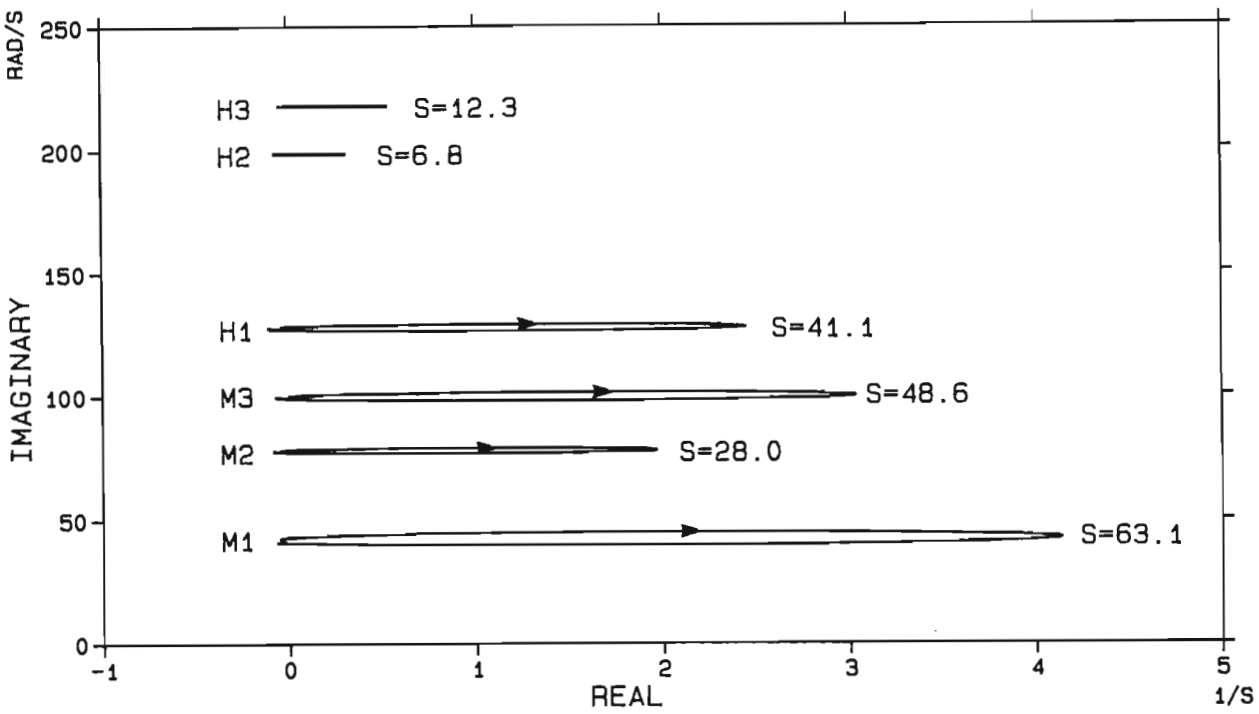

Fig 4.1 First three torsional mode eigenvalue loci calculated for the Koeberg shaft (M1 to M3) and for the Hammons generator shaft (H1 to H3) as the series compensation is varied.

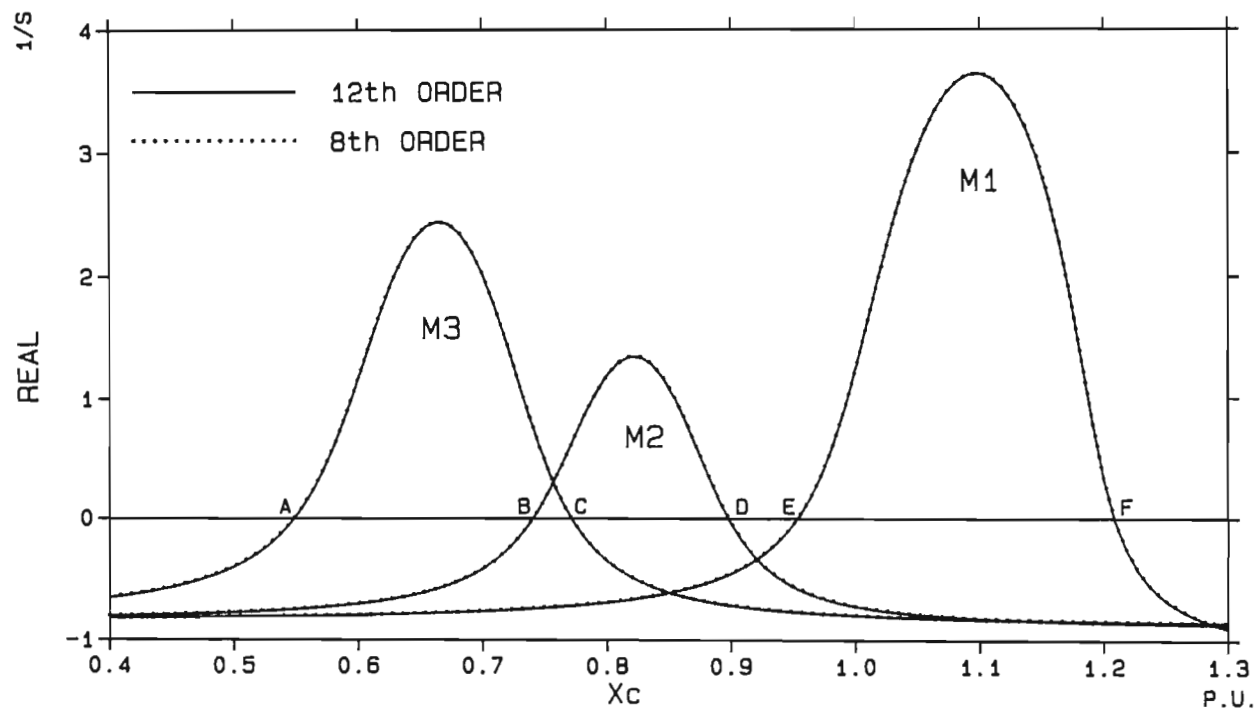

Fig 4.2 Real part of modes M1 to M3 calculated with the 12th order shaft model and the 8th order shaft model.

4.3.2 Reduction to fourth order model

A further reduction in the model order considers the possibility of neglecting all the torsional modes except one. Thus in order to study the stability of mode 1 (M1) a 4th order model containing M0 and M1 is used. Similarly, M0 and M2 are considered for mode 2 while for mode 3, M0 and M3 make up the shaft model. It is necessary in each case to include mode 0 so these fourth order models constitute the minimum order model that can be used to study a torsional mode.

The real parts of the eigenvalues in Fig 4.2 are recalculated with each mode represented separately in a 4th order model with mode M0. The results appear as the broken curves in Fig 4.3 which also shows the 12th order model results as the solid curves. The reduced order models give a good approximation to the true accurate curves in both the strength of interaction (amount of positive damping added) and the region of interaction. The values of capacitance at which the modes cross the stability boundary (points A to F) as predicted by the reduced 4th order models are compared with the accurately predicted values in Table 4.3 and they show that the errors incurred are less than 2%. In particular the mode 3 critical compensation level (CCL) at point A which governs the overall CCL of the system is determined with an error of only 1.6% (0.009 p.u.).

Table 4.3 Predicted stability limits of mechanical modes

MODE		X_c in per-unit		Percentage error
		12th order model	4th order model	
Mode 1	E	0.953	0.938	-1.6
	F	1.209	1.203	-0.5
Mode 2	B	0.740	0.732	-1.1
	D	0.898	0.894	-0.5
Mode 3	A	0.548	0.557	1.6
	C	0.771	0.778	0.9

The error incurred by the fourth order models is acceptable since it is less than the error that occurs due to uncertainties in the mechanical damping; however for a different shaft system this error could be greater. The approximation error occurs due to the fact that the mechanical modes become coupled through the electrical network as soon as the generator is synchronized. It can also be considered that the value of a mechanical eigenvalue, M3 for instance, is determined by all the modal parameters although its value is predominantly influenced by the mode 3 parameters. This aspect is discussed further in Sect 5.2.

The mechanical modes M1 to M3 move into the right-half-plane (RHP) and become unstable due to their interaction with the electrical subsynchronous mode E2. However, E2 does not interact exclusively with each mode in turn but rather interacts with all the modes simultaneously for all values of capacitance although in some regions it interacts more strongly with some modes than others. For instance at X_c = 0.667 p.u., E2 and M3 are at maximum interaction (see Fig 4.2) and the movement of E2 into the left-half-plane is predominantly due to M3, however at this point E2 is also interacting with M2 and to a lesser extent M1. Hence the mechanical modes influence each other through their simultaneous interaction with E2.

Figure 4.4 shows the effect the mechanical modes have on the real part of E2 and compares the case where M1 to M3 are represented together in a 12th order model, with that where each of them is represented separately in a 4th order model. It is clear from Fig 4.4 that the real part of E2 (while it is in a region of strong interaction with a mechanical mode) calculated with a 12th model containing all the modes, is different to that calculated with the 4th order model containing only the relevant mechanical mode.

With regard to the movement of the mechanical modes into the RHP of even greater importance is the influence these modes have on the frequency of E2. Figures 4.5(a) to 4.5(c) show the effect of a single mechanical mode (represented alone in a 4th order model) on the frequency of E2. The frequency of E2 calculated with no torsional modes (mechanical system represented by the inertial mode M0 only) is taken as the reference

frequency for E2 and curves 4, 5 and 6 show the difference between the E2 frequency calculated when modes 1, 2 and 3 are represented separately in a 4th order model and the reference. In each case, the real part of the torsional mode included in the 4th order model is drawn on the same axes as the E2 frequency difference curves and appear as curves (1), (2) and (3) for modes M1 to M3 respectively.

The interaction between a mechanical mode and E2 causes the frequency of E2, in the region leading up to maximum interaction with the mechanical mode, to be reduced below that which it would be without the mechanical mode, while in the region after maximum interaction the mechanical mode causes the frequency of E2 to be greater than that for no mechanical mode. In other words, the frequency of E2 is drawn towards the mechanical mode frequency thereby increasing or decreasing in value depending on whether it is greater or less than the mechanical mode frequency. When all the mechanical modes are included together, they simultaneously interact with E2 so for certain values of capacitance some mechanical modes will tend to increase the frequency of E2 while others will tend to decrease it. The resultant effect on the E2 frequency is a combination of the individual effects of each mechanical mode and is shown in Fig 4.5(d) (solid curve) as the difference between the E2 frequency calculated with the 12th order model and the E2 reference frequency (no torsional modes). The broken curve is the summation of curves 4 to 6 in Figs 4.5(a) to (c) and shows the extent to which the resultant effect from all the mechanical modes on E2 is the combined effect of each mechanical mode's individual influence.

The understanding of the influence of the mechanical modes on the frequency of E2 enables an explanation of the errors incurred in the critical compensation levels (CCLs) determined by the 4th order models in Fig 4.3. The difference between the E2 frequency calculated with the 12th order model and that calculated with the M1-, M2- and M3 4th order models is shown in Figs 4.6(a), (b) and (c) respectively. For the M3 4th order model (Fig 4.6(c)) the difference in the E2 frequency at the M3 CCL (point A in Fig 4.3) is -0.7 rad/s. This means that the frequency of E2 calculated with the 4th order model is higher than that calculated with the

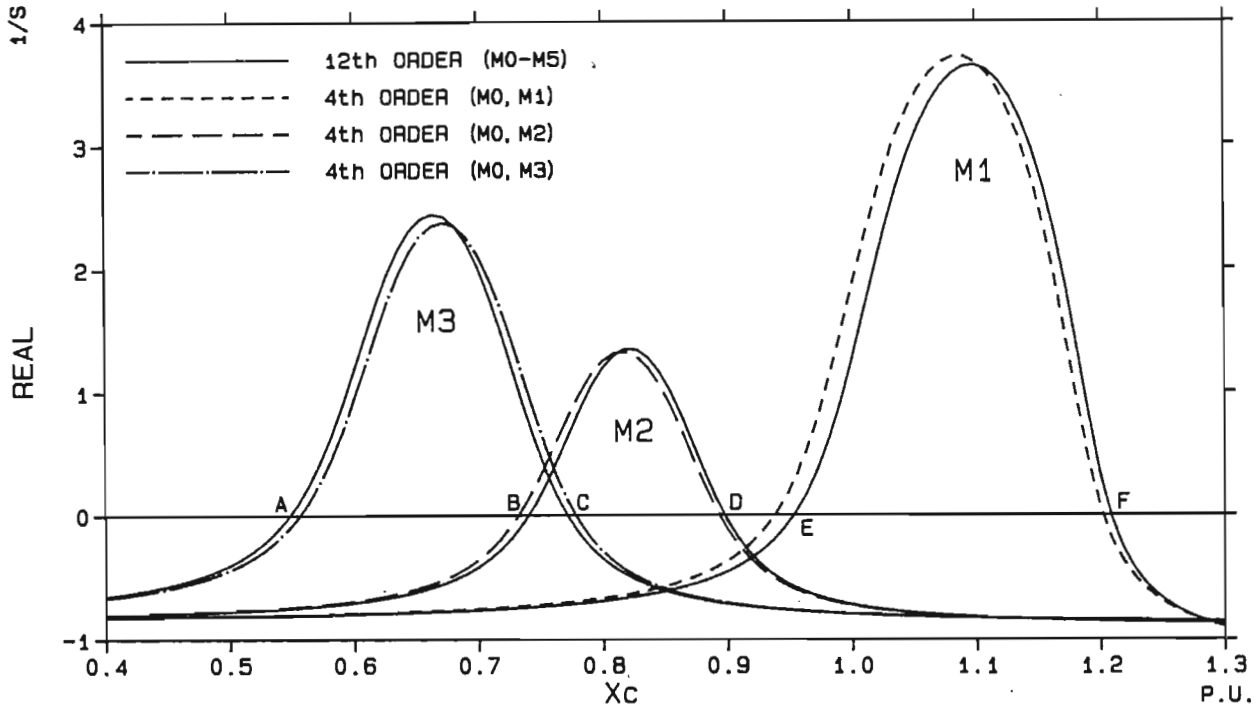

Fig 4.3 Real part of modes M1 to M3 calculated with the 12th order shaft model and three 4th order shaft models.

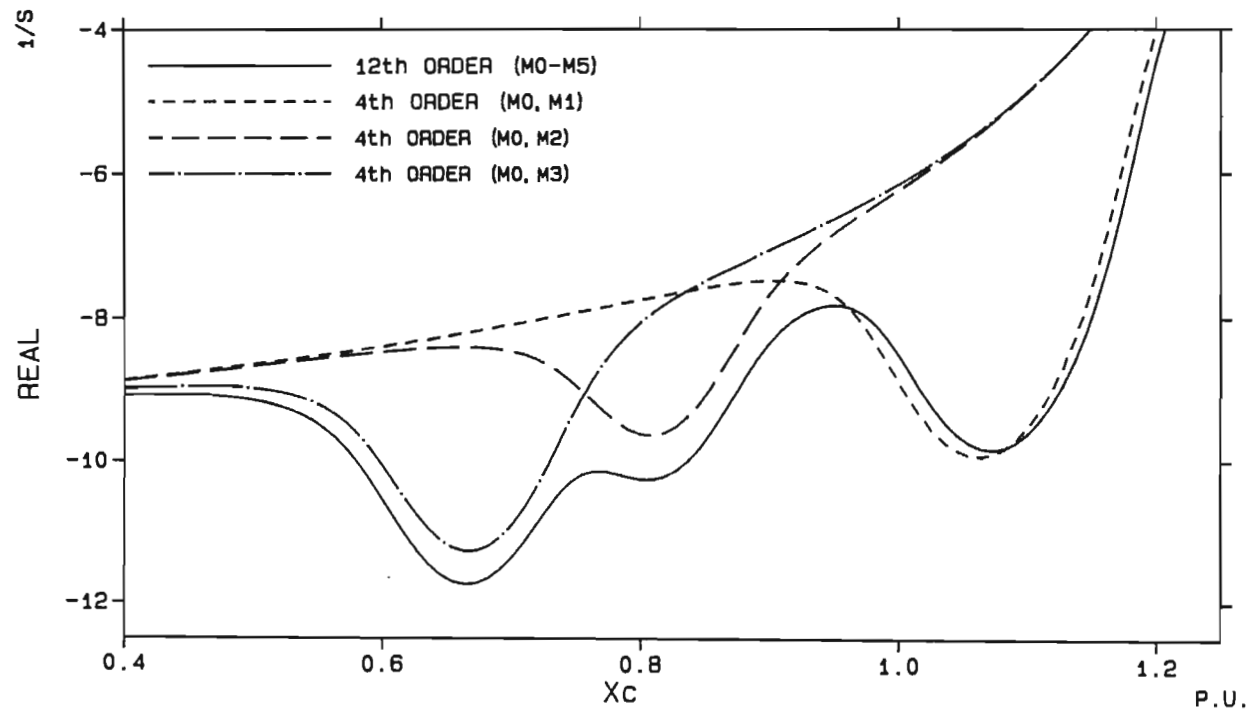

Fig 4.4 Real part of the electrical subsynchronous mode E2 calculated with the 12th order shaft model and three 4th order shaft models.

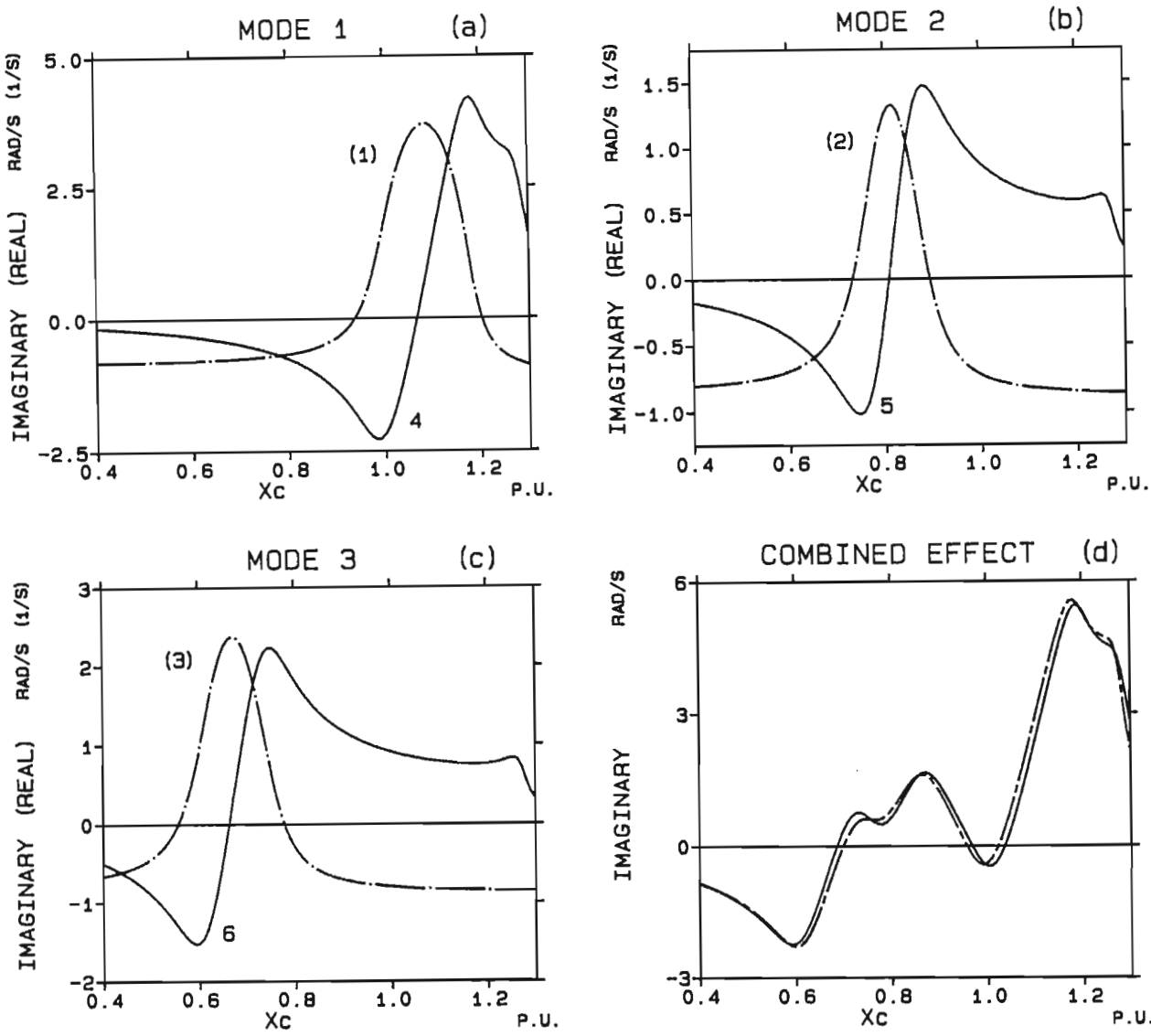

Fig 4.5 Curves to show the effect of the mechanical modes on the frequency of E2; curves (1), (2) and (3) are the real parts of M1, M2 and M3 calculated with a 4th order model; curves 4, 5 and 6 are the difference between the imaginary part of E2 calculated with a 4th order model (one torsional mode) and that calculated with no torsional modes; the combined effect of M1, M2 and M3 on the imaginary part of E2 is shown in (d).

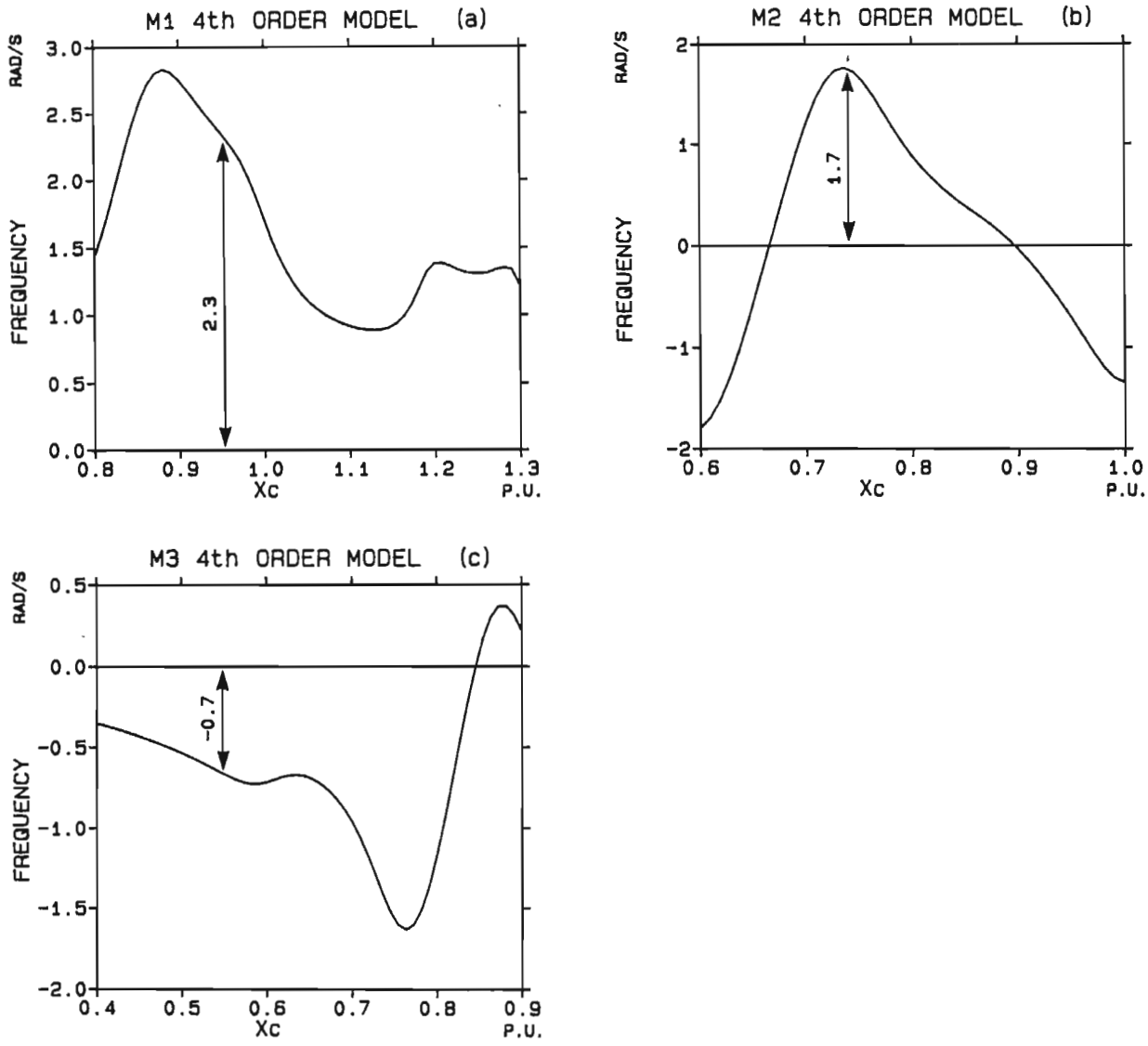

Fig 4.6 Difference between the E2 frequency calculated with the 12th order model and that calculated with the 4th order models.

12th order model at the CCL and hence M3 in the 4th order model will interact with E2 at higher values of X_c. This causes the shift in the 4th order M3 curve to the right in Fig 4.3. Similarly, the E2 frequency difference between the 12th order model and the 4th order models at the CCLs for M1 and M2 are 2.3 rad/s for M1 (point E in Fig 4.3) and 1.7 rad/s for M2 (point B in Fig 4.3). Both these values are positive, thereby resulting in the shift to the left for the M1 and M2 4th order model curves in Fig 4.3.

The errors incurred by the 4th order models are small and are much less than those due to damping uncertainties; however for a different shaft system these errors may be different. The M1- and M2 4th order models fail to safety and thus do not cause much concern, however the M3 CCL, which determines the CCL of the whole system, is optimistic and hence the M3 4th order model does not fail to safety. It is thus necessary to determine which factors influence the magnitude of this error and whether this error could become large enough to cause concern.

It was stated earlier that the error incurred by the 4th order models is because they do not represent the coupling between the mechanical modes. Therefore, two new systems are considered to investigate the extent to which the strength of the coupling between the mechanical modes affects the value of the error incurred by the M3 4th order model. In the first hypothetical system, mode 3 is assumed to be at 20 Hz (M3') and the coupling with mode 2 (12.4 Hz) is therefore weak; in the second hypothetical system mode 3 is moved to 13.5 Hz (M3") and the coupling with mode 2 is stronger. At these new hypothetical frequencies for mode 3, the values of mode shape, mode decrement factor and mode excitability remain unchanged. The real parts of the eigenvalues of the new modes M3' and M3" calculated with a full 12th order model and also with a reduced 4th order model are shown in Fig 4.7. The error in the CCL is greatest when M3 is closer to M2 and M1. For M3' in Fig 4.7 the error in the CCL is only 0.003 p.u. (0.8%) whereas for M3" the CCL error is 0.02 p.u. (3.2%). The damping of E2 calculated with the 12th order and 4th order models for these two cases is compared in Fig 4.8(a) while the difference in the E2

frequency between the full order and reduced models is shown in Fig 4.8(b) for both cases. The difference in the CCL error between the two cases is largely due to the E2 frequency difference being only -0.38 rad/s at the CCL for the M3' case whereas for the M3" case this frequency difference is 0.95 rad/s.

This effect is summarized in Fig 4.9(a) which shows the error in the CCL as the frequency of mode 3 is varied from 12.5 Hz to 20 Hz; the error increases rapidly as M3 moves closer to M2 and at 12.5 Hz the error is as much as 7%. However it is likely that if M2 and M3 were as close as 12.37 Hz and 12.5 Hz then one would not consider neglecting either mode if one was interested in the stability of the system around that frequency.

The effect of the system operating point on the CCL error is seen in Figs 4.9(b) and 4.9(c) (calculated with the nominal mode 3 frequency). Figure 4.9(b) shows the CCL error as the bus real power P_b (for the network in Fig 2.1) is varied from 0.05 p.u. to 0.9 p.u. with zero reactive power at the bus and Fig 4.9(c) shows the CCL error as the bus reactive power Q_b is varied from -0.5 p.u. to 0.5 p.u. while P_b remains at 0.8 p.u. The CCL error is greater for higher values of power since at higher current levels the interaction between the mechanical modes through the electrical system is more pronounced. Furthermore, the magnitude of the error is dependent on the power factor and is greater at lagging power factors (Q positive).

The results in this section have shown that for eigenvalue stability studies the order of the mechanical system can be greatly reduced by neglecting certain modes, including active modes, and acceptable results still attained.

4.4 Transient Analysis with Reduced Order Models

This section investigates the feasibility of using reduced order mechanical models to determine generator shafts torques resulting from a system disturbance such as a temporary reduction in the infinite bus voltage (in

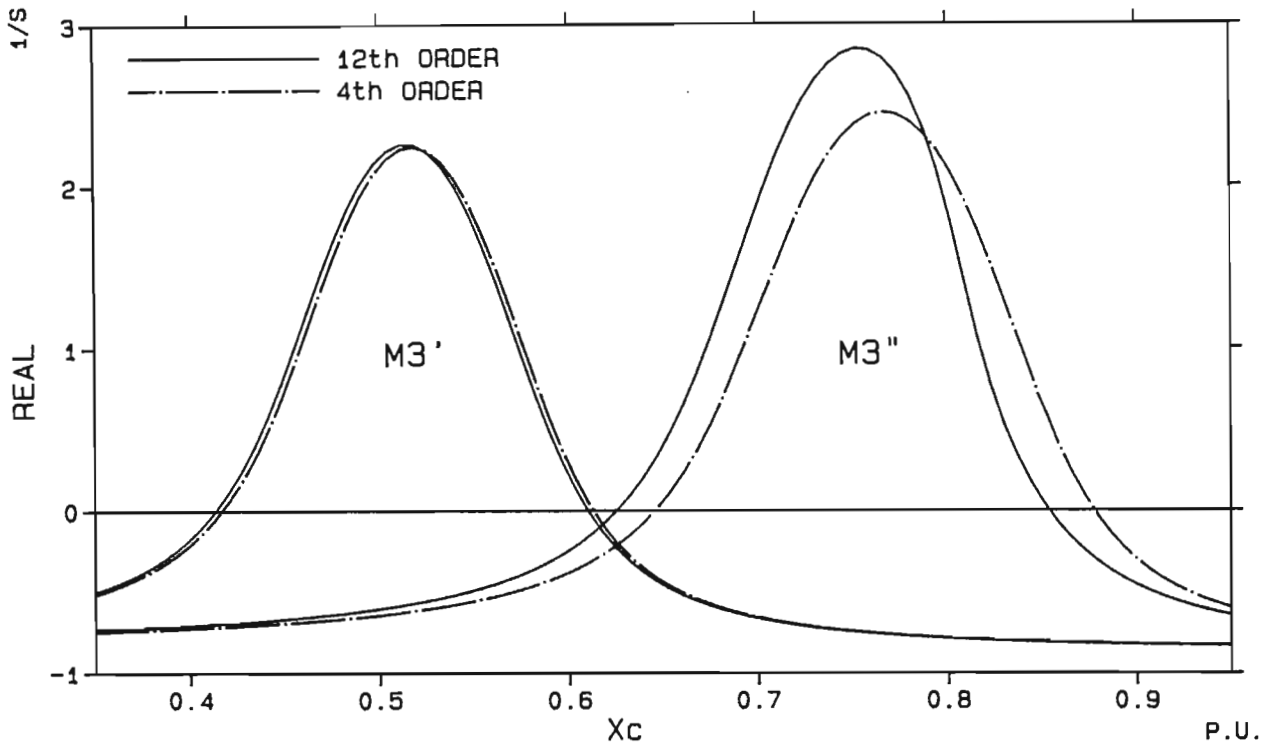

Fig 4.7 Real part of mode M3' (hypothetically assumed at 20 Hz) and M3" (hypothetically assumed at 13.5 Hz) calculated with a 12th order model and a 4th order model.

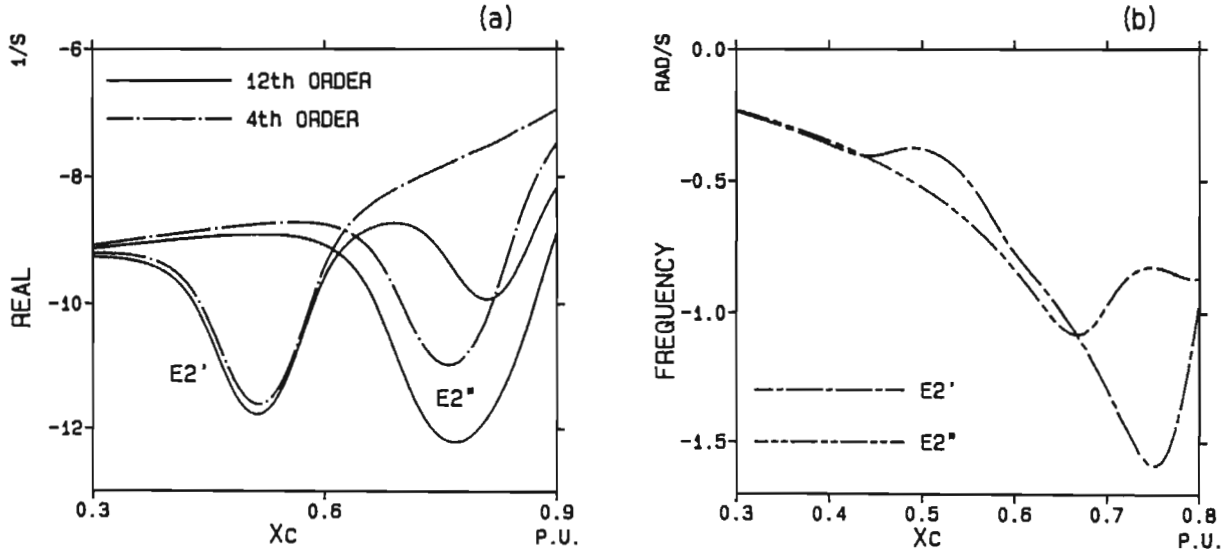

Fig 4.8 (a) Real part of E2' (E2 for the system with M3') and E2" (E2 for the system with M3") calculated with a 12th and 4th order model.
(b) Difference between the E2' and E2" frequencies calculated with a 12th order model and those calculated with a 4th order model.

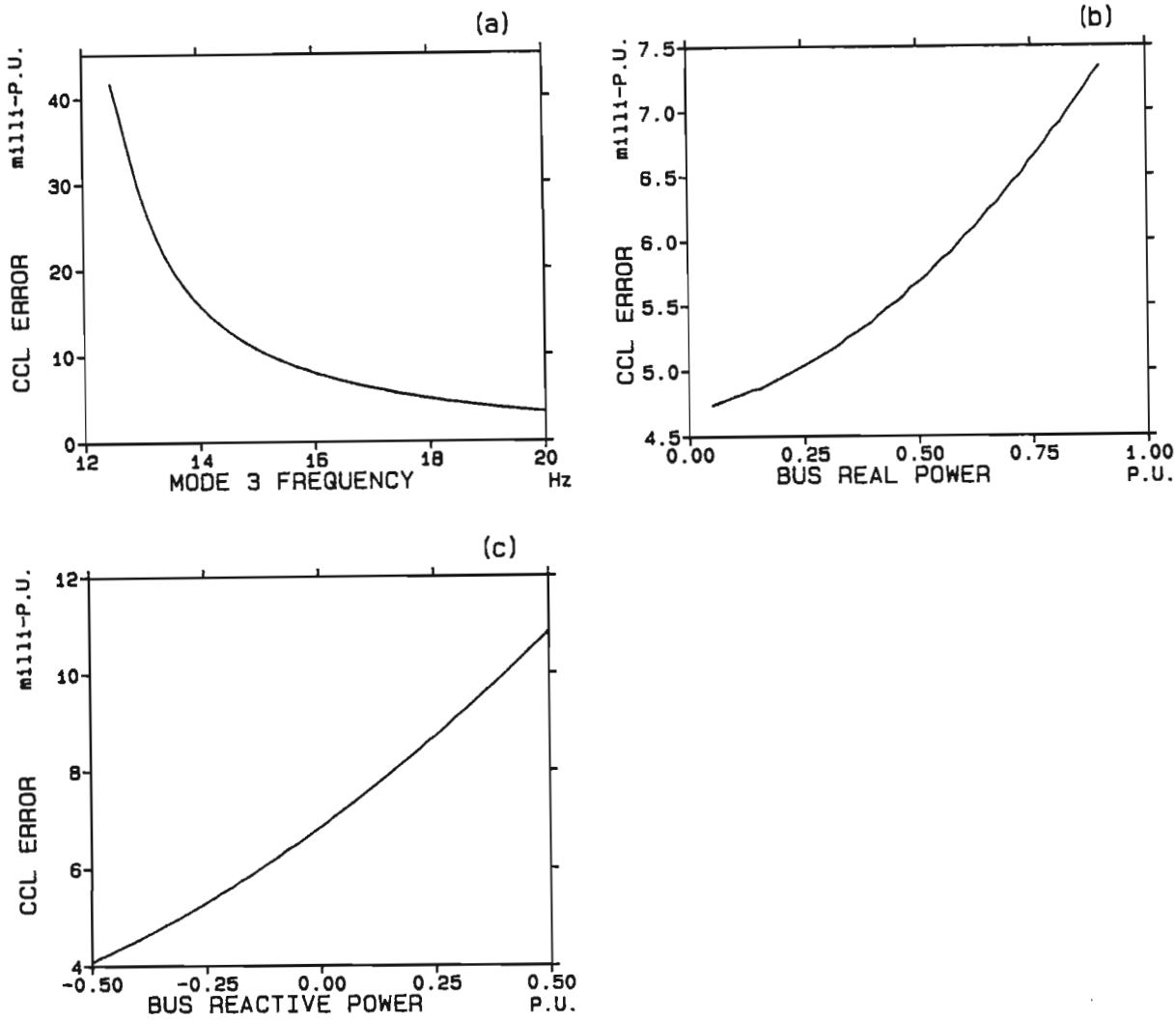

Fig 4.9 Error in the critical compensation level (CCL) calculated by the M3 4th order model as: (a) the M3 frequency is varied, (b) the real power at the bus is varied, (c) the reactive power at the bus is varied.

Fig 2.1) to zero; the pre-fault conditions in all cases are V_b = 1.0 p.u., P_b = 0.8 p.u. and Q_b = 0.2 p.u. The results focus on the LP2-LP3 and the LP3-GEN shaft sections since their torques are generally the most troublesome and are predicted in Table 4.2 to have the largest mode torque susceptibility (MTS) values.

4.4.1 No series capacitance

Firstly, the case of an uncompensated system is considered where the torque amplification phenomenon does not come into effect. The MTS values in Table 4.2 indicate that for the LP2-LP3 shaft section, mode 1 is the most susceptible to high torques (A^1_{34} = 56.1) and of the active modes, mode 2 is the least susceptible (A^2_{34} = 31.7). However, as stated in Sect 4.2 the actual magnitude of a particular mode torque depends on the excitation of that mode and this will generally not be the same for all modes; a higher mode frequency is generally excited to a lesser extent than a lower one.

Figure 4.10(a) shows the LP2-LP3 peak torque (half the maximum peak-to-peak value) as a function of fault duration calculated with different shaft models while Fig 4.10(b) shows the peak torque components of modes 1 to 3 for this shaft section as calculated with the full 12th order model. The mode peak torques show the characteristic cyclic variation at a period corresponding to the mode frequency and their relative contributions agree well with the MTS predictions bearing in mind that the lower frequency modes have a higher level of excitation. In Fig 4.10(a) the peak torque is shown calculated with four different mechanical models of varying complexity. They are labelled according to the torsional modes included in the model; all models include M0. The result obtained with the 8th order model (neglecting M4 and M5) is practically identical to the accurate 12th order curve due to the low MTS values of 0.82 and 0.01 for mode 4 and 5 respectively. A simple 4th order model containing the mode with the highest MTS (mode 1) gives only an approximate value of the peak torque with errors of up to 25%. The inclusion of mode 3 in a 6th order model improves the accuracy to within 10% for most of the range considered.

Figure 4.11 shows similar results to those in Fig 4.10 but calculated for the LP3-GEN shaft section. The mode components in Fig 4.11(b) show mode 3 to be the largest as predicted by the MTS values while mode 1 and 2 are about the same magnitude (in spite of mode 2 having a larger MTS) due to the greater excitation of mode 1. Once again the low values of MTS for modes 4 and 5 result in the 8th order model predicting the same peak torque as the full 12th order model. The 4th order model with mode 3 as the only torsional mode does not produce good results for this shaft section and incurs a 35% error for worst case peak torque around a fault duration of 100 ms. The inclusion of either M1 or M2 in a 6th order model improves the accuracy with an error in worst case peak torques between 10% and 15%.

In Fig 4.12 the LP2-LP3 and LP3-GEN torques are shown calculated with a 4th, 6th and the full 12th order models when the fault duration is 100 ms; from the magnitudes of the component torques in Figs 4.10(b) and 4.11(b) M1 and M3 were chosen as the modes to be included in the 6th order model. However, M2 could have been chosen instead of M1 for the LP3-GEN section based on the MTS values alone, without any reference to the frequency spectrum of the excitation torque although this would not have made much difference to the accuracy. The response of a 4th order model is seen to be much different to that of the accurate curve. The 6th order model predicts the shape of the curve much better than the 4th order model but is unable to accurately reproduce the peaks.

4.4.2 With series capacitance

In this section series capacitance is included in order to investigate the use of reduced order models when the torque amplification effect is present; a series capacitor of 0.667 p.u. is considered in order to give maximum interaction between the electrical system and M3. However, this results in an unstable M3 as seen from Fig 4.2 and transient results under such conditions would be meaningless since the torque amplification effect would be swamped by the instability due to torsional interaction. This unstable value of damping for M3 is the resultant combination of the mechanical damping and a large negative electrical damping component; in

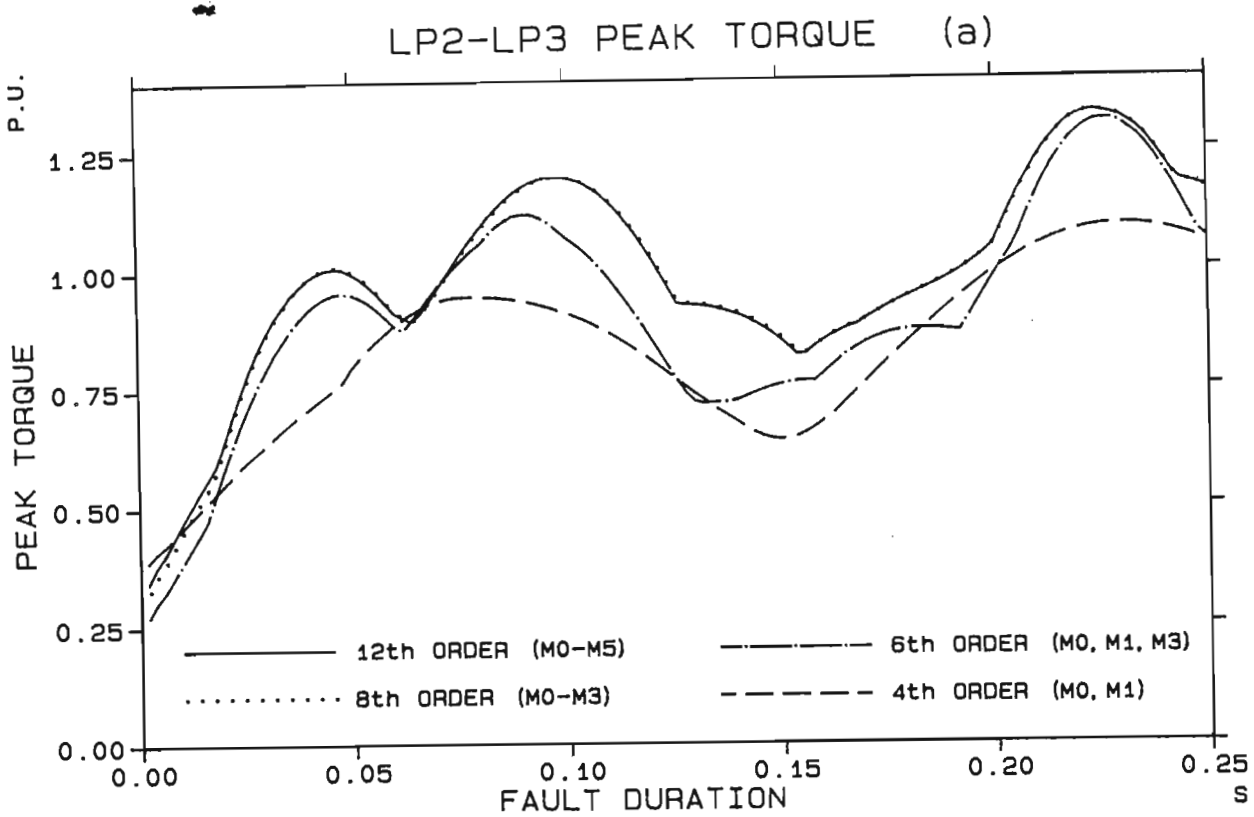

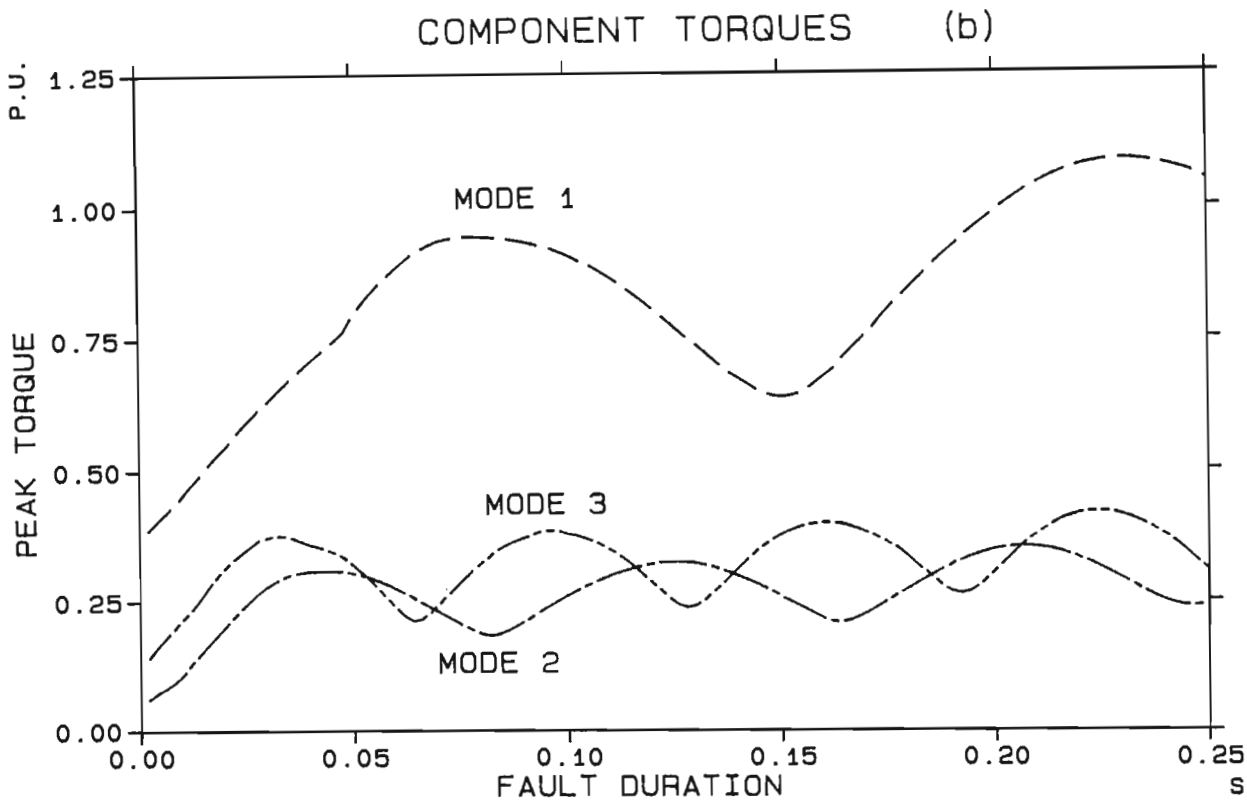

Fig 4.10 LP2-LP3 peak shaft torque calculated with different order models and the component torques due to different modes, all as a function of fault duration for a temporary three phase short circuit at the infinite bus with no series compensation.

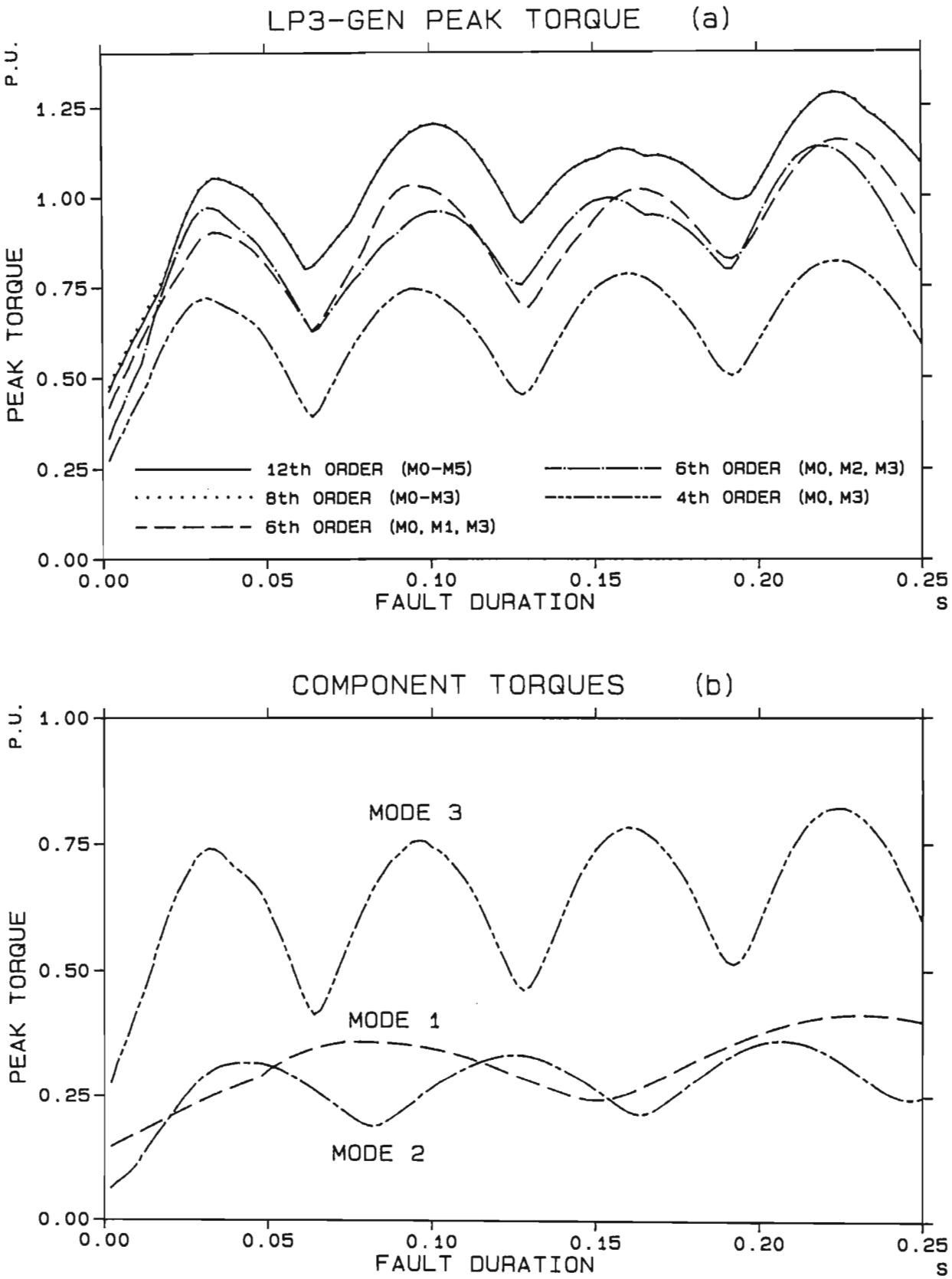

Fig 4.11 LP3-GEN peak shaft torque calculated with different order models and the component torques due to different modes, all as a function of fault duration for a temporary three phase short circuit at the infinite bus with no series compensation.

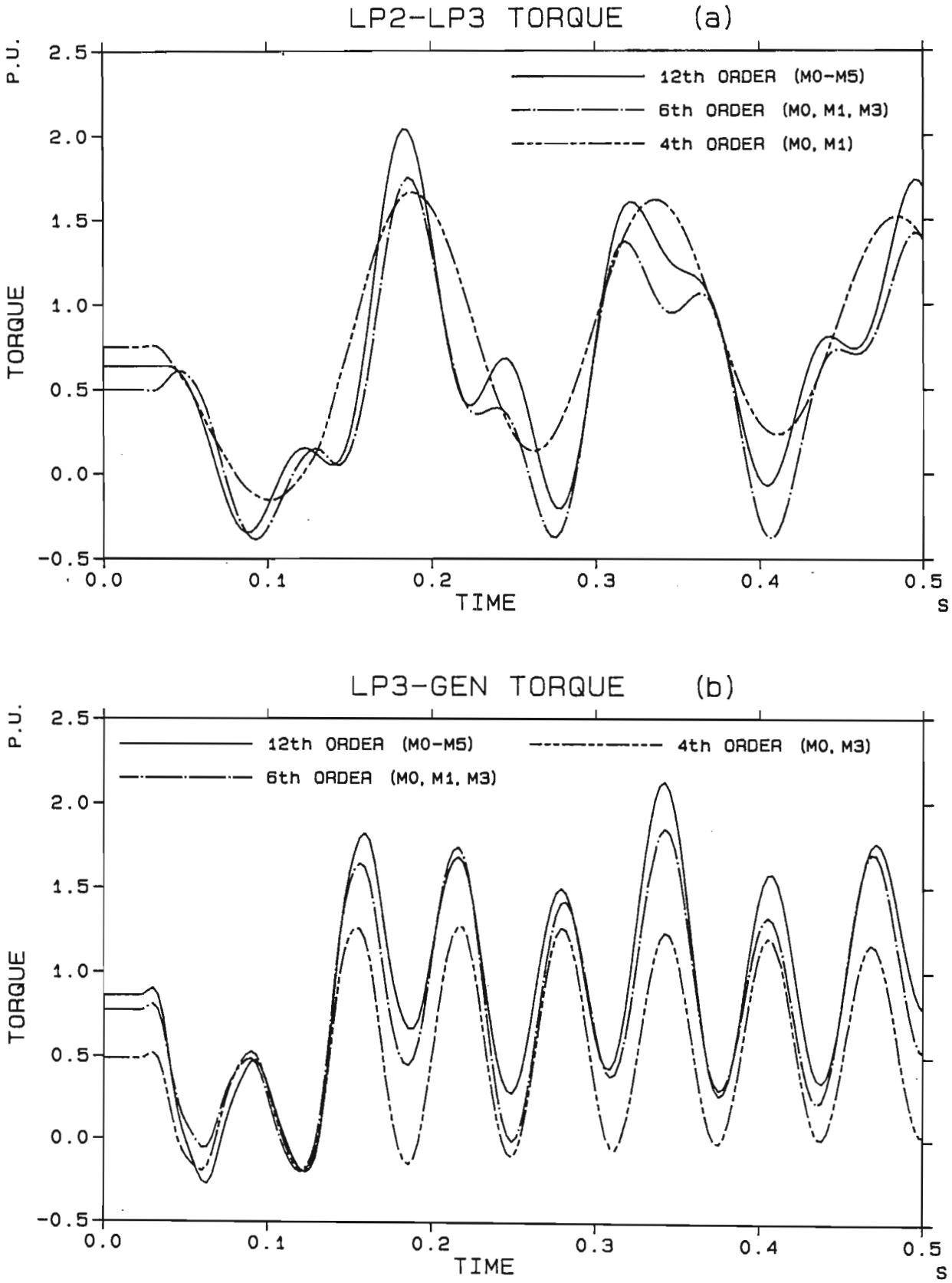

Fig 4.12 LP2-LP3 and LP3-GEN shaft torques calculated with 4th, 6th and 12th order shaft models for a 100 ms fault duration with no series compensation.

order to separate the torque amplification and torsional interaction effects, the mechanical dampings of the modes are increased so that the resultant mode dampings are the same as those of the uncompensated system in Sect 4.4.2.

The LP2-LP3 peak torque calculated with different order models and the peak torque of the mode components are shown as a function of fault duration in Fig 4.13. Under conditions of series capacitance it is difficult to make assessment of mode contributions to torque from the MTS values alone and ideally one should look at the frequency response of the transfer function between the electrical torque and the disturbance.

The effect of torque amplification can be seen by comparing Fig 4.13(b) with Fig 4.10(b). Mode 3 is amplified by a factor of between 4 and 6 while mode 2 is amplified about 3 times. Torque amplification thus affects all modes simultaneously but by different amounts depending on the tuning of the electrical system. The accuracy of the reduced order models is shown in Fig 4.13(a) and once again the 8th order model is accurate while the 4th order model gives totally unacceptable results with errors approaching 50%. The 6th order model gives reasonable results (10% to 15% error for higher torques) over most of the range except for a fault duration around 30 ms.

The results for the LP3-GEN section in Fig 4.14 show that in this case the 6th order model gives good results (less than 5% error) due to the small contribution from mode 1 compared to the amplified response of modes 2 and 3. The time response of the two shaft torques calculated with different models for a 100 ms fault appear in Fig 4.15 and the inadequacy of the reduced order models in predicting the peaks, particularly for the LP2-LP3 section, is clearly evident.

Overall the results illustrate that the determination of maximum shaft torques is a complex process which is generally not suited to using reduced order models which neglect active subsynchronous modes. Certainly a degree of reduction is possible from 12th order to 8th order by only

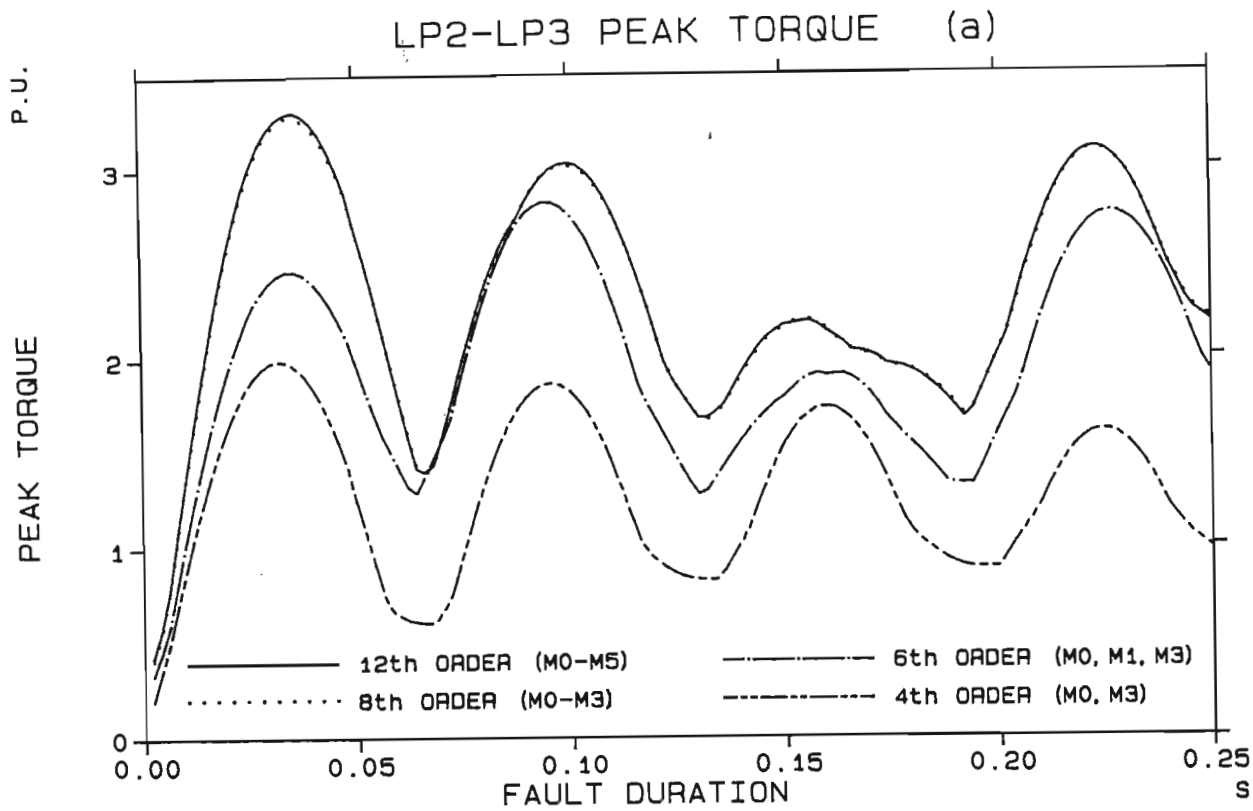

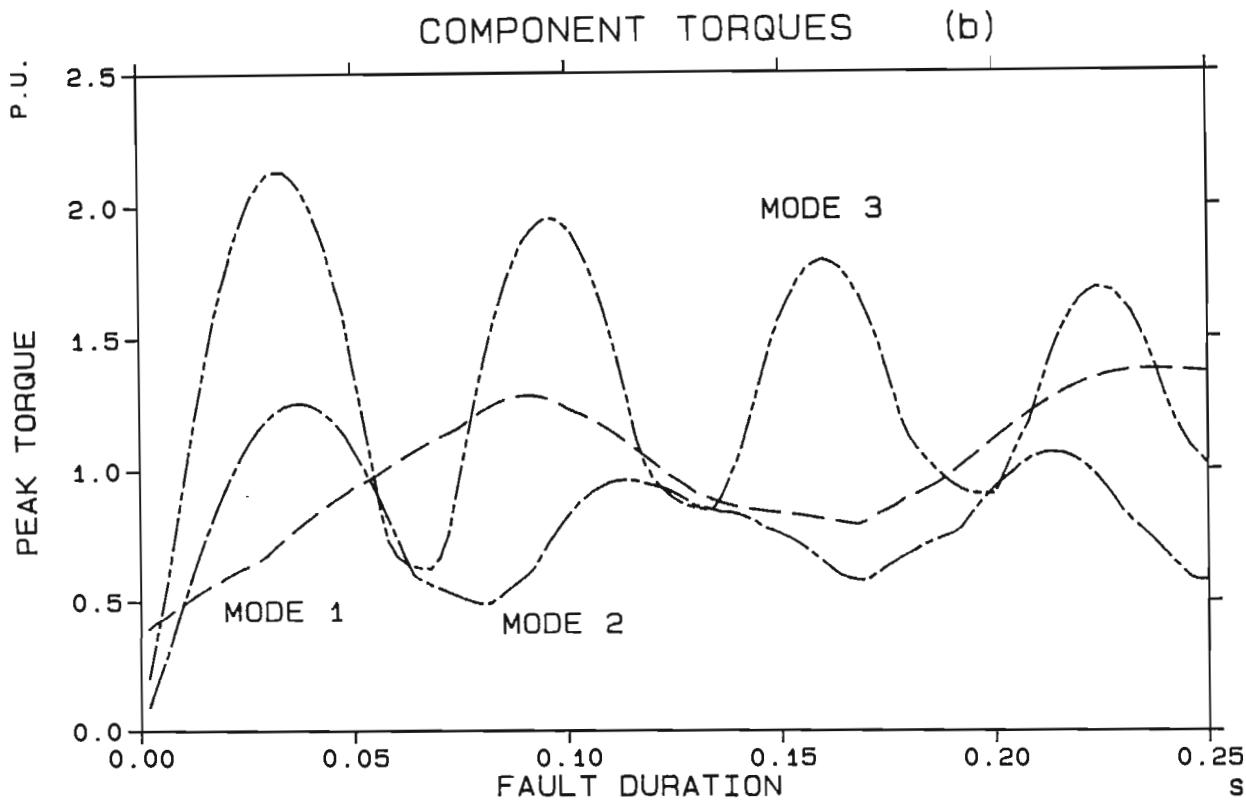

Fig 4.13 LP2-LP3 peak shaft torque calculated with different order models and the component torques due to different modes, all as a function of fault duration for a temporary three phase short circuit at the infinite bus; the compensation level is such that it produces maximum torque amplification for mode 3.

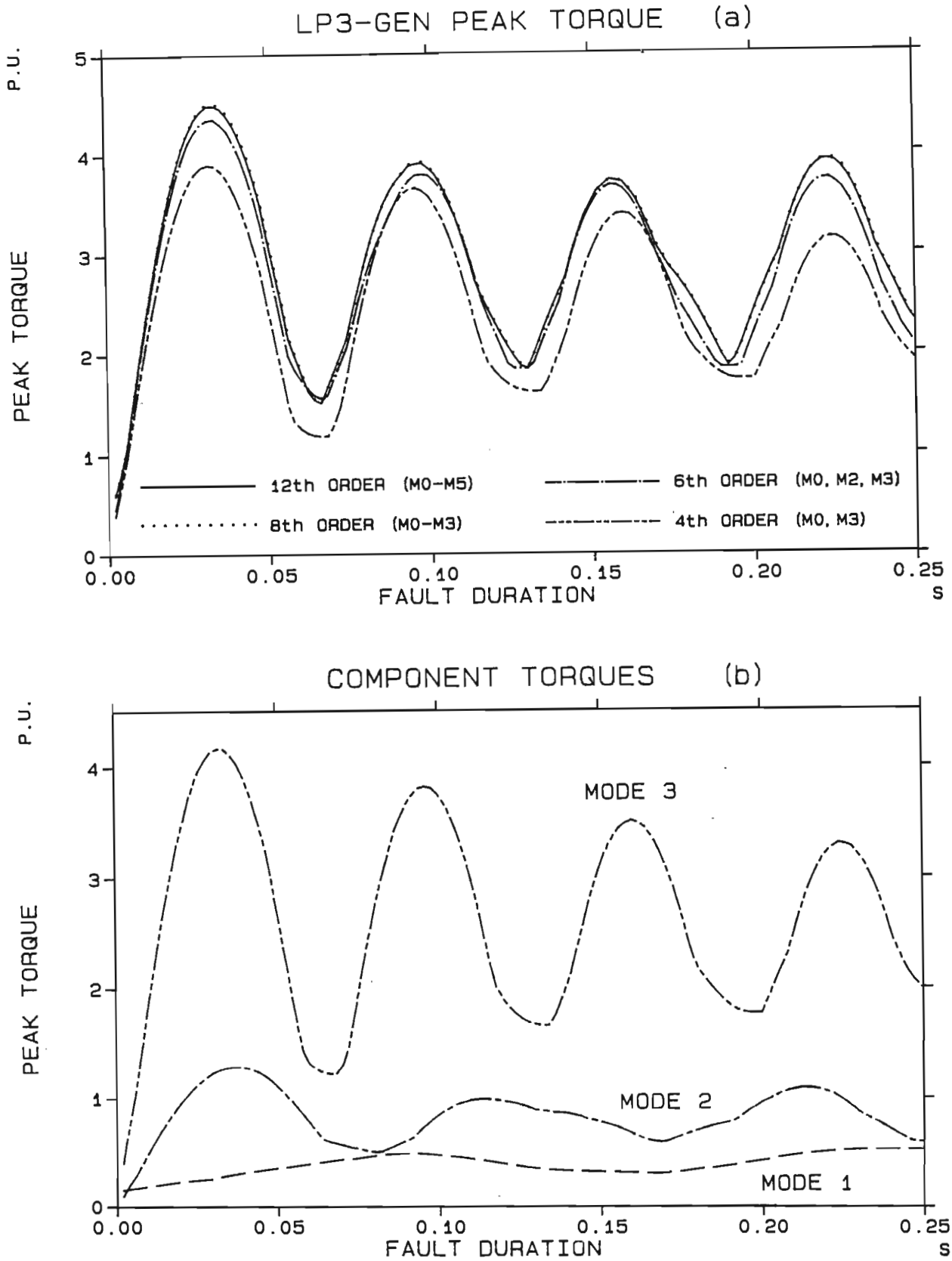

Fig 4.14 LP3-GEN peak shaft torque calculated with different order models and the component torques due to different modes, all as a function of fault duration for a temporary three phase short circuit at the infinite bus; the compensation level is such that it produces maximum torque amplification for mode 3.

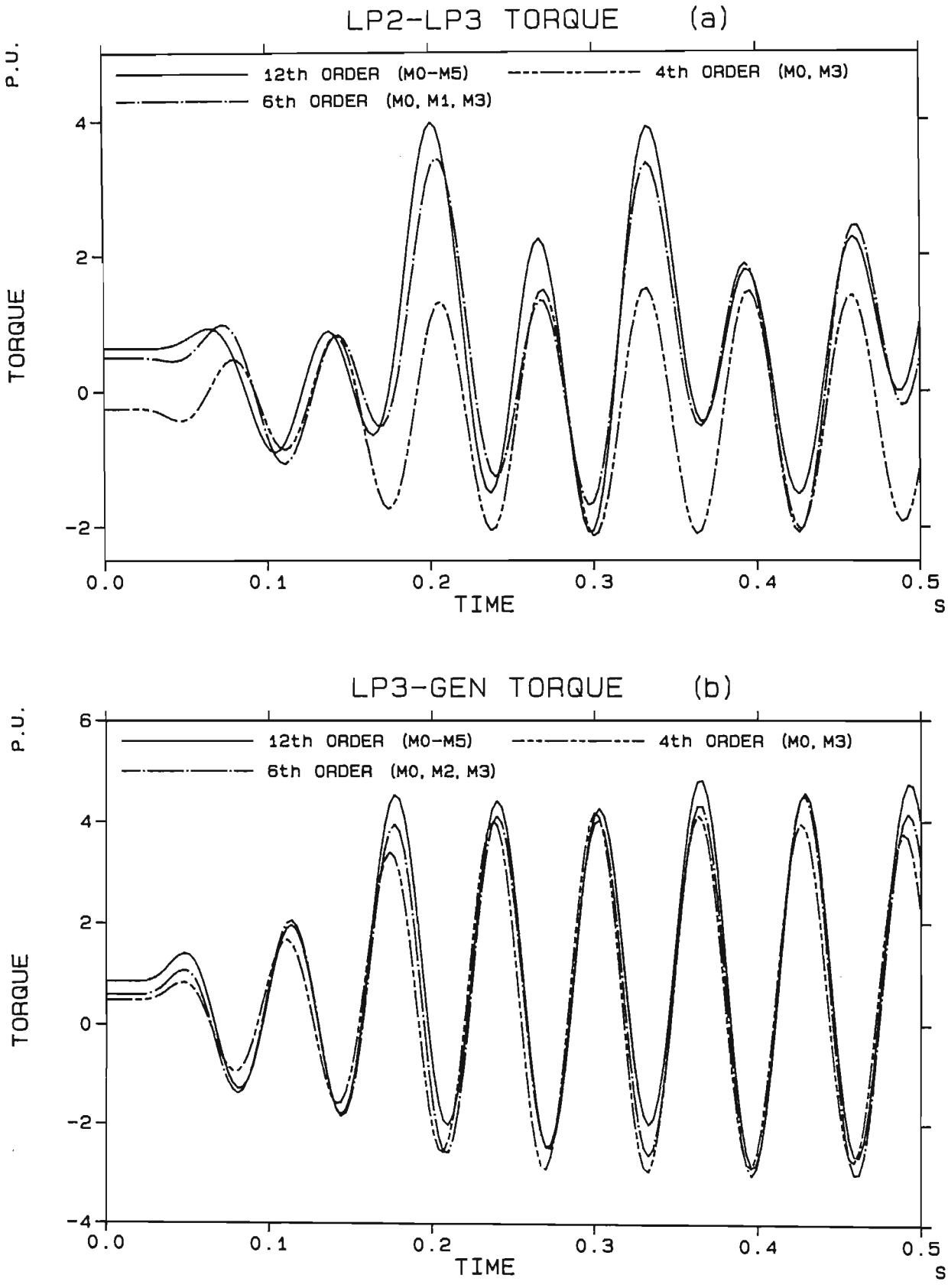

Fig 4.15 LP2-LP3 and LP3-GEN shaft torques calculated with 4th, 6th and 12th order shaft models for a 100 ms fault duration; the compensation level is such that it produces maximum torque amplification for mode 3.

considering active subsynchronous modes with accurate results being attained; however for the HP-LP1 section it would probably be necessary to include mode 4 and for the GEN-EXC section mode 5. However, the torques in these shaft sections are smaller than for the centre three sections and would probably not be a problem regarding possible shaft failure. A reduced order model (6th order for instance) can in some instances give reasonable approximations to the true values of maximum torques however this may not always be the case and each generator will have to be analysed as a separate case.

4.5 Conclusions

This chapter has investigated the possibility of using reduced order modal models of the mechanical system in small-signal and transient stability studies with particular attention to the calculation of the Critical Compensation Level (CCL) and the determination of turbogenerator shaft torques. The reduction in the order of the mechanical system is achieved by neglecting certain modes including some subsynchronous modes which interact appreciably with the electrical system (active modes).

To help in the understanding of the torsional nature of a certain shaft, parameters such as mode excitability, torsional interaction susceptibility (TIS) and mode torque susceptibility (MTS) are introduced which enable comparisons between modes of a turbogenerator and also between modes from different turbogenerators. These parameters can be used to assist in the selection of reduced order models.

The results show that for small-signal stability studies large reductions in the model order can be achieved with acceptable results still being attained. In fact, for a Koeberg turbogenerator an error of less than 2% can be achieved in the CCL with a reduction in the mechanical system order from 12 to 4; this model reduction will be of great benefit in multi-machine studies.

For transient stability calculations the possibility of model reductions is not as feasible as for small-signal stability studies. For simply determining subsynchronous stability or instability it may be possible to use reduced order models, however the results show that for the determination of accurate magnitudes of rotor variables, in particular shaft torques, not much reduction in the model order can be made before errors start becoming significant. In fact, in order to obtain results with less than 5% error one should probably always include all active subsynchronous modes, but this would depend on the particular turbogenerator shaft.

CHAPTER FIVE

DETERMINATION OF MODE PARAMETERS

5.1 Introduction

The previous two chapters have described the modal representation of a turbogenerator shaft and have discussed the usefulness of this model in power system stability studies. One of the main advantages of a modal representation is that the mode parameters can be measured thereby enabling an accurate representation of the shaft's torsional characteristics. Since many important power system phenomena such as torsional interaction and shaft torque amplification are dependant on the torsional nature of the shaft, it is important to model the shaft accurately to predict with any degree of certainty results related to these phenomena. To this end present research efforts still strive to improve the identification of the torsional characteristics of turbogenerators [44].

The process of determining mode parameters for a system is well known and has been applied in many fields to date. In power system engineering, since the first occurrence of SSR, it has become common to perform tests on turbogenerators to determine the mode parameters which characterize their torsional behaviour [28,36,37,45]. The tests which are usually performed on turbogenerators can be separated into two groups: firstly those which are performed with the generator at standstill such as

- harmonic torque excitation (as described in Ref [45]);
- engagement and disengagement of the shaft turning gear;

and secondly those performed with the machine synchronized thereby using the generator's electrical torque to excite the shaft and these include

- manual out-of-phase synchronization;
- sinusoidal variation of the exciter power output;
- a system disturbance such as series capacitor switching.

These tests are all described in detail in Refs [28,36,37,45]. The mode parameter values obtained from these tests may differ, particularly between those tests performed on an unsynchronized machine and those performed on a synchronized machine. It is important to have a clear understanding of the modal concept and the reasons for any differences that may occur between parameters from different tests before one attempts to use these mode parameters in theoretical studies.

This chapter firstly verifies that parameters used in the modal representation described in Chapter Three can be determined from measured transient data and relates these parameters to those which may be obtained from the tests described above. Although this work is not new, it is included here since it provides a more complete picture of the modal analysis concept and will help a reader not conversant in the field of modal analysis to understand the subject.

One of the main problems associated with the modal testing of turbogenerators is to separate the measured dampings into mechanical and electrical components as described in the following section. This chapter concludes by proposing a method whereby this separation can be performed.

5.2 Mechanical Modes and System Modes

It is important to understand that two different torsional systems exist for a turbogenerator; one when the generator is synchronized to the electrical network and the other when it is not synchronized.

The mechanical system of an unsynchronized generator can be represented by the torsional spring-mass model shown in Fig 5.1. When the generator is synchronized, the torsional system effectively has an additional spring and damper between the generator and a fixed reference (the infinite busbar) represented by K_e and D_e in Fig 5.2. This spring and damper represent the synchronizing torque coefficient and the electrical damping respectively and are functions of load, system impedance, machine electrical parameters and frequency [11]. This means that a different set of mode dampings, mode shapes, mode inertias and mode frequencies exist for the generator when synchronized and when unsynchronized. In order to distinguish between these two cases, the mode parameters related to the unsynchronized generator are referred to in this chapter as mechanical modes and are denoted by a subscript 'm' while those related to the synchronized generator are referred to as system modes and are denoted by a subscript 's'.

To illustrate the differences which may occur between mechanical and system modes, the following example is given. The theoretical mechanical mode parameters of the Koeberg turbogenerator shaft, determined from the physical model parameters, appear in Appendix I and are restated here in Table 5.1 for convenience.

Table 5.1 Mechanical mode parameters for the Koeberg turbogenerator

		Mode					
		0	1	2	3	4	5
f_{mi}	(Hz)	0.0	6.68	12.37	15.84	17.49	92.59
σ_{mi}	(s^{-1})	0.785	0.785	0.785	0.785	0.785	0.785
J_{Mi}	(p.u.)	3.62E-2	1.72E-2	1.28E-2	9.71E-3	1.24E-3	2.31E-4
MODE SHAPES	HP	1.00	-1.00	1.00	-0.52	1.00	0.00
	LP1	1.00	-0.83	0.43	-0.04	-0.14	-0.00
	LP2	1.00	-0.17	-0.85	0.31	0.06	0.00
	LP3	1.00	0.67	-0.01	-0.64	-0.03	-0.00
	GEN	1.00	0.95	0.75	0.97	0.03	0.05
	EXC	1.00	0.96	0.76	1.00	0.03	-1.00

Now consider the Koeberg generator connected to an infinite busbar through an uncompensated transmission line of impedance 0.02+j0.2 p.u. and with the infinite busbar operating point at V_b = 1.0 p.u., P_b = 0.6 p.u. and Q_b = 0.2 p.u. The turbogenerator torsional system now appears as in Fig 5.2; the mode parameters for this system are determined from the eigenvalues and eigenvectors of the full linearized system equations (Appendix C). The system mode dampings and frequencies are obtained from the eigenvalues while the system mode shapes are obtained from the eigenvectors and these all appear in Table 5.2. The system mode inertias are not readily obtained from the small-signal calculations and are difficult to obtain from measurements on the system.

Table 5.2 System mode parameters for the Koeberg turbogenerator synchronized to an infinite bus

		Mode					
		0	1	2	3	4	5
f_{si} (Hz)		1.09	6.90	12.47	16.02	17.49	92.59
σ_{si} (s^{-1})		1.541	0.928	0.847	0.831	1.052	0.787
MODE SHAPES	HP	1.00	-1.00	1.00	-0.50	1.00	0.00
	LP1	0.99	-0.82	0.42	-0.02	-0.14	-0.00
	LP2	0.97	-0.13	-0.86	0.27	0.06	0.00
	LP3	0.93	0.73	0.04	-0.59	-0.03	-0.00
	GEN	0.88	0.95	0.73	0.97	0.03	0.05
	EXC	0.88	0.95	0.74	1.00	0.03	-1.00

The electrical spring coefficient K_e is much smaller than the mechanical spring constants for the shaft so the differences in mode frequencies and mode shapes between the system modes and mechanical modes are not so significant. The most obvious difference occurs for mode 0 which has a frequency of 0 Hz in the unsynchronized case whereas in the synchronized case its frequency is 1.09 Hz. Similarly for the mode shape, mode 0 shows the largest difference between the system and mechanical mode with a difference in the deflections at the GEN and EXC locations of 12% of the maximum deflection. However, for the torsional modes the differences in

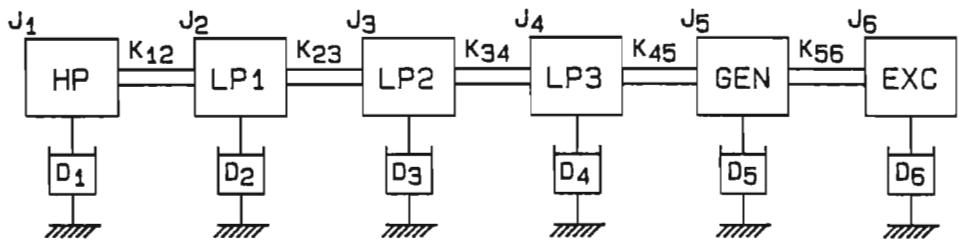

Fig 5.1 Torsional model of an unsynchronized turbogenerator.

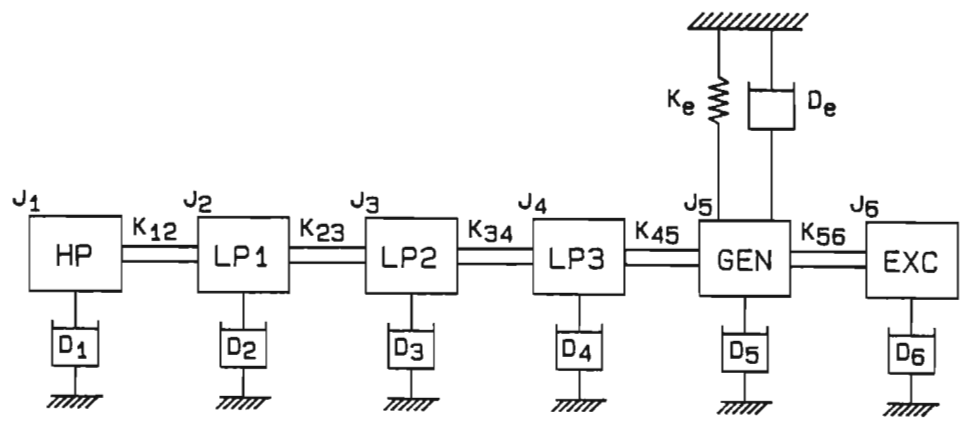

Fig 5.2 Torsional model of a synchronized turbogenerator.

frequency and mode shape between system and mechanical modes are not as severe.

The electrical damping D_e presents a different problem though since its value may not be small in comparison to the mechanical dampings of the shaft. It is useful to consider the system mode damping σ_{si} and the mechanical mode damping σ_{mi} to be related by the following equation:

$$\sigma_{si} = \sigma_{mi} + \sigma_{ei}$$

where σ_{ei} is the contribution to the system mode damping from the electrical damping D_e. Thus the dampings of the system modes, being a combination of the electrical and mechanical dampings, may be quite different from those of the mechanical modes. This difference is clearly evident in comparing the mechanical and system modes in Tables 5.1 and 5.2 and could be even greater if series capacitors were present.

The mechanical mode frequencies, inertias and mode shapes are constants while the mechanical mode dampings vary with load (due to steam forces) and strain level. However, at a particular steady-state load level even the mechanical mode dampings are constant. The system mode parameters, in contrast, are not constants but depend on the operating point, network configuration and the presence of any controllers.

The mode parameters required to be used in the modal model as described in Chapter Three are those pertaining to the mechanical modes and not those pertaining to the system modes. The error incurred if system mode frequencies and system mode shapes are used instead of mechanical mode values may not be significant (except perhaps for mode 0), however it is important to ensure that the damping values used are not system mode dampings but mechanical mode dampings. The use of system mode dampings will result in the electrical component of the damping being represented twice in any subsequent mathematical simulation. In some applications such as shaft torque calculations, the modal model of the shaft is used in a two-step process where the generator torque is first calculated using an

electrical transient program and this torque time record is then applied as a disturbance to a mechanical transient program [29]. In such cases where the electro-mechanical interaction of the torsional modes is not represented, it is necessary to use the system mode parameters in the modal model.

Measurements taken on an unsynchronized generator, such as those mentioned in the first group in the previous section, provide information related to mechanical modes. Those tests performed on a synchronized generator using the electrical torque to excite the generator shaft provide information related to system modes. Direct measurement of mechanical mode parameters on a synchronized generator requires the electrical torque to be measured (or defined) so that the mechanical system can be isolated from excitation point to response point. This aspect is discussed further in a later section.

5.3 Mode Parameter Extraction Process

It should be noted that no practically measured transient results on a turbogenerator were available. Instead, transient results were theoretically predicted by computer simulation and these were taken to represent actual measured results. The 'measurements' were thus noise free and enabled easy digital processing. This is not meant to belie the actual difficulty associated with obtaining good noise-free measurements on a real turbogenerator.

Mode parameters are extracted from the 'measured' transient data using the Hewlett-Packard Modal Analysis Software Package [46] on a Hewlett-Packard 5451B Fast Fourier Analysis System. The extraction technique is well known and the theory involved will not be described here. The Modal Analysis Package determines the transfer function between a time-domain transient excitation signal and a time-domain transient response signal using Fast Fourier Transform techniques. It then analytically curve-fits this transfer function to a known transfer function equation where the

parameters in this equation are the required mode parameters. This process is more fully described in Appendix E.

In the following sections, transient results are calculated for a turbogenerator of known mode parameters (given in Table 5.1) and the mode parameters are obtained from the transient results using the above-mentioned extraction techniques.

5.4 Unsynchronized Generator

The first test considers the generator to be at standstill and a short duration step torque is applied at the HP turbine. This test represents the engagement of the shaft turning gear at a particular location on the shaft. The actual nature of the torque and the position of application will differ in a practical test. The speed at each inertia stage along the rotor is calculated and the transfer function between speed and torque excitation $\omega_i(s)/T(s)$ is determined for each speed ω_i as shown in Fig 5.3. In practice it is not possible to measure the speed at each rotor stage but only at a few shaft locations; this makes it impossible to determine the complete mode shape and the measurements have to be used in conjunction with the manufacturer's parameters to obtain a final mode shape. The mechanical mode parameters determined by curve fitting the transfer functions in Fig 5.3 are shown in Table 5.3 and should be compared with the parameters in Table 5.1 used to generate the transient curves.

The frequencies, dampings and mode shapes are determined accurately with a maximum error in frequency of 0.04%, a maximum error in damping of 0.2% and a maximum error in mode shape of 0.9% of the maximum deflection. There is however a fair degree of error (up to 12%) in some of the determined values of mode inertia. This can be explained by considering the torque excitation pulse and the digital representation of this pulse. Data was written to file every 5 ms (corresponding to the sampling interval in a real measurement) so the torque excitation dropped from its step value to zero in 5 ms. In the program the step actually dropped to zero in one

integration interval of 1 ms so there was an error in the step representation as shown by the shaded region in Fig 5.4.

Table 5.3 Mechanical mode parameters determined for a temporary step torque at the HP turbine

		Mode			
		1	2	3	4
f_{mi}	(Hz)	6.68	12.37	15.84	17.49
σ_{mi}	(s^{-1})	0.787	0.785	0.786	0.787
J_{Mi}	(p.u.)	1.91E-2	1.33E-2	9.84E-3	1.17E-3
MODE SHAPES	HP	-1.00	1.00	-0.52	1.00
	LP1	-0.83	0.43	*	-0.14
	LP2	-0.17	-0.85	0.31	0.06
	LP3	0.67	*	-0.64	-0.03
	GEN	0.95	0.74	0.97	0.03
	EXC	0.96	0.76	1.00	0.03

* No value obtained (approximately zero)

The magnitudes of the frequency spectrums of the accurate and approximate torque pulses over the frequency range of interest are compared in Fig 5.5. The approximate torque pulse has more energy at the mode 1 and 2 frequencies, approximately the same energy at the mode 3 frequency and less energy at the mode 4 frequency. This results in an error of 11.3% in J_{M1}, 4.2% in J_{M2}, 1.9% in J_{M3} and -5.7% in J_{M4}. This underlines the importance of correctly defining the excitation in a modal analysis study, especially with regard to mode inertia measurement.

No data was obtained for modes 0 and 5 in this test. Mode 0 is not a torsional mode and its damping and inertia can be determined by normal methods for a stiff-shaft generator; its frequency is known to be 0 Hz and its mode shape is known to be equal deflections at all elements. Mode 5 was not excited due to its very low mode excitability at the HP turbine. In order to obtain parameters for mode 5 it is therefore necessary to

excite the shaft at a different location. This is done with the step torque applied at the exciter and the transfer functions obtained are shown in Fig 5.6(a) and (b); they are very different from those shown in Fig 5.3 with the torque excitation at the HP turbine. The mode 5 parameters determined from these transfer functions are given below and should be compared with the correct mode 5 values in Table 5.1.

f_{m5} = 92.57 Hz (0.02% error)
σ_{m5} = 0.787 s^{-1} (0.14% error)
J_{M5} = 0.58E-3 p.u. (152% error)

Maximum error in mode shape is 0.2% of maximum deflection

The large error in the mode inertia is again due to the incorrect representation of the torque pulse. Although these results serve to show that mode parameters can be determined from excitation tests, in practice it is nevertheless difficult to generate a broadband excitation force with sufficient energy across the frequency spectrum of interest. One way of doing this is to use the electrical torque of the generator to excite the shaft, but to achieve this, the generator has to be synchronized to a fixed supply.

5.5 Synchronized Generator

In this section the generator is synchronized and the shaft is excited by the electrical torque of the generator following a system disturbance. As mentioned in Sect 5.2, the synchronized generator has a different set of mode parameters to those of the unsynchronized generator. After a disturbance, the system will respond according to the frequencies and dampings of the system modes (as determined by the system eigenvalues) and not those of the mechanical modes. Frequency analysis of the transient response waveforms will provide the system mode frequencies while band-pass filtering these signals at the system mode frequencies will provide system mode dampings.

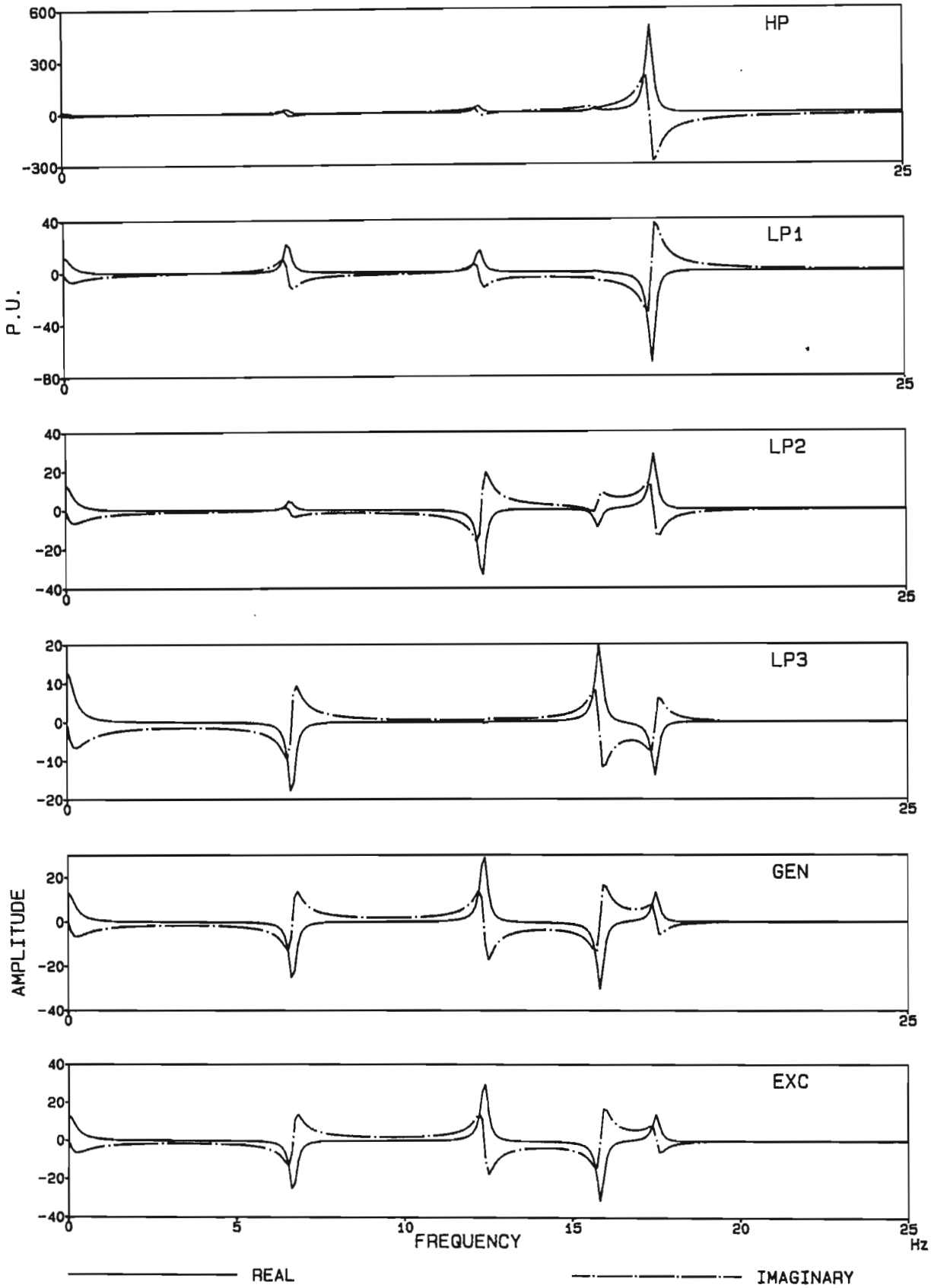

Fig 5.3 Transfer functions between torque excitation and shaft speeds for a temporary step torque at the HP turbine.

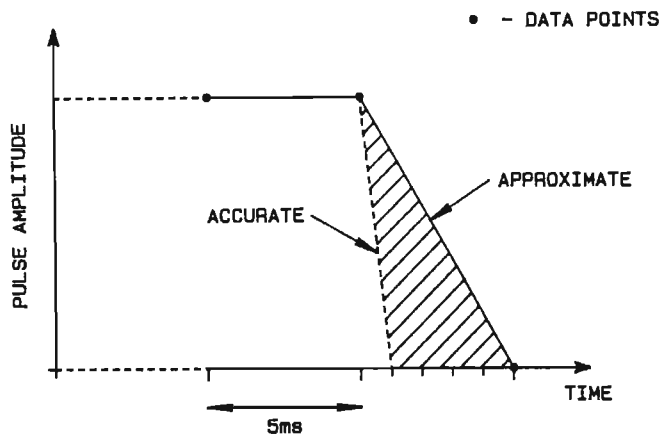

Fig 5.4 Error in the torque pulse representation due to the difference in the integration time-step and the period with which data was written to disc (sampling interval).

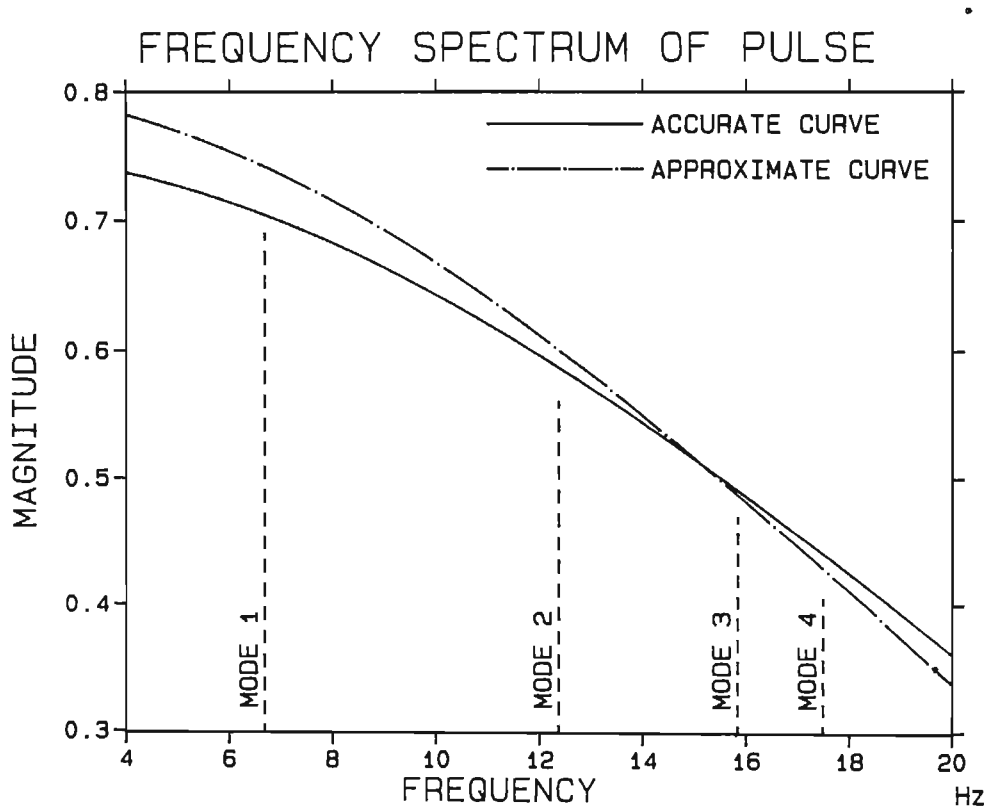

Fig 5.5 Comparison of the frequency spectrums of the accurate and approximate torque pulse.

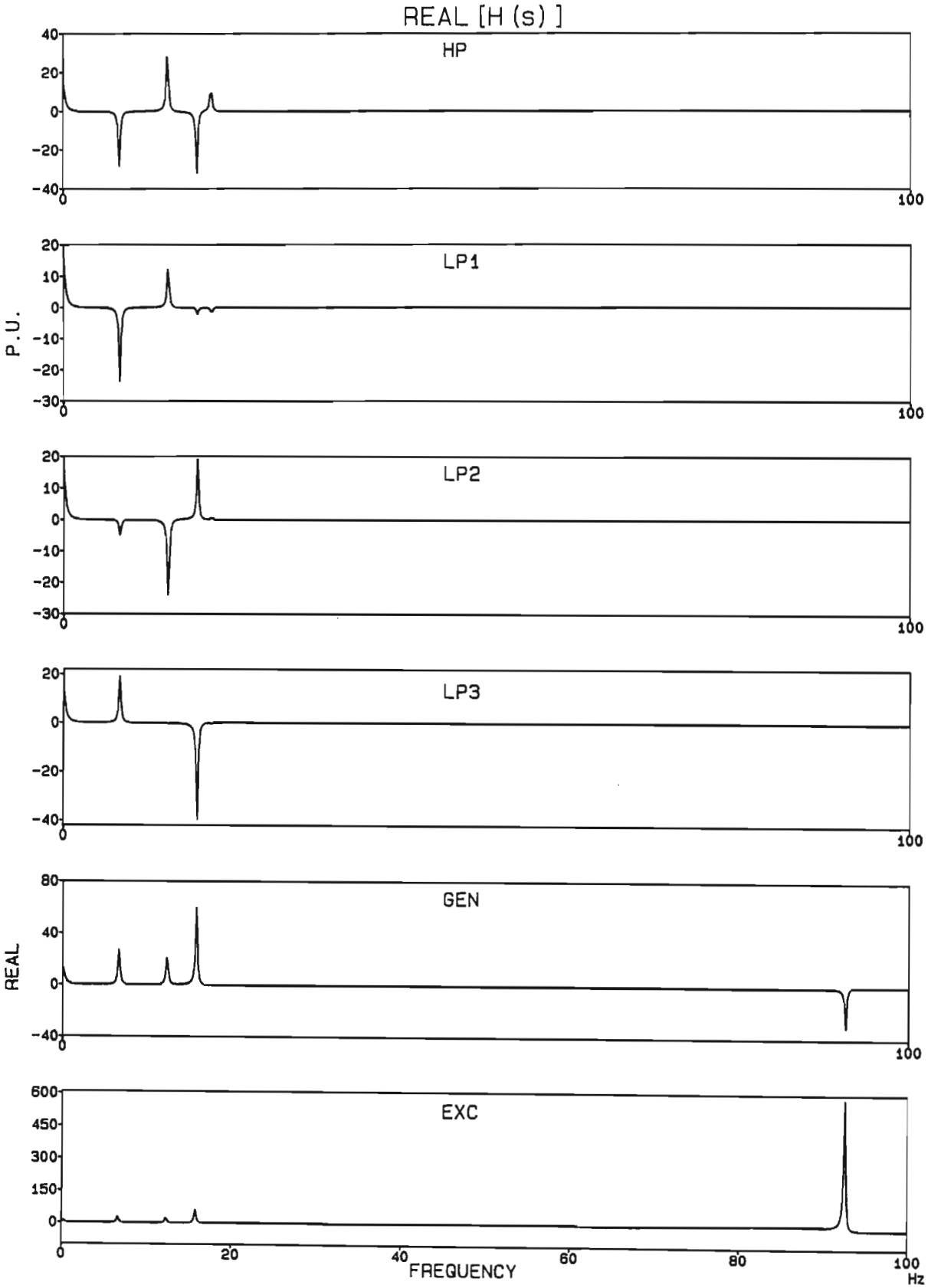

Fig 5.6 (a) Real part of the transfer functions between torque excitation and shaft speeds for a temporary step torque at the exciter.

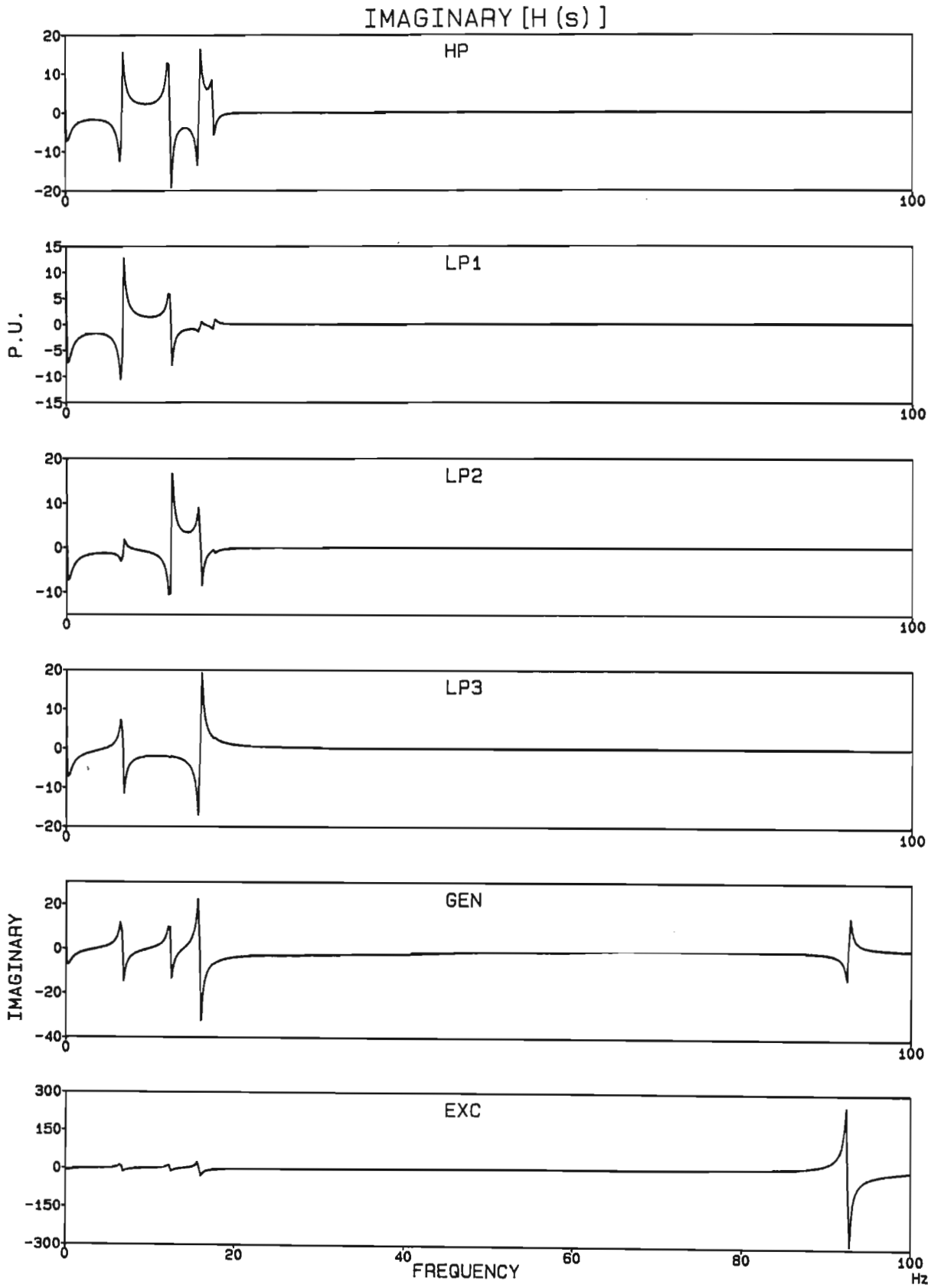

Fig 5.6 (b) Imaginary part of the transfer functions between torque excitation and shaft speeds for a temporary step torque at the exciter.

To directly measure the mechanical mode parameters, it is necessary to take a transfer function between the torque signal exciting the shaft (the electrical torque) and the response signals; this requires the electrical torque to be known. Direct measurement of the electrical torque is very difficult but it can be estimated from measurements of generator terminal electrical quantities or from torsional monitoring equipment if available [47,48].

Numerous results were computed with the generator synchronized and the transfer functions calculated between the rotor speeds ω_i and the electrical torque; it was not necessary to deduce the electrical torque since it was available as an output from the simulation program. A typical set of transfer functions obtained is shown in Fig 5.7(a) and (b) and they are similar, both in frequency content and magnitudes (except for mode 5), to those in Fig 5.6 obtained with the torque applied at the exciter. From the numerous results taken, two selected examples are presented below; for both cases the fault considered was a permanent 5% drop in the infinite bus voltage. The network considered is the same single-generator-infinite-bus system considered in the previous three chapters (shown in Fig 2.1), the parameters for which are given in Appendix I.

(1)-Generator at no-load with series compensated transmission line; for this test the infinite bus real power was 0.01 p.u. and a series capacitance of 0.48 p.u. was included in the transmission line. The system modes for these conditions are calculated from the linearized system equations (Appendix D) using the mechanical mode parameters in Table 5.1 and appear in Table 5.4 below.

Table 5.4 System modes as determined by eigenvalues for the generator at no-load and with a series capacitance of 0.48 p.u.

	Mode					
	0	1	2	3	4	5
f_{si} (Hz)	0.81	6.81	12.44	16.01	17.49	92.59
σ_{si} (s^{-1})	1.502	0.809	0.748	0.457	0.785	0.787

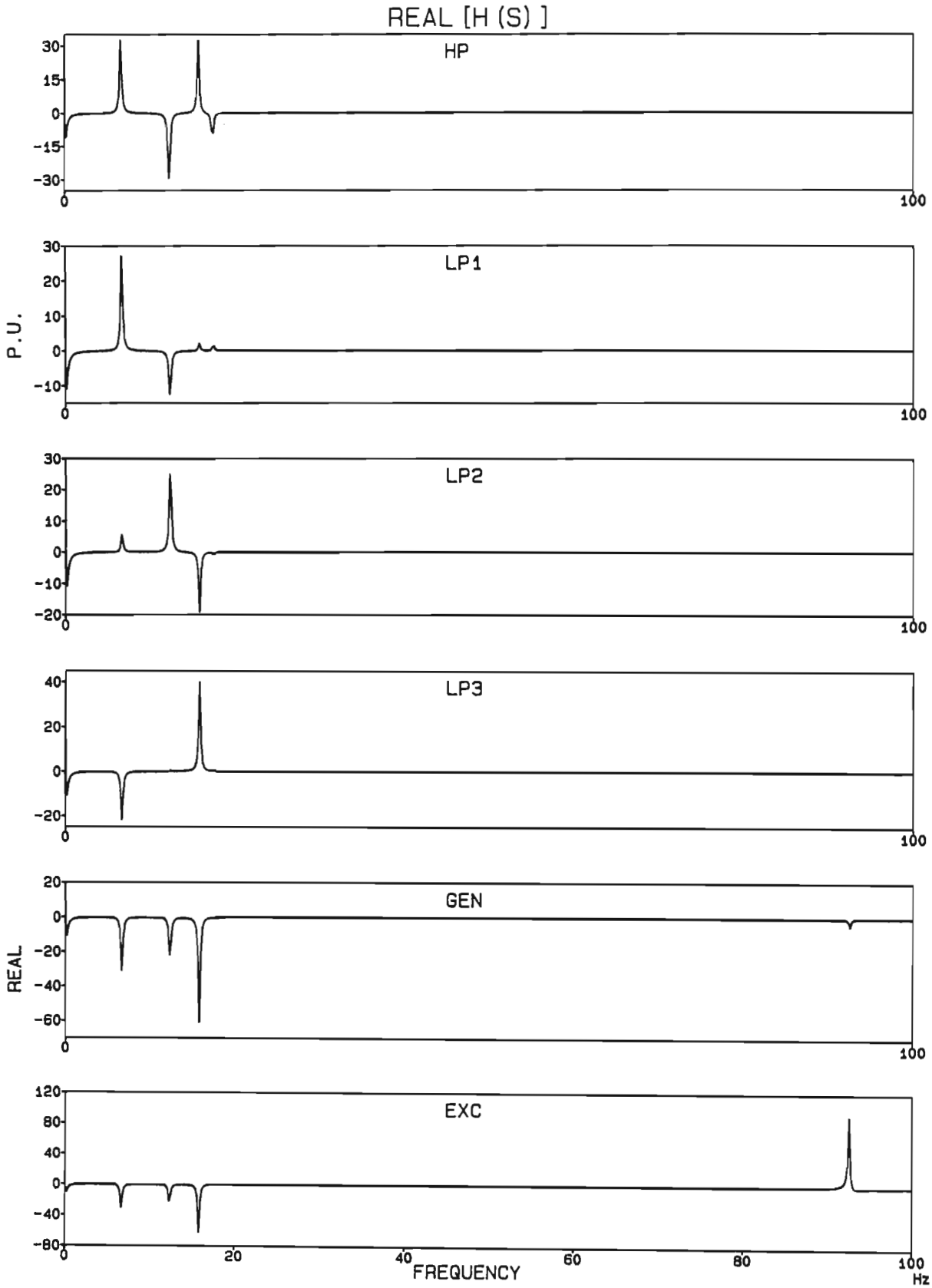

Fig 5.7 (a) Real part of the transfer functions obtained between electrical torque and shaft speeds.

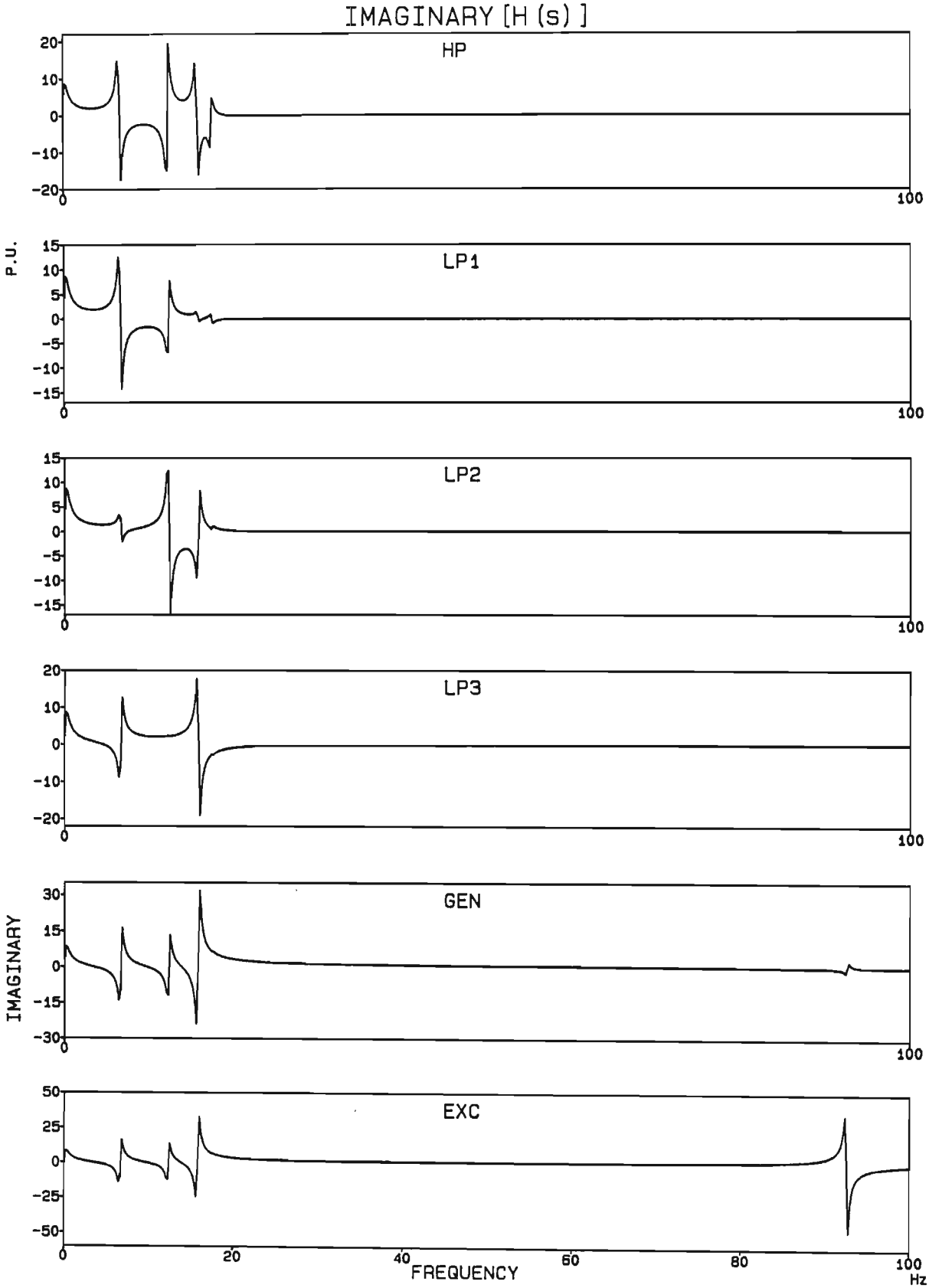

Fig 5.7 (b) Imaginary part of the transfer functions obtained between electrical torque and shaft speeds.

The series capacitance results in a negative electrical contribution to the system mode 3 damping which is 0.457 s^{-1} compared to the 0.785 s^{-1} of the mechanical mode. The frequencies and dampings in Table 5.4 determine the system behaviour following a disturbance; these are the parameters which would be obtained from tests such as the sinusoidal modulation of the exciter power and the band-pass filtering of shaft speed signals following a system disturbance or manual synchronization [28,36,37]. The mode parameters determined from the 'measured' transfer functions between rotor speeds and electrical torque are shown in Table 5.5.

Table 5.5 Mechanical mode parameters determined from 'measured' transfer functions for generator at no-load with series capacitance

Mode	f_{mi} (Hz)	Error (%)	σ_{mi} (s^{-1})	Error (%)	J_{Mi} (p.u.)	Error (%)
1	6.68	0.01	0.786	0.03	1.70E-2	0.70
2	12.37	0.01	0.785	0.06	1.28E-2	0.00
3	15.84	0.00	0.779	0.82	9.68E-3	0.30
4	17.49	0.01	0.784	0.19	*	*
5	92.59	0.00	0.768	2.22	*	*

Mode shapes: maximum error = 1.0% of the maximum deflection

* Unable to obtain value

Due to the low excitability of modes 4 and 5 from the generator rotor, data obtained for these modes may not be reliable; in this case, the frequencies and dampings are determined accurately, but in a practical measurement the presence of noise and the inability to excite these modes with sufficient energy will probably prevent any parameters being determined for them. Even without noise it was not possible to determine the inertia of these modes. This problem with modes 4 and 5 is not serious since it has been shown that they are not important in an SSR stability study and it is only necessary to obtain parameters for modes 1 to 3.

Table 5.5 shows that the mechanical mode 1 to 3 parameters are determined accurately. This proves that if the transfer function is taken between the electrical torque and the rotor variable then the mechanical system is isolated and the identified mode parameters are those due solely to the mechanical system.

(2)-Generator at load with series compensated transmission line; for this test the infinite bus (see Fig 2.1) real power was 0.6 p.u., the reactive power was 0.2 p.u. and a series capacitance of 0.43 p.u. was included. For these conditions, the system mode frequencies of the first three torsional modes were 6.83, 12.46 and 16.04 Hz while the corresponding dampings were 0.813, 0.772 and 0.490 s^{-1}. The mechanical mode parameters identified from the 'measured' transfer functions appear in Table 5.6.

Table 5.6 Mechanical mode parameters determined from 'measured' transfer functions for generator at load with series capacitance

Mode	f_{mi} (Hz)	Error (%)	σ_{mi} (s^{-1})	Error (%)	J_{Mi} (p.u.)	Error (%)
1	6.68	0.01	0.821	4.6	1.71E-2	0.47
2	12.37	0.00	0.826	5.2	1.27E-2	0.31
3	15.84	0.01	0.802	2.1	9.77E-3	0.55

Mode shapes: maximum error = 1.3% of the maximum deflection

In this case with the generator at load, the identification of the mechanical mode dampings was not as accurate as for the generator at no-load. Nevertheless, an error of 5.2% in the determined damping is not excessive.

These results have shown how mechanical mode parameters can be obtained for a turbogenerator from transient response data recorded when the machine is excited from the electrical system. The major limitation of this method is the requirement that the electrical torque should be known accurately. This is not easy due to saturation and other non-linear effects within the

generator and it has already been seen how an ill-defined excitation signal can affect the accuracy of the results. In order to overcome this problem, a method is suggested in the next section whereby mechanical mode parameters can be determined from measured system mode parameters thereby eliminating the need to determine the electrical torque accurately.

5.6 Determining Mechanical Modes from System Modes

System mode parameters are much easier to determine accurately than mechanical mode parameters and are therefore the parameters most commonly determined in power station tests [28,36,37]. Such tests normally provide the system mode frequencies, f_{si}, system mode dampings, σ_{si} and some information about the system mode shapes $\underline{Q}_{si}$. This section proposes a method to determine the mechanical mode parameters by an eigenvalue-eigenvector scanning program which scans the mechanical mode parameters f_{mi}, σ_{mi} and $\underline{Q}_{mi}$ until the calculated system mode parameters are the same as the measured values. The measured system mode parameters can be used as the starting point for the mechanical mode parameters; convergence is fast and does not even require a good initial estimate of the mechanical parameter values. The eigenvalue-eigenvector scanning program calculates f^*_{si}, σ^*_{si} and $\underline{Q}^*_{si}$ and uses the errors $f^*_{si}-f_{si}$, $\sigma^*_{si}-\sigma_{si}$ and $\underline{Q}^*_{si}-\underline{Q}_{si}$ to update the mechanical mode parameters f_{mi}, σ_{mi} and $\underline{Q}_{mi}$.

Nevertheless one remaining problem is that the eigenvalue-eigenvector scanning method does not give any information about the mode inertias. The system mode damping σ_{si} is determined by the mechanical and electrical components of damping $(\sigma_{mi}+\sigma_{ei})$, and the electrical component σ_{ei} in turn depends on the value of the the mode inertia J_{Mi}. Hence, a particular value of J_{Mi} determines σ_{ei} which then determines the value of σ_{mi} obtained from the scanning program. It is thus necessary to be able to determine the mode inertia as well, or else the mechanical mode damping determined will be in error. The mode inertias are obtained by attempting to digitally regenerate the 'measured' transient response waveforms using the last updated values of mechanical mode parameters; the calculated and

'measured' waveforms then both then have the same frequency and damping content. The FFT of the calculated response is then compared to the FFT of the 'measured' response. Since the mode inertia determines the amplitude of oscillation of a particular mode, the mode inertias can be adjusted by the ratio of the frequency peaks of the two FFTs. The process can be summarized as follows where the superscript 'j' denotes the j'th iteration:

1) Measure the system mode parameters f_{si}, σ_{si} and $\underline{Q}_{si}$;

2) Assume initial values J^0_{Mi}, $f^0_{mi} = f_{si}$, $\sigma^0_{mi} = \sigma_{si}$ and $\underline{Q}^0_{mi} = \underline{Q}_{si}$;

3) Use the last updated values of mechanical mode parameters J^j_{Mi}, f^j_{mi}, σ^j_{mi} and $\underline{Q}^j_{mi}$ in the scanning program to obtain f^{j+1}_{mi}, σ^{j+1}_{mi} and $\underline{Q}^{j+1}_{mi}$;

4) Use J^j_{Mi}, f^{j+1}_{mi}, σ^{j+1}_{mi} and $\underline{Q}^{j+1}_{mi}$ to calculate the transient response and from the FFT of the transient response obtain J^{j+1}_{Mi};

5) Repeat 3) and 4) until a specified convergence criterion is achieved.

The process is illustrated by way of an example. The generator is assumed to be at the same operating point as in example 2 of Sect 5.5 (P_b = 0.6 p.u., Q_b = 0.2 p.u., X_c = 0.43 p.u.) and the system is subjected to a 5% drop in the infinite bus voltage for a duration of 70 ms. The resulting generator and HP turbine speeds are shown in Fig 5.8. In order to check the accuracy of the method it is initially assumed that the system mode parameters are known exactly so that any error that may result in the identified mechanical mode parameters can be ascribed to the identification method rather than to initial errors in determining the system mode parameters. The system mode parameters as determined from the system eigenvalues and eigenvectors appear below in Table 5.7.

Table 5.7 System mode parameters for the generator at load and with series capacitance

		Mode					
		0	1	2	3	4	5
f_{si} (Hz)		0.920	6.832	12.456	16.038	17.493	92.593
σ_{si} (s^{-1})		1.164	0.813	0.772	0.490	1.059	0.787
MODE SHAPES	HP	1.00	-1.00	1.00	-.50	1.00	.00
	LP1	1.00	-.83	.42	-.02	-.14	-.00
	LP2	.98	-.14	-.86	.27	.06	.00
	LP3	.95	.71	.03	-.59	-.03	-.00
	GEN	.92	.95	.73	.97	.03	.05
	EXC	.92	.96	.75	1.00	.03	-1.00

The mechanical mode 0 frequency and mode shape are not fitted since they are known (f_{m0} = 0 Hz, $\underline{Q}_{m0} = [1,1,1,1,1,1]^T$), however information about f_{s0} can be used as discussed in Sect 5.7.

The initial mechanical mode inertias are assumed to all be equal to 0.1 p.u. and these values are used in the scanning program to determine the mechanical mode frequencies, mode dampings and mode shapes which result in the system modes in Table 5.7. The rotor speeds are then calculated using these mechanical mode parameters and the first 0.8 s of these curves for the generator and HP turbine are compared in Fig 5.9 with the true 'measured' curves; the initial time is that at which the fault is removed. In all the figures the solid curves are the true curves (or would be measured curves in practice) and the dotted curves are the fitted curves. The FFTs of these fitted curves are shown together with the FFTs of the true curves in Fig 5.10. The mode inertias are then updated from these FFTs and in order to see the effect of this update, the speed signals are recalculated with the new mode inertias and appear as the high amplitude broken curves in Fig 5.9. (This last calculation is not normally done in the process). Note the change in the system mode frequencies after the mode inertias have changed.

The updating of the mode inertias concludes the first iteration. The process is repeated 5 times and Figs 5.11 and 5.12 show the transient and FFT curves for iteration 2 and 3 (except for the FFT of the HP speed which shows iteration 2 and 5). The convergence of the mode parameters is shown in Tables 5.8, 5.9 and 5.10.

Table 5.8 Convergence of mechanical mode inertias

	Mode Inertia J_{Mi} (milli-p.u.)					
Iteration	0	1	2	3	4	5
0	100.0	100.0	100.0	100.0	100.0	100.0
1	37.05	17.12	11.94	8.703	2.251	0.236
2	35.61	17.14	12.85	9.803	1.358	0.231
3	36.40	17.14	12.69	9.700	1.294	0.230
4	36.03	17.12	12.70	9.703	1.269	0.230
5	36.21	17.15	12.70	9.706	1.256	0.230
Correct	36.17	17.16	12.77	9.713	1.241	0.231
Error (%)	0.11	0.05	0.55	0.08	1.22	0.23

Table 5.9 Convergence of mechanical mode frequencies

	Mechanical Mode Frequency f_{mi} (Hz)				
Iteration	1	2	3	4	5
0	6.832	12.456	16.039	17.493	92.593
1	6.808	12.446	16.020	17.494	92.593
2	6.680	12.366	15.814	17.493	92.591
3	6.681	12.374	15.839	17.493	92.591
4	6.680	12.373	15.837	17.494	92.591
5	6.681	12.373	15.837	17.493	92.591
Correct	6.681	12.371	15.836	17.493	92.590
Error (%)	0.00	0.00	0.00	0.00	0.00

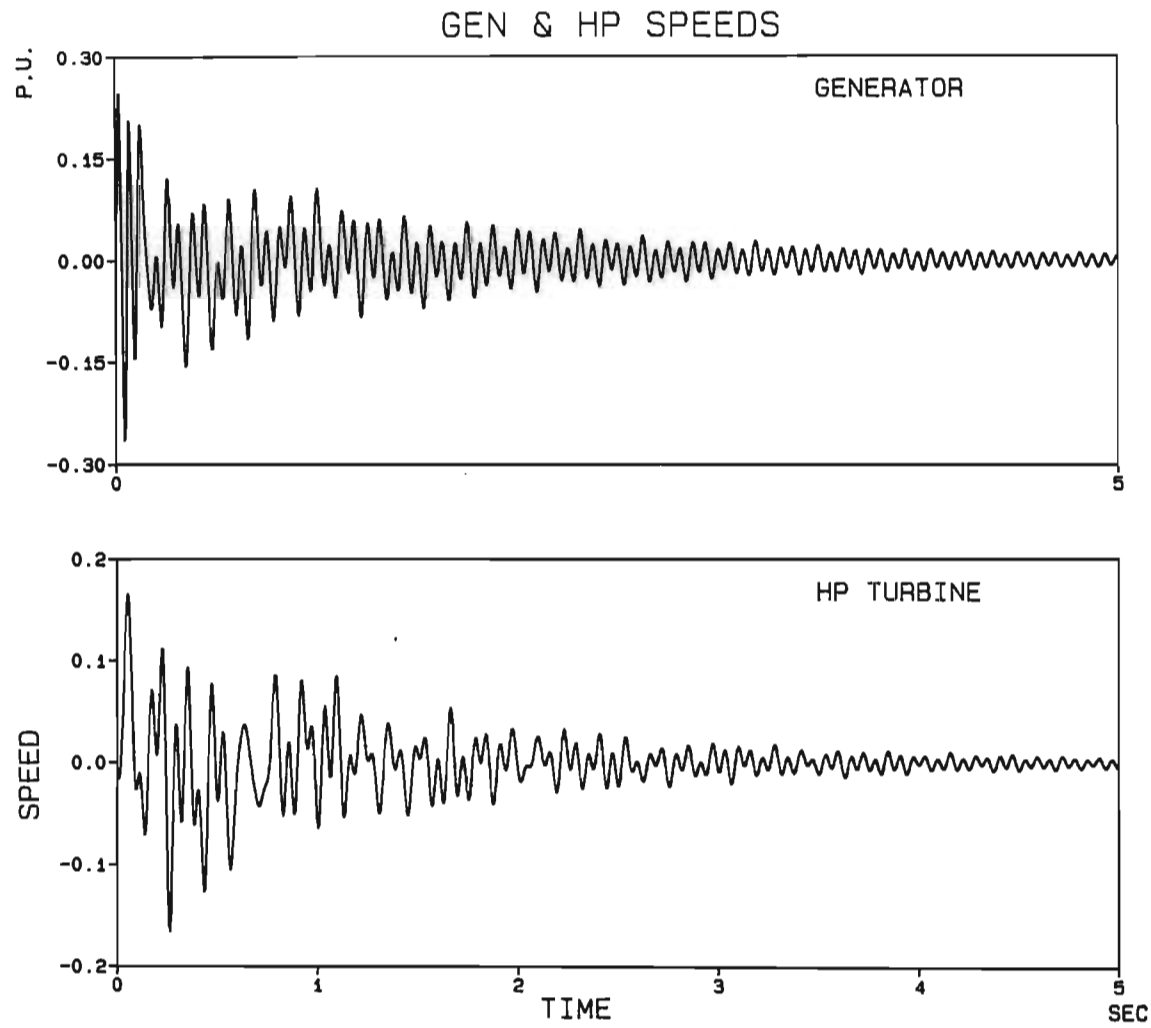

Fig 5.8 Generator and HP turbine speeds for a 5% drop in the infinite bus voltage for a duration of 70 ms when the generator is at load and with a series capacitor of 0.43 p.u. in the line; zero time is taken at fault removal.

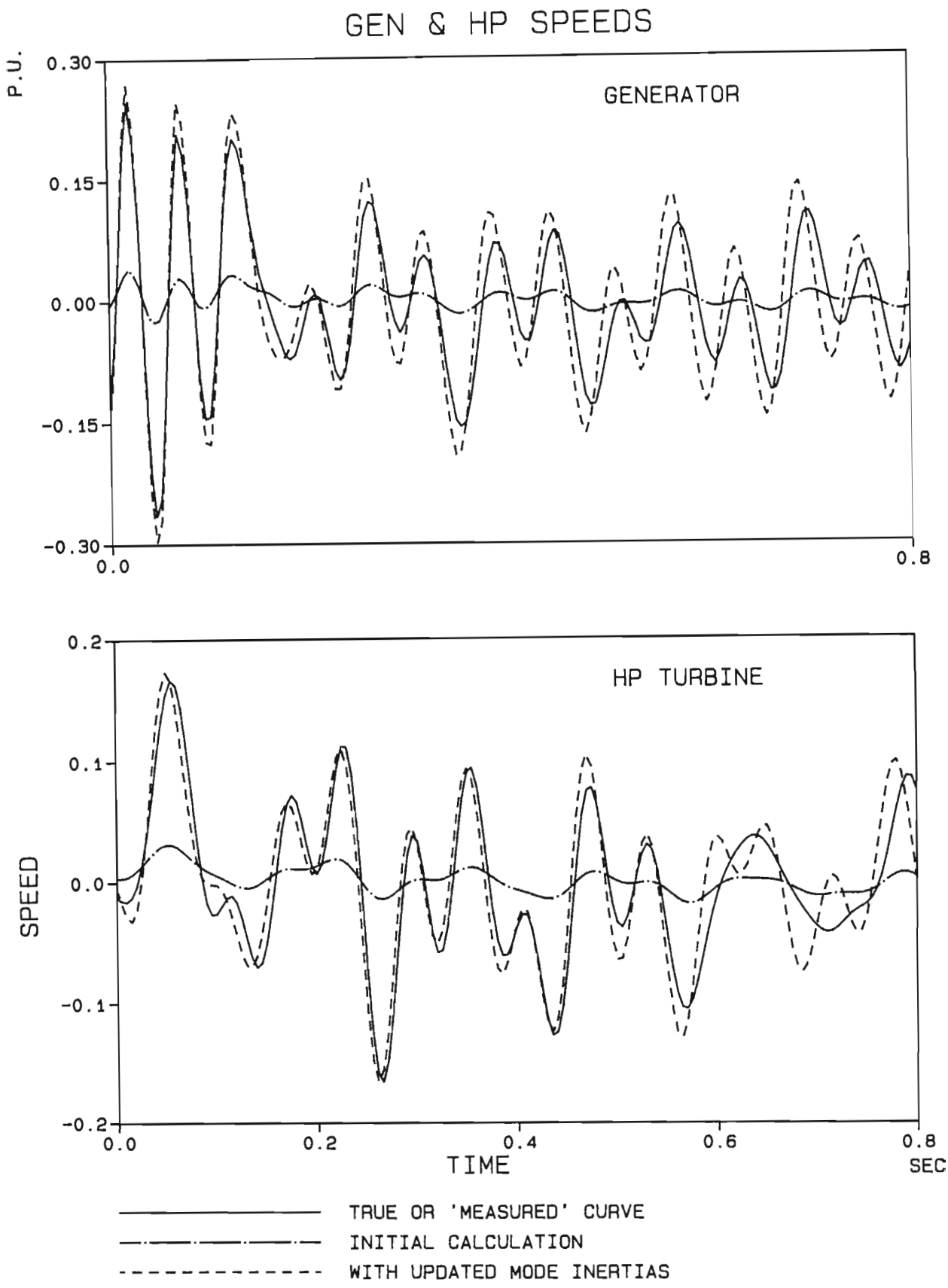

Fig 5.9 Generator and HP turbine speeds comparing the 'measured' curves, the initial fitted curves (with guessed mode inertias) and the fitted curves after the first update of mode inertias.

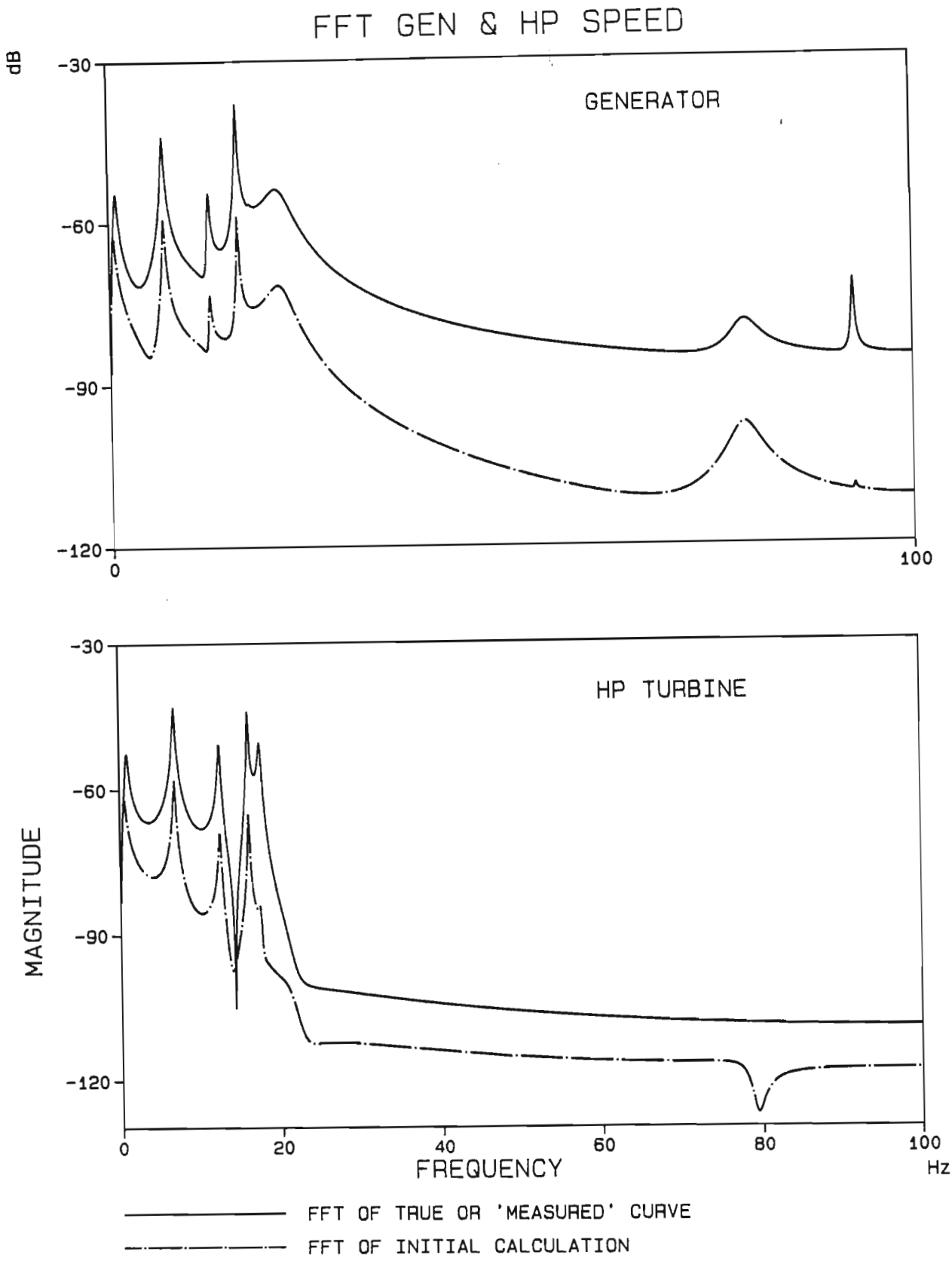

Fig 5.10 FFTs of the 'measured' generator and HP turbine speeds compared to those of the initial calculation before updating the mode inertias; the difference between the magnitudes of the peaks of these FFTs are used to update the mode inertias.

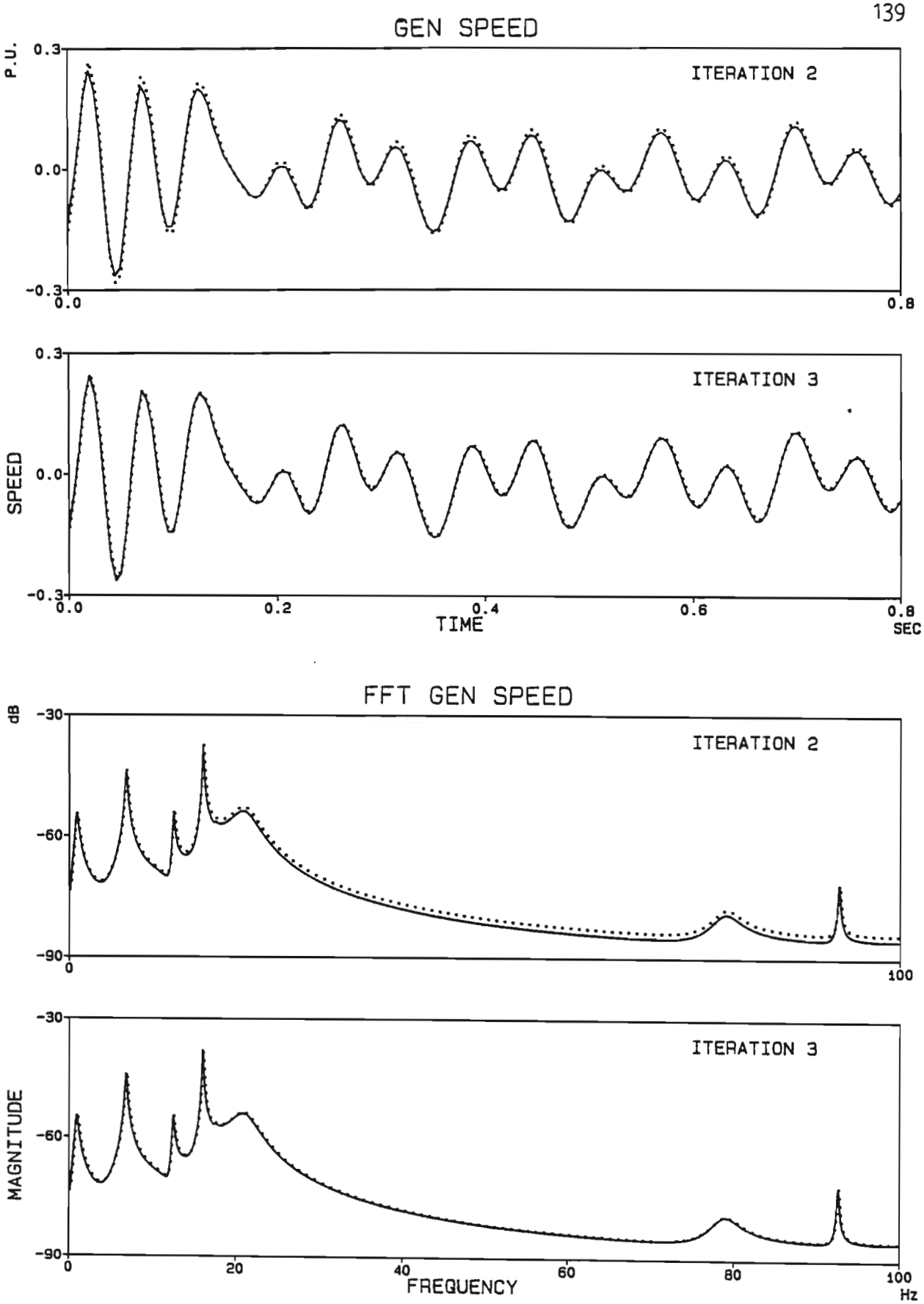

Fig 5.11 'Measured' and fitted generator speed, and the FFTs of these curves, for the second and third iterations.

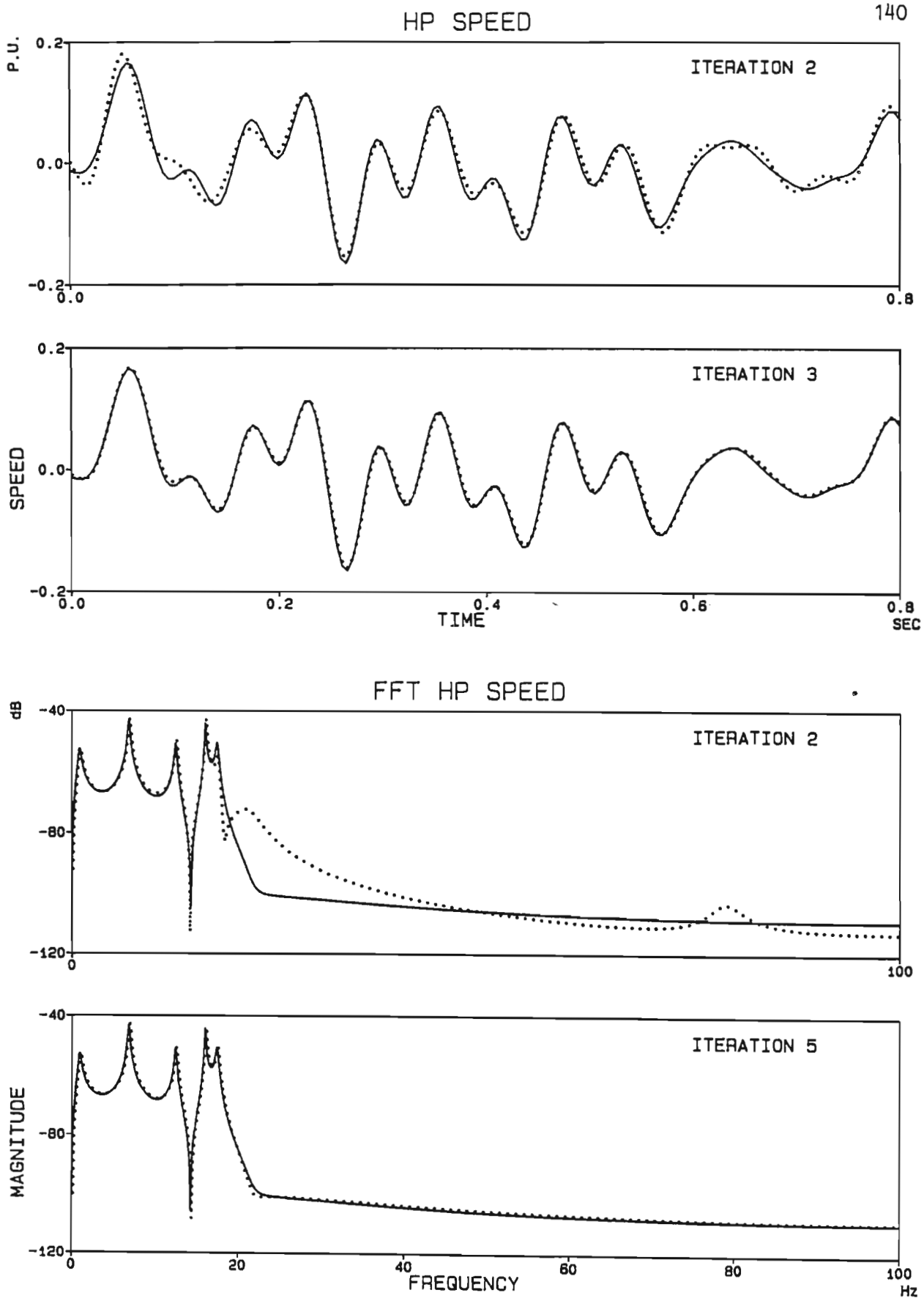

Fig 5.12 HP turbine speed showing 'measured' and fitted transient curves for iterations 2 and 3, and the FFTs of the 'measured' and fitted curves for iterations 2 and 5.

Table 5.10 Convergence of mechanical mode dampings

Iteration	Mechanical Mode Dampings σ_{mi} (s^{-1})					
	0	1	2	3	4	5
0	1.116	0.813	0.772	0.490	1.059	0.787
1	0.870	0.808	0.773	0.517	1.056	0.787
2	0.790	0.785	0.787	0.820	0.908	0.785
3	0.783	0.785	0.785	0.783	0.809	0.785
4	0.787	0.785	0.786	0.786	0.797	0.785
5	0.785	0.785	0.786	0.786	0.789	0.785
Correct	0.785	0.785	0.785	0.785	0.785	0.785
Error (%)	0.04	0.00	0.01	0.04	0.43	0.00

The mechanical mode parameters are all obtained to a high degree of accuracy and at a fast rate of convergence. The convergence of the mode shapes is not shown; they were however identified to within 0.06% of the maximum deflection in each mode shape. The convergence is slower for mode 4 due to the fact that it is the least interactive with the electrical system.

This example has demonstrated the feasibility of this process given the identification of the system modes. The process is now repeated here except in this case transfer functions between the rotor speed signals and the infinite bus voltage are calculated and the system modes extracted from these using the Hewlett-Packard Modal Analysis Package. The transfer functions obtained are shown in rectangular form in Fig 5.13 and they are different to those obtained between electrical torque and rotor speed as shown in Fig 5.7. In particular the system electrical modes at 21 Hz and 78 Hz are evident in the transfer functions involving the bus voltage as the input; these are clearly seen in the log magnitude plots of these transfer functions shown in Fig 5.14.

The system mode data identified from the transfer functions appears in Table 5.11 and should be compared with the values in Table 5.7 obtained from the system eigenvalues and eigenvectors.

Table 5.11 System mode parameters identified from transfer functions

		Mode					
		0	1	2	3	4	5
f_{si} (Hz)		0.925	6.832	12.456	16.038	17.495	92.591
σ_{si} (s^{-1})		1.187	0.810	0.770	0.479	1.054	0.785
MODE SHAPES	HP	1.00	-1.00	1.00	-.50	1.00	.00
	LP1	1.00	-.83	.43	-.02	-.15	-.00
	LP2	.98	-.14	-.86	.26	.05	.00
	LP3	.95	.71	.04	-.59	-.03	-.00
	GEN	.92	.95	.74	.97	.03	.05
	EXC	.92	.96	.75	1.00	.03	-1.00

The system mode parameters are determined accurately; slight inaccuracies are incurred due to the fact that during the disturbance (V_b = 0.95 p.u.) the system eigenvalues are different to those during steady state. This effect is minimized by starting the 'measurement' upon the removal of the fault.

The identified system mode parameters are used as the starting values of the mechanical mode parameters and the initial values of mechanical mode inertias are chosen as 0.05 p.u. The calculated HP turbine speed for the first three iterations and the FFT of this speed for the 1st, 2nd and 4th iterations are shown in Figs 5.15 and 5.16 respectively. The mechanical mode parameters converge rapidly to their true values and the final parameters after 5 iterations are shown in Table 5.12.

The identification yields relatively accurate results for the mechanical mode parameters. In particular, mode 3 which has a negative damping influence from the electrical system (σ_{s3} = 0.49 s^{-1}) is identified correctly. Errors in the resultant mechanical mode parameters can be ascribed to errors in the identified system mode parameters. Hence, the accuracy of the mechanical mode parameters depends on how accurate the system mode parameters are identified.

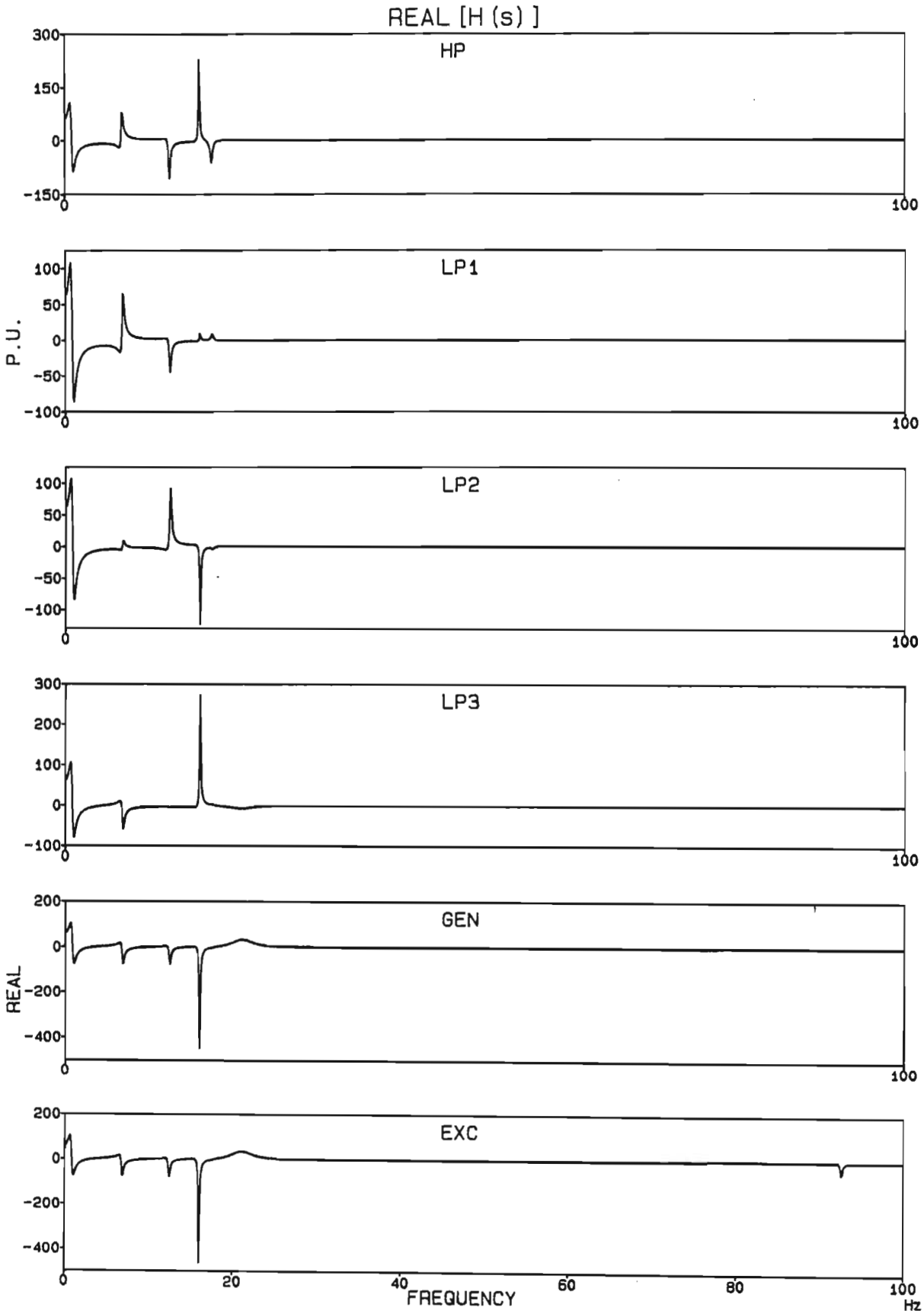

Fig 5.13 (a) Real part of transfer functions between infinite bus voltage and shaft speeds for a 70 ms duration 5% drop in the infinite bus voltage.

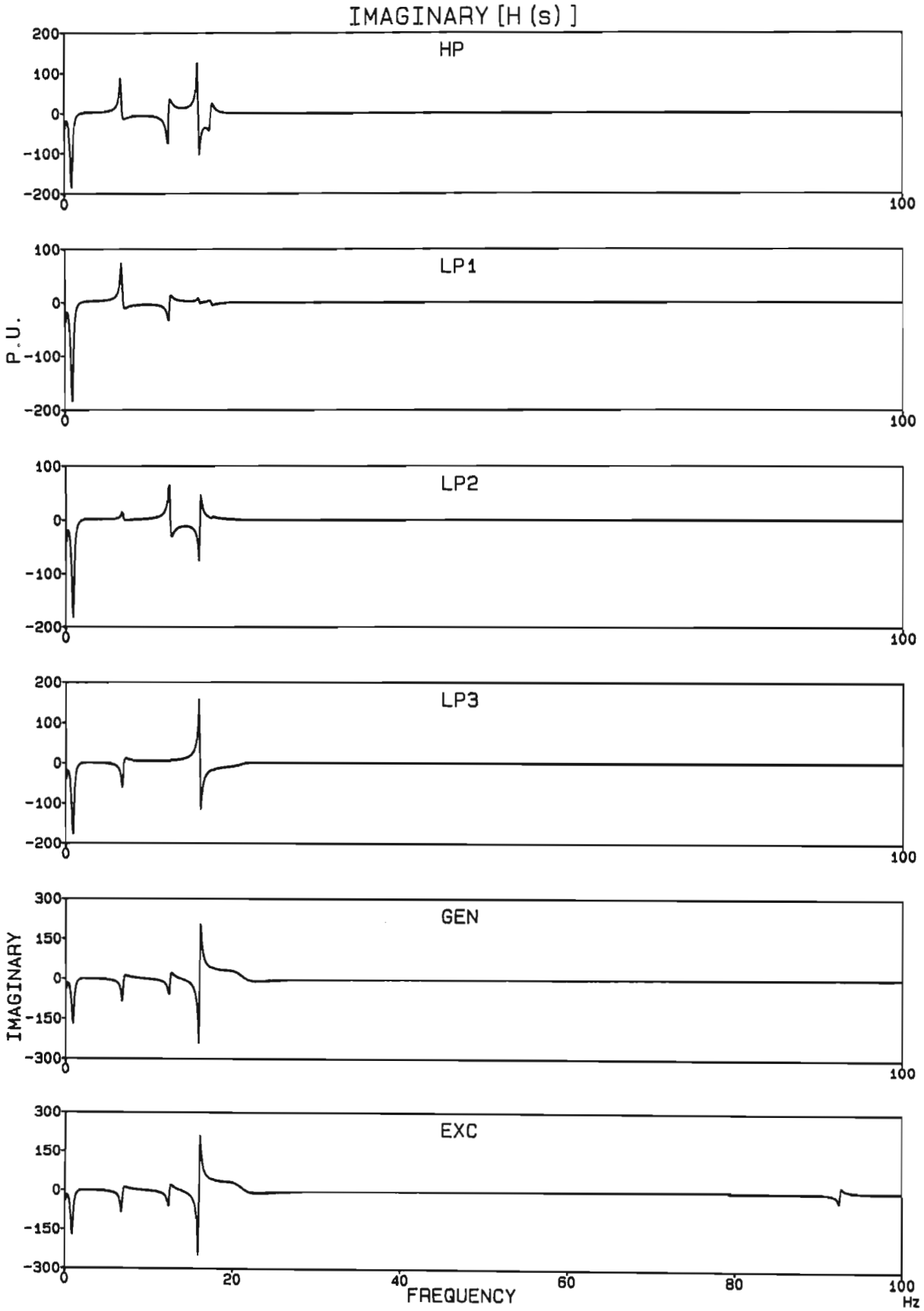

Fig 5.13 (b) Imaginary part of transfer functions between infinite bus voltage and shaft speeds for a 70 ms duration 5% drop in the infinite bus voltage.

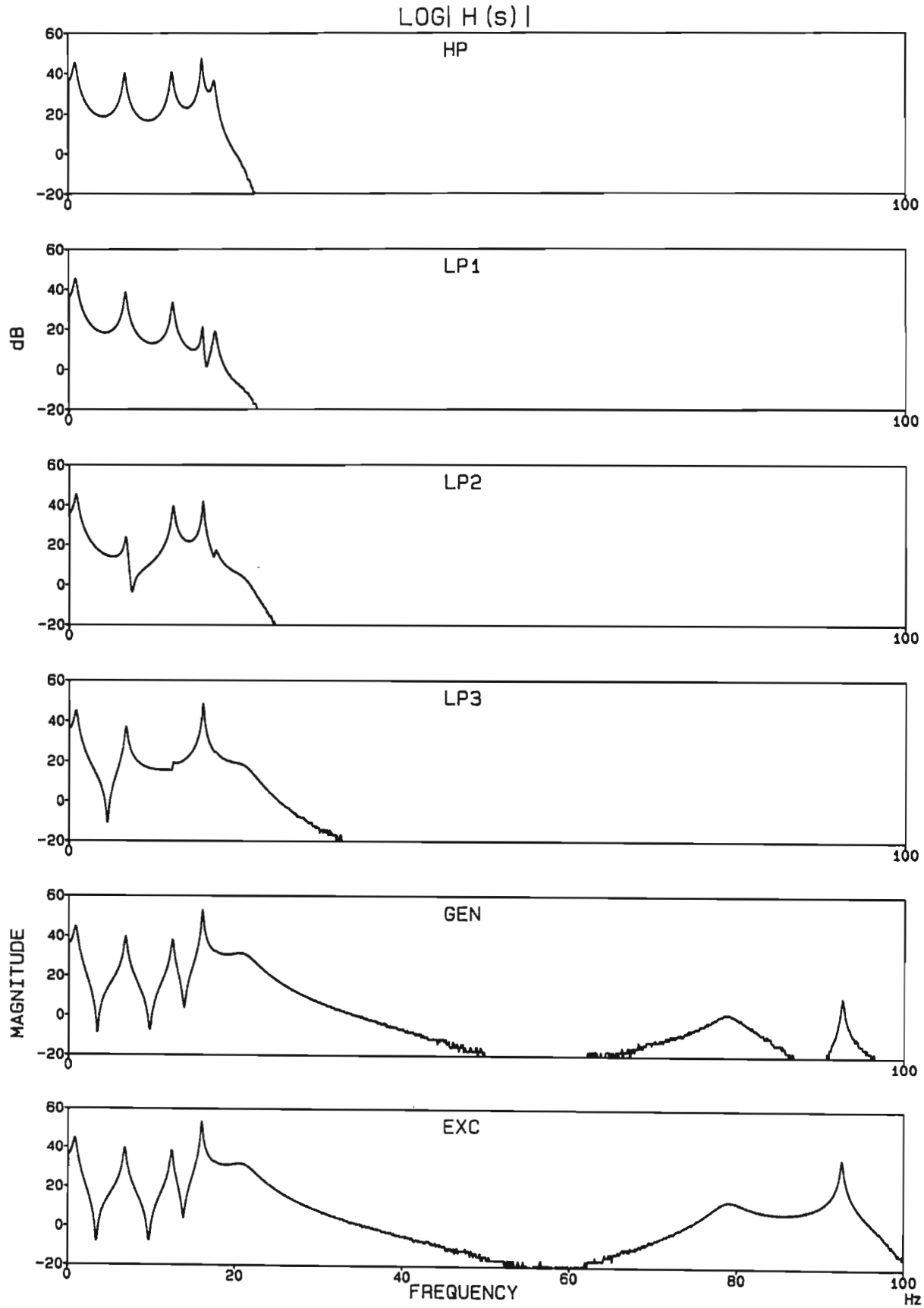

Fig 5.14 Log magnitude plots of the transfer functions in Fig 5.13.

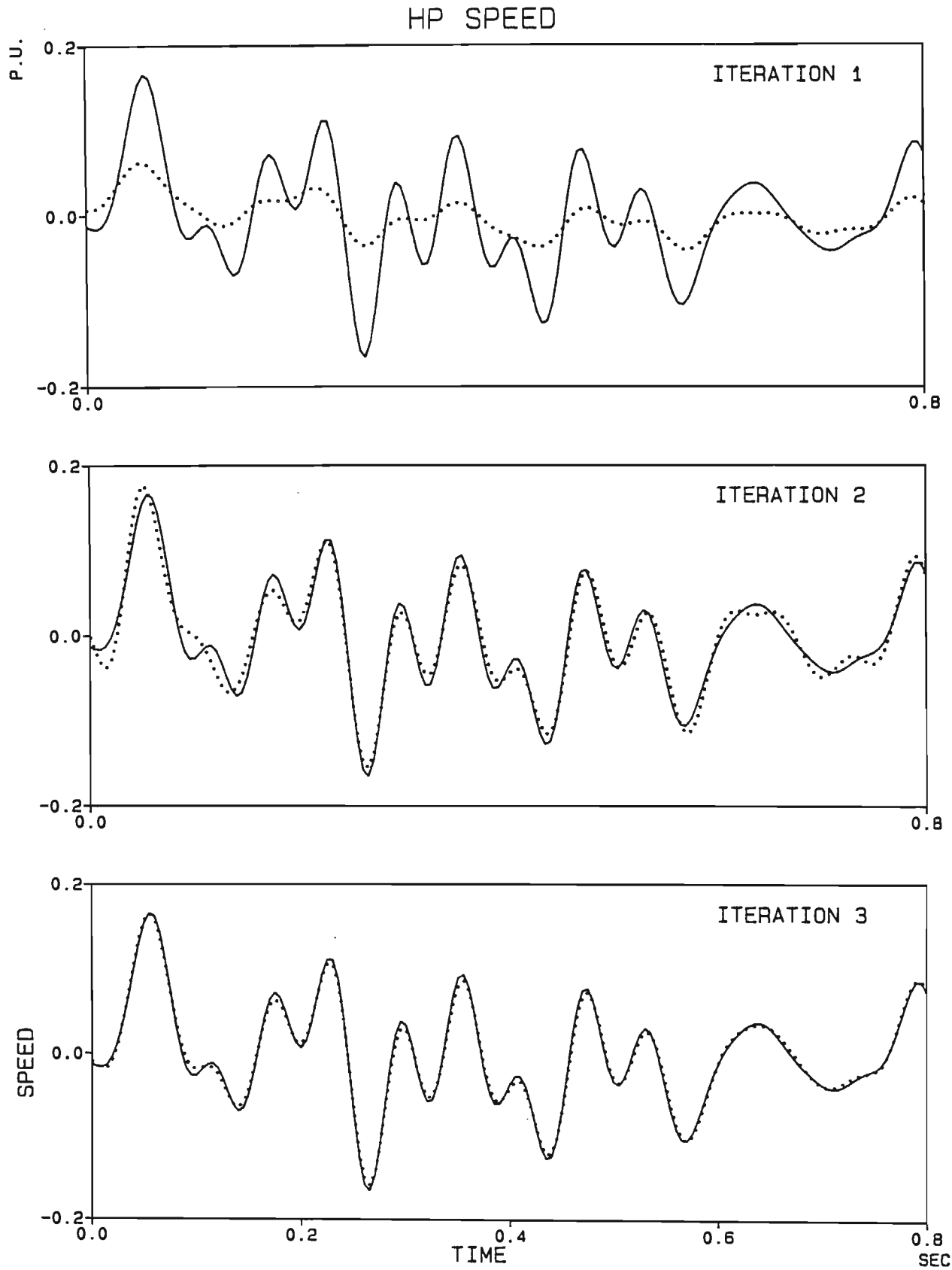

Fig 5.15 Comparison of 'measured' and fitted HP turbine speeds for the first three iterations.

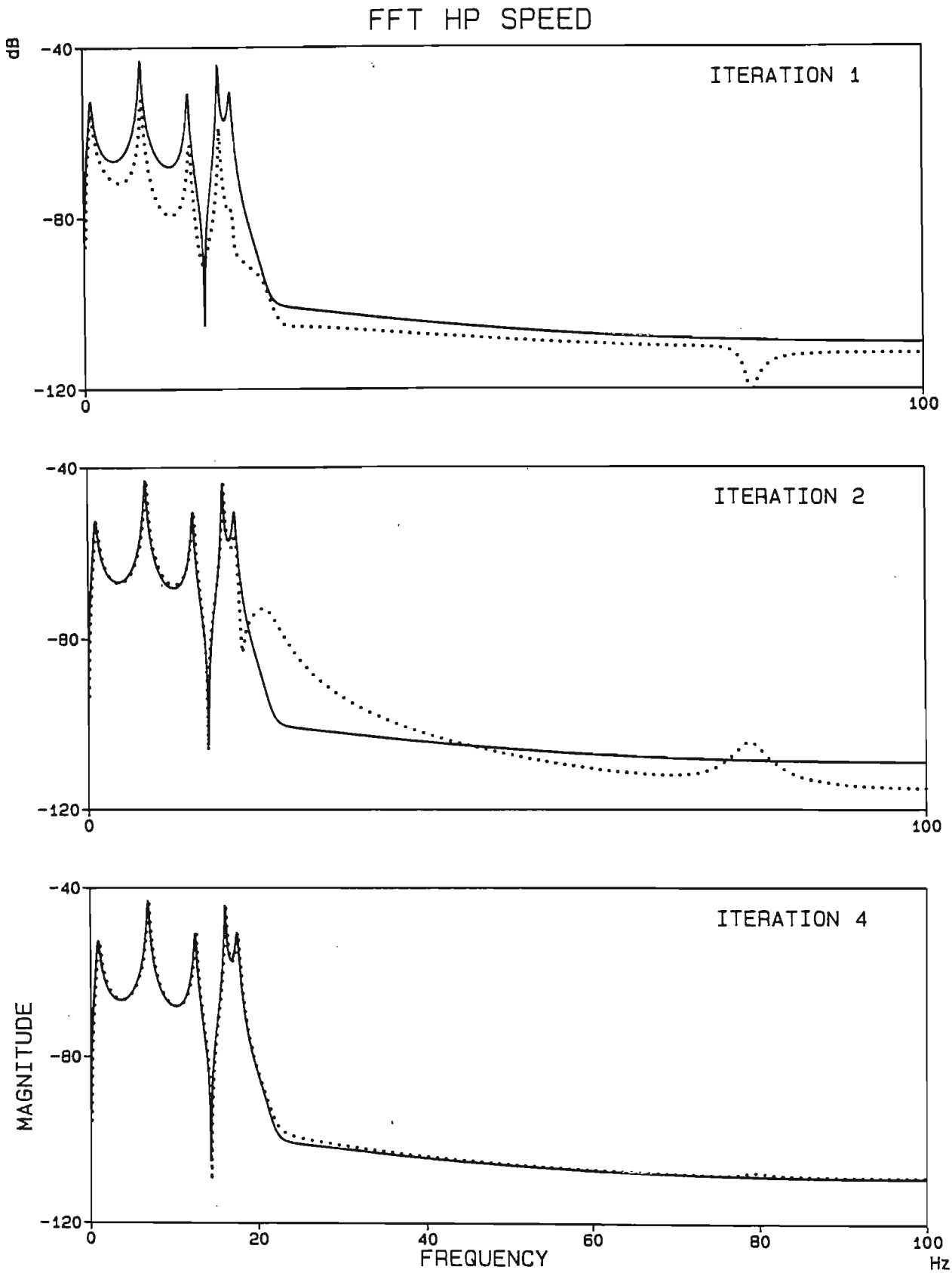

Fig 5.16 Comparison of FFTs of 'measured' and fitted HP turbine speeds for the first, second and fourth iterations.

Table 5.12 Final values of mechanical mode parameters obtained from identified system modes

Mode	f_{mi} (Hz)	Error (%)	σ_{mi} (s^{-1})	Error (%)	J_{Mi} (p.u.)	Error (%)
0	0.00	0.00	0.806	2.57	3.58E-2	0.93
1	6.68	0.01	0.782	0.38	1.73E-2	0.71
2	12.37	0.00	0.784	0.14	1.28E-2	0.21
3	15.84	0.03	0.767	2.34	9.95E-3	2.39
4	17.49	0.01	0.766	2.52	1.18E-3	4.76
5	92.59	0.00	0.783	0.31	2.32E-4	0.51

Mode shapes: maximum error = 0.6% of the maximum deflection

5.7 Correction of Transmission System Parameter Errors

The transfer functions (in Fig 5.14) taken between the bus voltage and the shaft speeds show additional modes around 20 and 80 Hz; these are the electrical subsynchronous and supersynchronous modes respectively. These modes are identified by the modal analysis software package and are compared with the true values obtained from the system eigenvalues below:

	Calculated	Identified	Error
Subsynchronous	σ = 9.96 s^{-1}	= 10.00 s^{-1}	0.39%
	f = 21.00 Hz	f = 21.01 Hz	0.05%
Supersynchronous	σ = 10.93 s^{-1}	= 11.17 s^{-1}	2.12%
	f = 78.78 Hz	f = 78.71 Hz	0.09%

This identification of the super- and more important, subsynchronous electrical modes is useful as previous investigations have shown that the contribution of the electrical damping to the overall damping of a system mode is strongly dependant on the frequency and damping of the electrical subsynchronous mode. Since any inaccuracy in the electrical damping contribution results in a corresponding inaccuracy in the mechanical

damping ($\sigma_{mi} = \sigma_{si} - \sigma_{ei}$), it is important that the electrical damping be accurately represented. Identifying the electrical subsynchronous mode enables one to adjust the transmission system parameters to ensure that the calculated electrical subsynchronous mode is the same as that measured. This enables the correction of errors that may occur due to inaccuracies in the specified values of transmission system parameters. In addition to the electrical subsynchronous mode, information about the system mode 0 frequency can be used in the correction of transmission system parameters.

Once the subsynchronous electrical mode damping σ_s, the subsynchronous electrical mode frequency f_s and the system mode 0 frequency f_{s0} have been identified, then the errors $\Delta\sigma_s$, Δf_s and Δf_{s0} can be determined by a comparison with the values predicted by the system eigenvalues. These errors are then used to calculate the changes required in the total external circuit resistance ΔR_e, the total external inductive reactance ΔX_e and the series capacitance ΔX_c according to the equation:

$$\begin{bmatrix} \Delta\sigma_s \\ \Delta f_s \\ \Delta f_{s0} \end{bmatrix} = \begin{bmatrix} \partial\sigma_s/\partial R_e & \partial\sigma_s/\partial X_e & \partial\sigma_s/\partial X_c \\ \partial f_s/\partial R_e & \partial f_s/\partial X_e & \partial f_s/\partial X_c \\ \partial f_{s0}/\partial R_e & \partial f_{s0}/\partial X_e & \partial f_{s0}/\partial X_c \end{bmatrix} \begin{bmatrix} \Delta R_e \\ \Delta X_e \\ \Delta X_c \end{bmatrix}$$

The matrix of partial derivatives is derived in Appendix F. The iterative identification process is as follows where the superscript 'j' denotes the j'th iteration:

1) Measure the system mode parameters f_{si}, σ_{si} and $\underline{Q}_{si}$ and the electrical subsynchronous mode parameters f_s and σ_s;

2) Assume initial values R_e^0, X_e^0, X_c^0, J_{Mi}^0, $f_{mi}^0 = f_{si}$, $\sigma_{mi}^0 = \sigma_{si}$, $\underline{Q}_{mi}^0 = \underline{Q}_{si}$;

3) Use the last updated values of mechanical mode parameters J_{Mi}^j, f_{mi}^j, σ_{mi}^j and $\underline{Q}_{mi}^j$, and the last updated values of transmission line parameters R_e^j, X_e^j and X_c^j in the scanning program to obtain f_{mi}^{j+1}, σ_{mi}^{j+1}, $\underline{Q}_{mi}^{j+1}$, R_e^{j+1}, X_e^{j+1} and X_c^{j+1};

4) Use J_{Mi}^{j}, f_{mi}^{j+1}, σ_{mi}^{j+1}, Q_{mi}^{j+1}, R_e^{j+1}, X_e^{j+1} and X_c^{j+1} to calculate the transient response and from the FFT of the transient response obtain J_{Mi}^{j+1};

5) Repeat 3) and 4) until a specified convergence criterion is achieved.

The process is illustrated by way of an example; the system is considered to be operating under the same conditions as the example in the previous section (P_b = 0.6 p.u., Q_b = 0.2 p.u., X_c = 0.43 p.u.). In order to demonstrate the convergence on the correct transmission system parameters and test the accuracy of this method, it is assumed that the system modes and the electrical subsynchronous mode are known exactly so that any errors can be ascribed to the identification method. Furthermore, since the identification of the mechanical mode inertias by FFT measurements has been demonstrated in the previous section, it will be assumed here that the mechanical mode inertias are known, thereby eliminating step 4 above. However, it should be noted that the errors in the identified values of R_e, X_e and X_c at each step are strongly dependant on the value of the mode 0 inertia. Thus for a bad initial guess of mode 0 inertia the values of R_e, X_e and X_c will have large errors (although they will give the correct values of σ_s, f_s and f_{s0}). This problem can be overcome by only updating R_e, X_e and X_c after the first or second iteration for J_{M0}. However, in general J_{M0} is known quite accurately for a generator and hence the initial value used should not be a 'bad' starting point.

The system mode parameters are used as the starting point for the mechanical mode parameters and it is assumed that there is an error in the transmission system parameters. The true values used to generate the system modes are:

R_e = 0.0845 p.u. X_e = 1.0097 p.u. X_c = 0.43 p.u.

while the starting values (say as supplied by a utility) are:

R_e = 0.0945 p.u. X_e = 1.3197 p.u. X_c = 0.38 p.u.

The above convergence algorithm is applied successfully and all parameters converge on their correct values after 5 iterations. The convergence of the transmission system parameters is shown below:

Iteration	R_e	X_e	X_c
0	0.0945	1.3197	0.3800
1	0.0760	0.8783	0.4057
2	0.0820	0.9681	0.4180
3	0.0848	1.0096	0.4297
4	0.0846	1.0110	0.4304
5	0.0845	1.0097	0.4300

Thus the identification of the subsynchronous electrical mode and the system mode 0 frequency has enabled the transmission system parameters to be modified to their correct values. Had the identification proceeded as in Sect 5.6 with the incorrect values of R_e, X_e and X_c then the identified mechanical parameters (especially the mode 3 damping) would have been in error, as the subsynchronous electrical frequency and damping would have been incorrect resulting in an incorrect representation of the subsynchronous electro-mechanical interaction.

5.8 Conclusion

This chapter has investigated the problem of determining mode parameters for a turbogenerator. Mechanical mode parameters can be obtained from transient tests on the turbogenerator at standstill. However, the measurement of mechanical mode parameters directly, while the generator is synchronized, requires an accurate knowledge of the generator electrical torque. This is difficult to achieve and a method is therefore proposed whereby mechanical mode parameters are determined from system mode parameters. Results of a few examples show that by using eigenvalue-eigenvector scanning techniques and FFT analysis of measured and predicted responses, mechanical mode parameters can be determined quite accurately from system mode parameters. This method becomes less accurate as the

severity of the disturbance used to excite the system increases, due to the use of the linearized system model for the eigenvalue-eigenvector scanning section. However, accurate results (less than 0.6% error for torsional modes) have been obtained for a 100 ms 10% drop in the infinite bus voltage.

A requirement for obtaining mechanical parameters from system mode data is the ability to do a transient simulation and eigenvalue calculation with the shaft represented in modal form. This is because it is not possible to independently adjust mode frequencies, dampings, inertias and mode shapes with a physical model of the shaft. Adjustment of one of the parameters of the physical model will alter all the parameters of the modal model.

In the determination of mechanical mode parameters from system mode parameters it is important that the rest of the system is represented accurately, particularly the transmission system. It has been shown in this chapter that if the system electrical modes can be identified, then it is possible to correct the errors in the assumed values of transmission system parameters at the same time as identifying the mechanical mode parameters.

CHAPTER SIX

SUBSYNCHRONOUS RESONANCE OF THE KOEBERG POWER STATION WITH TWO IDENTICAL GENERATING UNITS

6.1 Introduction

Since the appearance of the first paper in 1979 on Subsynchronous Resonance in the Koeberg system [15] much work has followed related to Koeberg, dealing with topics such as system modelling, multi-machine SSR and possible SSR countermeasures [20,24,25,41,49-53]. These studies, with the exception of Ref [20], dealt with the first phase of the Koeberg project in which a single 1072 MVA turbogenerator was to be commissioned. Thus the majority of the work related to Koeberg was done as single machine studies; even the multi-machine studies in Refs [24,25] considered the Koeberg station to consist of a single 1072 MVA generator and investigated the effect of other generating stations on the single generator stability of Koeberg. At a later stage a second nominally identical 1072 MVA turbogenerator was commissioned and this necessitated the extension of the earlier single machine studies to consider the effects of the increased generating capacity at Koeberg. Ref [20] did consider a generating capacity of 2144 MVA at Koeberg but it represented this as a single equivalent generator; moreover, it did not represent the torsional characteristics of this increased generating capacity system and could thus make no conclusions regarding the subsynchronous stability of the two generator station. This chapter extends these earlier investigations and describes the analysis of the subsynchronous stability of the Koeberg power station with two nominally identical generating units; this work was the fore-runner to recent publications dealing with two generators at Koeberg [40,42].

Conventional representation in a stability analysis of a power station containing more than one generator usually 'lumps' all the generators into one equivalent generator with a rating equal to the sum of the ratings of the individual generators [54]. This is known to be a valid simplification if the stability study is concerned with the transient oscillations of energy between the electrical network and the rotating inertias of the generators. However, an SSR investigation also includes an analysis of the oscillation of energy between the various individual inertias of a generator shaft interacting with the electrical system. Thus the shaft's natural frequencies and the torsional modelling of the shaft become important. If two generators are considered to be a single equivalent generator of increased rating, then the station is transformed from two coupled identical resonant systems to a single resonant system, and a certain amount of detail about the station's mechanical resonance characteristics is lost. (The combined resonant properties of two coupled identical resonant systems are different from those of one of the systems individually [55]). Moreover, this simplification of representing two generators by an equivalent generator would not be possible without great loss in accuracy if the individual generators had different shaft torsional characteristics.

This chapter investigates two aspects of the increase in the generating capacity at Koeberg. It firstly reconsiders this station's potential SSR problem with particular emphasis on the effects of adding the second generator. The results obtained by an eigenvalue analysis agree with those obtained by frequency scanning techniques [56] where it was shown that an increase in the number of generators at a station would most often result in a relatively less stable system.

It then investigates the torsional characteristics of the power station with the two generators modelled as separate units. A comparison is made between the two-generator representation and the equivalent single larger generator representation to determine the error in SSR predictions due to the loss in detail in the station's torsional characteristics when creating the single equivalent generator. The results show that this loss in

detail does not seriously affect the SSR stability studies of this system, particularly for CCL calculations.

In Chapter 7 the investigation is extended to consider non-identical units. This analysis is greatly assisted by the representation of the generator shaft in modal form which allows the effects of variations in mode damping, frequency, inertia and mode shape to be analysed separately. With a physical shaft representation, it is not possible to vary mode inertia, damping, frequency and mode shape independently as a change in the parameters of the physical shaft model changes the torsional characteristics of all the modes.

The results obtained are compared with those obtained by others in studies involving multiple units at power stations [57-60]. Ref [57] considered the torsional interaction of truly identical generators but did not consider systems with series capacitor compensation. Ref [58] extends the analysis of Ref [57] to include series capacitors in the transmission system and also considers non-identical units; however the shaft system is modelled by a physical representation. Ref [59] considers two different generators having a common torsional mode with identical frequencies but different inertias, dampings and mode shapes; the effect of these differences in mode parameters as compared to truly identical modes is not considered, nor is the difference in the SSR stability of the common mode compared with one and two generators synchronized. Ref [60] considers two generators with modal shaft representations and different mechanical dampings transmitting power over a HVDC link; apart from damping the generators are identical.

6.2 Single Per-Unit Equivalent Generator

Traditionally, a number of generators are replaced by a single equivalent generator with a rating equal to the sum of ratings of the individual generators. Thus, the two generators in Fig 6.1 can be simplified to the equivalent generator in Fig 6.2 which has a rating of 2144 MVA, i.e. twice

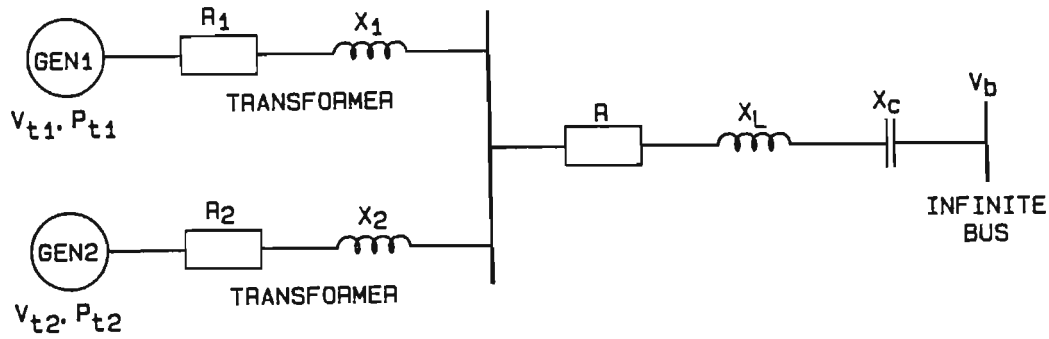

Fig 6.1 Schematic diagram of the two-generator system.

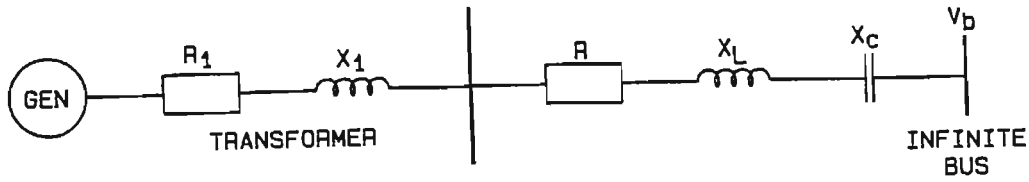

Fig 6.2 Schematic diagram of the one-generator system and the equivalent generator system.

that of a single generator. The base values for one of the Koeberg generators (1072 MVA) and those for the equivalent generator (2144 MVA) are given in Appendix A.3.

The per-unit values of the electrical parameters in the equivalent system of Fig 6.2 are given by the per-unit values in the two-generator system of Fig 6.1 multiplied by the ratio of equivalent-generator base power to single generator base power, that is by a factor of two. However, since the generator and transformer in Fig 6.2 represent the parallel combination of generators and transformers in Fig 6.1, their parameters in physical units are half those of a single generator and transformer in Fig 6.1. Thus in per-unit, the generator and transformer in Fig 6.2 all have the same electrical parameters as those in Fig 6.1.

For the equivalent generator's mechanical system to be equivalent to that of the two generator system, its shaft's total inertia must be equal to the sum of the total inertias of the two generators in order to have the same quantity of stored rotational energy at synchronous speed. However, since the base inertia for the equivalent generator is twice that of a single generator, the per-unit values of inertia will be the same for both systems.

Similarly, to carry through the torsional characteristics of the shaft to the equivalent generator, the physical values of shaft stiffnesses of the equivalent generator must be twice those of the single generator's shaft. As in the case with the inertia, due to the doubling of the base value of stiffness for the equivalent generator, the per-unit values of shaft stiffness will be the same in both cases.

The inertia constant H in seconds is the same for all generators since both the stored kinetic energy at synchronous speed and the base power increase by a factor of two for the equivalent generator.

The equivalent system is summarized below in Table 6.1 where the elements in the table give the ratio of equivalent generator system values to the single generator system values.

Table 6.1 Ratio of Equivalent Generator System Parameters to Single Generator System Parameters

Generator mechanical		Generator electrical and transformer		Transmission line	
p.u.	physical	p.u.	physical	p.u.	physical
1	2	1	0.5	2	1

6.3 The Multi-Machine System Model

The previous chapters have all dealt with a single-generator infinite-busbar system and have modelled the generator in a rotor reference frame [11]. However, in a multi-machine system the rotors of individual generators rotate at different speeds during a transient, while under steady state conditions individual generators have different rotor angles. Thus the d,q reference frames of the generators move with respect to each other during a transient and are out of phase during steady state. The modelling of a multi-generator system thus requires different techniques to those used in modelling a single generator system to be able to relate variables from different generators.

In this thesis the two-generator system in Fig 6.1 is analysed using a multi-machine program developed by Lahoud [20] which allows the user to specify an arbitrary network with any number of generators and induction motors as well as the loads at each busbar. A description of the original program and it's capabilities appears in Refs [20,61,62]; this program has been extended by the author to include:

(a) the modal representation of generator shaft dynamics for any of the generators in the system;

(b) the modelling of any number of Shunt Reactor Stabilizers in the system with the order of each shunt reactor controller independently specified.

The ability to represent the generator shaft dynamics in modal form is particularly useful in the investigation of dissimilarities between nominally identical units as is done in Chapter Seven.

The multi-generator system equations including modal shaft dynamics and shunt reactor stabilizers are described in Appendix G. In the multi-machine model, the generator is represented by an equivalent non-linear voltage source b which does not neglect transformer voltage terms, in series with the stator phase resistance R_a and an equivalent inductance L_g^*

as shown in Fig 6.3 as part of an ac equivalent circuit of the transmission network. The generators and network equations are thus represented in steady ABC variables for the initial load-flow calculations and the whole system, including the network equations, are transformed into a common synchronously rotating D,Q reference frame for the transient and small-signal calculations. The linearized form of the system equations in terms of the synchronously rotating D,Q reference frame required for eigenvalue and mode shape calculations are described in Appendix H.

The state-space formulation of the entire system can be summarized in the following form (Appendix G):

$$[P]p\underline{x} = [E]\underline{x} + [S]\underline{u} \tag{6.1}$$

The state vector $\underline{x}$ for the system in Fig 6.1 is a composite vector consisting of the following components:

$$\underline{x} = [\underline{i}_{ED}^T, \underline{i}_D^T, \underline{i}_{EQ}^T, \underline{i}_Q^T, \underline{v}_{CtD}^T, \underline{v}_{CtQ}^T, [\underline{\psi}_{dr}]^T, [\underline{\psi}_{qr}]^T, \underline{F}_m^T,]^T \tag{6.2}$$

and

$$\underline{u} = [v_{bD}, \underline{b}_D^T, v_{bQ}, \underline{b}_Q^T, [\underline{v}_{dr}]^T, \underline{P}_m^T]^T \tag{6.3}$$

where the various components are defined in Appendix G.

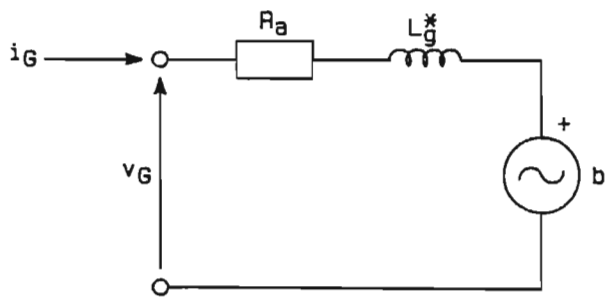

Fig 6.3 Multi-machine model of a generator suitable for inclusion in the transmission network.

The transient results in this chapter are calculated from numerical integration of eqn (6.1) (since it has non-linearities in [E]) while the eigenvalues and mode shapes are calculated from eqn (H.12) which is a linearized form of eqn (6.1). The system parameters appear in Appendix I and for all transient and small-signal calculations in this chapter, unless otherwise stated, the initial conditions are V_b = 1.0 p.u., V_t = 1.1 p.u. and P_t = 0.6 p.u.

6.4 Effect of Second Generating Unit

In this section the effect of adding a second generating unit on the previously calculated stability performance of the single-generator system is investigated. The increased capacity two-generator system is represented as a single equivalent generator as described in Sect 6.2 so that the comparison between the two systems is performed as two single-machine studies and conclusions arrived at are due solely to the increase in generating capacity. Sections 6.5 and 6.6 compare the behaviour of this equivalent generator system with that of the actual system of two separate generators.

6.4.1 Simple radial transmission system

Fig 6.4 shows the eigenvalue loci in the direction of the arrows calculated for one 1072 MVA generator at Koeberg as the compensation level in the transmission line in Fig 6.2 is varied from around 10% to 105% where the percentage compensation level N is defined as:

$$N = 100(X_c/X_L) \tag{6.4}$$

This is the same result as calculated earlier in Fig 3.3 except for small differences that exist between the two figures due to the different way in which the initial conditions were specified for each calculation. The single machine program used in Chapter 3 specifies the infinite busbar real power, reactive power and voltage at each compensation level whereas the

multi-machine program specifies infinite busbar voltage, generator terminal voltage and generator real power as initial conditions at each compensation level.

The effect of an increase in the generating capacity of Koeberg by the addition of a second generating unit can be seen by comparing Fig 6.5 with Fig 6.4 where Fig 6.5 is calculated for an equivalent 2144 MVA generator at Koeberg. Table 6.2 contains a set of eigenvalues from each of these figures calculated with a compensation level of 74% (X_c=0.4 ohm). This is the same value of X_c that was used in the first study on this system [15].

Table 6.2 One-generator and equivalent generator eigenvalues calculated for a compensation level of 74%

		Single Machine		Equivalent Machine	
Mode		Real	Imaginary	Real	Imaginary
E1	Supersynch. flux	-9.94	±539.8	-11.3	±558.9
E2	Subsynch. flux	-9.67	±88.8	-10.5	±69.8
M5	Supersynch. mech.	-0.79	±581.8	-0.79	±581.8
M4	Subsynchronous mechanical	-1.05	±109.9	-1.05	±109.9
M3		+0.25	±98.2	-0.72	±99.2
M2		-0.12	±78.8	-0.30	±77.3
M1		-0.76	±43.2	-0.61	±42.9
M0	Inertial mode	-1.24	±5.98	-1.04	±5.10
M	Magnetic stability	-0.17	0.0	-0.11	0.0
R1	Damper circuits	-1.18	0.0	-1.10	0.0
R2		-11.4	0.0	-10.8	0.0
R3		-18.0	0.0	-17.5	0.0

The main differences between the loci of Figs 6.4 and 6.5 can be explained by noticing that the the effect of adding a second generator, and hence a doubling of the power transfer capability between the power station and the infinite busbar, is the same as a per-unit equivalent generator transferring power across a transmission line of twice the distance.

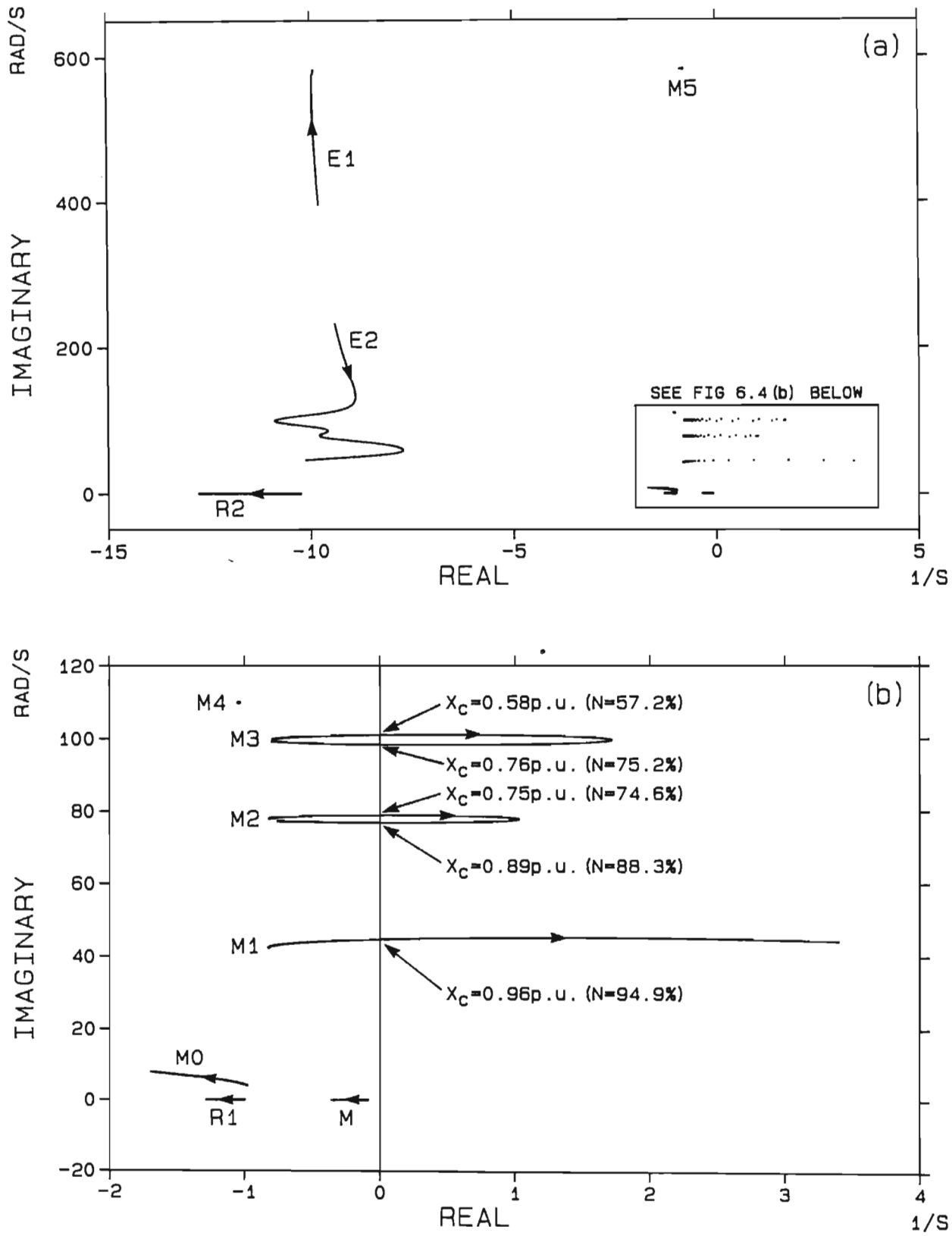

Fig 6.4 Eigenvalue loci for the one-generator system (1072 MVA) as the compensation N is varied from 10% to 105%.

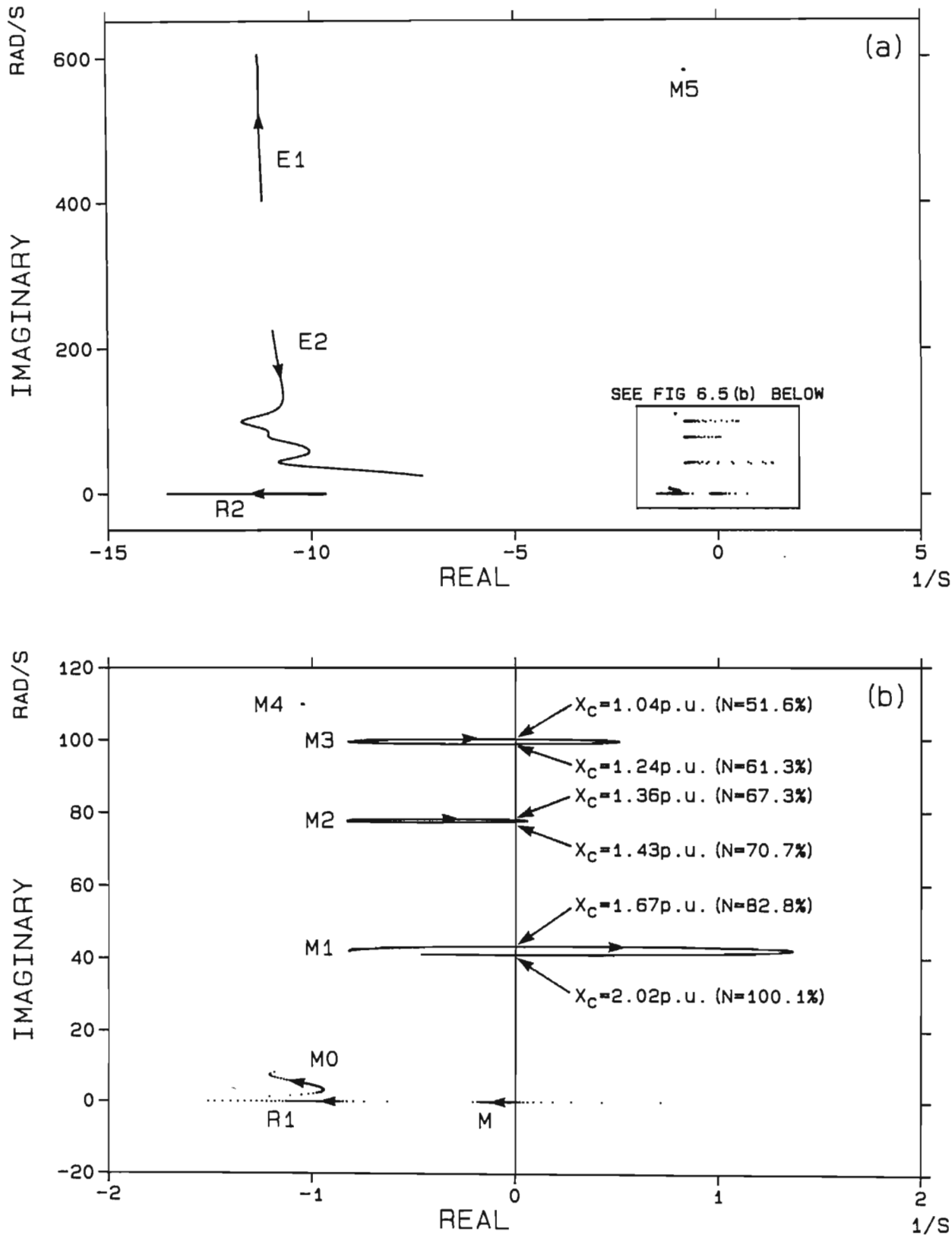

Fig 6.5 Eigenvalue loci for the equivalent generator system (2144 MVA) as the compensation N is varied from 10% to 105%.

Hence, since the transmission line resistance and reactance have doubled in per-unit whereas the generator and transformer parameters are the same as before, there is an increase in the per-unit values of R, X_L and X_c between the internal voltage of the equivalent generator and the infinite bus of 96.5% in R, 69.4% in X_L and 100% in X_c. This results in the following:

(a) for a low value of compensation, there is an effective higher value of reactance between the equivalent generator's internal voltage and the infinite bus. Thus, since the generator is not modelled with a voltage regulator, the locus at M in Fig 6.5(b), which is associated with the electromagnetic stability of the generator [11], is unstable for low compensation levels and starts in the right-half-plane (RHP). Furthermore, this increased reactance means that there is a weaker electrical coupling between the equivalent generator and the infinite bus, and this results in a decrease in the damping and frequency of the hunting mode M0 as can be seen in Table 6.2;

(b) the damping of the electrical modes E1 and E2 has increased with the addition of the second generator. This is due to the fact that the real parts of the eigenvalues for an RLC circuit are given by -R/2L and the per-unit resistance has increased by more than the per-unit inductance. The effect of this is that mode E2 does not interact as strongly with the equivalent generator mechanical modes and this is one of the reasons why M1, M2 and M3 do not move as far into the RHP;

(c) for any compensation level, the frequency of mode E1 has increased and that of mode E2 has decreased. This is due to the fact that the imaginary parts of the eigenvalues of an RLC circuit can be approximated to $1/\sqrt{LC}$ for $(R/2L)^2 \ll 1/LC$ and, since the increase in L is less than the decrease in C (increase in X_c), the resonant frequency of the RLC circuit between the equivalent generator internal voltage and the bus voltage is higher. The consequence of this is that the subsynchronous mode E2 interacts with the mechanical modes at a lower value of X_c. Thus at high compensation levels the hunting mode M0 starts to interact with the subsynchronous mode E2 and changes direction towards the RHP.

The above effects are all caused by the change in the interconnecting transmission system characteristics that occurs with the addition of a second generator. Differences in the mechanical systems of one generator and an equivalent generator also have a noticeable effect on the eigenvalue loci. The shaft of the equivalent generator has an inertia twice that of a single generator and this means that the excitability values (see Sect 4.2) of the equivalent generator's modes will be half those of a single generator. This results in the mechanical modes of the equivalent generator having a lower value of torsional interaction susceptibility (TIS) and they are thus not pushed as far into the RHP as seen by comparing Fig 6.4(b) and 6.5(b).

The effect of (b) above and the change in the mode excitability is to make the equivalent generator system more stable whereas the effect of (c) is to make the equivalent generator system less stable. The combined effect can be determined by looking at the real parts of the mechanical mode eigenvalues as a function of the compensation. This is shown for both the one-generator system and the equivalent generator system in Fig 6.6.

The one-generator system is seen to be stable for compensation values less than B and between G and H. The region up to B is considered a safe stable region and it is in this region that a system without any SSR countermeasure will be operated. The region GH is an unsafe stable region since a reduction in the compensation can cause the onset of SSR. The system with two generators has two unsafe stable regions, CD and EF, and a safe stable region below A. In the regions CD and EF, the system is stable with two generators but not with one generator; similarly in the regions AB and GH, one generator is stable but not two. Fig 6.6 therefore shows that for certain values of compensation, the system can be put into subsynchronous resonance by merely synchronizing or desynchronizing the second generator. Especially significant is the fact that part of the safe stable region AB for one generator is an unstable area for two generators.

It is thus seen from Fig 6.6 that the effect of (c) above predominates and instability occurs at a lower compensation level with two generators. The

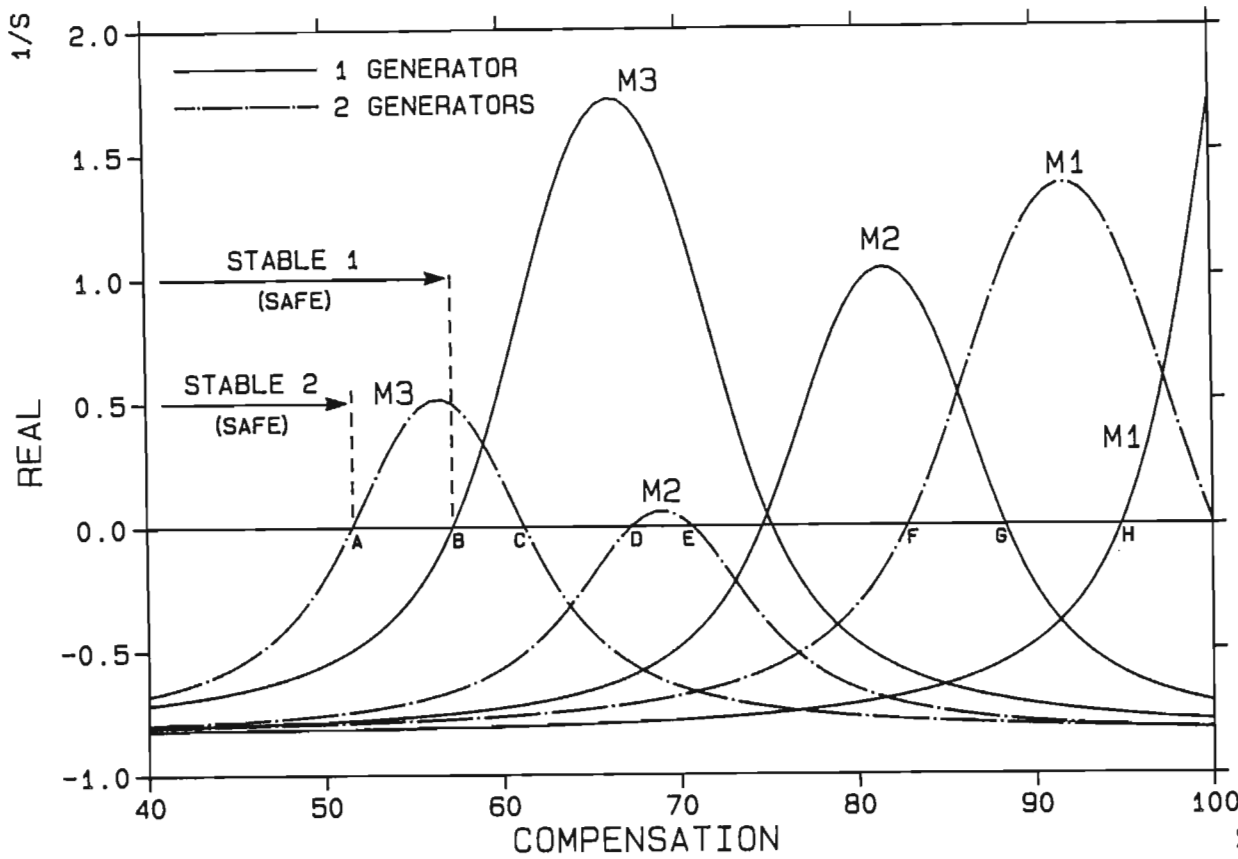

Fig 6.6 Real part of modes M1 to M3 for the one-generator system (1072 MVA) and the equivalent generator system (2144 MVA).

compensation levels at which the mechanical modes first go unstable for one generator and for two generators are compared below in Table 6.3.

Table 6.3 Compensation N(%) giving instability of mechanical modes for one and two generators at Koeberg

	Mechanical Mode		
	M1	M2	M3
One generator	94.9	74.6	57.2
Two generators	82.8	67.3	51.6

The stability characteristics of the system with one and two generators are markedly different as the compensation level is varied and so the second generator must be considered in a stability study.

6.4.2 Effect of transmission line configuration

The reason for the large difference in the stability limits of the mechanical modes for one and two generators is the effect that the addition of the second generator has on the transmission system characteristics. The previous section has shown that a reduction in the maximum permissible value of X_c of about 10% may have to be made when the second generator is added, however this result was calculated for a simple radial transmission line, a system which seldom exists in reality. A previous investigation [24] has shown that the correct representation of the transmission system is important for accurate predictions of SSR and that the single-line equivalent of a more complex system is only valid at a single frequency and compensation level. For this reason the investigation of Sect 6.4.1 is extended here to include a more realistic representation of the transmission system.

Figure 6.7 shows a more accurate representation of the transmission system between the Koeberg power station and the infinite bus where a section of the line consists of a pair of separately compensated parallel lines. The parameter values for this system appear in Appendix I. The following three eigenvalue scans are considered for this system and they are the same as those which were done in an earlier study [24] which considered only one generator at Koeberg:

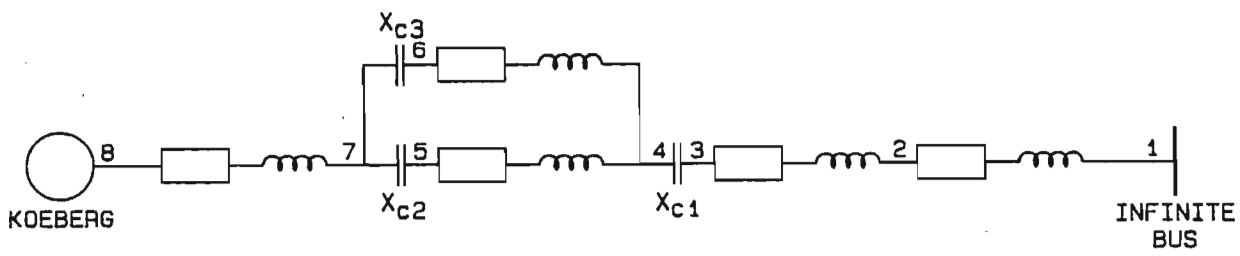

Fig 6.7 More detailed representation of the transmission system between Koeberg and the infinite busbar.

(a) With line 4-5-7 at 60% compensation (X_{c2} = 0.448 p.u.) and line 4-6-7 at 60% compensation (X_{c3} = 1.222 p.u.), the compensation in line 2-3-4 is varied from 40% to 100%.

(b) With line 2-3-4 at 60% compensation (X_{c1} = 0.277 p.u.) and line 4-6-7 at 60% compensation (X_{c3} = 1.222 p.u.), the compensation in line 4-5-7 is varied from 40% to 100%.

(c) With line 2-3-4 at 60% compensation (X_{c1} = 0.277 p.u.) and line 4-5-7 at 60% compensation (X_{c2} = 0.448 p.u.), the compensation in line 4-6-7 is varied from 40% to 100%.

The per-unit values given above are for the one-generator system (1072 MVA base); for the equivalent generator system they are double. The above three eigenvalue scans are performed in each case for both the one-generator and equivalent generator systems.

Case (a):

The real parts of the three active subsynchronous modes M1 to M3 calculated for the two systems as the line 2-3-4 compensation is varied, appear in Fig 6.8. Only M3 goes unstable for these conditions, however M2 is close to being unstable around 90% compensation for two generators whereas it is easily stable for one generator. A comparison between the two M3 curves shows the same effects as were seen in the simple radial transmission line case (Fig 6.6); the mechanical mode is destabilized to a greater degree for one generator than for two and the first occurrence of instability occurs at a lower compensation level with two generators.

Case (b):

Fig 6.9 shows the real parts of modes M1 to M3 as the compensation in line 4-5-7 is varied. The results are similar to those in Fig 6.8 and the same comparisons between the two M3 curves can be made here. Once again there are large regions (51%<N<63% and 75%<N<100%) where the system is stable with one generator but unstable with two and vice

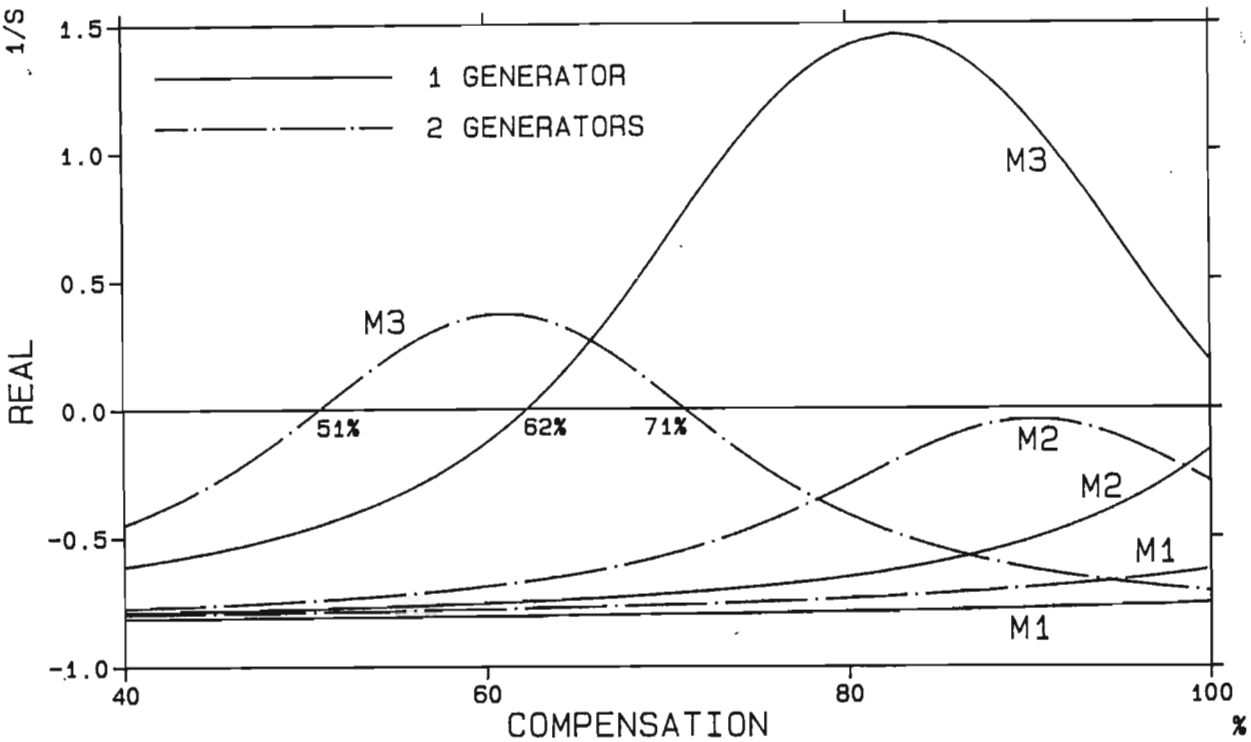

Fig 6.8 Real part of modes M1 to M3 for the one-generator and equivalent generator systems as a function of line 2-3-4 compensation while lines 4-5-7 and 4-6-7 are kept at 60% compensation.

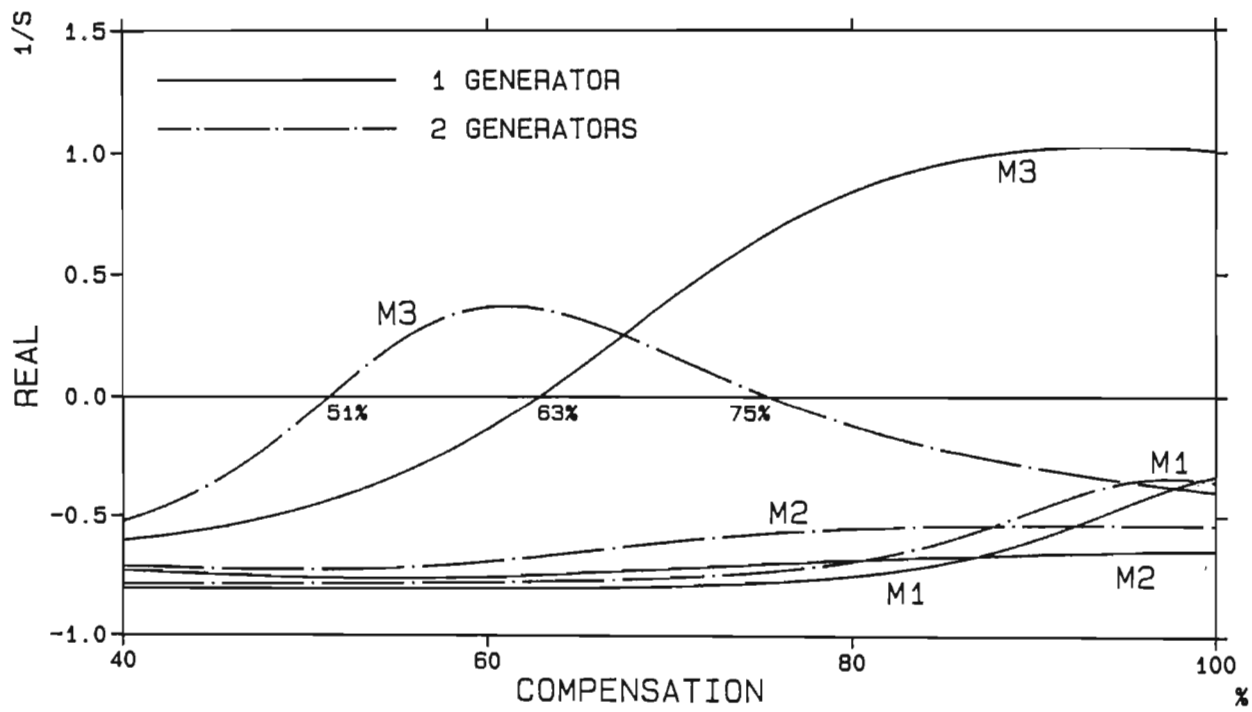

Fig 6.9 Real part of modes M1 to M3 for the one-generator and equivalent generator systems as a function of line 4-5-7 compensation while lines 2-3-4 and 4-6-7 are kept at 60% compensation.

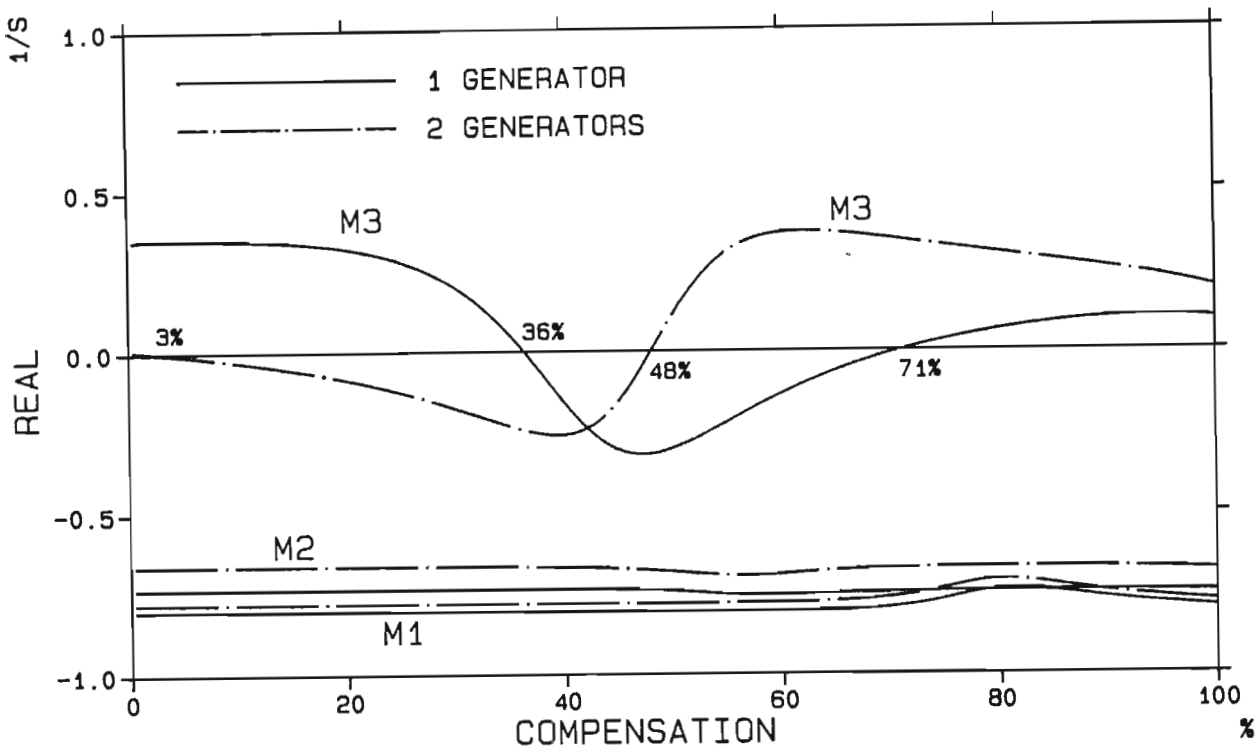

Fig 6.10 Real part of modes M1 to M3 for the one-generator and equivalent generator systems as a function of line 4-6-7 compensation while lines 2-3-4 and 4-5-7 are kept at 60% compensation.

versa. For both case (a) and (b), the reduction in the maximum permissible compensation before the first occurrence of SSR with two generators is greater than that which occurred for the simple single line transmission system.

Case (c):

The real parts of modes M1 to M3 for the compensation variation of line 4-5-6 are shown in Fig 6.10 and they are very different to those of the previous two cases. Mode M3 is destabilized to the same extent with one generator as with two but the regions of instability are vastly different; more so than in the previous two cases. Particularly interesting is the instability of mode M3 with zero compensation in this line and the difference in the stability of the two systems at low compensation levels (3%<N<36%).

The results in this section have shown that the differences in the SSR stability limits for the one and two generator systems, predicted by the simple single line transmission system, were not unrealistic and were not exaggerated by the simplified transmission line. In fact, greater disparities exist between the one generator and two generator stability limits when a more detailed transmission system is considered which makes a case for using the more detailed representation.

6.4.3 Transient calculations

In order to verify the predictions of the small-signal stability calculations in the previous sections, the transient response of both the one-generator station and the equivalent generator station are calculated when the system is subjected to a temporary symmetrical 10% reduction in the infinite bus voltage for a duration of 200 ms. The single line transmission system of Fig 6.1 is assumed and the compensation level chosen is 74% (X_c = 0.746 p.u.; 1072 MVA base); the eigenvalues given in Table 6.2 govern the system dynamic behaviour. The response is shown in Fig 6.11 for the one-generator station and in Fig 6.12 for the equivalent generator station; in each case the variables shown are the generator current, load angle, electric torque and shaft torque on either side of the generator as well as the Fast Fourier Transform (FFT) of certain variables.

The eigenvalues in Table 6.2 for the one-generator station indicated that mode M3 would be unstable and this is seen in Fig 6.11 where the transient curves contain a growing oscillatory component. The FFTs of the shaft torques contain the mechanical mode frequencies at 6.9, 12.6, 15.6 and 92.6 Hz. These compare well with the frequencies predicted by the eigenvalues in Table 6.2 and shown in Table 6.4. Mode M4 at 17.5 Hz is not clearly seen due to its non-excitability from the electrical network. The frequency components at 25, 28 and 31 Hz are due to the mutual coupling between the armature and field circuits [63]. The FFT of the generator current contains the frequency components 34.4, 37.4, 43.1, 50, 56.9, 62.6

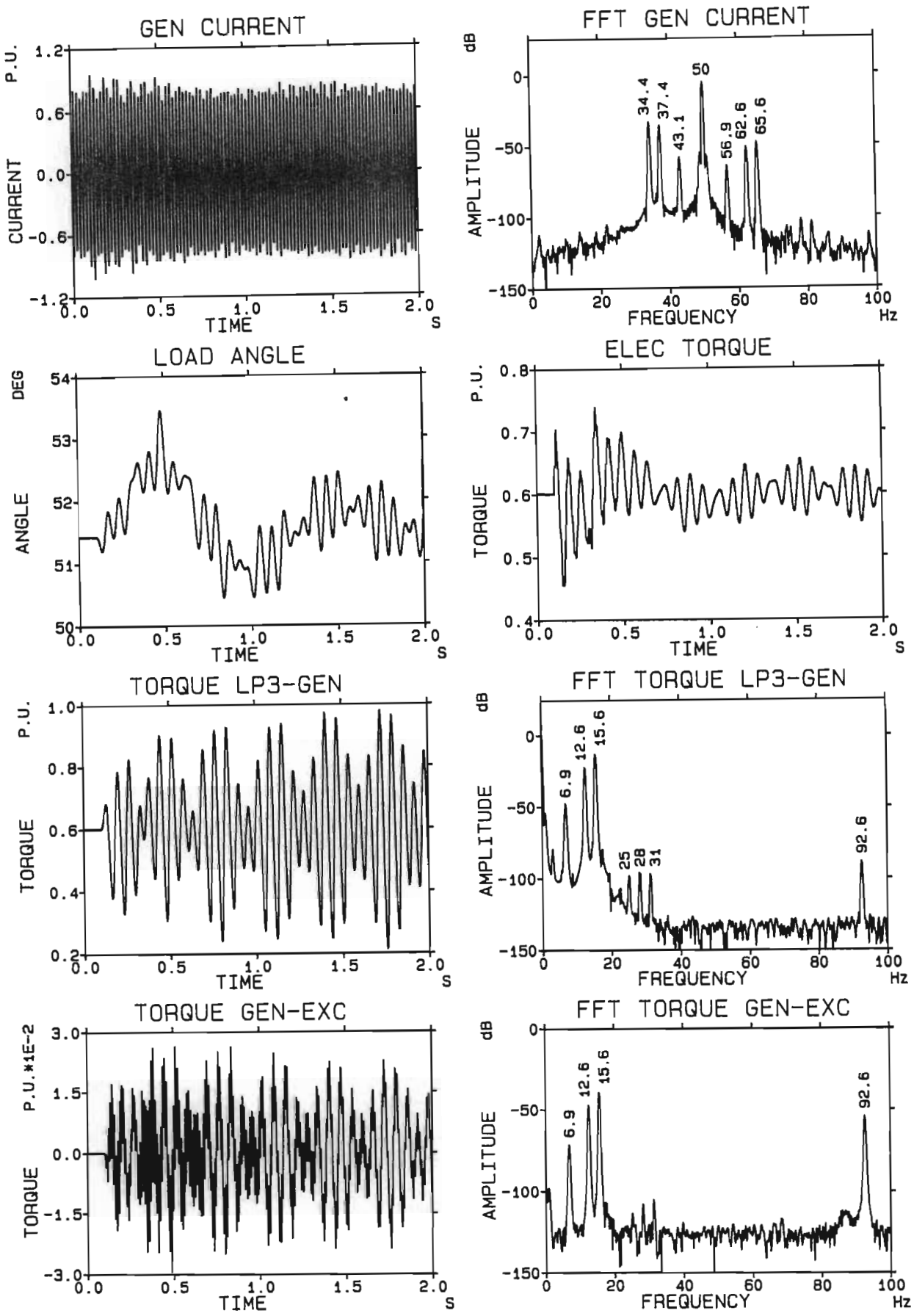

Fig 6.11 Transient response curves for the one-generator system (1072 MVA) after a 200 ms 10% reduction in the infinite busbar voltage at a compensation level of 74%.

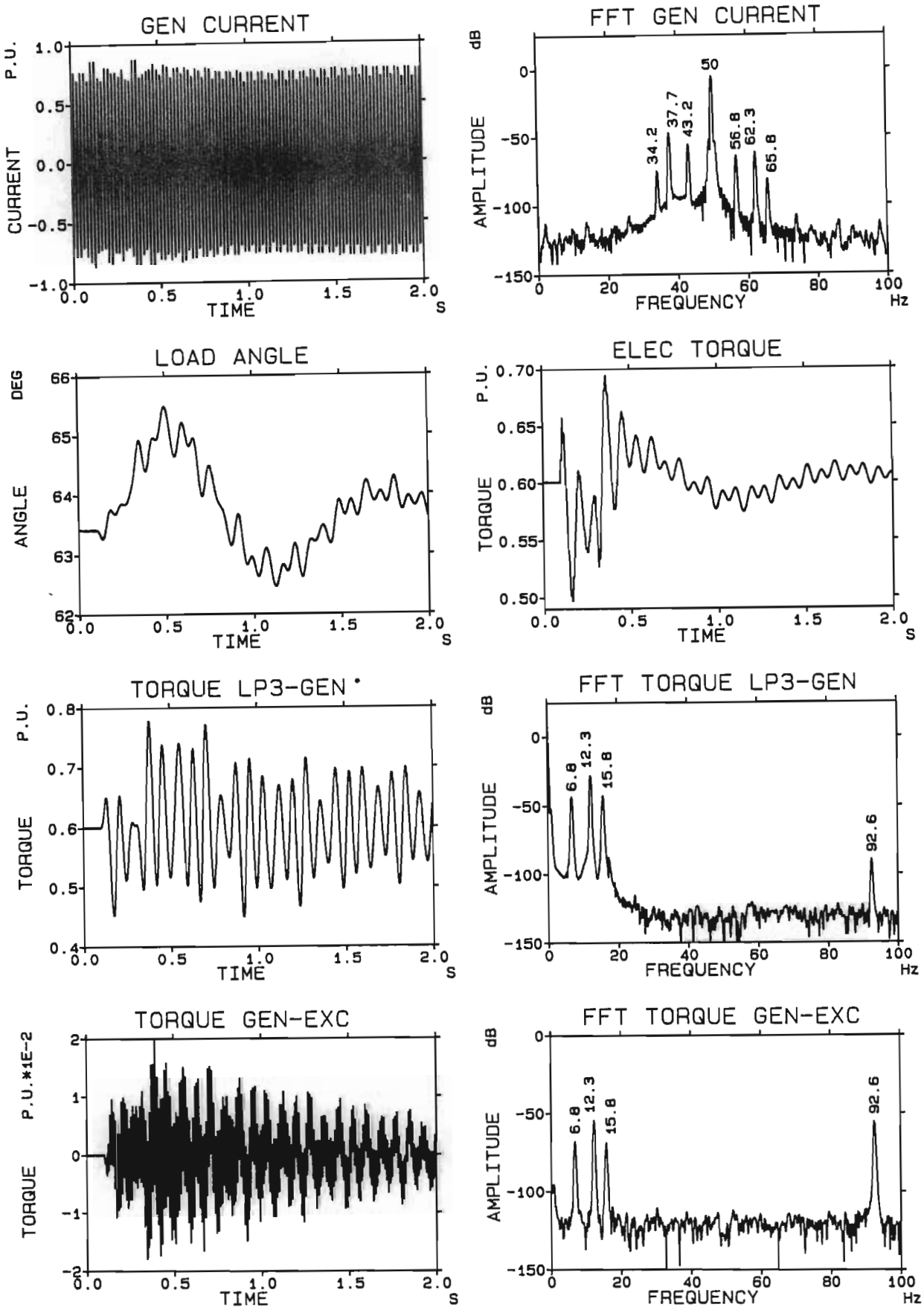

Fig 6.12 Transient response curves for the equivalent generator system (2144 MVA) after a 200 ms 10% reduction in the infinite busbar voltage at a compensation level of 74%.

and 65.6 Hz. These components are the complementary mechanical frequencies and appear at $50 \pm f_{mi}$, where f_{mi} are the natural frequencies of the multi-mass shaft [63].

The eigenvalues in Table 6.2 indicated that the equivalent generator station would be stable and this is seen to be true by the decaying oscillations of the displayed transient curves in Fig 6.12. However, this is not a safe operating point as discussed earlier, for if one of the two generators (represented by the equivalent generator) was switched out, then the resulting one-generator system would experience subsynchronous instability as seen in Fig 6.11. The FFTs of the current and shaft torques show similar frequency components to those of the one-generator system in Fig 6.11 and agree well with the values predicted by the eigenvalues in Table 6.2 and shown in Table 6.4.

Table 6.4 Mechanical mode frequencies predicted by eigenvalues in Table 6.2

Mode	Frequency (Hz)	
	One generator	Equivalent generator
0	0.95	0.81
1	6.87	6.83
2	12.55	12.31
3	15.63	15.79
4	17.49	17.49
5	92.59	92.59

The results have shown that the addition of the second generator alters the damping of some the system mechanical modes (and hence their stability), but only has a small effect on the frequency of these modes. Although the effect on the frequency is small, it could be important if there is possible torsional interaction with other turbogenerators in the system (see Chapter Seven).

6.5 Two-Generator Multi-Machine Representation

In this section the torsional characteristics of the Koeberg power station are investigated when the 2144 MVA generating capacity is represented as a multi-generator system as shown in Fig 6.1. The results obtained with this station representation are compared with those obtained in Sect 6.4 using an equivalent generator representation.

The eigenvalue scan in Fig 6.5 obtained for the equivalent generator system is repeated with the two generators represented separately and the results appear in Fig 6.13. Table 6.5 contains a set of eigenvalues from these loci calculated at a compensation level of 74%.

Table 6.5 Two-generator system eigenvalues calculated for a compensation level of 74%

Mode	Common mode			Anti-mode		
		Real	Imaginary		Real	Imaginary
Supersynch. flux	E1	-11.3	±558.9			
Subsynch. flux	E2	-10.5	±69.8			
Synch. flux	E3	-2.91	±314.1			
Supersynch. mech.	M5	-0.79	±581.8	M5a	-0.79	±581.8
Subsynchronous mechanical	M4	-1.05	±109.9	M4a	-1.05	±109.9
	M3	-0.72	±99.2	M3a	-0.87	±100.9
	M2	-0.30	±77.3	M2a	-0.87	±78.5
	M1	-0.61	±42.9	M1a	-0.98	±43.6
Inertial mode	M0	-1.04	±5.10	M0a	-1.68	±7.36
Magnetic stability	M	-0.11	0.0	Ma	-0.19	0.0
Damper circuits	R1	-1.10	0.0	R1a	-1.41	0.0
	R2	-10.8	0.0	R2a	-12.8	0.0
	R3	-17.5	0.0	R3a	-19.1	0.0

A comparison of Fig 6.5 with Fig 6.13 and the eigenvalues in Table 6.2 with those in Table 6.5 shows that the modelling of the two generators separately does not produce a duplicate set of modes (the six mechanical modes M0 to M5 and the four rotor circuit modes R1, R2, R3 and M) of a single generator system. Instead, for each generator mode of Fig 6.5 there now appears a pair of modes in Fig 6.13. These pairs are the so-called common (or symmetrical) and anti- (or anti-symmetrical) modes associated with symmetrical resonant systems [55] and have been reported on previously [57,58] in studies on other systems.

Figure 6.14 shows the mode shapes for the mechanical system common modes and anti-modes determined from the system eigenvectors. Only the real parts are shown since the imaginary parts are all zero. It is clearly seen that the common modes represent an in phase oscillation between the generators and the anti-modes an out-of-phase oscillation. The common- and anti-mode mode shapes are compared for one of the generators in Fig 6.15 and it is seen that although there is a small noticeable difference in the rotor deflections for the two modes of oscillation they are essentially the same. For mechanical modes M4 and M5, only one mode is seen as in each case the common mode and anti-mode are almost coincident; this is because these modes are only weakly excited from the electrical network and are thus weakly coupled.

The anti-mode loci of the two-generator system are only slightly affected by a change in compensation level. However, the common mode loci are identical to the loci of the equivalent generator system. Thus, for the system in Fig 6.1, the level of compensation permitted before the onset of instability can be calculated with either a two-generator multi-machine representation or a single equivalent generator representation (assuming the two generators are identical).

The next section investigates the anti-modes in more detail, particularly how they are affected by the electrical operating conditions at the generator terminals.

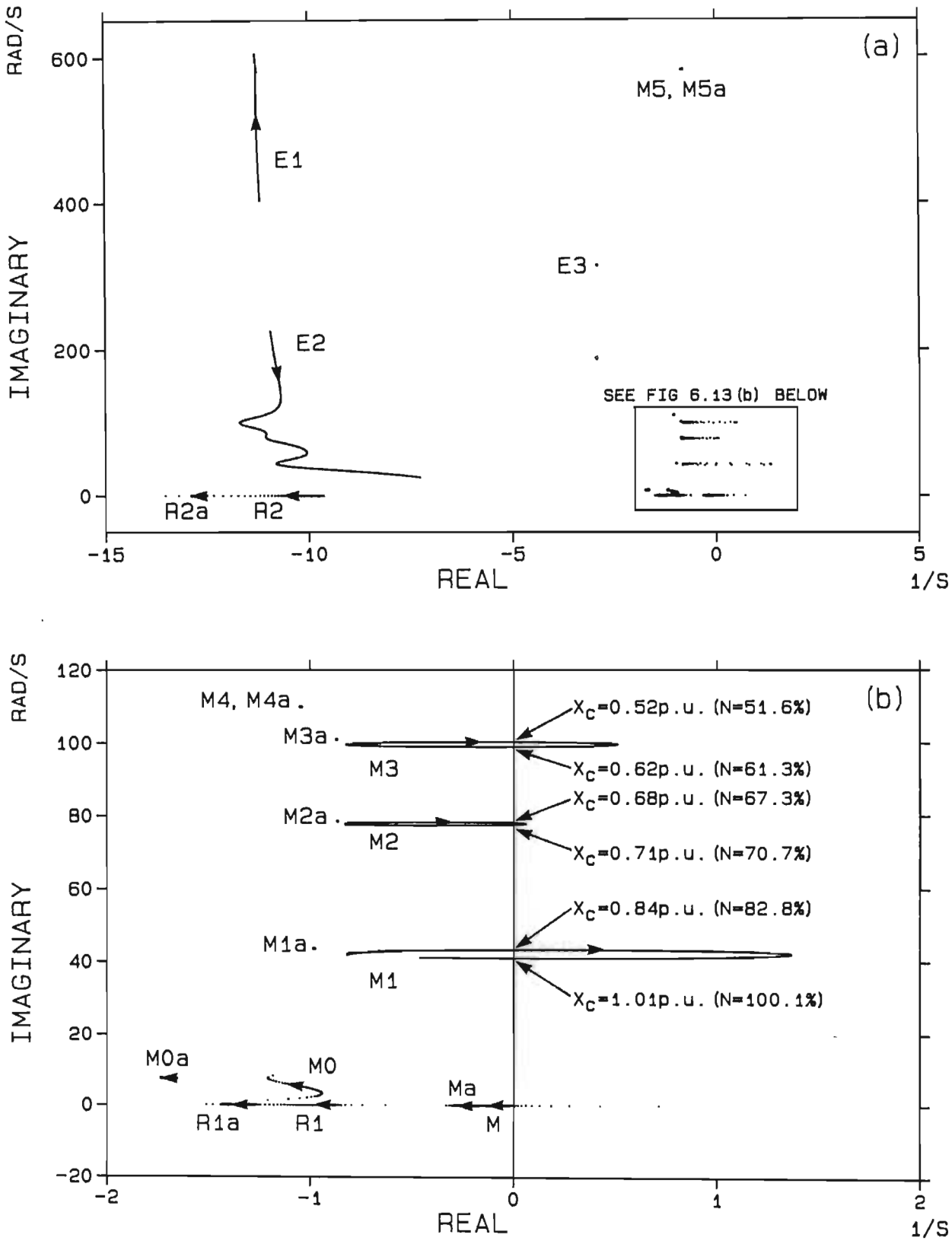

Fig 6.13 Eigenvalue loci for the two-generator system in Fig 6.1 as the compensation N is varied from 10% to 105%.

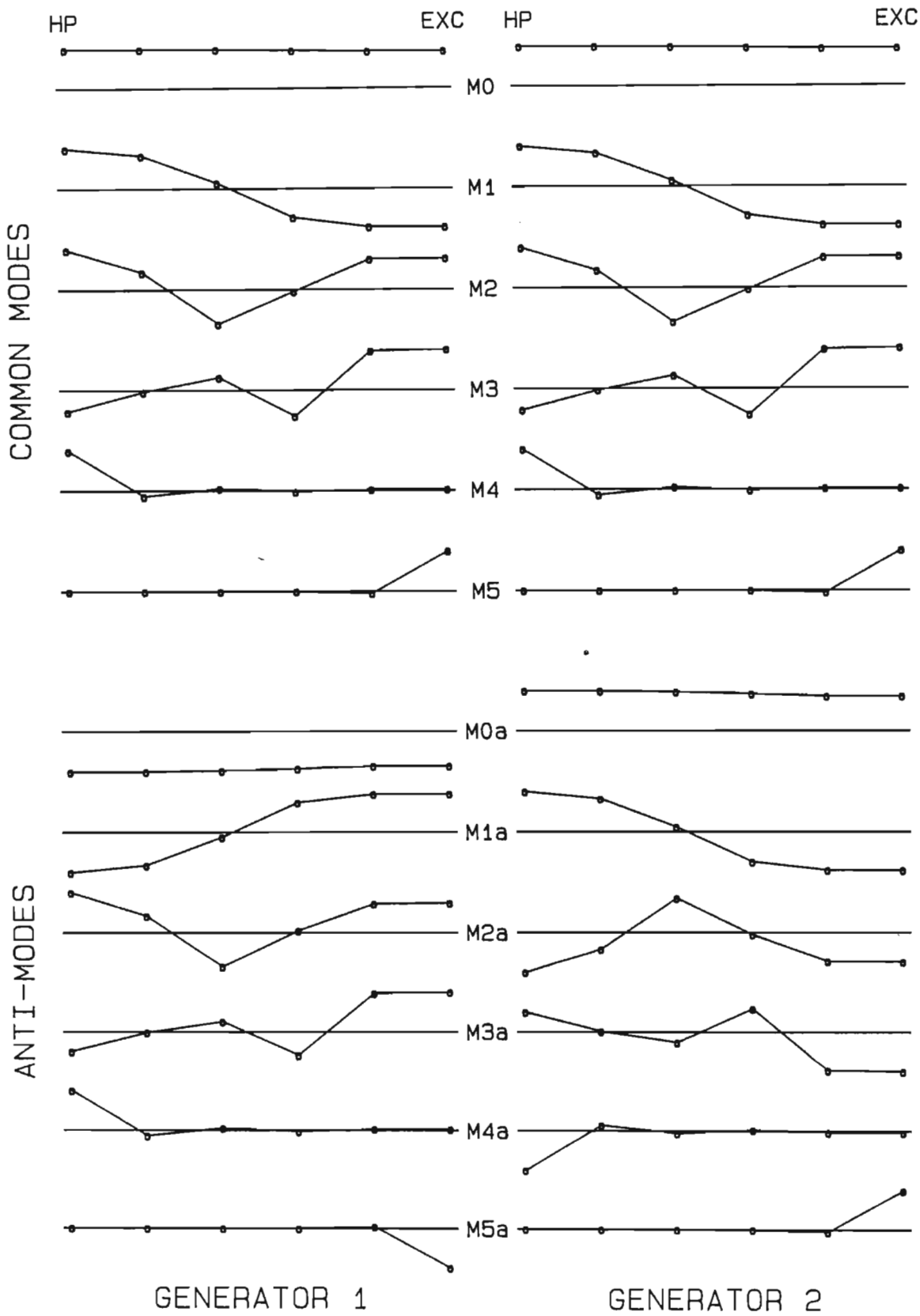

Fig 6.14 Generator mode shapes for the common modes M0 to M5 and the anti-modes M0a to M5a.

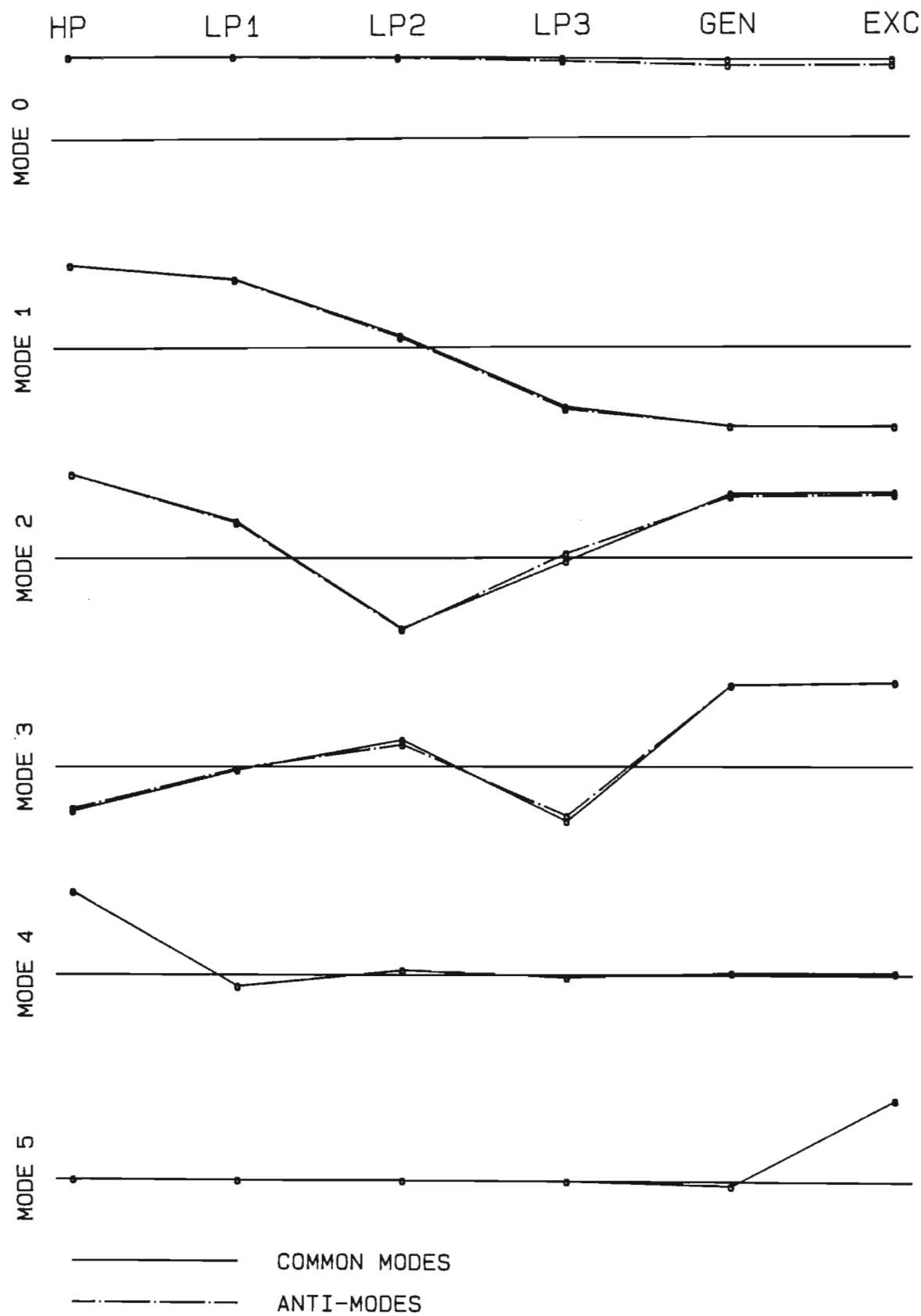

Fig 6.15 Comparison of shaft deflections for the common and anti-modes.

6.6 Investigation of anti-modes

6.6.1 Small-signal analysis

The effect of active power variation on the anti-mode loci can be seen in Fig 6.16 which shows a selection of the eigenvalues in the subsynchronous range as the terminal power of each generator is increased from 0.05 p.u. to 0.95 p.u. at a compensation level of 74%. The anti-modes M0a, R1a, Ma and M4a all show large variations in their dampings as the power transmitted increases and this variation is in each case in the same direction as occurs for the corresponding common mode. However, the anti-modes M1a, M2a and M3a corresponding to the active subsynchronous common modes are hardly affected by changes in the total power transferred.

Since the anti-modes involve inter-unit oscillations, it is interesting to investigate the effect on them of differences in the operating points between the two generators. Fig 6.17(a) shows a selection of the subsynchronous eigenvalue loci calculated at 74% compensation as the generator-2 terminal voltage is varied from 1.0 p.u. to 1.1 p.u. while the generator-1 terminal voltage is held constant at 1.1 p.u. The M3 and M3a modes shapes for the first and last scans are shown in Fig 6.17(b) where 'first scan' is the unbalanced condition with V_{t1} = 1.1 p.u., V_{t2} = 1.0 p.u. and 'last scan' is the balanced conditions with both terminal voltages equal to 1.1 p.u.; the imaginary values for the last scan are zero. Differences in the voltages of the generators only has a small effect on the subsynchronous torsional eigenvalues while the mode shapes (illustrated by M3 and M3a) are practically the same for equal and unequal voltages.

The results of Fig 6.17 are repeated in Fig 6.18 but this time an active power difference between the two generators is considered. Generator-1 power is varied from 0.05 p.u. to 0.45 p.u. while generator-2 power is varied from 0.95 p.u. to 0.55 p.u. so that the power transmitted to the infinite bus is maintained at 1.0 p.u. The eigenvalue loci in Fig 6.18(a) show that the active subsynchronous mechanical modes and their anti-modes are unaffected by the unbalance in the power between the generators.

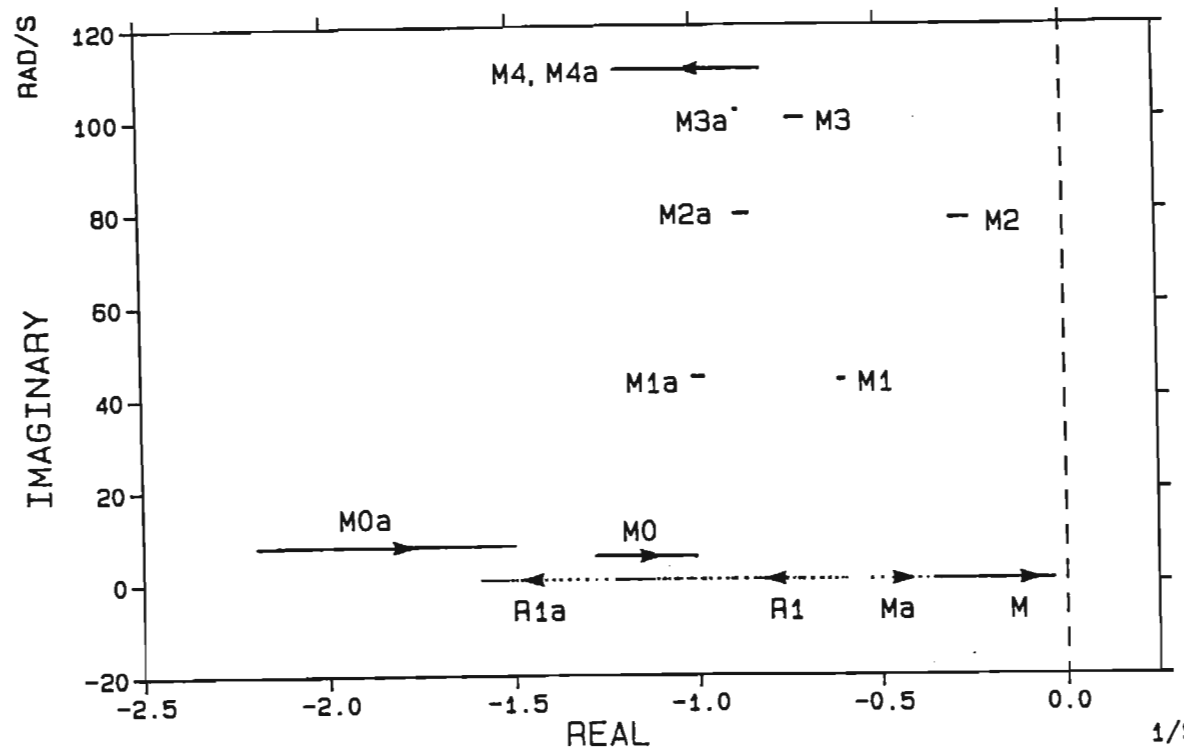

Fig 6.16 Selected eigenvalue loci for the two-generator system in Fig 6.1 at a compensation level of 74% as P_{t1} and P_{t2} are simultaneously varied from 0.05 p.u. to 0.95 p.u.

However, the mode shapes in Fig 6.18(b) indicate that during an unbalanced power condition the common modes are not totally in phase, and the anti-modes are not totally out-of-phase. This effect is not significant though with the phase shift in generator oscillations away from truly in-phase and out-of-phase modes being no more than 9 degrees.

6.6.2 Transient analysis

The transient results in Fig 6.12 calculated with the equivalent generator station representation, were repeated with the two-generator representation and the results for the two-generators were exactly the same as those obtained in Fig 6.12 with the equivalent generator. The mechanical common

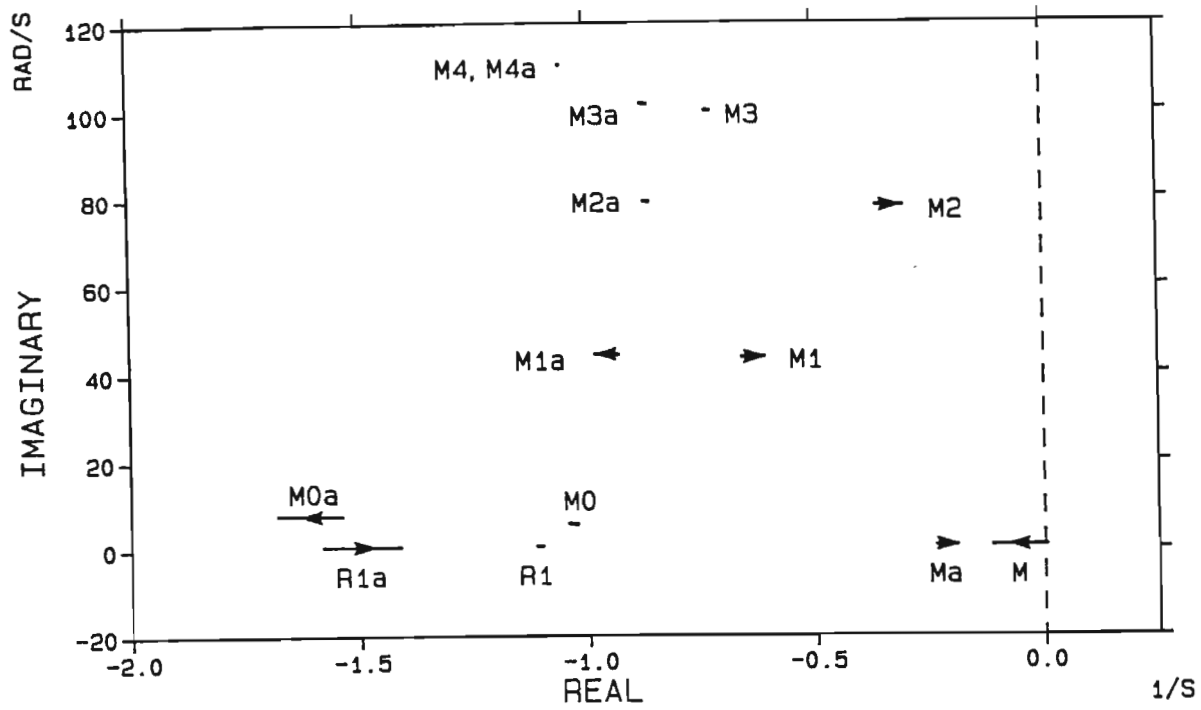

Fig 6.17(a) Selected eigenvalue loci for the two-generator system in Fig 6.1 at a compensation level of 74% as V_{t2} is varied from 1.0 p.u. to 1.1 p.u. and V_{t1} is held at 1.1 p.u.

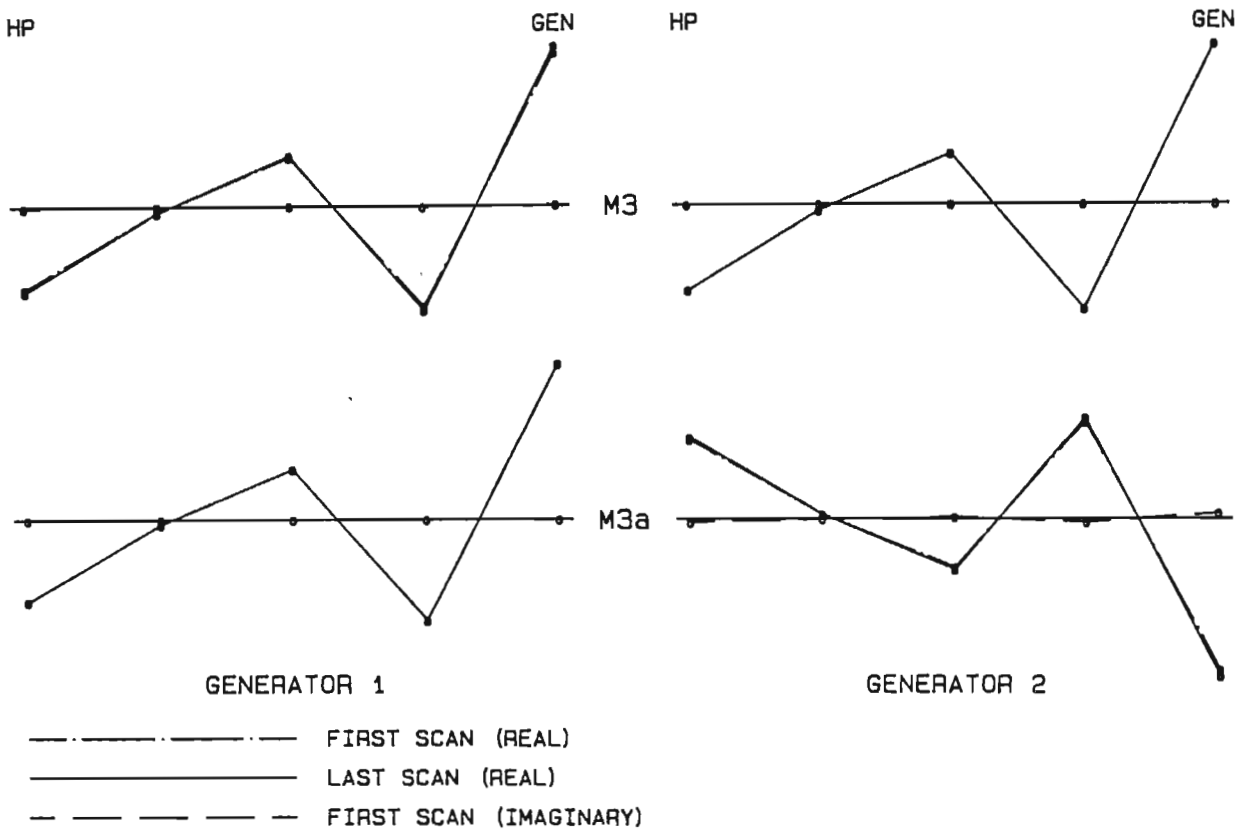

Fig 6.17(b) M3 and M3a mode shapes corresponding to loci in Fig 6.17(a); 'First Scan': V_{t1} = 1.1 p.u., V_{t2} = 1.0 p.u.; 'Last Scan': $V_{t1} = V_{t2}$ = 1.1 p.u.

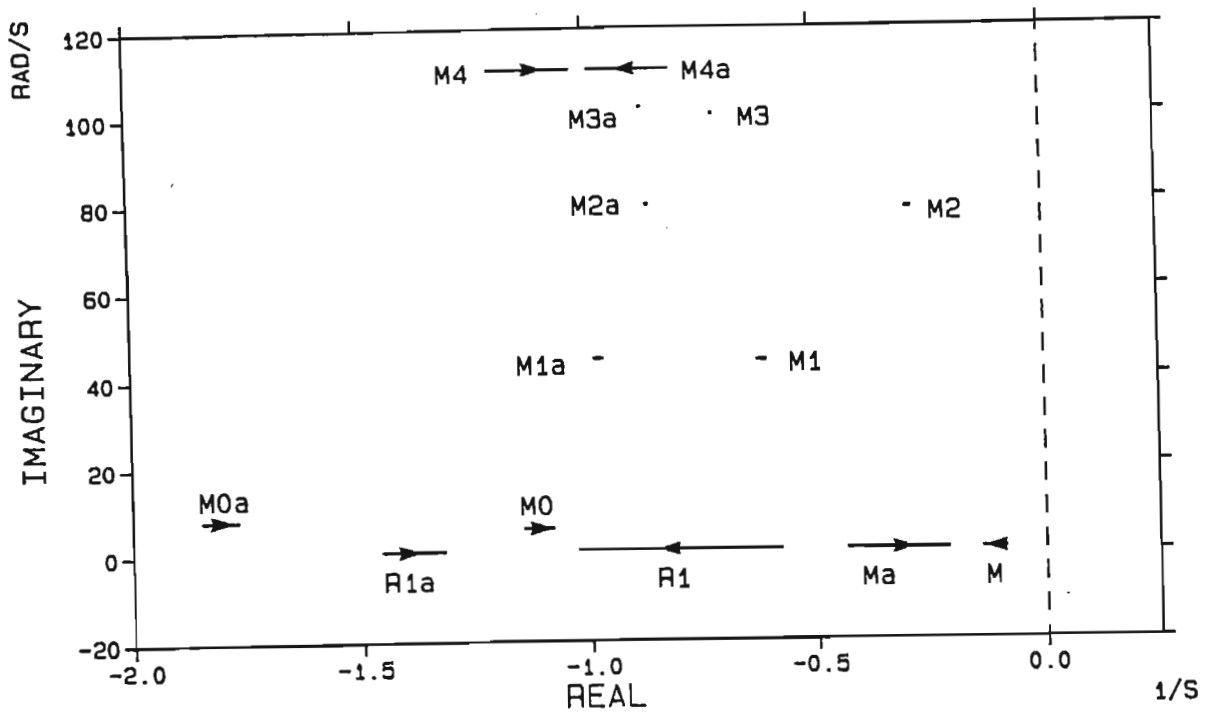

Fig 6.18(a) Selected eigenvalue loci for the two-generator system in Fig 6.1 at a compensation level of 74% as P_{t1} is varied from 0.05 to 0.45 p.u. and P_{t2} is varied from 0.95 to 0.55 p.u.

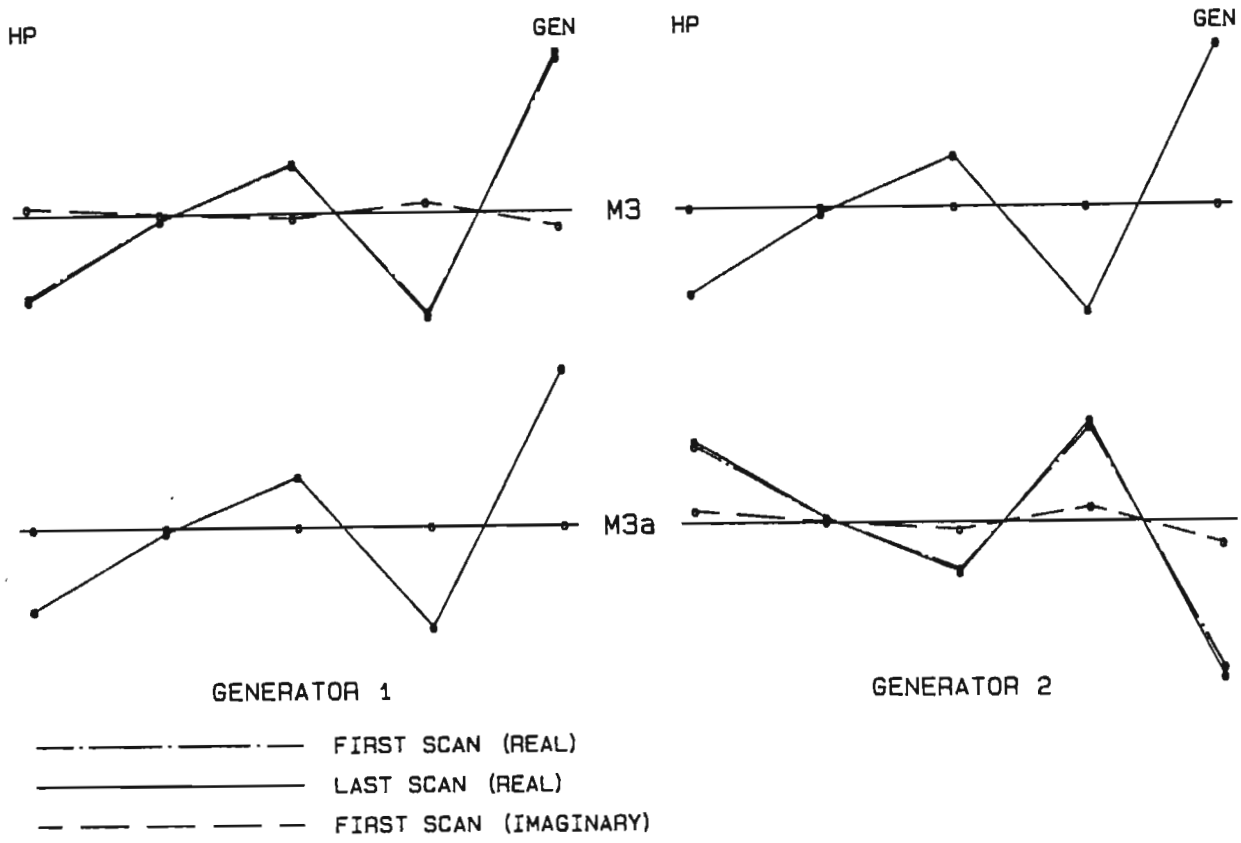

Fig 6.18(b) M3 and M3a mode shapes corresponding to loci in Fig 6.18(a); 'First Scan': P_{t1} = 0.05 p.u., P_{t2} = 0.95 p.u.; 'Last Scan': P_{t1} = 0.45 p.u., P_{t2} = 0.55 p.u.

mode and anti-mode frequencies shown in Table 6.6 (as predicted by the system eigenvalues in Table 6.5) indicate that only the common modes are excited for this fault and system condition. The anti-modes are not excited since both generators were operating under identical conditions and the fault was remote from the station. To induce anti-mode oscillations, the generators must be at different operating points or the fault must not be symmetrical to the two-generators.

Table 6.6 Mechanical mode frequencies of two-generator system as predicted by eigenvalues in Table 6.5

Frequency (Hz)			
Common Mode		Anti-Mode	
M0	0.81	1.17	M0a
M1	6.83	6.94	M1a
M2	12.31	12.49	M2a
M3	15.79	16.06	M3a
M4	17.49	17.49	M4a
M5	92.59	92.59	M5a

In order to illustrate anti-mode oscillations the transient response of the two-generator system is calculated for a temporary change in the generator shaft powers lasting 100 ms. The shaft power of generator 1 is decreased by 5% and that of generator 2 is increased by 5% so that the total power transmitted to the infinite bus remains constant. This results in pure anti-mode oscillations as can be seen from the generated transient results in Fig 6.19 which show the generators oscillating exactly 180 degrees out-of-phase in all variables. The FFT of the LP3-GEN torque confirms the frequencies present as being those corresponding to the anti-modes in Table 6.6.

The fault considered in Fig 6.19 is a symmetrical fault in terms of anti-mode excitation resulting in transient transfers of energy between the generators but not between the station and the infinite bus. In Fig 6.20

the transient response of certain variables are shown for a 200 ms increase in the transformer reactance X_2 in Fig 6.1 to 0.2 p.u. The speed of the mode 1, 2 and 3 inertias (pq_1, pq_2 and pq_3) are shown for a short period after the fault and then again after a few seconds. These speeds are translated into all physical rotor variables through the mode shape vectors $\underline{Q}_1$, $\underline{Q}_2$ and $\underline{Q}_3$.

For this fault, rotational energy is exchanged between the generators as well as between the station and the infinite bus, resulting in both the common and anti-modes being excited. Thus, for a particular mode, the generators oscillate both in-phase and out-of-phase but at slightly different frequencies. The result is that the two generators oscillate at a phase between 0 and 180 degrees depending upon the relative amplitudes of the common and anti-modes. Immediately after the fault, the anti-mode amplitude is relatively large resulting in large phase shifts as evident in the initial mode 1, 2 and 3 speeds (Fig 6.20(c), (e) and (g)). For all three modes, the anti-mode are more damped (see eigenvalues in Table 6.5) so as time progresses the anti-mode amplitudes become less than the common mode amplitudes and the generator mode speeds become in-phase (Fig 6.20(d), (f) and (h)). The time interval for this to occur depends on the difference in the damping of the common and anti-modes and is seen to be much shorter for mode 2 due to the larger difference in the mode 2 common and anti-modes dampings as seen in Table 6.5.

The occurrence of both common mode and anti-mode oscillations together is further verified in Fig 6.21 by transient and FFT calculations. Figs 6.21(b) and (d) show the FFTs of two transient signals from the fault in Fig 6.20 and the presence of double peaks corresponding to common modes and anti-modes is clearly evident for some of the modes. Mode 2 does not show this well in either signal due to the common mode being much less damped and thus having a much larger magnitude. In Fig 6.21(a) the angle of the generator-2 mode 3 inertia is shown calculated when each generator is modelled with only mode 0 and mode 3. The phase relationship between the common mode and anti-mode oscillations for a certain mode within a

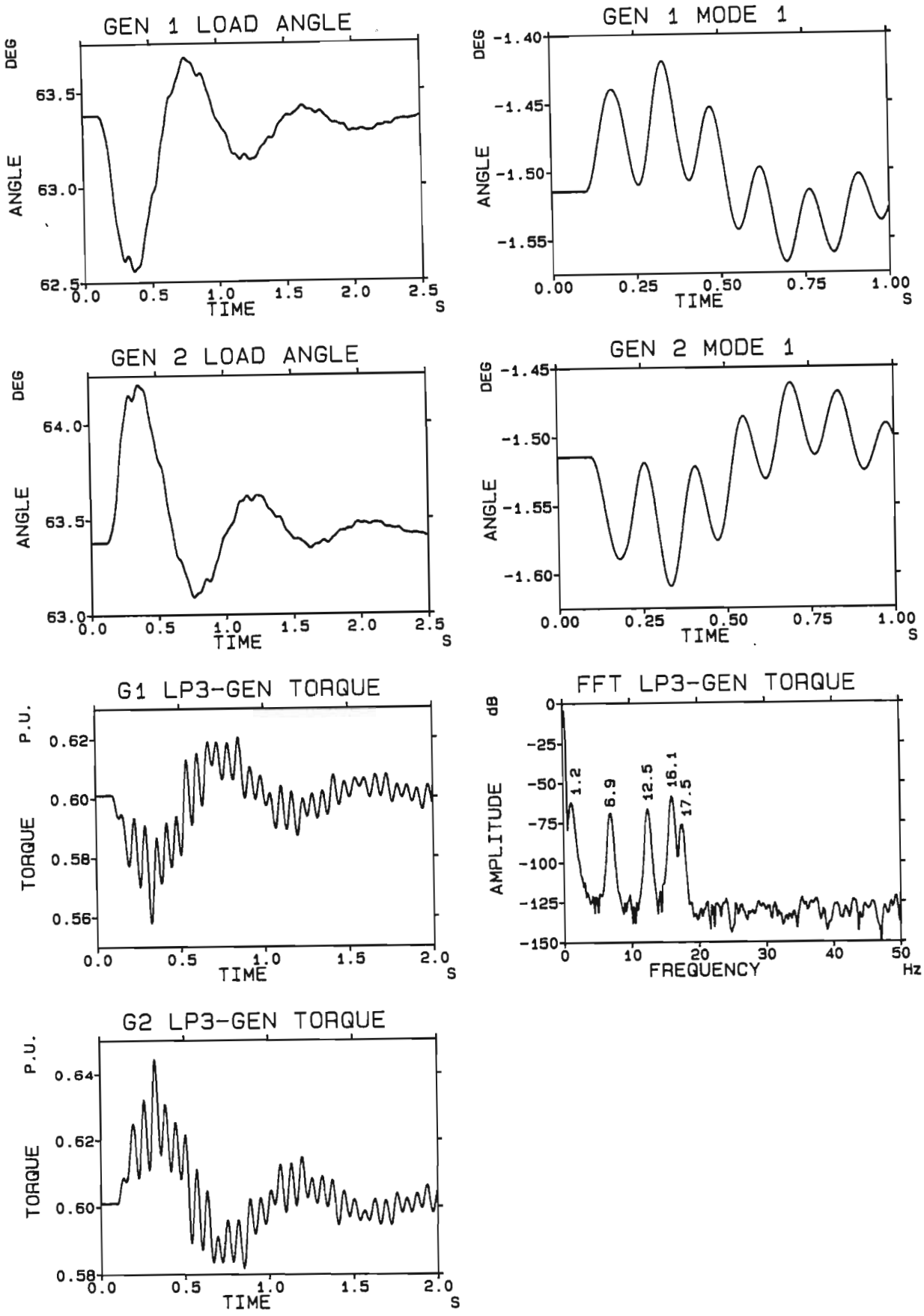

Fig 6.19 Transient response of the two-generator system at 74% compensation to a simultaneous 5% decrease in generator-1 shaft power and 5% increase in generator-2 shaft power lasting 100 ms.

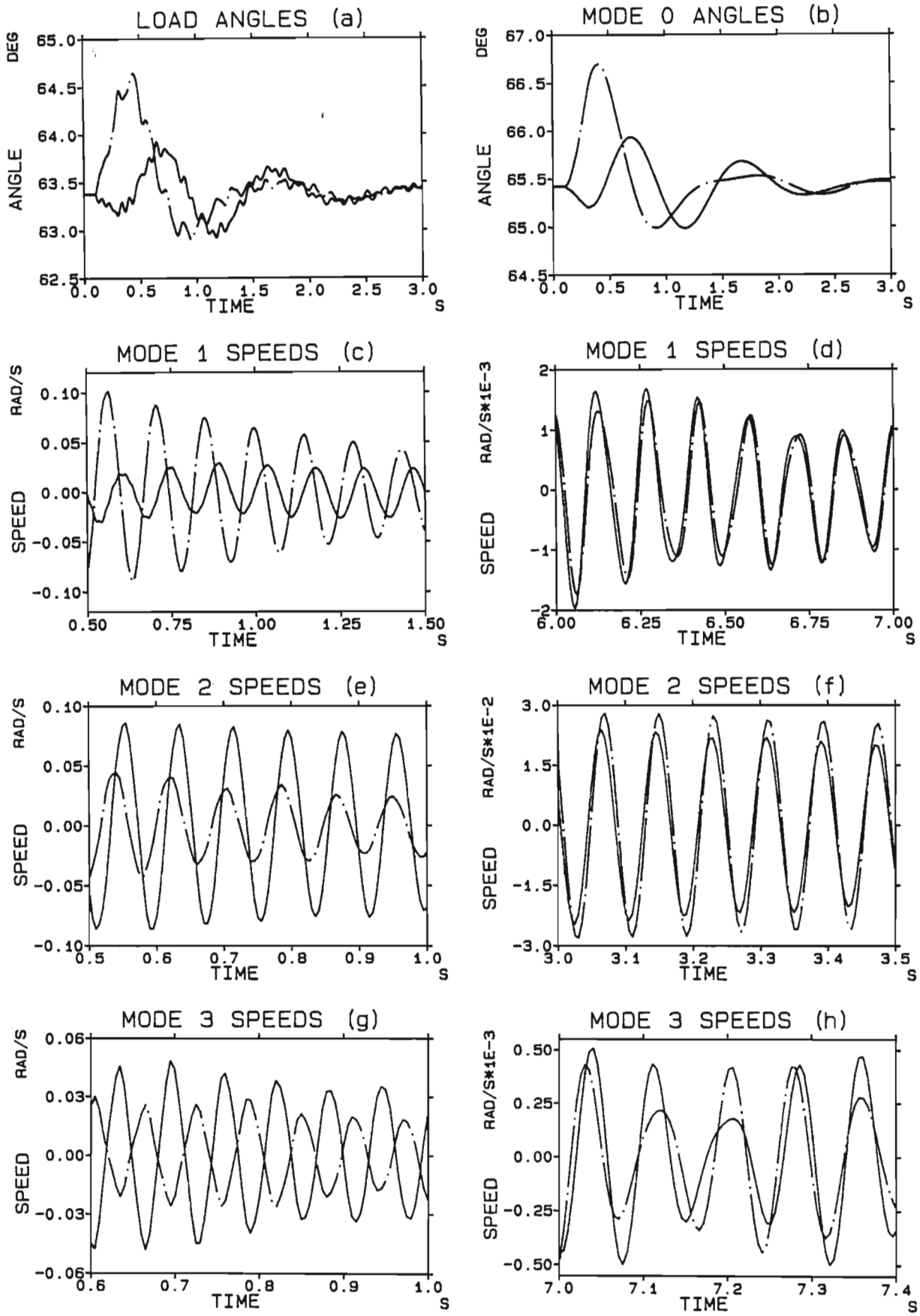

Fig 6.20 Transient response of the two-generator system, at a compensation level of 74%, to a 200 ms increase in X_2 in Fig 6.1 from 0.15 p.u. to 0.2 p.u.

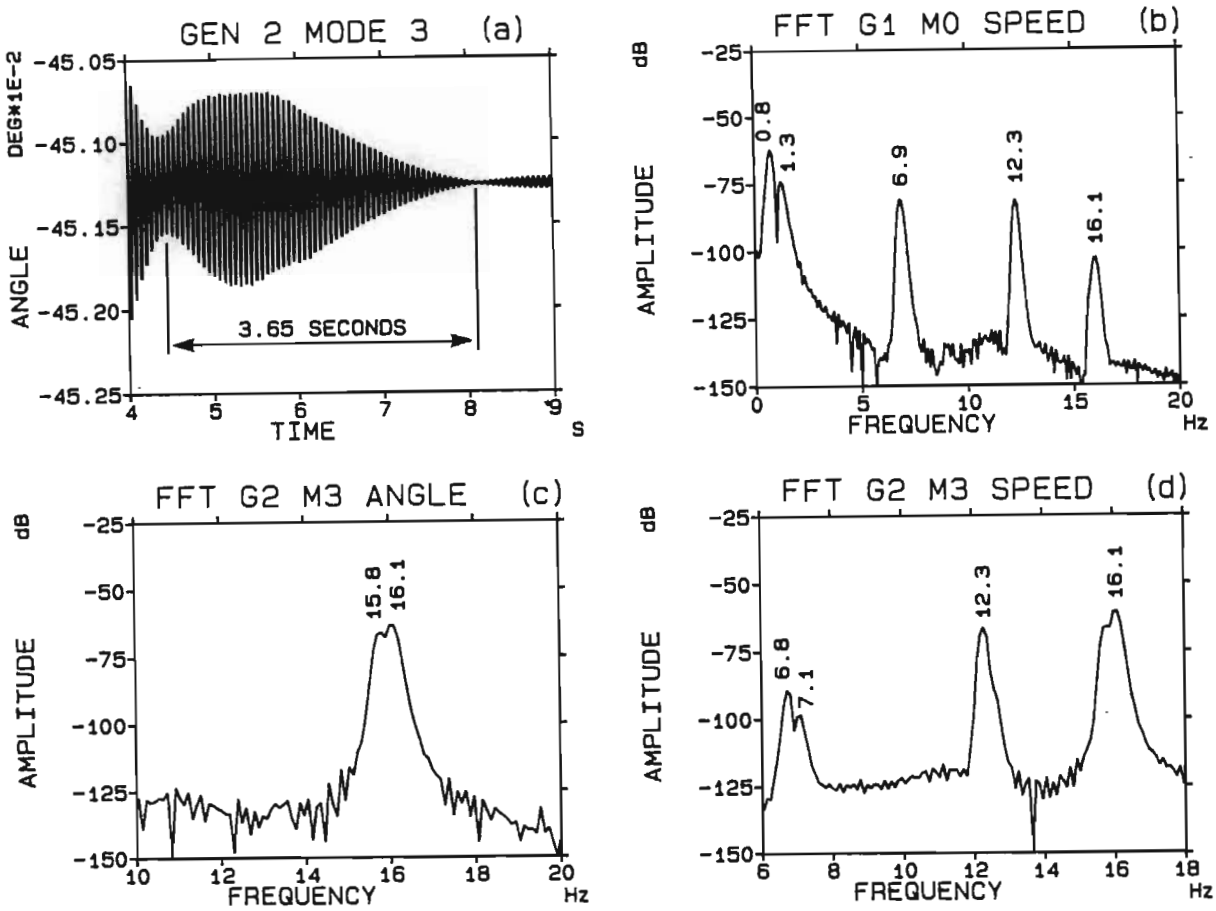

Fig 6.21 Further transient and FFT results for the fault in Fig 6.20.

particular generator will vary since their frequencies are different. At some time they will enhance each other and at a later time they will cancel each other. The period of this cyclic interaction will depend on the difference in the frequencies of the two oscillations. From Table 6.6, the difference in the mode 3 common and anti-mode frequencies is 0.27 Hz and this corresponds to a cycle of constructive and destructive interference of period 3.70 seconds. The 3.65 second period amplitude modulation obtained in Fig 6.21(a) thus verifies the presence of both modes of oscillation as does the FFT of this signal in Fig 6.21(c).

6.7 Conclusions

This chapter has investigated the effect of adding a second 1072 MVA turbogenerator to an existing one at the Koeberg power station which feeds a series capacitor compensated transmission system. It has compared the effect of modelling the new two-generator system as a single equivalent generator or as a multi-machine system consisting of two separate generators. The following conclusions can be drawn from the results presented:

(a) The addition of a second generating unit effectively alters the interconnecting transmission system characteristics, and so previous stability studies for one generator are no longer valid, but are generally rather optimistic.

(b) There are certain operating conditions when a stable operating point (with one generator) may become unstable when a second generator is added (and vice versa). Hence, the system can be put into an unstable subsynchronous condition by merely synchronizing or desynchronizing the second generator at certain values of capacitive compensation.

(c) The modelling of two generators as a multi-machine system introduces anti-resonant modes which represent an out-of-phase resonance between the two generators. For the purpose of maximum permissible capacitor compensation calculations, these anti-modes appear to have little effect, and no advantage is gained by modelling the two generators separately rather than as an equivalent single generator.

(d) It is possible to have common mode and anti-mode oscillations present at the same time during a transient; in fact this is likely to be the norm rather than the exception. This results in varying phase relationships between oscillations of the two generators.

CHAPTER SEVEN

TORSIONAL INTERACTION BETWEEN NON-IDENTICAL GENERATING UNITS

7.1 Introduction

The previous chapter has investigated the torsional characteristics of the Koeberg power station with two separate generating units and although differences in the operating point between the two units were considered, at all times it was assumed that the two generators were identical. This is rarely the case and in practice there will always be some degree of dissimilarity between the parameters of the two machines due to manufacturing tolerances. Moreover, it is possible that two markedly different generators at a power station may have a common torsional mode and it is important to know how these generators will interact, especially in the presence of capacitively compensated networks.

Although some work has been done on the torsional interaction between non-identical adjacent units [58-60], it would appear that the understanding of this subject is far from complete. This chapter therefore extends the work of Chapter Six by considering non-identical adjacent units and in addition investigating the possibility of torsional interaction between remote generators in a network.

The damping of SSR oscillations in a turbogenerator by means of a Controlled Shunt Reactor (or Shunt Reactor Stabilizer) is well known and many publications are available in the literature dealing with this topic. More lately, the damping of SSR oscillations in two interacting adjacent turbogenerators has been investigated [40,42] and it was proposed to damp

out SSR oscillations in these adjacent units by means of a single controlled shunt reactor (connected at the common high voltage side of the two generator step-up transformers) controlled by the sum of the speed signals of the two units. These studies only considered truly identical turbogenerators operating under identical conditions; under such conditions the speed signals are always in phase and a single equivalent generator could be used to model the system. This chapter extends the previous work of Refs [40,42] by again considering a single controlled shunt reactor but for non-identical adjacent generators and for identical units but at different operating points; in such cases the speed signals may have an appreciable phase difference. It is not the purpose of this section to consider the design of the controller for such a system, but rather to investigate the effect of dissimilarities between the units (and the resultant phase variation in the speed signals) on the operation of a previously designed controller [40] which did assume that the units were identical and running at the same operating point.

The system considered for the analysis of adjacent units is the same two-generator system used in Chapter Six (shown in Fig 6.1) and the parameters for this system appear in Appendix I. For all results, unless otherwise stated, the initial conditions are V_b = 1.0 p.u., $V_{t1} = V_{t2}$ = 1.1 p.u. and $P_{t1} = P_{t2}$ = 0.6 p.u. The parameters in Appendix I of identical generators are altered (by varying amounts) in the following sections to realistically portray non-identical units.

7.2 Differences in Mechanical Damping

The most probable difference that will occur between the parameters of adjacent units, and the most crucial in terms of SSR, will be the values of the mechanical damping since this is highly dependant on the loading of the unit and may be quite different even for nominally identical units. In Sect 6.6.1 the effects of differences in electrical loading were investigated and it was assumed that the mechanical mode dampings of the two units were identical and independent of electrical loading. This is

in fact not strictly correct, however it enabled the effect of differences in electrical damping to be investigated separately to that of mechanical damping differences. In the same vein, in this chapter the mechanical damping is varied while the electrical loading on a unit remains constant, thereby enabling the effects of mechanical damping differences to be investigated free from influences of electrical damping.

In order to investigate the effect of mechanical damping differences between the two generators, the system in Fig 6.1 is reconsidered without any series capacitance and with a transmission line reactance of X_L = 0.2637 p.u. (which is the effective value of reactance corresponding to a compensation level of 74%). The system eigenvalues are calculated as the generator-1 mode dampings are varied from 0.0 to 0.785 s^{-1} and the generator-2 mode dampings are simultaneously varied from 1.57 s^{-1} to 0.785 s^{-1} resulting in the total combined damping for each mechanical mode being constant at each calculation (and equal to the combined damping of the identical units in Chapter Six). The resultant eigenvalue loci for the active subsynchronous modes are shown in Fig 7.1.

As the mechanical damping difference between the generators increases, the anti-modes become more damped while the common modes become less damped indicating that the anti-mode damping is related more strongly to the damping of the highest damped generator while the common mode damping is determined more by the lowest damped generator. At the extreme case of generator-1 having zero damping, the common mode dampings are considerably less than that for equally shared damping; however the common mode dampings are greater than those which occur for the single generator on its own without any mechanical damping. This shows that adjacent units <u>do not</u> share torsional damping (which would have resulted in no movement in the loci in Fig 7.1) and this contradicts the results of Ref [60] in which there was no movement in the common mode or anti-mode loci for variations in the damping distribution. The results do however show that a lightly loaded unit will gain <u>some</u> damping benefit from an adjacent more highly loaded unit (with a common torsional mode) and this is in agreement with the results of Ref [58].

In order to investigate the nature of the torsional oscillations that would occur under unequal damping conditions the common and anti-mode mode shapes are calculated (at a compensation level of 74%) as the damping is varied in a similar manner as was done for terminal voltage and power in Sect 6.6.1. The results obtained for mode 3 (similar to modes 1 and 2) are presented in Fig 7.2 where 'first scan' corresponds to the maximum difference in the damping conditions of generator-1 and generator-2 (dampings being 0.0 and 1.57 s^{-1} respectively) and 'last scan' corresponds to a condition of equal dampings.

The most obvious effect of a damping difference is its influence on the phase relationship between the oscillations of the two generators when excited in either the common mode or anti-mode. With unequal damping conditions the common mode oscillations are no longer totally in-phase, while the anti-mode oscillations are no longer totally out-of-phase. In fact for the maximum difference in damping considered here the mode 3 common mode oscillations of the generators are phase displaced by 68 degrees while those of the anti-mode are phase displaced by 112 degrees. A second effect of the damping difference, not easily seen in Fig 7.2, is that for the common mode, the mode shape amplitude of the lesser damped generator (generator-1) is greater than that the more damped generator, whereas the opposite is true for the anti-mode.

The results therefore show how a difference in damping between the two generators tends to destabilize the common modes and cause variations in the phase relationship between the generators' oscillations in both the common and anti-modes. It is necessary to know how these effects influence the subsynchronous resonance stability of the system and furthermore, how the interaction of the two generators with the electrical network resonance(s) affects their combined torsional characteristics under unequal damping conditions.

The generators are assumed to be operating at the maximum unequal damping conditions stated previously and the eigenvalues of the system in Fig 6.1 are calculated as the line's series capacitor compensation level (see

eqn (6.4)) is varied from 10% to 105%. The resulting active subsynchronous mode loci are presented in Fig 7.3. The common modes are destabilized in a similar manner as occurred for the case of equal dampings (cf Fig 6.13(b)) however the anti-modes now show a distinct interaction with the electrical network although they remain stable. It is interesting to note that the electrical network affects each anti-mode in a different manner; M1a's stability is improved, M2a's is worsened while M3a moves both left and right depending on the compensation level.

The destabilization of the common modes in Fig 7.3 is compared with the condition of equal dampings (from Fig 6.6) in Fig 7.4 which shows the real part of the eigenvalues as a function of compensation level. The unequal damping system has worse subsynchronous resonance characteristics in two aspects: firstly, the degree of destabilization is greater (eigenvalues are pushed further into the right-half-plane) and secondly, the onset of instability occurs at a lower compensation level for all three modes. In fact, M3 goes unstable for the unequal damping case at a compensation level 6% lower. Figure 7.5 shows the Critical Compensation Level (CCL) in per-unit as a function of the damping difference where a damping difference of 0.0 represents equal dampings and 1.0 represents the maximum damping difference. The CCL displays a favourable lower sensitivity to damping differences at smaller differences. This means that for small differences in the dampings of the two generators a single equivalent generator with a damping equal to the combined damping of the two generators (in real units) could be used without much error; however for large damping differences between the generators an equivalent generator representation should not be used. This contradicts Ref [60] which claims that adjacent generators share torsional damping in the common mode; this would mean that an equivalent generator could always be used with no error.

So far this chapter has investigated the effect of damping differences on the SSR stability limits of the various modes. It is also interesting to examine how the series compensation affects the torsional characteristics of the two-generator system with unequal dampings. This is done by calculating the mode shapes corresponding to the eigenvalue loci in

Fig 7.3; however due to the complex manner in which the mode shapes vary with changing compensation level, it is not possible to present the results in a simple mode diagram such as Fig 7.2. Instead the results are presented as real versus imaginary components such as in Fig 7.6 for M3 and M3a. Each locus corresponds to a particular shaft position with the generator number in brackets and the mode shape is normalized at each calculation with the largest deflection having an amplitude of one and a zero imaginary component. Each locus is meaningless in itself but should be compared to the corresponding locus for the same shaft position on the other generator (eg LP3(1) and LP3(2)) to determine the magnitude and phase relationship between the separate oscillations of the two generators when excited in that mode.

A comparison of the GEN(1) and GEN(2) loci shows that for the common mode, generator 1 (lower damping) has a higher amplitude of oscillation over the whole compensation range while the opposite is true for the anti-mode. Furthermore, the relative amplitude and phase of both the common and anti-mode oscillations change as the compensation level is varied. At low and high compensation levels (beginning and end of each locus of points in Fig 7.6) there is a phase difference of just less than 90 degrees between the generators' common mode oscillations and just greater than 90 degrees between their anti-mode oscillations. In this respect the common and anti-modes are very similar at these compensation levels. As the compensation level approaches the region of strong interaction between the electrical system and the mechanical mode, the generators' common mode oscillations become more in-phase (30 degrees) while their anti-mode oscillations become more out-of-phase (160 degrees). At the same time, the difference in the relative amplitudes of the individual generator oscillations in the common and anti-modes increases so that around maximum interaction between mode 3 and the electrical system, the generator-2 common mode oscillations are only 30% as great as those of generator-1 whereas at low and high compensation levels they are 50 to 80% as great.

In order to verify some of the eigenvalue calculations the system transient response is calculated for the case of maximum damping difference when the system is subjected to a temporary 10% drop in the infinite bus voltage for

a duration of 200 ms. The results are calculated firstly with a series capacitance of 0.635 p.u. (63% compensation level) in the line; the small-signal studies at this compensation level predict the M3 eigenvalue to be at -0.08 + j99.2 and the mode shape indicates the amplitude of generator-2 oscillations to be 74% of the size of those of generator-1 and lagging generator-1 in phase by 43 degrees. The calculated mode 3 speeds (speed pq_3 of the mode 3 inertia in the modal model) for both generators (which are translated into the rotor speed signals) appear in Fig 7.7(a) for the initial fault period and in Fig 7.7(b) an interval of time later. During the initial period the speed signals are similar, however after a short while they behave exactly as predicted by the small-signal calculations. Although the individual dampings of the two generators are vastly different (0.0 s^{-1} and 1.57 s^{-1}) the oscillations of both generators exhibit the same damping.

Figures 7.7(c) and (d) show the mode 3 speeds for a series capacitance of 0.505 p.u. (50% compensation) at which the M3 eigenvalue is +0.25 + j100.4 and the mode shape predicts the magnitude of generator-2's oscillation as 28% of generator-1's and lagging generator-1's by 41 degrees. During the fault period (0.1 to 0.3 s) both speed signals increase rapidly; after the fault is lifted, generator-1's oscillations continue to grow at the predicted unstable damping rate while generator-2's oscillations firstly decay until they reach 28% of generator-1's at which time they follow the rate of increase of generator-1's oscillations. This is in accordance with the small-signal predictions.

The results of Figs 7.7(c) and (d) are recalculated but using an equivalent single generator with a damping corresponding to the total mode 3 damping of the two generators (ie assuming the two generators share their torsional damping equally). The M3 eigenvalue for this case is -0.23 + j100.2 and this agrees with the stable decaying mode 3 speed oscillations seen in Fig 7.7(e). This further underlines the important finding that in terms of SSR stability, the total mechanical damping of a mode is not the only determining factor but the distribution of that damping between the two generators is important.

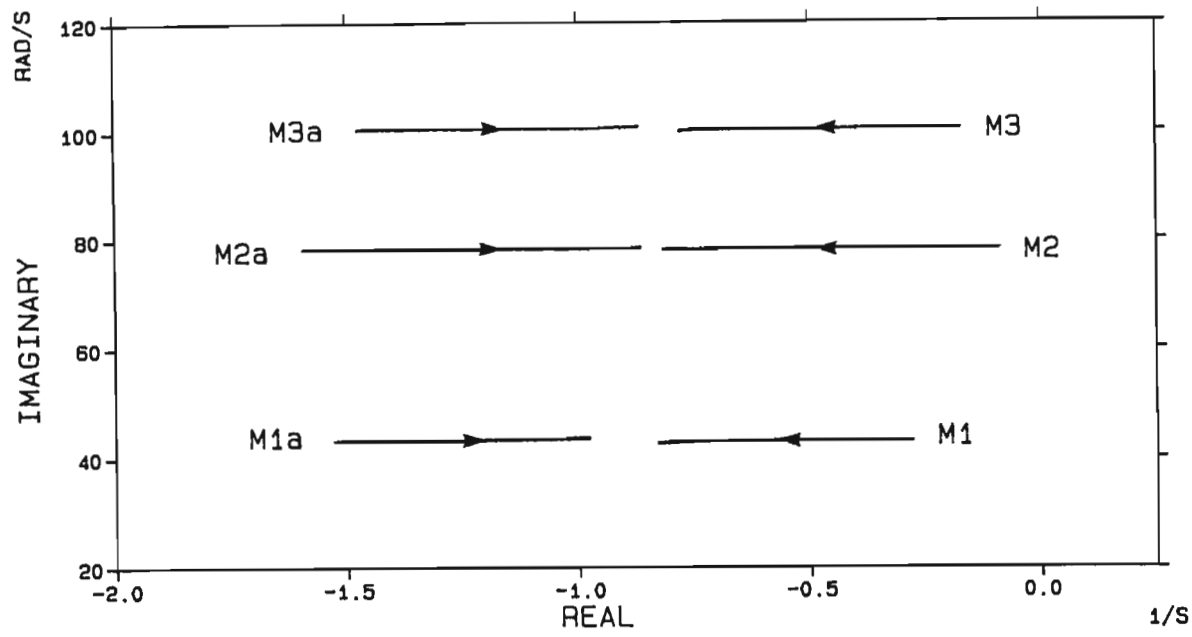

Fig 7.1 Selected eigenvalue loci as the generator-1 and generator-2 mode dampings are varied from 0.0 to 0.785 1/s and from 1.57 to 0.785 1/s respectively; no series compensation.

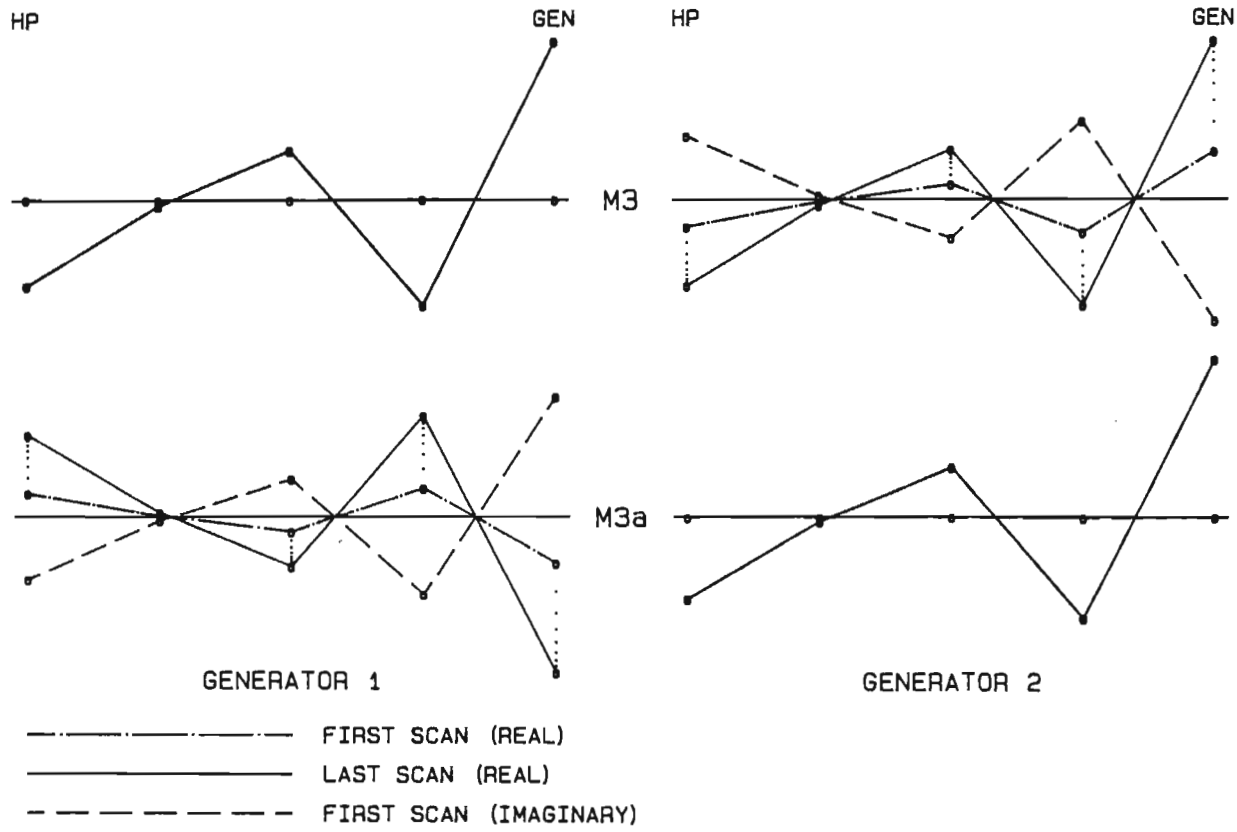

Fig 7.2 M3 and M3a mode shapes calculated for the same damping variation as in Fig 7.1, but with a compensation level of 74%;

'First Scan': Gen-1 σ_{mi} = 0.0 1/s, Gen-2 σ_{mi} = 1.57 1/s;

'Last Scan': Gen-1 σ_{mi} = 0.785 1/s, Gen-2 σ_{mi} = 0.785 1/s.

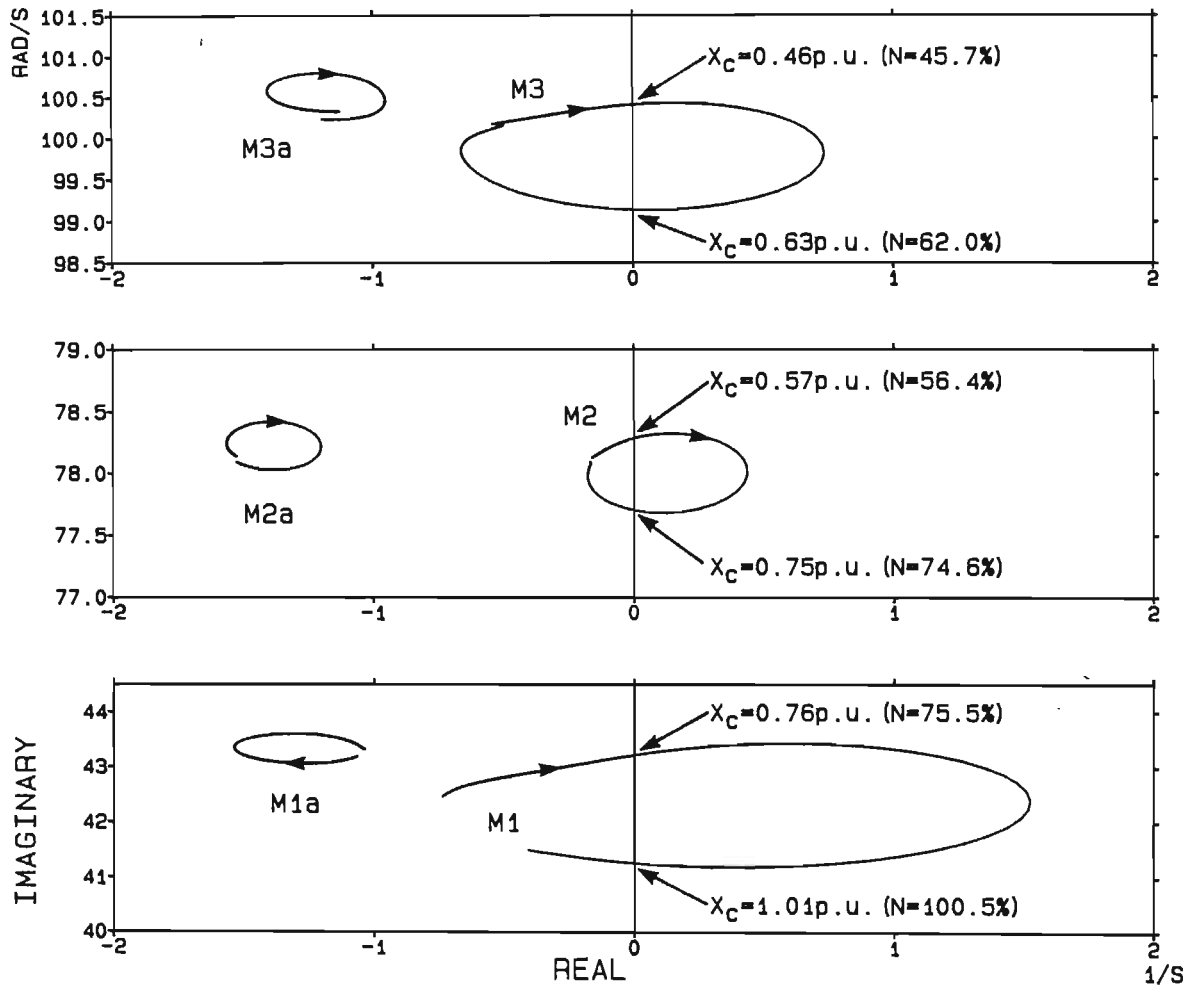

Fig 7.3 Selected eigenvalue loci for the maximum damping difference as the compensation level is varied from 10% to 105%; (Gen-1 σ_{mi} = 0.0 1/s and Gen-2 σ_{mi} = 1.57 1/s).

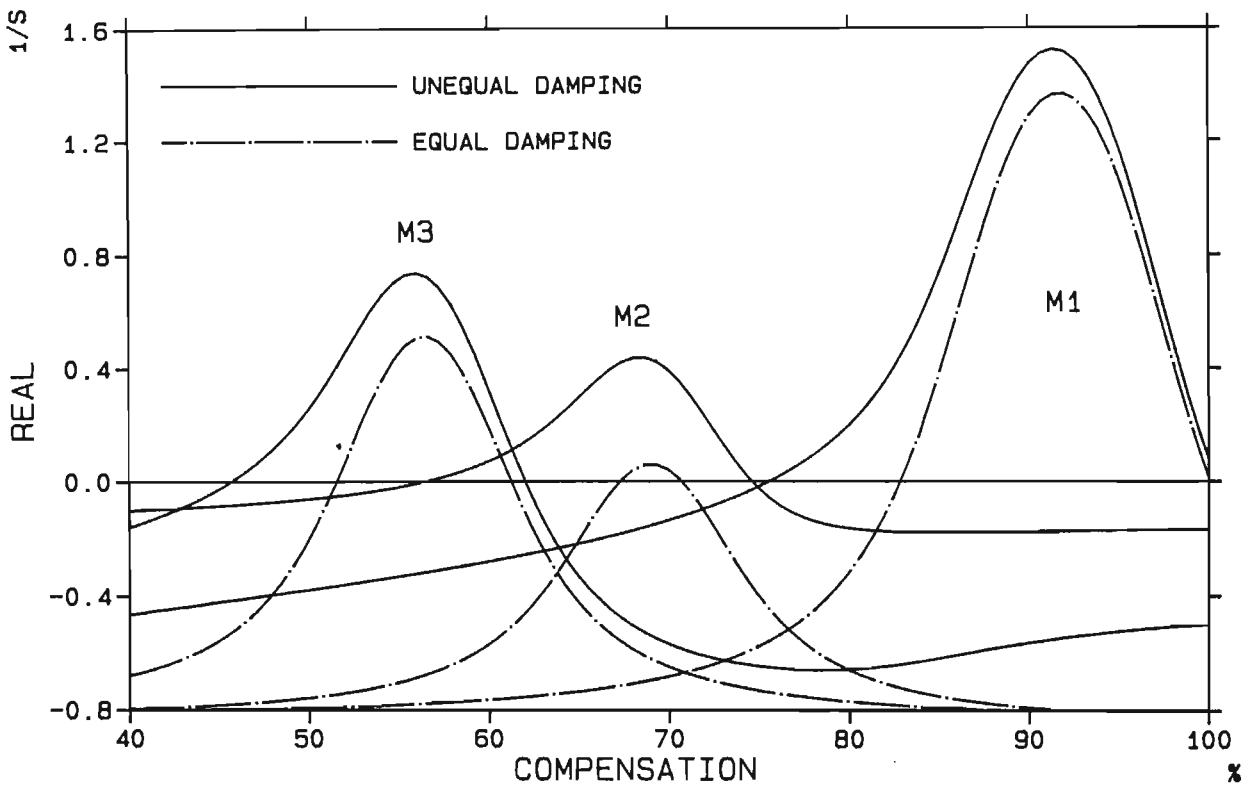

Fig 7.4 Real part of modes M1 to M3 from Fig 7.3 for unequal damping compared with that obtained for equal damping from Fig 6.6.

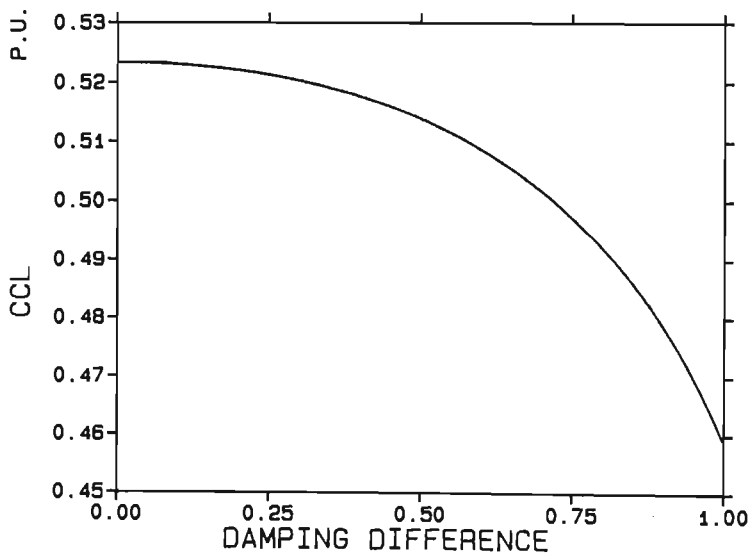

Fig 7.5 Change in the CCL (expressed as the per-unit value of X_c) as a function of the damping difference; 0.0 represents equal damping and 1.0 represent the maximum difference.

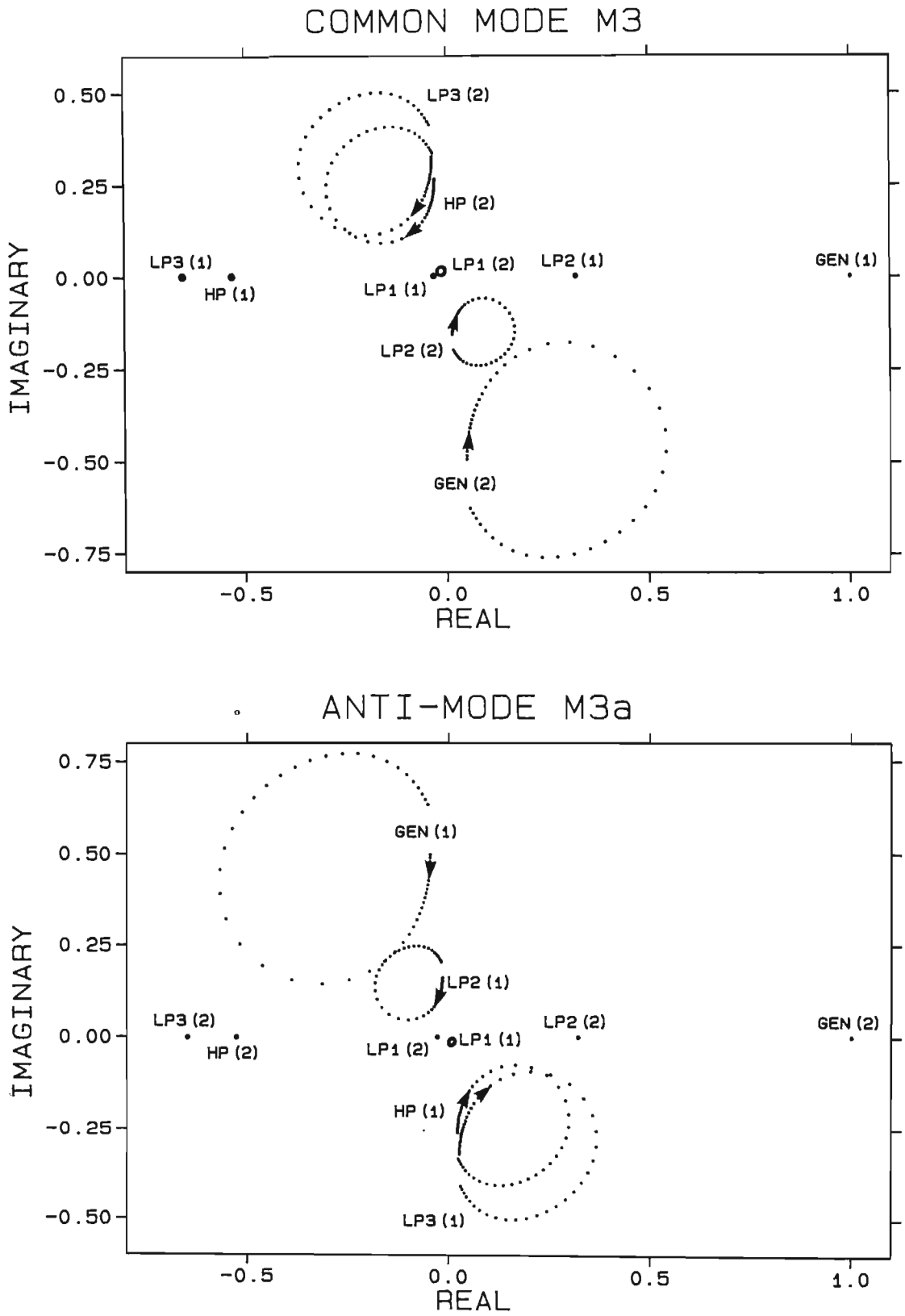

Fig 7.6 M3 and M3a mode shape loci corresponding to the eigenvalue loci in Fig 7.3; maximum damping difference between the generators and the compensation level varied from 10% to 105%.

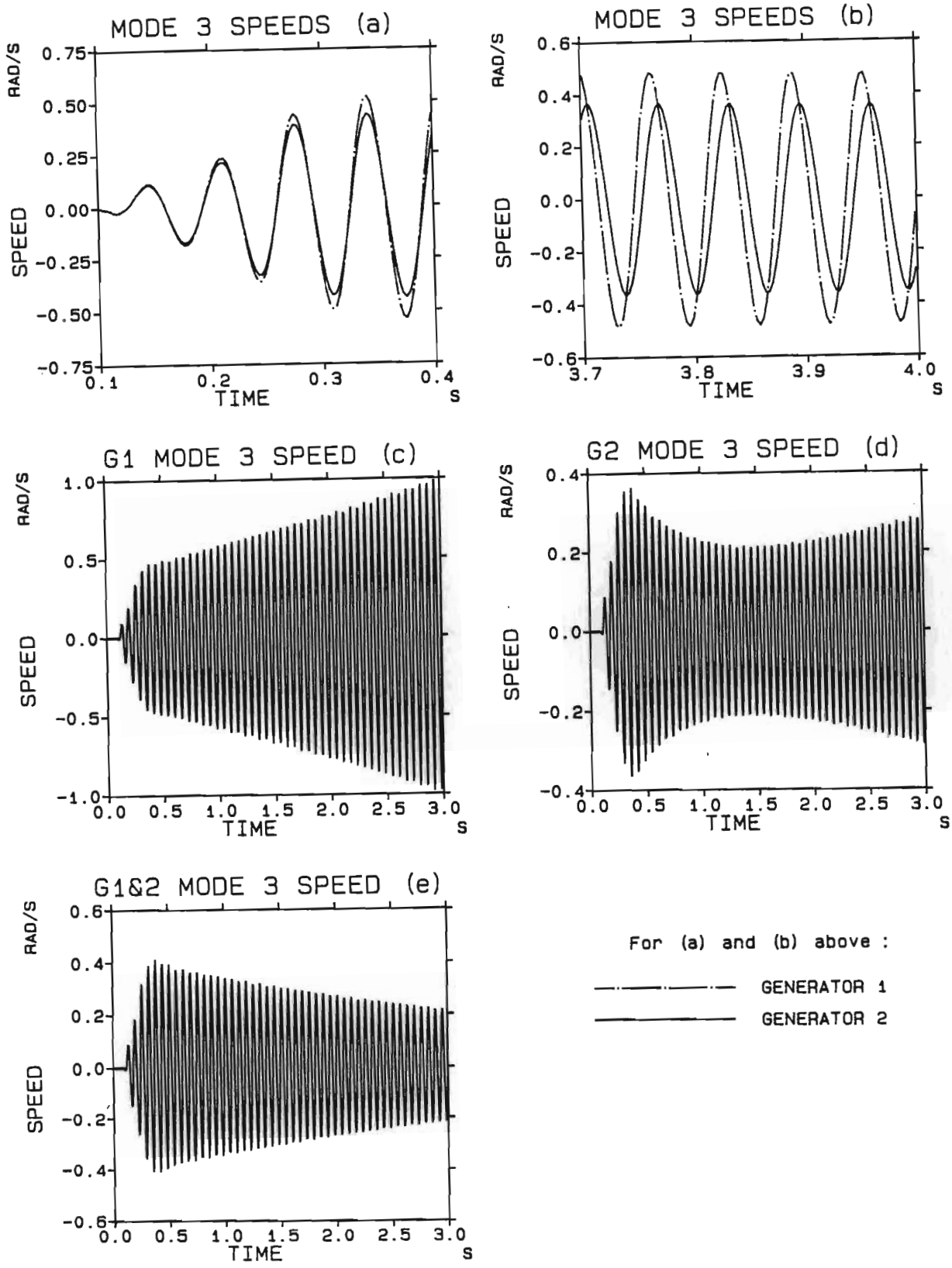

Fig 7.7 Transient response curves for a 200 ms 10% reduction in the infinite bus voltage; (a), (b) - unequal dampings and compensation level of 63%; (c), (d) - unequal dampings and compensation level of 50%; (e) - equal dampings and compensation level of 50%.

7.3 Differences in Mode Inertia

Nominally identical units in a power station will always have slight disparities in shaft inertia due to manufacturing tolerances; this includes differences in the distribution of the total inertia between various stages. This means that the mode inertias of the two generators will not be identical but will differ slightly. Moreover, it is possible that at a power station two different generators may have a common torsional mode, in which case it is likely that the mode inertias of that mode will be markedly different. This section therefore investigates the effect of non-identical mode inertias on the SSR stability and torsional performance of a two-generator power station.

The eigenvalue calculations in Fig 7.1 (no series capacitance) are repeated in Fig 7.8 with the mode inertias being scanned instead of the mode damping values. Generator-1's mode inertias are scanned from 150% to 100% of the nominal values in Appendix I while generator-2's mode inertias are simultaneously scanned from 50% to 100% of the nominal values. This variation in mode inertias is not chosen to suggest that such a large disparity may exist for nominally identical units, but rather to include the possibility of different units having a common mode. At each calculation the total inertia of the two generators as well as the total combined inertia of each mode remains constant. The results show that the common modes M1, M2 and M3 are not greatly affected by the differences in the mode inertias of the two generators and this is expected since the common modes represent the oscillation of both generators together against the infinite bus and are concerned mainly with the total inertia. The anti-modes however represent the exchange of energy between the two generators and in this respect the relative values of the mode inertias are important. As the differences in the mode inertias between the two generators becomes smaller, the anti-modes become less damped.

The effect of mode inertia differences on the torsional characteristic of the two-generator system is investigated in Fig 7.9 where the M3 and M3a mode shapes are shown as the mode 3 inertias are scanned in a similar

manner as in Fig 7.8 but this time at a series compensation level of 74% (cf Fig 7.2). Only the first and last scans are drawn fully where 'first scan' is the initial calculation with maximum inertia difference (Gen-1 150% and Gen-2 50% of nominal values) and 'last scan' is the final calculation with equal inertias where the imaginary component is zero.

At this compensation level, a difference in mode inertia does not have much affect on the phase relationship between the generator oscillations in either the common or anti-mode as seen by the small imaginary component for the 'first scan', however it does affect the relative amplitude of the oscillations for both modes. The generator with the larger inertia (generator 1) has the smaller amplitude of oscillation in both modes although this is far more noticeable in the anti-mode. This is expected since the smaller inertia generator must have a higher magnitude of oscillation for the same amount of torsional energy being transferred between the machines.

In order to see the effect of mode inertias differences on the SSR stability of a two-generator power station the system eigenvalues are calculated as the series compensation is scanned with generator-1's mode inertias at 50% of the nominal values and generator-2's at 150%. The loci for the active subsynchronous modes appear in Fig 7.10 and a number of noticeable differences are evident compared to the case of identical machines (Fig 6.13). Firstly, the M3a and M2a anti-modes are destabilized appreciably at some compensation levels whereas for identical generators they showed no movement at all. Secondly, and the most obvious difference, is the movement of the M1 and M1a loci with the anti-mode going unstable and the common mode remaining stable. In order to explain this it is necessary to examine the combined torsional characteristics of the generators in the presence of series capacitors and this is done by determining the mode shapes corresponding to the loci in Fig 7.10.

Due to the complex nature in which the mode shapes vary it is not possible to present the results as in Fig 7.6; instead they are presented as in Fig 7.11. The amplitude graphs (a), (c) and (e) show the difference in

the magnitude of the mode shape deflections at the generator rotors (denoted AMP1 and AMP2) as a fraction of the larger deflection (denoted |AMAX|). This value thus varies from +1, when generator-2 has zero amplitude of oscillation in the particular mode, to -1 when generator-1 has zero amplitude of oscillation. A value of 0 indicates that the generators oscillate with equal amplitude in that mode. The angle graphs (b), (d) and (f) show the angle of generator-2 oscillations with respect to generator-1 oscillations when the two-generator system is excited in the relevant mode.

The mode 3 magnitude curves indicate that in the anti-mode (broken curve in Fig 7.11(a)), generator-2's (larger inertia) oscillation is always smaller than generator-1's, being a minimum of 20% of generator-1's oscillation at a compensation level of 47%, and a maximum of 60% of generator-1's at at 55% compensation. For the common mode, generator-2 has a larger amplitude at lower compensation levels while generator-1 has a larger amplitude at higher compensation levels. Around maximum destabilization of M3, both generators respond with the same magnitude in the common mode. The phase results for mode 3 in Fig 7.11(b) show that at low compensation levels the generator common mode oscillations are in-phase, however as the compensation level approaches the region of maximum destabilization of M3 (around 57% compensation) the generator oscillations become phase shifted reaching a phase displacement of around 65 degrees just before maximum destabilization. At high compensation levels, the generator oscillations once again become almost totally in-phase. Similarly, for the anti-mode M3a, at low and high compensations the generators oscillate almost totally out-of-phase whereas their oscillations become only 115 degrees out-of-phase around maximum destabilization of M3.

The results for mode 2 in Fig 7.11(c) and (d) display similar effects to those described above for mode 3. The mode 1 results are however markedly different to those of mode 2 and 3. The most obvious difference occurs in the phase relationships shown in Fig 7.11(f); at low compensation levels the common mode represents an in-phase oscillation of the generators and the anti-mode represents an out-of-phase oscillation. However, as the

compensation is increased, the M1 and M1a oscillations become less in-phase and out-of-phase respectively until around 82% compensation at which the generator-2 oscillations lag those of generator-1 by 90 degrees in both the common and anti-mode. At this point it is not possible to discern between common and anti-mode oscillations without looking at either their frequencies or the relative magnitude of the generator oscillations in each mode. At high compensation levels the common mode becomes the out-of-phase mode and the anti-mode becomes the in-phase mode. Thus, although in Fig 7.10 the anti-mode M1a goes unstable, the unstable oscillations will be more in-phase than out-of-phase (less than 90 degrees phase displacement).

Hence when non-identical generators are being considered the idea of the common mode being the in-phase mode and the anti-mode being the out-of-phase mode is incorrect since this may depend on the compensation level.

A comparison of the stability limits with unequal mode inertias and equal mode inertias is made in Fig 7.12 in the same way as it was done in Fig 7.4 for unequal mode damping. The results in Fig 7.12 show that the modes are all destabilized to a greater degree when the mode inertias are different; however the CCL for each mode depends on the amount of mechanical damping (which determines the vertical positioning of the curves). It may be higher at some damping levels while at other damping levels it may be lower. The variation in the M3 CCL, for the damping level chosen in this case, as a function of the mode 3 inertia difference, is presented in Fig 7.13 where 0.0 represents equal inertias and 1.0 represents the maximum difference (Gen-1 inertias at 50% of nominal values and Gen-2 inertias at 150% of nominal values.

Figure 7.10 showed that at a low level of mechanical damping, M3a and M3 may both go unstable. The variation of their real parts as a function of compensation level is displayed in Fig 7.14 and it is seen that at some damping levels M3a may go unstable before M3; however in this case the reduction in the CCL due to M3a going unstable first would not be very large.

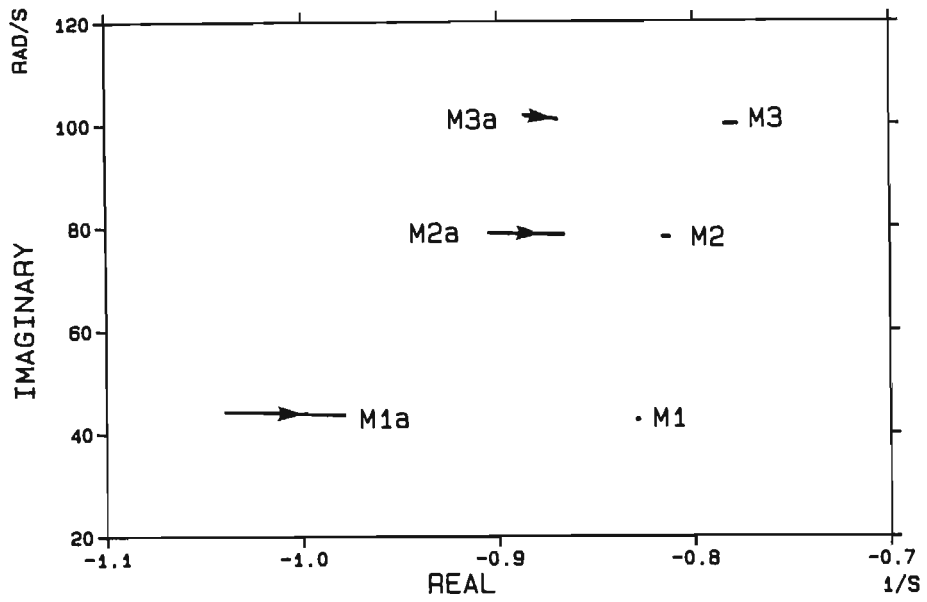

Fig 7.8 Selected eigenvalue loci as the generator-1 and generator-2 mode inertias are varied from 150% to 100% and from 50% to 100% of their nominal values respectively; no series compensation.

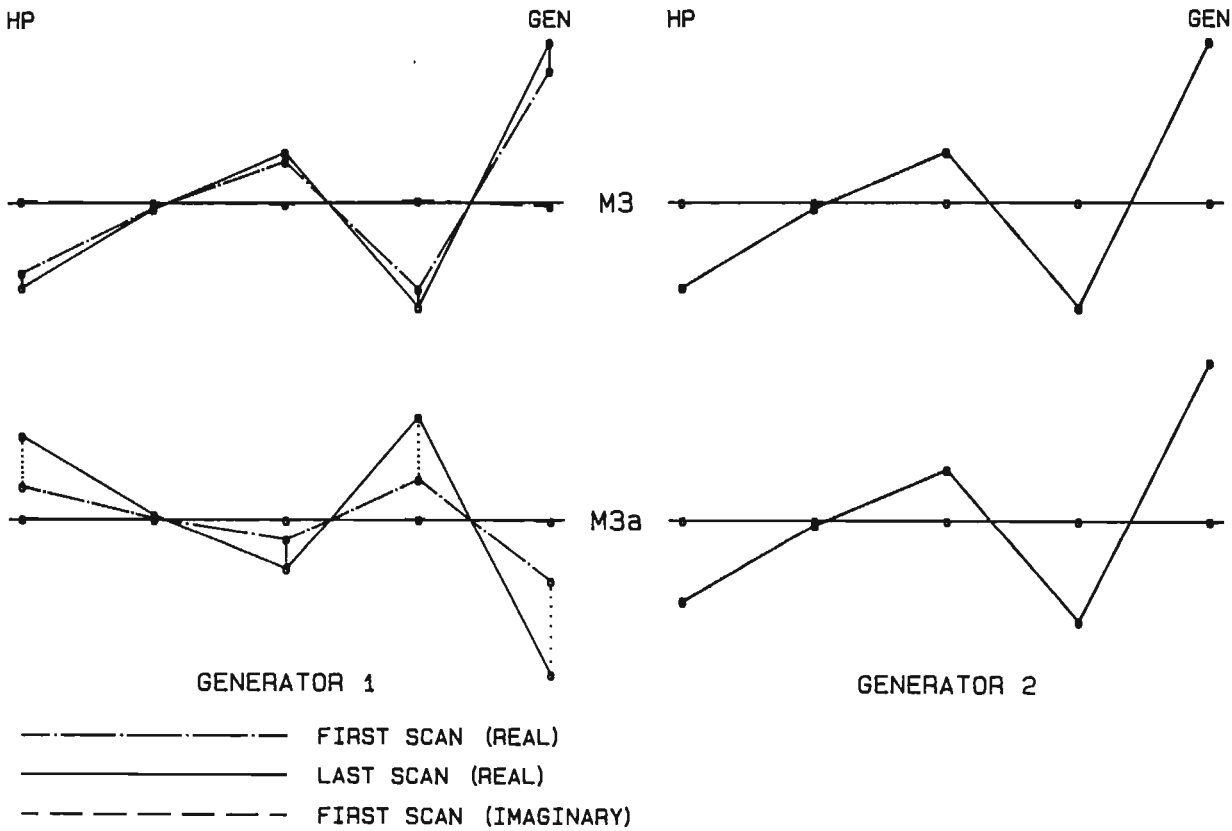

Fig 7.9 M3 and M3a mode shapes calculated for the same mode inertia variation as in Fig 7.8, but with a compensation level of 74%;
'First Scan': Gen-1 J_{Mi} = 150% nominal, Gen-2 J_{Mi} = 50% nominal;
'Last Scan': Gen-1 J_{Mi} = Gen-2 J_{Mi} = nominal values.

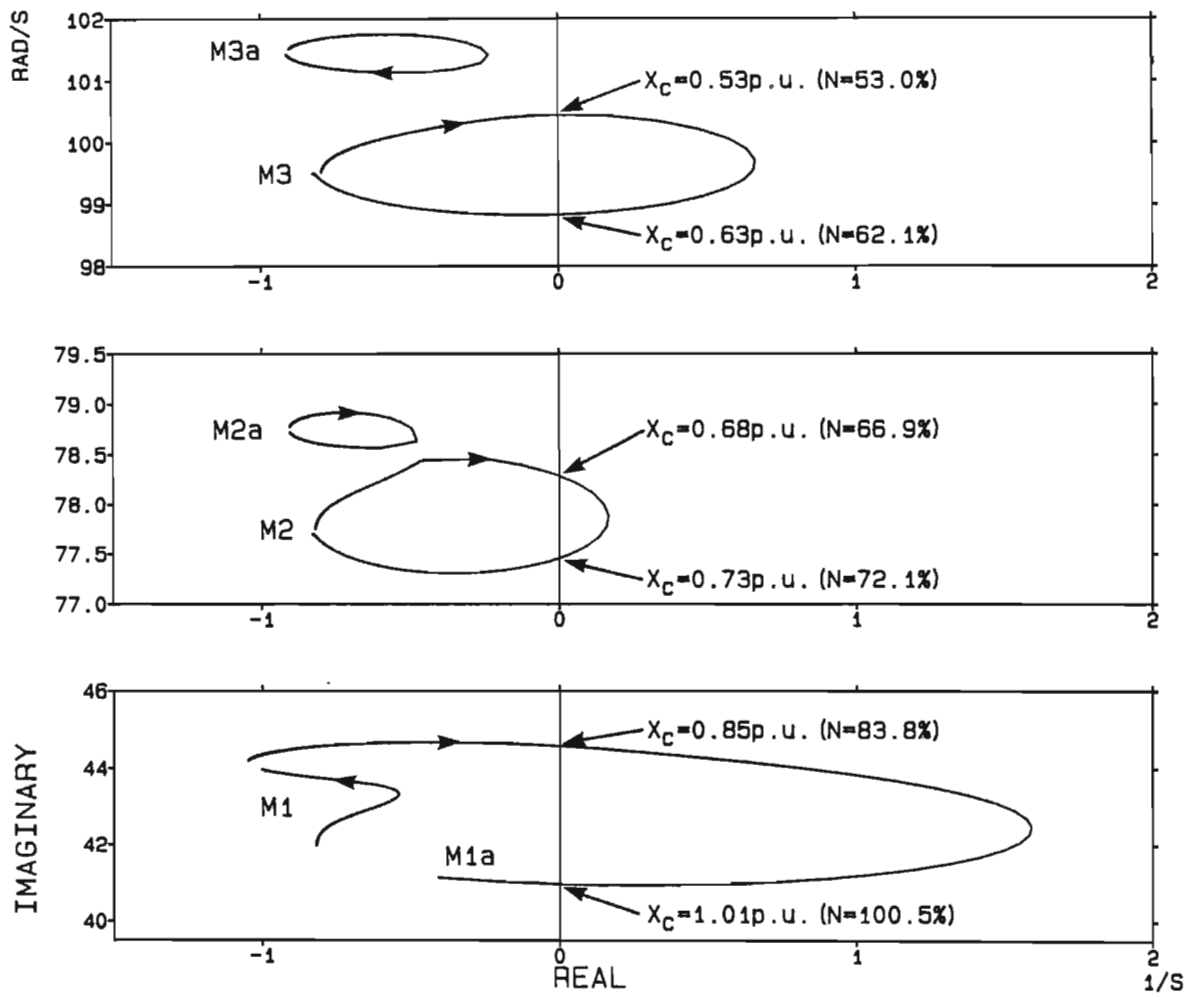

Fig 7.10 Selected eigenvalue loci for a the maximum inertia difference as the compensation level is varied from 10% to 105%; (Gen-1 J_{Mi} = 150% nominal and Gen-2 J_{Mi} = 50% nominal).

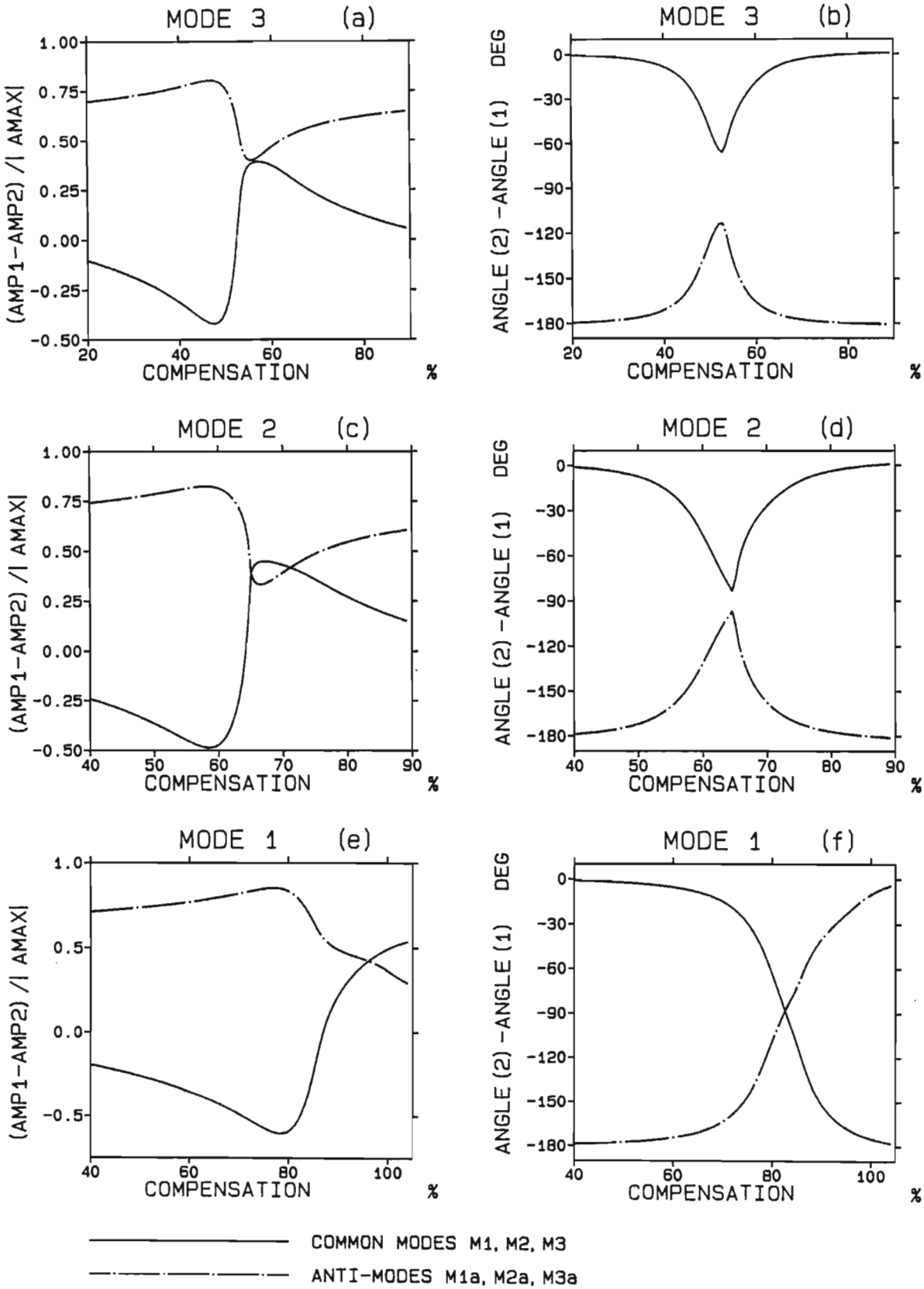

Fig 7.11 Mode shape information for unequal mode inertias corresponding to the eigenvalue loci in Fig 7.10

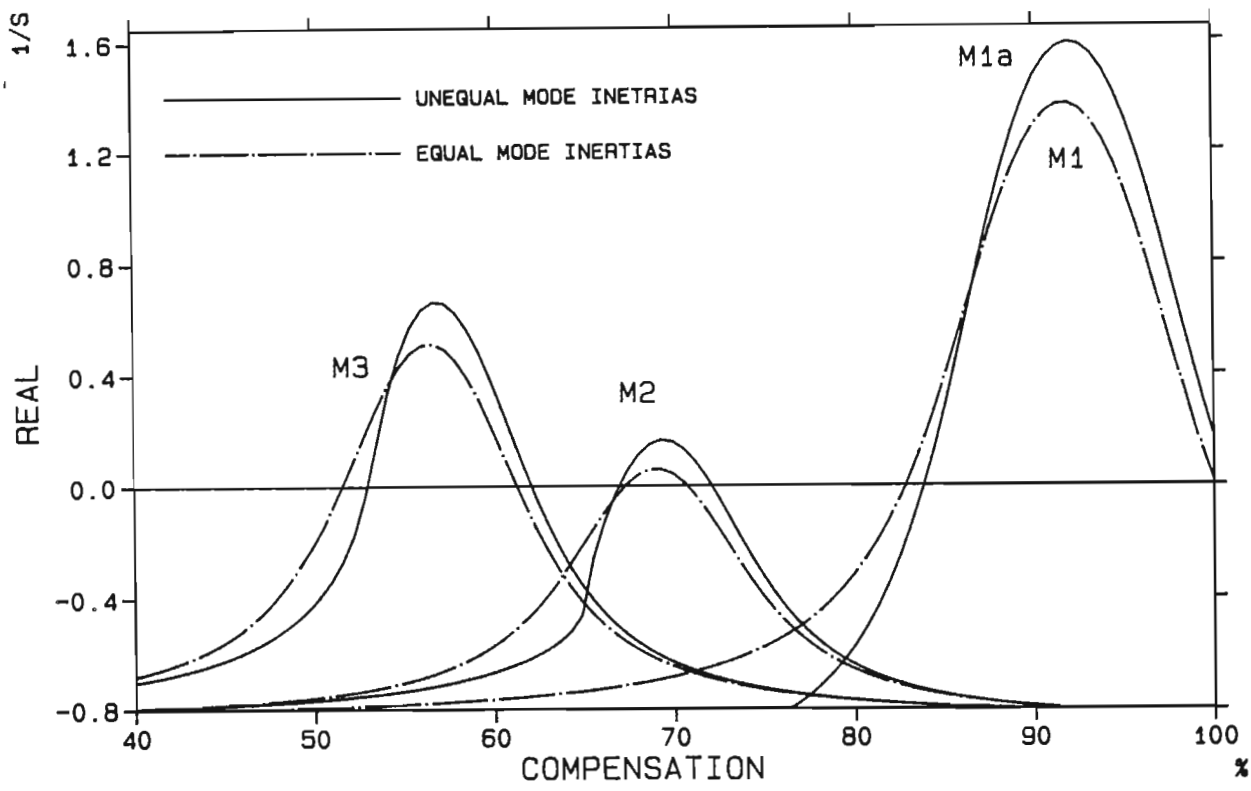

Fig 7.12 Comparison of real parts of destabilized modes for unequal mode inertias (from Fig 7.10) with that obtained for equal mode inertias (from Fig 6.6).

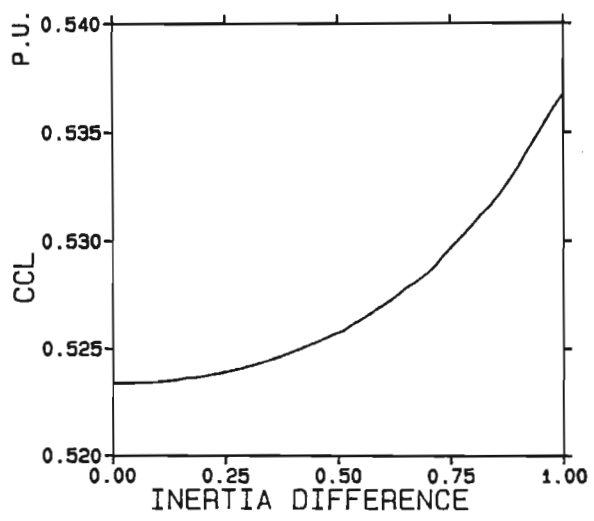

Fig 7.13 CCL (expressed as X_c in p.u.) as a function of the inertia difference.

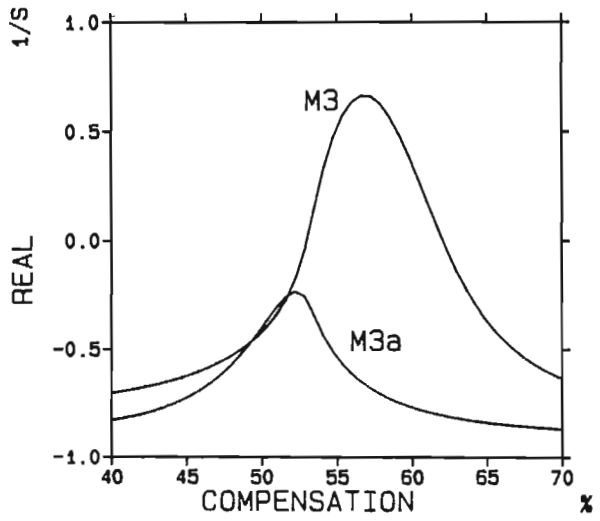

Fig 7.14 Real parts of M3 and M3a from Fig 7.10.

7.4 Differences in Mode Frequency

Of all the differences that may occur between parameters of adjacent nominally identical units, probably the most critical in terms of torsional interaction between the units is that difference which may occur in mode frequencies. Reference [58] showed that even for a small variation in frequency of 0.03 Hz there was a large reduction in the coupling between the generators and the anti-mode had a larger oscillation for the generator with the higher frequency while the common mode had a larger oscillation for the lower frequency generator. It further showed that there was practically no torsional interaction when the frequencies were 0.41 Hz apart, with the lower frequency generator having virtually zero involvement in the anti-mode and the higher frequency generator having zero involvement in the common mode. That analysis was however done with a physical representation of the generator shafts (instead of a modal representation) and the frequency variations were achieved by omitting the exciter inertia from one of the units and by modifying the shaft stiffnesses. Doing that altered not only the frequencies of the shaft but also the mode shapes and more importantly, the mode inertias (and thus the mode excitability values). Thus the results of Ref [58] were due not only to differences in mode frequency, but also to unspecified changes in the other mode parameters. Furthermore, Ref [58] did not investigate how the presence of series capacitors affects the torsional interaction of the adjacent units with small differences in mode frequencies. This aspect is investigated here and the effect of a frequency difference is isolated from that due to changes in other mode parameters by the use of the modal shaft representation which allows independent specification of any mode parameter.

Figure 7.15 presents the M3 and M3a mode shapes calculated at a compensation level of 74% as the generator-1 mode 3 frequency is varied from 16.336 Hz to its nominal value of 15.836 Hz while all the other generator parameters remain unchanged and equal to those of generator-2. The results in Fig 7.15 agree with those of Ref [58] in that the higher frequency generator becomes dominant in the anti-mode while the lower

frequency generator becomes dominant in the common mode; however the decoupling effect that occurs due to frequency differences is not as severe as described in Ref [58]. In this case, at a difference of 0.5 Hz there is still an observable amount of participation of both generators in both modes; however Ref [58] had almost zero combined participation at only 0.41 Hz, probably due to dissimilarities in mode excitability values incurred in their method of altering the frequency. The practically zero imaginary component in Fig 7.15 shows that at this compensation level the difference in frequency affects the relative magnitudes of the generator oscillations but does not have much effect on their phase relationship.

The effect of differences in mode frequency on the subsynchronous interaction between the electrical and mechanical systems is illustrated in Fig 7.16 which presents the mode 3 eigenvalue loci (as the compensation level is varied) when generator-2's mode 3 frequency is 16.336 Hz, that is, 0.5 Hz higher than generator-1's mode 3 frequency. Both the common mode and anti-mode interact with the electrical system resonances tending to less stable conditions although the common mode is more severely affected. In this case the undamping causes the common mode to go unstable but does not cause the anti-mode to go unstable. However, if the mode 3 mechanical damping was less than the assumed value of 0.785 s^{-1} (which is likely to be the case), then the anti-mode could go unstable and a situation could exist where both modes are unstable at the same time.

The real parts of the common and anti-modes in Fig 7.16 are shown together with those of the common mode for generators with identical mode frequencies (from Fig 6.6) in Fig 7.17 and show that the case with non-identical frequencies has a higher CCL. This is somewhat unexpected, since for a single generator, increasing the mode frequency causes the electrical subsynchronous frequency to interact with the mechanical mode at a lower compensation level resulting in a lower CCL and thus a less stable system. However for the two-generator case, increasing the frequency of one of the generators has increased the CCL; obviously increasing the frequency of both generators would lower the CCL. The stability of the system is improved in two ways with non-identical frequencies; firstly, the

CCL has increased and secondly, the extent to which the modes are destabilized is far less. In fact, for some modes a small difference in mode frequency between the generators could result in the mode no longer becoming unstable. An interesting and useful result of the decreased destabilization of the modes for the non-identical frequency case, is that regardless of the amount of mechanical damping (which determines the vertical position of the curves in Fig 7.17), the anti-mode does not go unstable before either common mode in spite of the fact that it reaches its position of maximum destabilization at a lower compensation level than both the common modes.

The results in Figs 7.16 and 7.17 apply to a specific frequency difference of 0.5 Hz. Figure 7.18 shows that the CCL varies fairly linearly as the difference between the mode 3 frequencies of the generators is increased from 0.0 Hz to 0.5 Hz.

The effect of series compensation on the torsional characteristics of a two-generator system with a small difference in the mode 3 frequency is investigated in Fig 7.19; it displays the mode shapes corresponding to the common mode and anti-mode loci in Fig 7.16 presented in the same manner as the modes shapes in Fig 7.11. The results confirm that the higher frequency generator (generator-2) has a larger amplitude in the anti-mode and a smaller amplitude in the common mode. The amount of interaction between the two generators is dependant on the compensation level; just before maximum destabilization of the common mode, generator-2's involvement in the common mode is only 13% of generator-1's whereas this increases to 33% just after maximum destabilization. Similarly, in the anti-mode the involvement of generator-1 varies from 13% to 33% of generator-2's involvement. The phase relationship of the generator oscillations in both modes is also dependant on the level of compensation with the common mode oscillations becoming less in-phase (55 degrees) during M3 destabilization and the anti-mode oscillations becoming less out-of-phase (125 degrees) during M3a destabilization.

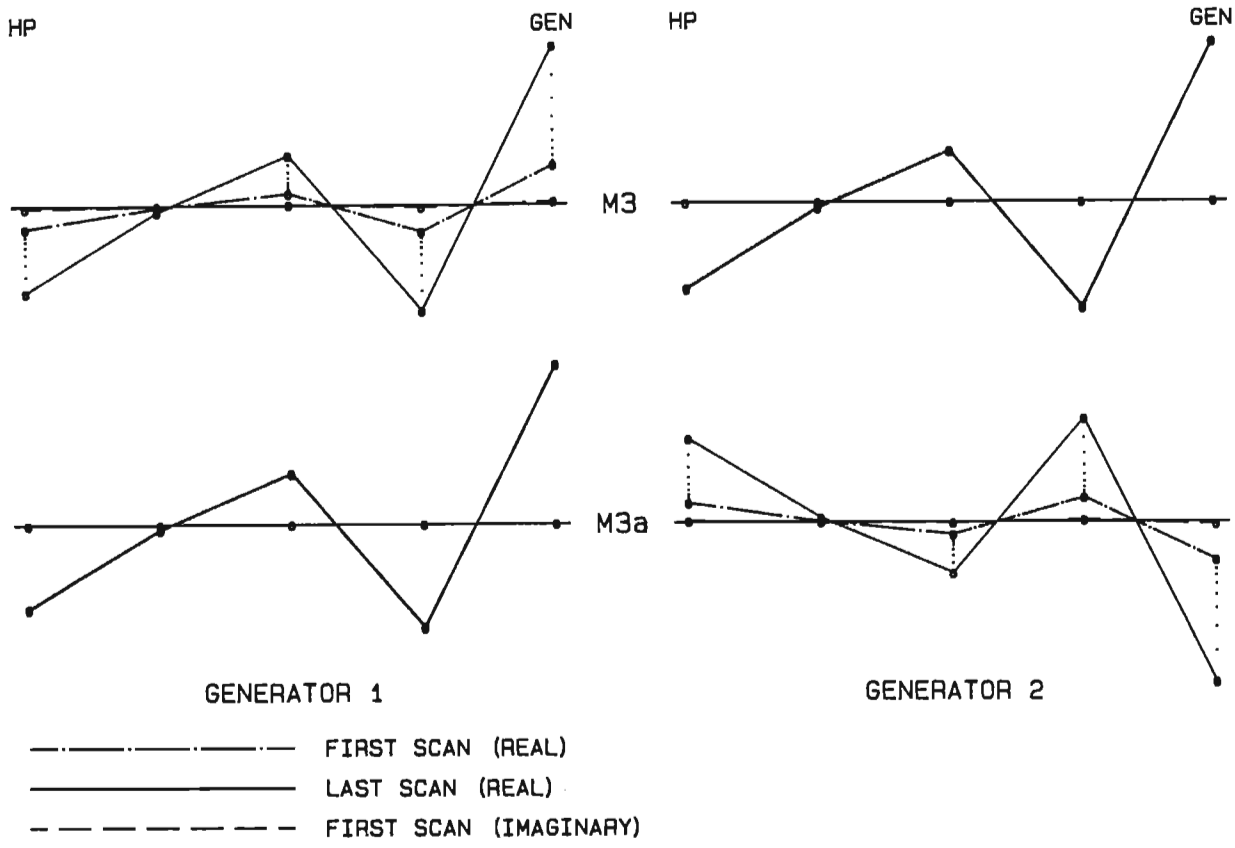

Fig 7.15 M3 and M3a mode shapes calculated at a compensation level of 74% as the Gen-1 mode 3 frequency is scanned from 16.336 Hz to its nominal value of 15.836 Hz;

'First Scan': Gen-1 f_{m3}=16.336 Hz, Gen-2 f_{m3}=15.836 Hz;

'Last Scan': Gen-1 f_{m3} = Gen-2 f_{m3} = 15.836 Hz.

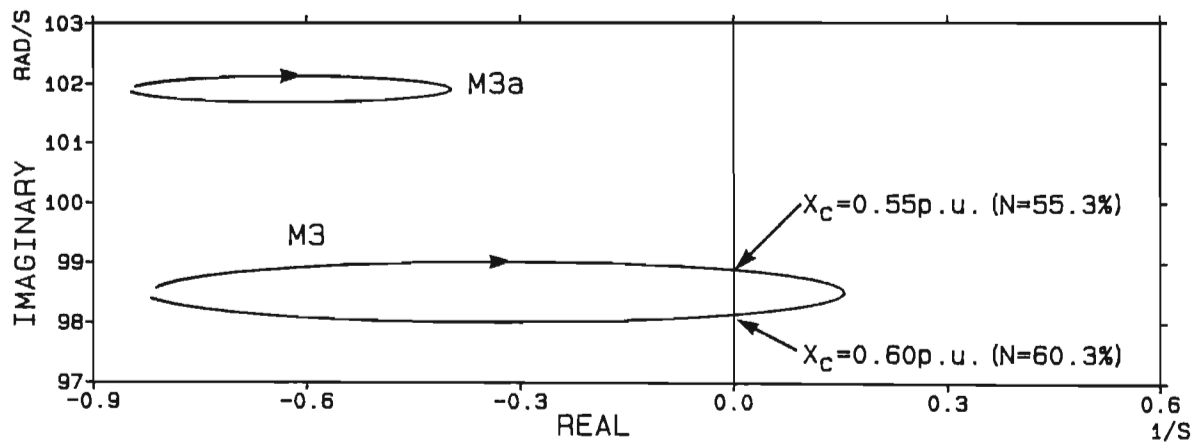

Fig 7.16 M3 and M3a eigenvalue loci as the compensation level is varied from 10% to 105% and the Gen-1 mode 3 frequency is at 16.336 Hz, 0.5 Hz higher than the Gen-2 mode 3 frequency.

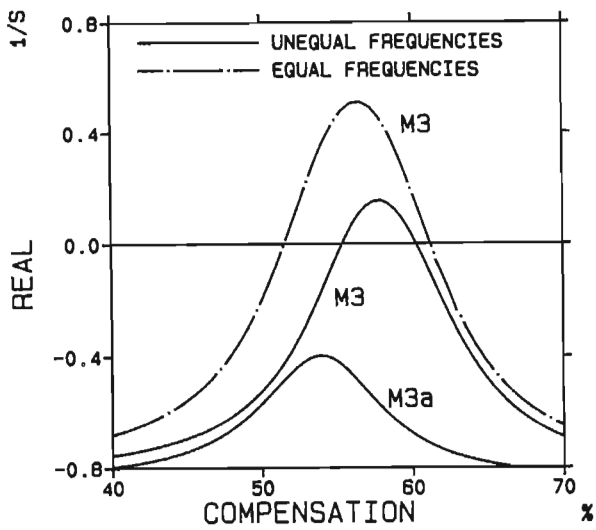

Fig 7.17 Real part of M3 and M3a for equal and unequal mode 3 frequencies.

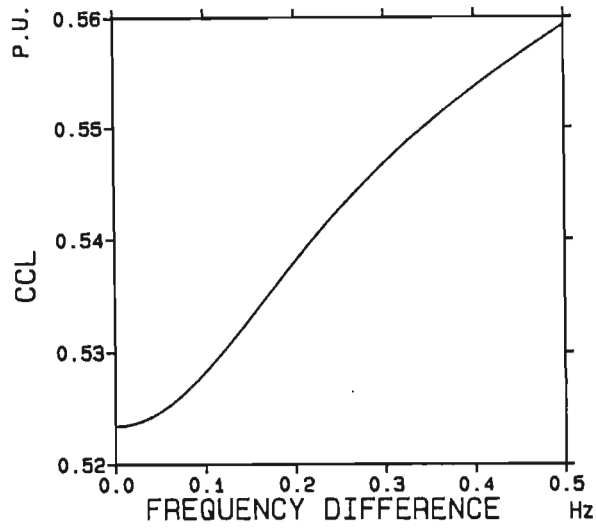

Fig 7.18 CCL (expressed as X_c in p.u.) as a function of frequency difference.

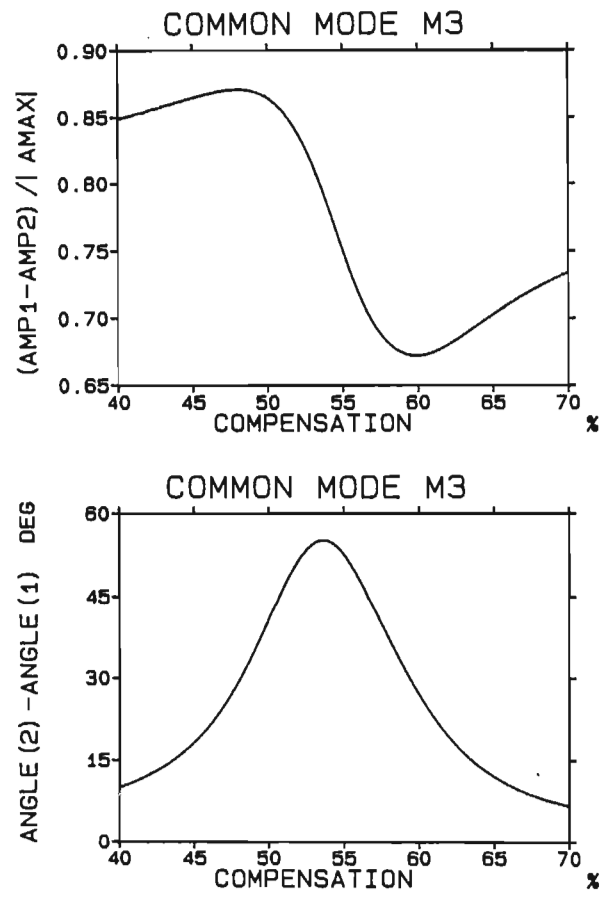

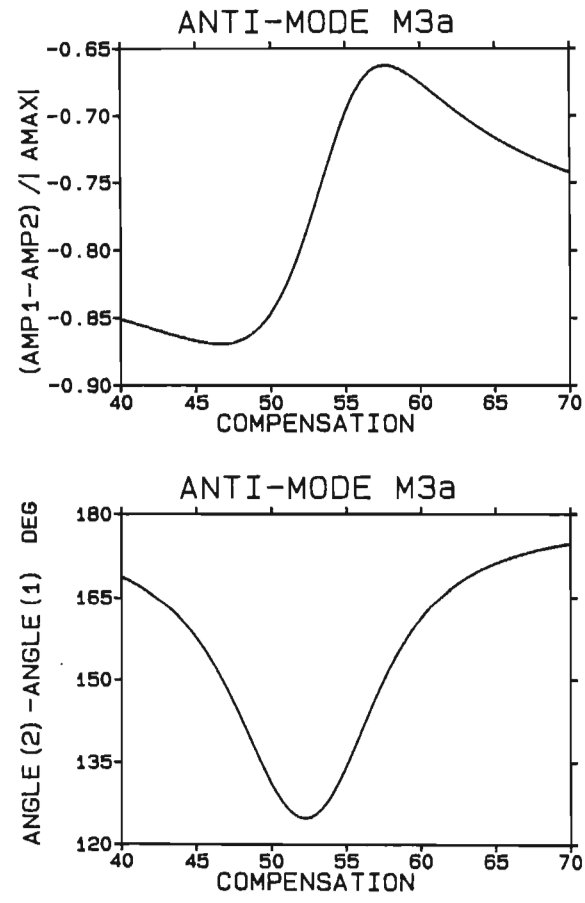

Fig 7.19 Mode shape information corresponding to the eigenvalue loci in Fig 7.16 for unequal mode 3 frequencies.

7.5 Differences in Mode Shape

In order to complete the investigation of differences in mode parameters between adjacent generators, the situation is considered where two generators have a mode of the same frequency, but not the same mode shape. In this instance, each generator is modelled by a fourth order mechanical system having only one torsional mode. Generator-1 has mode 3 as its torsional mode while generator-2's torsional mode has the same frequency as mode 3 but with the mode 1 mode shape. The mode 1 mode shape is altered so that the generator rotor deflection is the same as for mode 3. In order to restrict the analysis to differences in mode shapes, the mode 1 inertia is adjusted so that both modes have the same torsional interaction susceptibility (see Sect 4.2).

An eigenvalue analysis of this two-generator system shows two closely spaced modes at the torsional frequency in the same way as happens for identical mode shapes. The mode shapes of these two modes are presented in Fig 7.20 and it is seen that similar to identical mode shapes, a common mode and anti-mode exist where the two generator rotor deflections are in-phase for the common mode and out-of-phase for the anti-mode. The two generators thus interact torsionally as though their mode shapes were identical. This is somewhat expected since one generator does not 'see' the other generator but it only 'sees' the electrical system to which it is connected, and its torsional mechanical system interacts with currents at certain frequencies in that electrical system regardless of their origin.

The real part of the common mode is plotted as the compensation level is varied in Fig 7.21 and it is presented together with the result obtained for generators with identical mode shapes. The destabilization occurs in a similar manner in both cases although a small difference is discernible. This difference is attributed to the unequal mode deflections of corresponding turbine stages of the generators. This will results in small disparities in the torque distribution from the turbine stages along the shaft (assuming the power input at each stage is constant). A few calculations with different mode shapes showed in each case that for different mode shapes, the common mode was destabilized to a slightly lesser extent than for identical mode shapes.

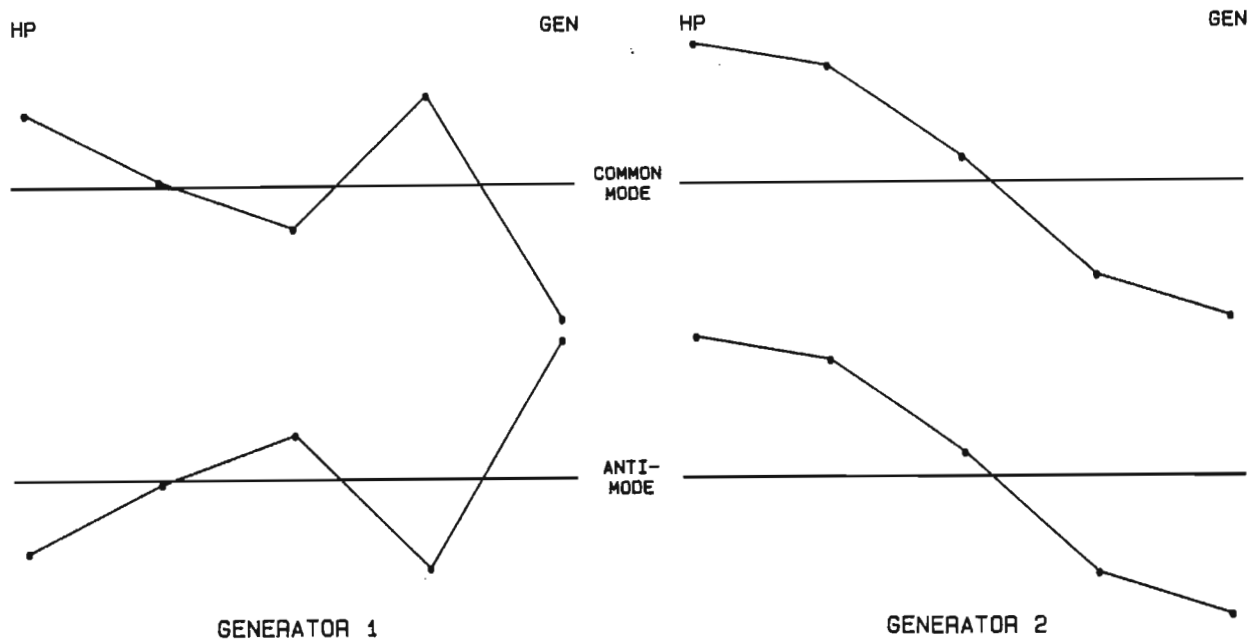

Fig 7.20 Generator mode shapes when the generator-1 mode 3 frequency and the generator-2 mode 1 frequency are the same.

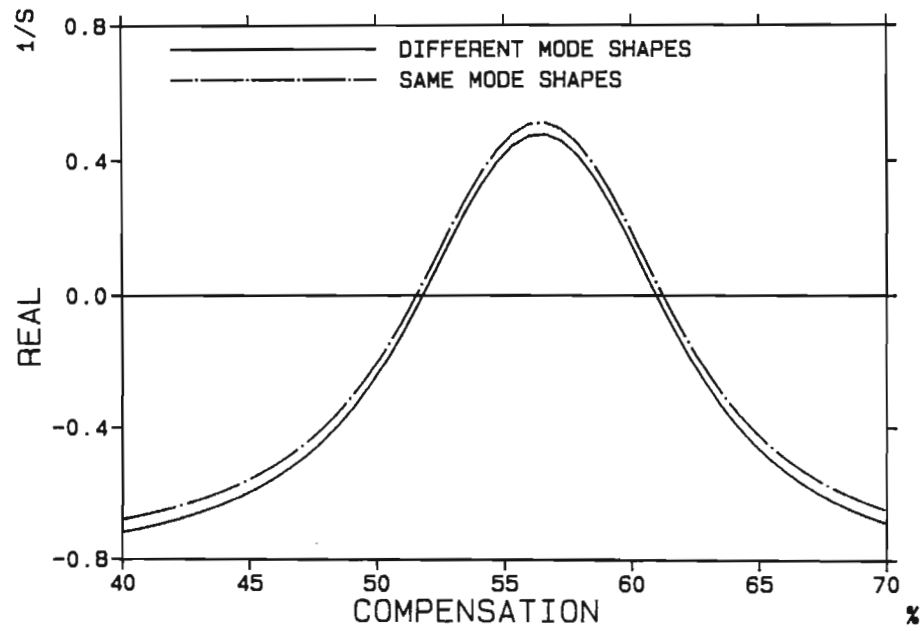

Fig 7.21 Real part of the common mode as the compensation is varied for coincident modes with different mode shapes compared with that obtained when the mode shapes are the same.

7.6 Torsional Interaction Between Remote Generators

The results and discussions so far have all dealt with two generators at the same power station. This section evaluates the torsional interaction between two generators which are electrically remote from each other. In order to investigate the effect of electrical distance between the generators on their torsional interaction, the mode shapes of the mode 3 common and anti-modes are calculated as generator-2 (in Fig 6.1) is moved away from the station busbar along the transmission line towards the infinite busbar. This is achieved by scanning the resistance and inductance representing generator-1's transformer (R_1 and X_1 in Fig 6.1) from 0.001 to 0.0771 p.u. and 0.15 to 1.0597 p.u. respectively while at the same time scanning the transmission line resistance and inductance (R and X_L) from 0.0845 to 0.0084 p.u. and 1.0097 to 0.1 p.u. respectively. This results in the resistance and inductance between generator-1 and the infinite bus remaining constant. The mode shapes (calculated without any series capacitance) appear in Fig 7.22.

Only the real parts of the mode shapes are shown since the imaginary parts are all very close to zero. Thus, although symmetry no longer exists, the concept of in-phase and out-of-phase modes still holds. As the generators become separated, the degree of torsional interaction becomes less with generator-1 being dominant in the common mode and generator-2 dominant in the anti-mode. Finally when generator-2 is close to the infinite bus and electrically far from generator-1 there is almost no interaction and the generator oscillations are mainly confined to different modes. These results refer to the system without series capacitors; in the presence of series capacitors, the torsional interaction between the generators can be markedly different.

Reference [20] considered remote generators in the presence of series capacitors when it investigated the influence of the Grootvlei power station on the SSR stability of Koeberg. The system considered was that shown in Fig 7.23 where the Grootvlei power station was represented at node 2. The Grootvlei generator (parameters given in Appendix I) had torsional frequencies at 23.5 Hz and 42.8 Hz and there was thus no

torsional interaction between it and the Koeberg generator. This earlier investigation of Ref [20] is extended here to consider the effect of the generator at Grootvlei and the generator at Koeberg having torsional modes at the same frequency. The possibility of torsional interaction occurring between these remote generators is investigated and the influence of the torsionally similar generator at Grootvlei on the SSR stability of Koeberg is determined.

As a first step, it is assumed that the generator at Grootvlei power station (generator-2) is identical to the Koeberg generator (generator-1). The capacitance in line section 2-3 is varied such that the compensation, expressed as a percentage of the line section 3-4 inductance, varies from 20% to 100% and the mode 3 common and anti-mode eigenvalue loci are shown in Fig 7.24. The common mode remains stable while the anti-mode goes unstable between 61% and 79% compensation; in order to determine the nature of these oscillations and the involvement of the generators in them it is necessary to look at the mode shapes corresponding to these eigenvalue loci. These are displayed in Fig 7.25 in the same form as the previously presented mode shapes.

At low compensation levels there is very little torsional interaction with generator-1 almost totally dominating in the common mode and generator-2 dominating in the anti-mode; these results agree with those in Fig 7.22 obtained with zero compensation. As the compensation level increases the mutual involvement of the generators in both modes increases until around 55% compensation when both generators show equal involvement in both modes. As the compensation level increases further, the mutual involvement decreases with the generators dominating in different modes; however unlike the situation at low compensation levels, generator-1 now dominates in the anti-mode and generator-2 dominates in the common mode. The angle plots indicate that around equal involvement of the generators in both modes (55% compensation) the common mode oscillations are less in-phase (60 degrees) while the anti-mode oscillations are more in-phase (132 degrees).

This therefore means that although the generators are electrically remote, in the presence of series capacitors strong torsional interaction can occur between them. At some compensation levels unstable SSR oscillations could

exist with both generators being involved and the phase angle of the M3a mode shape during the unstable period shows that these oscillations would involve exchanges of energy between generators 1 and 2 as well as between the infinite bus and the generators.

These results have shown that if the generators are identical then torsional interaction between them can occur. The possibility of torsional interaction occurring between non-identical units with a single coincident torsional frequency is investigated next. This is achieved by assuming that the original Grootvlei generator is at node 2 as in Ref [20], but its mode 1 frequency is shifted from 23.5 Hz to 15.84 Hz which is also the frequency of mode 3 of the Koeberg generator. All other mode 1 parameters of the Grootvlei generator are left unchanged and are thus not equal to the corresponding Koeberg mode 3 parameters. Figure 7.26 presents the common and anti-mode loci corresponding to this 15.84 Hz mode as the compensation is varied. They are labelled M and Ma without a number for the common and anti-mode respectively since they are related to mode 1 of the Grootvlei generator and mode 3 of the Koeberg generator. In this case the anti-mode remains stable and the common mode goes unstable; the nature of this instability can be determined from the mode shapes presented in Fig 7.27 corresponding to the loci in Fig 7.26.

The oscillations related to the common and anti-modes exhibit a different characteristic compared to the previous case of identical generators in Fig 7.25. In this case generator-1 is always dominant in the common mode and generator-2 is always dominant in the anti-mode, but the degree of mutual interaction differs between the two modes. The common mode reaches the point of maximum mutual interaction with generator-2 showing only 50% of generator-1's involvement whereas for the anti-mode at maximum mutual interaction both generators show almost equal involvement. The angle plots indicate that at low compensation levels the common mode is the 'in-phase' mode and the anti-mode is the 'out-of-phase' mode, while at high compensation levels this is reversed. Around 52% compensation generator-2 oscillations lag generator-1's by 90 degrees in both the common and anti-mode. The unstable common mode oscillations between 61% and 79% compensation level are 'out-of-phase' oscillations similar to those which occur for identical generators.

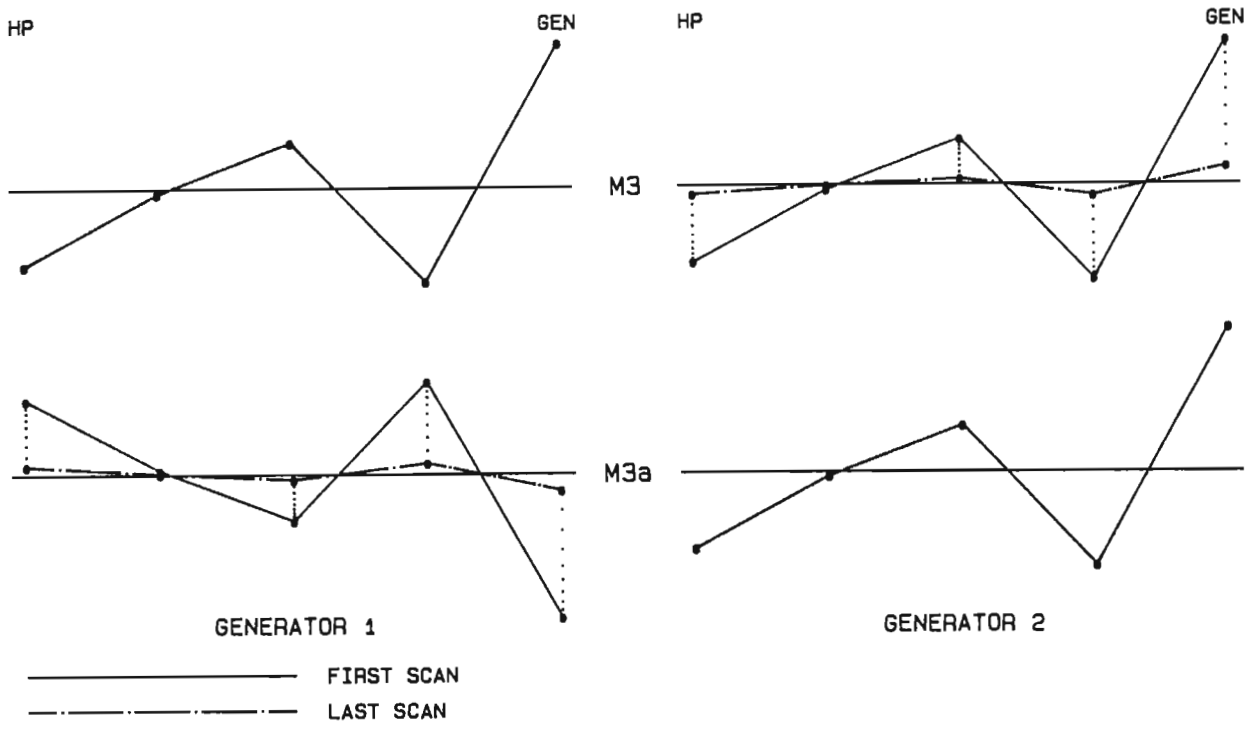

Fig 7.22 Real part of M3 and M3a mode shapes as generator 2 in Fig 6.1 is moved away from the station bus towards the infinite bus.

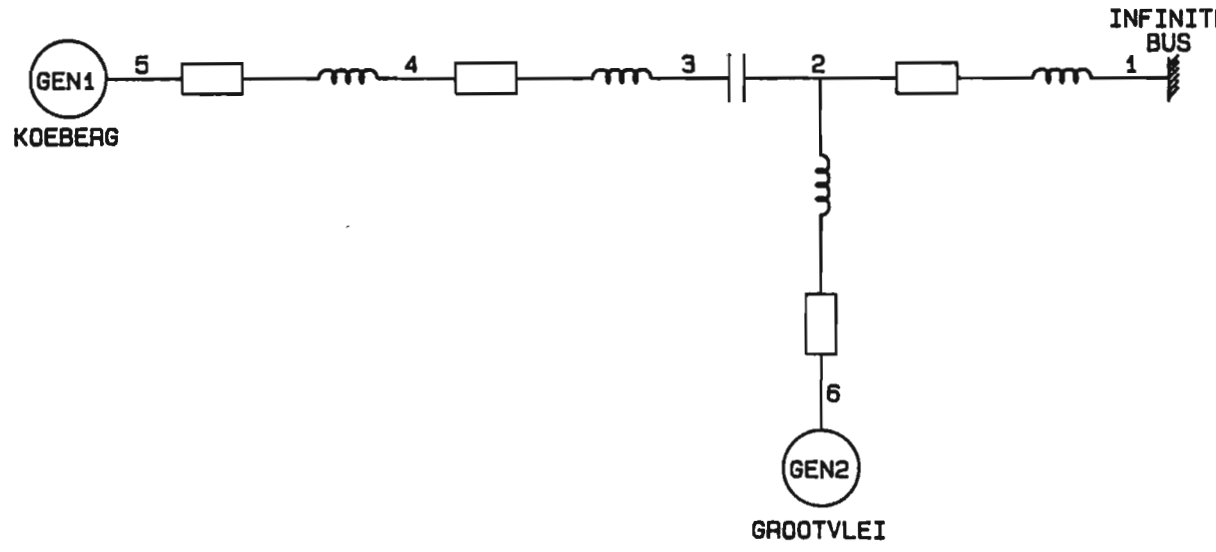

Fig 7.23 Schematic diagram of the system used to investigate interaction between generators at the Koeberg and Grootvlei power stations.

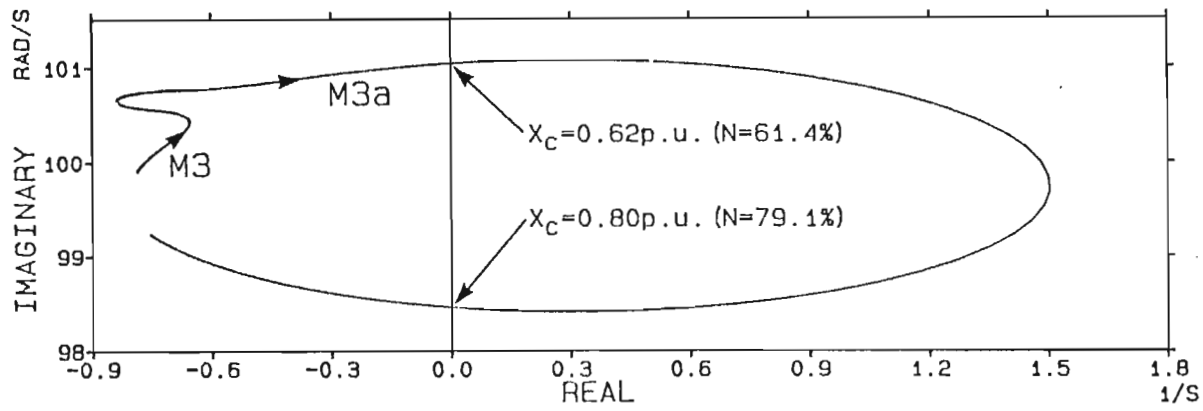

Fig 7.24 Mode 3 eigenvalue loci for the system in Fig 7.23 with identical generators at Koeberg and Grootvlei as the compensation in line 2-3-4 is varied from 20% to 100%.

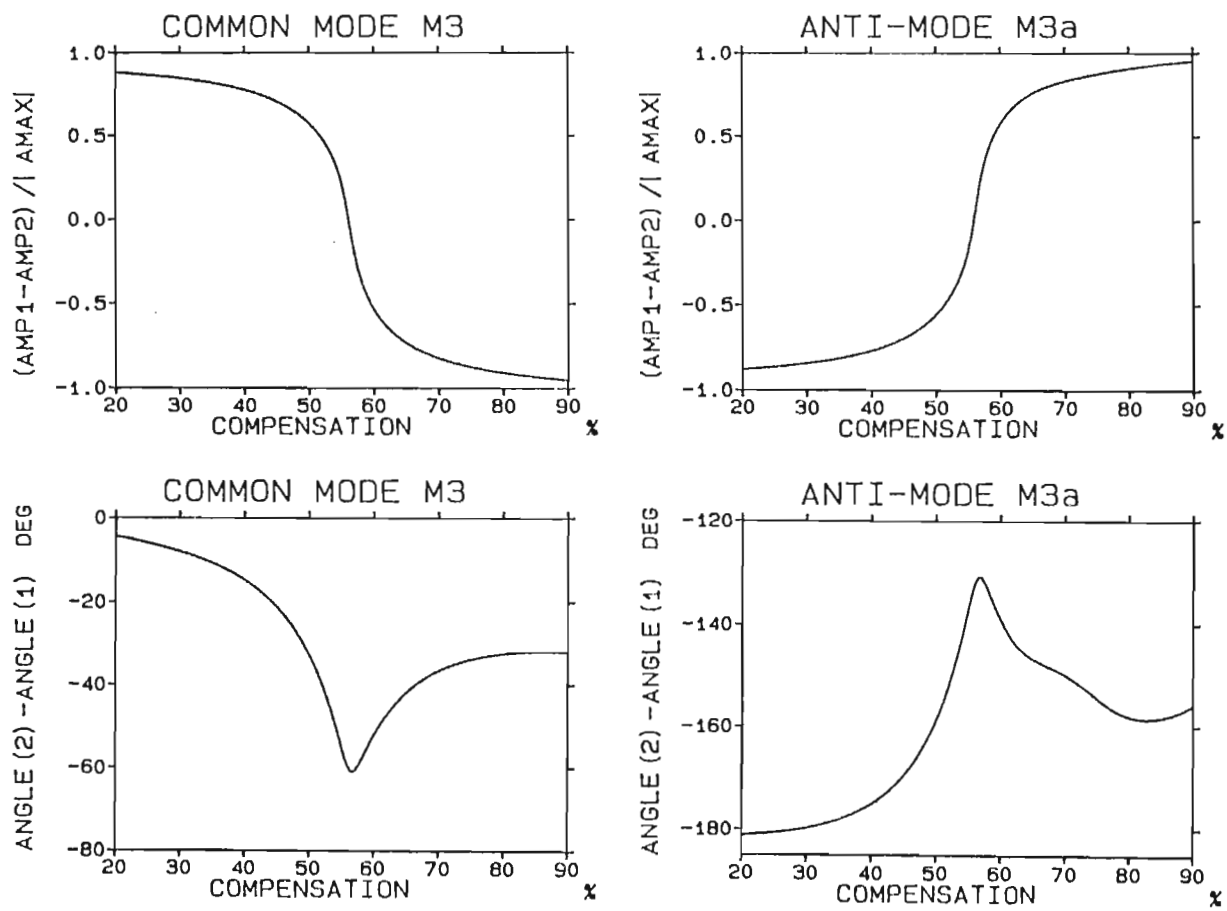

Fig 7.25 Mode shape information corresponding to the loci in Fig 7.24.

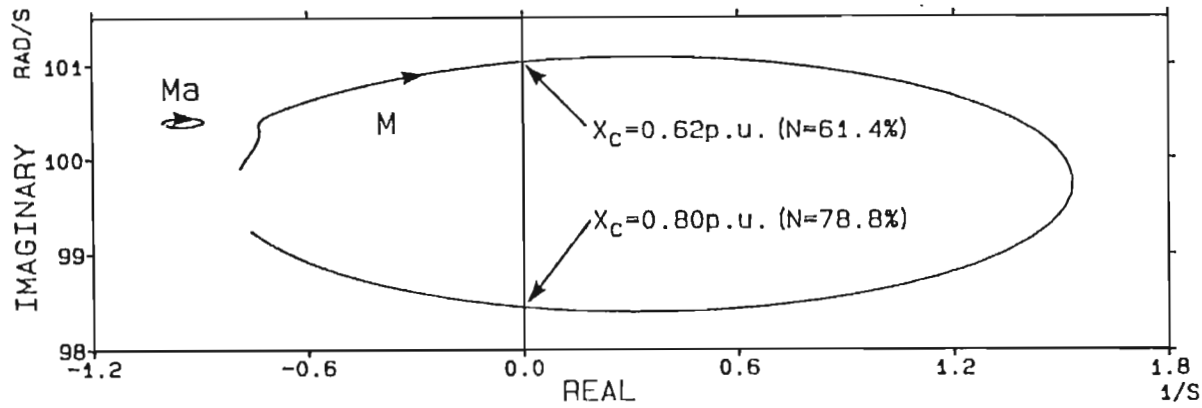

Fig 7.26 Common mode and anti-mode eigenvalue loci for the system in Fig 7.23 as the compensation level is varied from 20% to 100%; the Koeberg and Grootvlei generators are different except for a single coincident torsional mode.

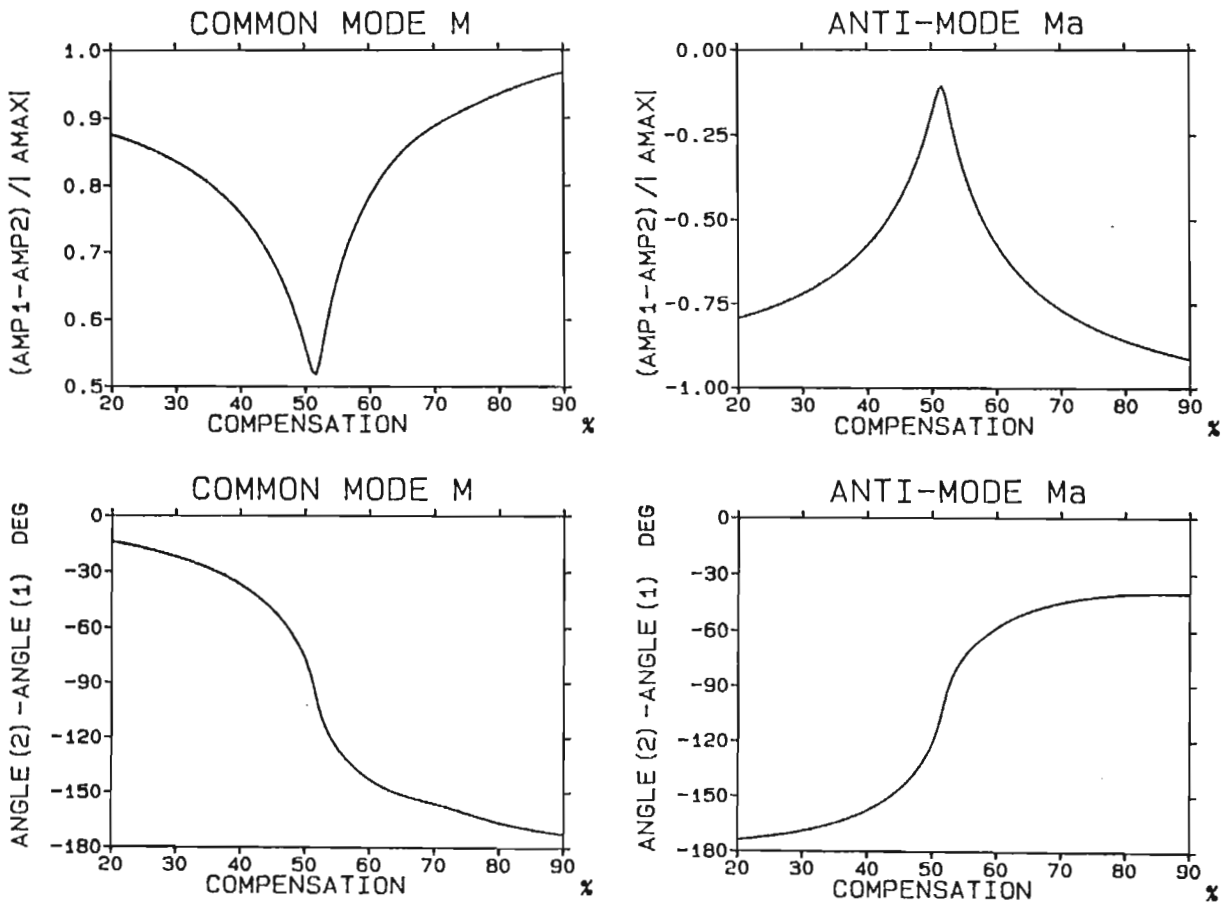

Fig 7.27 Mode shape information corresponding to the loci in Fig 7.26.

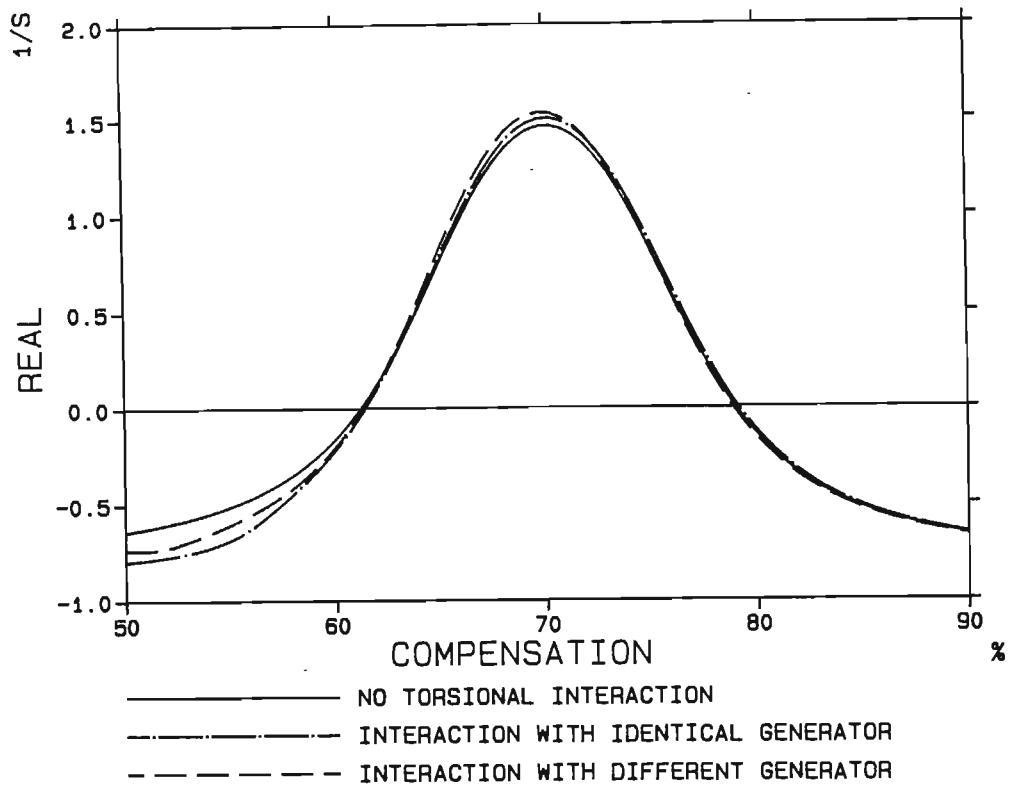

Fig 7.28 Real parts of destabilized modes from Figs 7.24 and 7.26 together with that obtained for no torsional interaction between Koeberg and Grootvlei.

Torsional interaction between remote generators is thus not restricted to identical units; remote non-identical units will also experience torsional interaction in the presence of series capacitors if they have a coincident torsional frequency.

In order to investigate the effect of the above displayed torsional interaction on the SSR stability limits of the Koeberg power station, the real parts of the unstable modes in Figs 7.24 and 7.26, together with that which occurs for the original Grootvlei generator with no torsional interaction (from Ref [20]), are displayed as a function of the compensation level in Fig 7.28. This interesting result shows that the SSR stability limit of the system is hardly affected by the torsional interaction of the Koeberg generator with another generator at the Grootvlei station; be it either an identical generator or a different generator with a coincident torsional mode.

7.7 Damping SSR Oscillations in Non-Identical Units with a Single Controlled Shunt Reactor

In this section the operation of a single controlled shunt reactor damping out SSR oscillations in two adjacent turbogenerators is investigated when the turbogenerators differ in either operating point or mechanical parameters. The system considered is shown in Fig 7.29; all the system parameters are given in Appendix I and they are the values at which the controller (also given in Appendix I) was designed [40]. The equations describing this multi-machine system with controlled shunt reactor are given in non-linear form in Appendix G and in linearized form in Appendix H. It should be noted that the equations used here to describe the system are different to those used previously in such studies for Koeberg [20,40,42,53] and to those used to design the controller [40]. In those earlier studies a simplification was made in which the rate of change of the shunt inductance was neglected; however, since the controlled shunt reactor is modelled as a varying inductance (eqn (G.24)) it is necessary to have an equation describing the rate of change of the shunt inductance (given by eqn (G.28)). This difference means that the controller designed as an optimal controller in Ref [40] will not be an optimal controller for the system as described by the equations in this thesis. This is not serious since this section is only concerned with comparing the operation of the controller with identical units to that with non-identical units.

Figure 7.30 shows the eigenvalue loci of the first three torsional modes (common and anti-) as the series compensation (as a percentage of the transmission line inductance X_L in Fig 7.29) is varied from 20% to 100% when the controller is not in operation. Only M1 and M3 go unstable although M2 comes close to an unstable condition. The eigenvalue loci for the same change in compensation when the controller is operational are presented in Fig 7.31. The electrical system now adds positive damping to the common modes and all three move further into the left-half-plane when interacting with the electrical system resonances. It is interesting to note that the electrical subsynchronous mode loci E2 and mechanical mode loci M3 interchange at some stage. The controller has no effect on the anti-modes and this is expected since for identical generators at the same

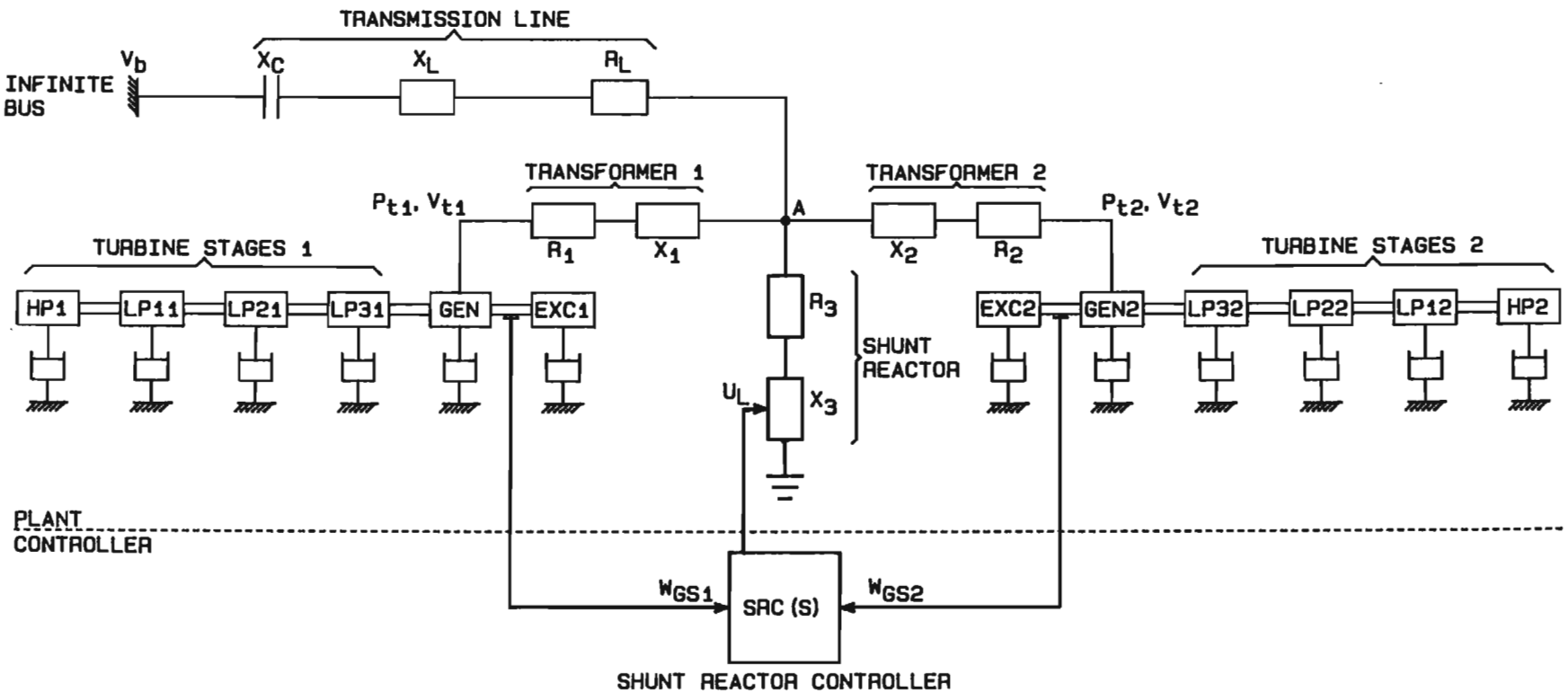

Fig 7.29 System with two generators and a single controlled shunt reactor.

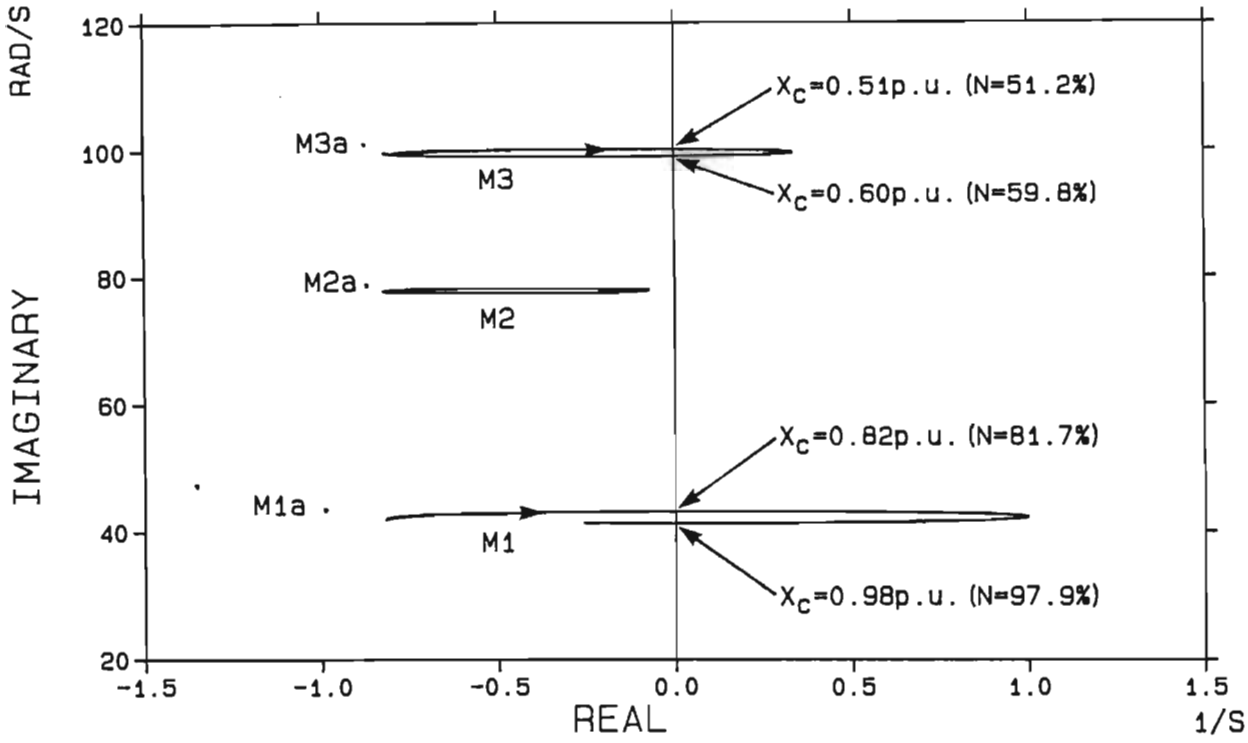

Fig 7.30 Selected eigenvalue loci for the system in Fig 7.29 with no controller as the transmission line compensation level is varied from 20% to 100%.

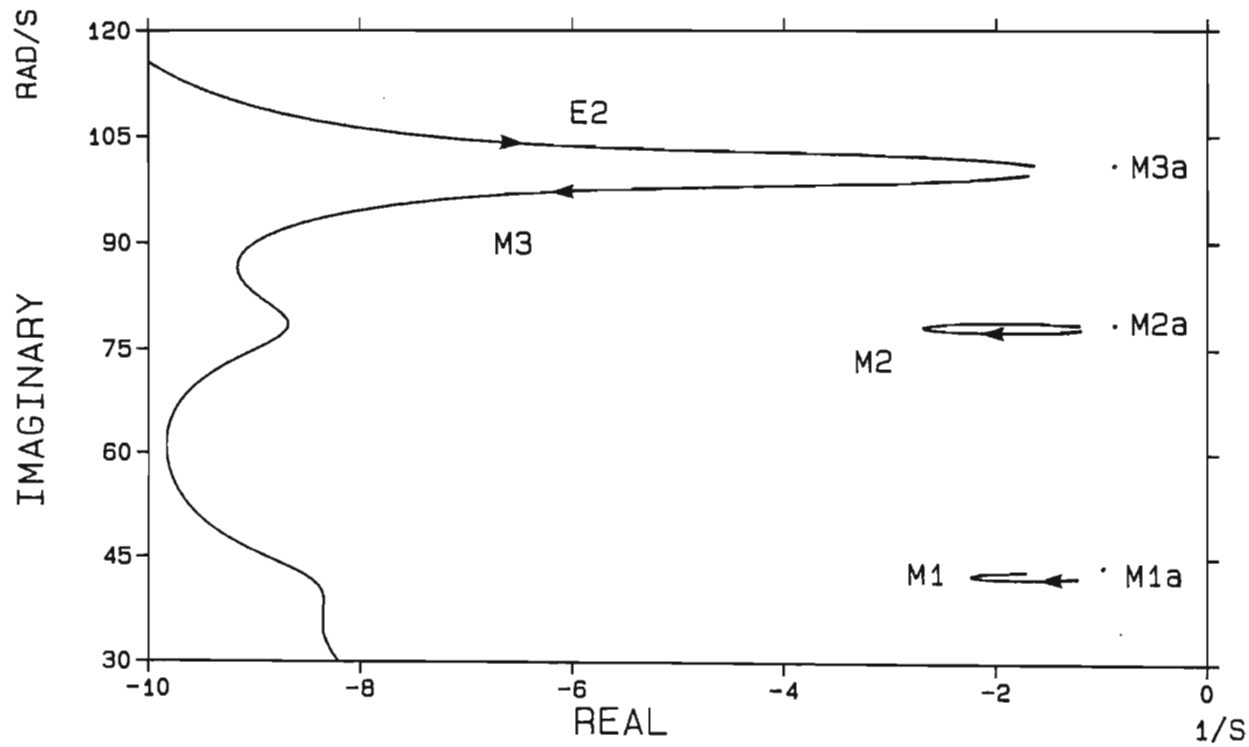

Fig 7.31 Selected eigenvalue loci for the system in Fig 7.29 with the controller in operation as the transmission line compensation level is varied from 20% to 100%.

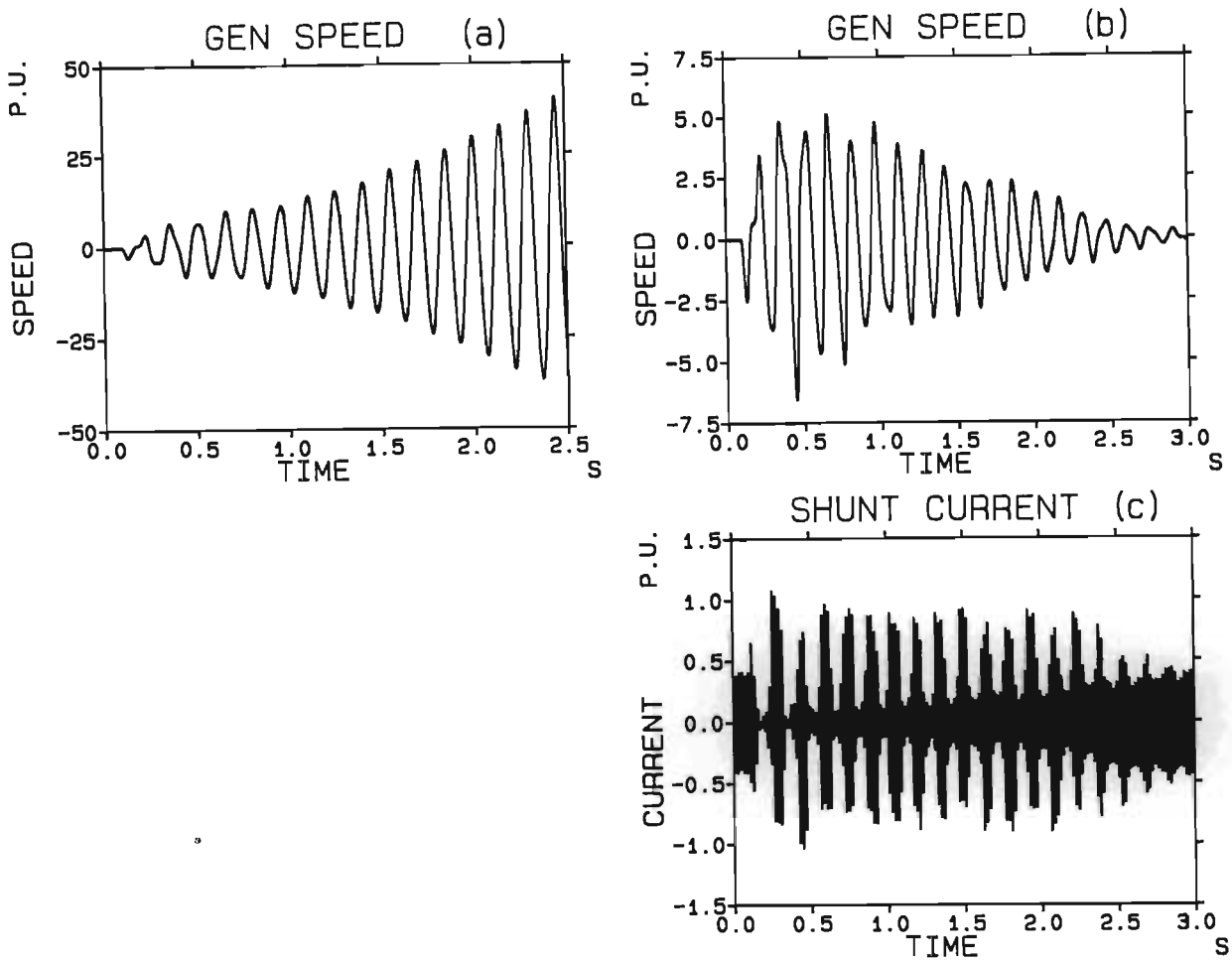

Fig 7.32 Transient response of the system following a 100 ms three-phase short circuit at the infinite bus at a compensation level of 90%; (a) - without controller, (b) and (c) - with controller.

operating points, the generator anti-mode speed signal contributions are 180 degrees out-of-phase and hence sum to zero as the input to the controller.

The system transient response is calculated for a temporary three phase short circuit at the infinite busbar lasting 100 ms with a series capacitor of 0.9 p.u. (90% compensation) in the line. This value of capacitance results in the maximum destabilization of M1 when no controller is present. Fig 7.32(a) shows the resulting generator speed with no controller while Figs 7.32(b) and (c) show the generator speed and shunt reactor current respectively when the controller is in operation. Clearly the transient response confirms the predictions of the eigenvalue calculations and the controller is successful in damping out the unstable oscillations.

7.7.1 Differences in electrical power

In this section the generators are assumed to be operating at different power levels (P_{t1} = 1.0 p.u. and P_{t2} = 0.2 p.u.) while all other generator parameters, including the mechanical damping, are equal. As explained earlier, the assumption that the mechanical damping does not depend on the electrical loading allows the effects of mechanical and electrical damping to be separated. Previous results (see Sect 6.1.1, Fig 6.18) showed that electrical loading differences hardly affected the active torsional mode loci and only had a small effect on their mode shapes, introducing a small out-of-phase component in the common mode oscillations and a small in-phase component in the anti-mode oscillations. This in-phase component in the anti-mode oscillations causes them to interact with the electrical resonance in the transmission system as evidenced in Fig 7.33 by the movement of the anti-mode loci as the capacitance is scanned. This interaction of the anti-modes with the electrical resonance will cause the controller to have some influence on their stability.

The controller maintains a stable system over the considered compensation range; in particular, at 90% compensation (X_c = 0.9 p.u.) M1 is stabilized from 1.03 s^{-1} without the controller to -2.07 s^{-1} with the controller. However, the controller adds a small negative damping to the anti-modes which have real components of -0.99, -0.87 and -0.87 s^{-1} for M1a to M3a respectively without the controller and -0.93, -0.82 and -0.81 s^{-1} respectively with the controller. It has been suggested (discussion and closure of Ref [42]) that an out-of-phase component in the common mode oscillations would detract from the controller's operation; this is not true and is discussed in the next section.

Figure 7.34 presents the two generator speeds calculated for a 100 ms three phase short circuit at the infinite bus with a compensation level of 90%. A comparison of these results with that of Fig 7.32(b) calculated for equal electrical loading on both generators shows that the difference in electrical power between the generators does not have much affect on the controller's operation.

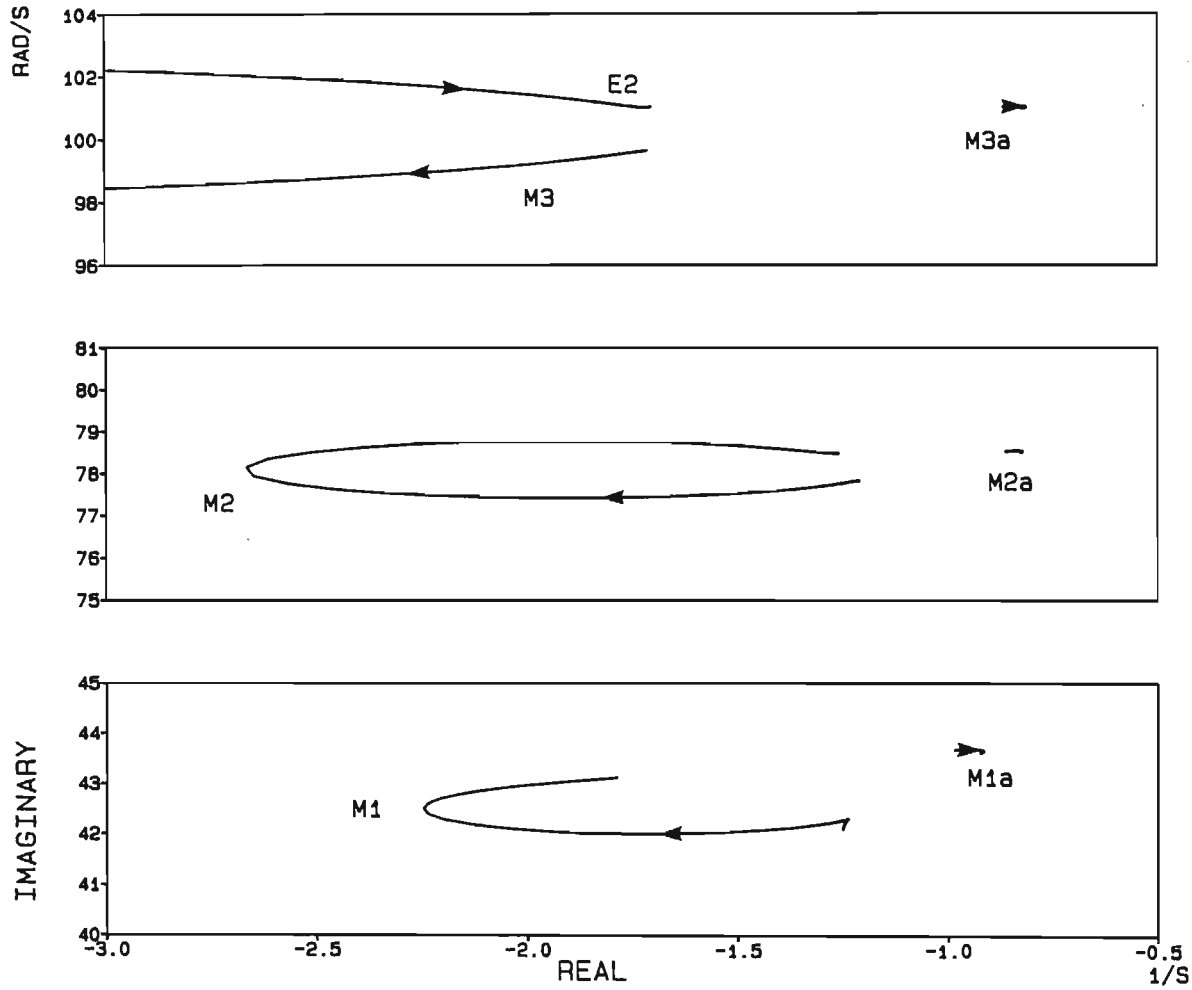

Fig 7.33 Selected eigenvalue loci for the system in Fig 7.29 with the generators at different power levels as the compensation level is varied from 20% to 100%; (P_{t1}=1.0 p.u., P_{t2}=0.2 p.u.).

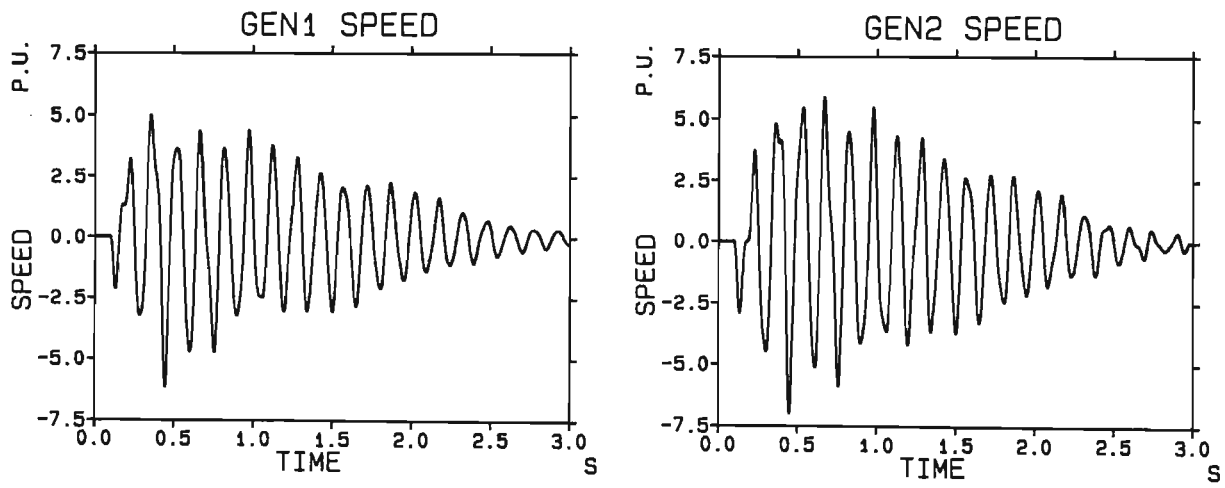

Fig 7.34 Generator speed signals following a 100 ms three-phase short circuit at the infinite bus at a compensation level of 90% when P_{t1} = 1.0 p.u. and P_{t2} = 0.2 p.u.

7.7.2 Differences in mechanical damping

In this section the generators are assumed to have different mechanical dampings (as in Sect 7.2) with generator-1's modes having zero mechanical damping and generator-2's modes all having a mechanical decrement factor σ_{mi} = 1.57 s^{-1}; the total mechanical damping for each mode is thus the same as that for the case of identical units in Fig 7.31.

Figure 7.35 presents some of the system eigenvalue loci for this unequal damping condition as the compensation level is varied from 20% to 100%. The results of Sect 7.2 showed that for unequal dampings the common and anti-mode oscillations of the generators both have in-phase and out-of-phase components. In fact, at 90% compensation (X_c = 0.9 p.u.) the generator oscillations for M1 are 29 degrees out-of-phase while those for M1a are 143 degrees out-of-phase, generator-1 leading in both cases. The in-phase components in the anti-modes results in them producing an input to the controller and they are thus affected by the controller.

The common mode oscillations of the generators contain quite large out-of-phase components when there is a damping difference between the generators (see Fig 7.6); however this phase difference does not in itself necessarily reduce the effectiveness of the controller. The common modes are in this case more damped than for equal dampings. For instance, at 90% compensation M1 has a real part of -2.39 s^{-1} compared to -2.10 s^{-1} for the case of equal mechanical dampings. The effect of out-of-phase speed signal components on the operation of the controller is described below.

Consider the action of the controller in damping a particular subsynchronous mode current in the transmission line. For two identical generators, the input signal to the controller (being the sum of the two generator speed signals) and the individual generator speed signals are all in-phase. The speed oscillations of the generators induce armature currents at $50 \pm f_m$ Hz (where f_m is the speed oscillation frequency) which are in-phase with each other; (for example the subsynchronous current of generator-1 is in-phase with that of generator-2). These current

components cause an amplitude modulation (at a frequency of f_m) of the armature currents which is in phase with the speed oscillations. The armature currents add to form an amplitude modulated total generator current which in the absence of a shunt reactor would be the transmission line current. The phase of the total generator current modulation is the same as that of each individual armature current and hence of each individual speed oscillation. The controller action is to produce an amplitude modulated shunt reactor current which has its amplitude modulations in phase opposition to the modulation in the total generator current. The amplitude modulation in the shunt reactor current is thus 180 degrees out of phase with the controller input signal (assuming zero phase shift through the controller) and this is seen in comparing Figs 7.32(b) and (c).

For generators with different mechanical dampings, the controller input signal at a particular mode frequency is the resultant of the vectorial addition of the individual generator speed oscillations at that frequency and will therefore have a phase angle between the phase angles of the individual speed oscillations of the two generators. In other words, the controller input signal will lead the one generator speed signal and lag the other generators speed signal. These 'mode speed oscillations' (speed oscillations at a particular mode frequency) produce amplitude modulations in the individual armature currents which are out-of-phase with each other by the same amount as the individual speed signals; when added to form the total generator current, the out-of-phase components cancel and the resultant amplitude modulations are in-phase with the controller input signal. Hence, since the out-of-phase components in the amplitude modulation of the armature currents cancel in the same way as the out-of-phase components in the generator mode speed signals do, the controller input will always have the correct phase with respect to the amplitude modulations in the total generator current. Even for a real controller with a phase shift between the input and output, the phase relationship between the controller input and the total generator current will be the same for the purely in-phase speed signals of identical generators and the phase displaced speed signals of non-identical generators. Moreover, the

magnitude of the total generator current amplitude modulations is determined by the magnitude of the in-phase components of the generator mode speed signals, which is the magnitude of the controller input.

The presence of a phase shift between the individual generator speed signals should thus not in itself affect the operation of the controller at all. The effectiveness of the controller when there is a damping difference between the generators depends on the design of the controller and may be better or worse than for identical units. The controller used in this thesis was designed as an optimal controller [40,42], but it can no longer be considered optimal since it was designed using simplified equations to describe the controller action as pointed out earlier. In general though, a controller may be designed as being optimal around a particular operating point so a change in the system conditions (for example the damping distribution) will result in the controller no longer being optimal. However, the effect of the controller may be better than for the original design conditions although not the best for the new conditions.

Figure 7.36 presents the generator transient speed signals following a temporary three phase short circuit at a compensation level of 90%. Generator-2 (higher damping) has a lower amplitude of oscillation than generator-1 and the response of both units is less damped than for identical units. This is due to the fact that for unequal dampings both the common modes and anti-modes are excited by a system fault and although the common modes are damped out quickly by the controller, the anti-modes have a lower damping (real part of $-0.7\ s^{-1}$) and persist longer. The damping of the mode 1 anti-mode is actually reduced by the controller; the real part of M1a being $-1.17\ s^{-1}$ without the controller and $-0.70\ s^{-1}$ with the controller. This is true also for M3a which moves from a real part of $-0.61\ s^{-1}$ to $-0.42\ s^{-1}$ when the controller is added.

The nature of the speed oscillations in Fig 7.36 are investigated further in Fig 7.37 in order to verify that they are in fact due to the anti-modes. The mode shapes predict generator-1 to lead generator-2 by 29 degrees and

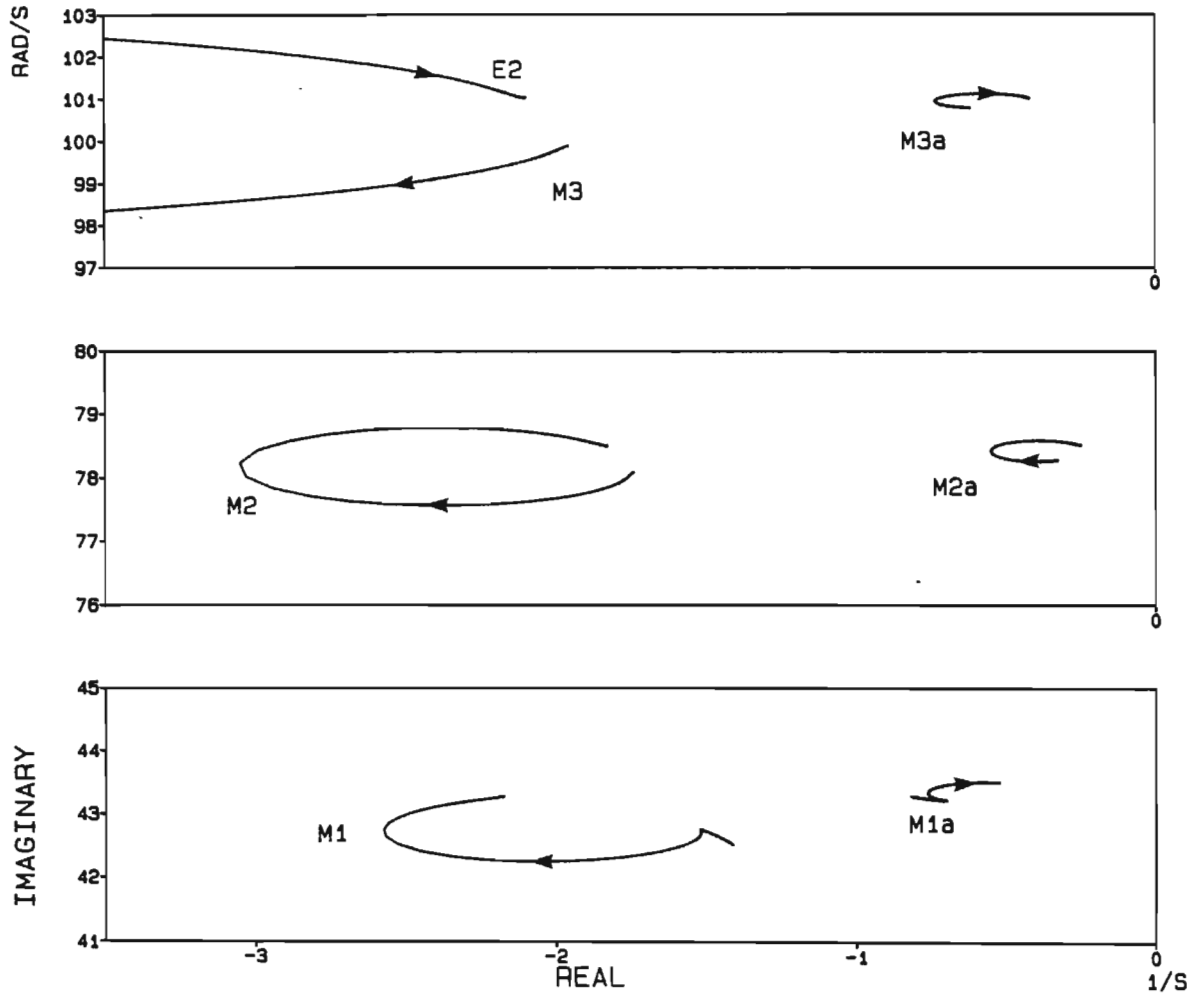

Fig 7.35 Selected eigenvalue loci for the system in Fig 7.29 with different generator dampings as the compensation level is varied from 20% to 100%; (Gen-1 σ_{mi} = 0.0 1/s, Gen-2 σ_{mi} = 1.57 1/s).

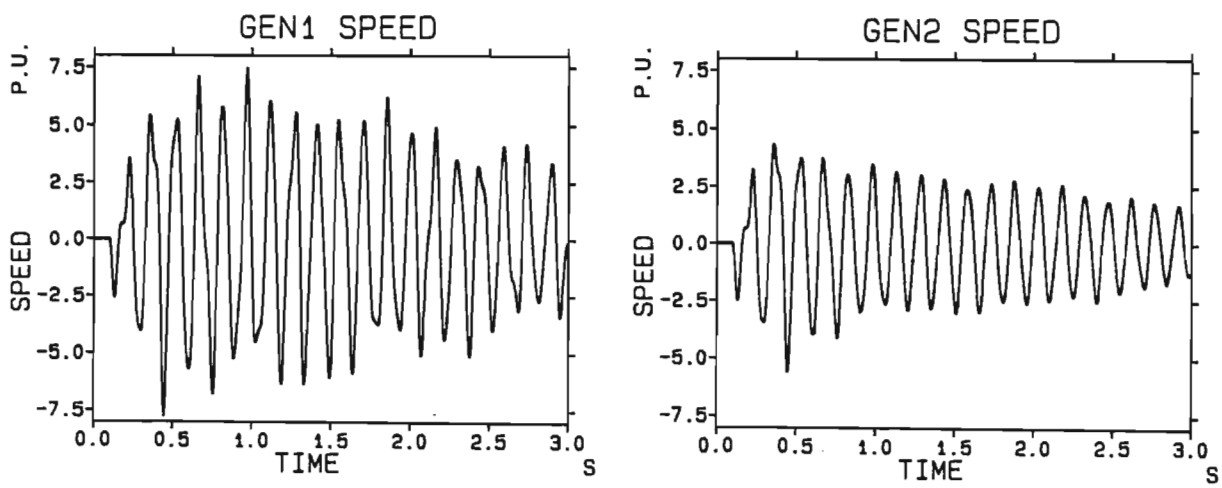

Fig 7.36 Generator speed signals following a 100 ms three-phase short circuit at the infinite bus at a compensation level of 90% when Gen-1 σ_{mi} = 0.0 1/s and Gen-2 σ_{mi} = 1.57 1/s.

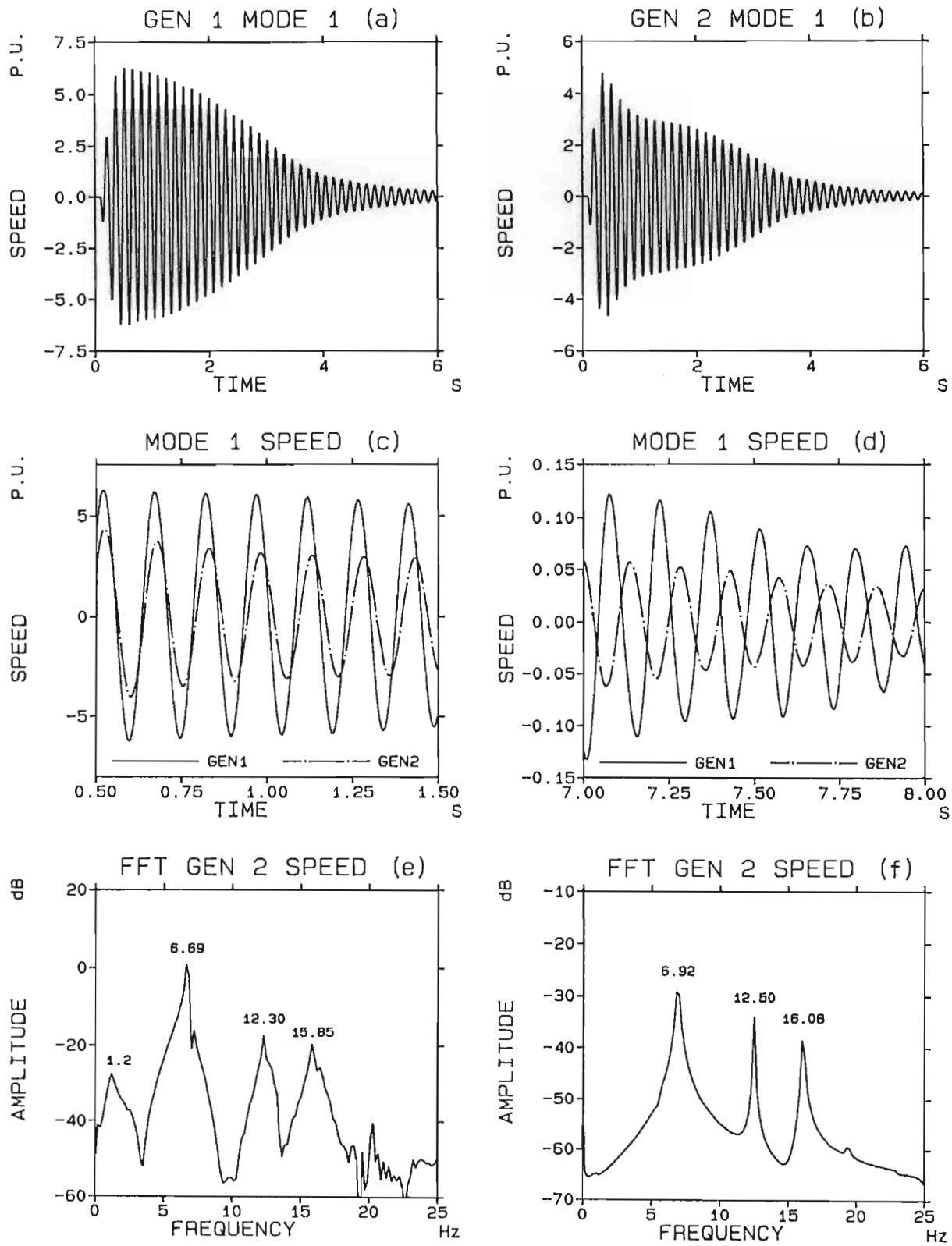

Fig 7.37 Further transient results for the fault in Fig 7.36.

have a magnitude 2.08 times larger than that of generator-2 for the common mode, while for the anti-mode generator-1 leads generator-2 by 143 degrees and has a magnitude 0.48 times that of generator-2. The mode 1 inertia speeds of generator 1 and 2 are shown in (a) and (b) respectively; generator-2's oscillations are dominated by the common mode initially as seen by the higher decay rate immediately after fault removal while generator-1's oscillations are dominated by the anti-mode as seen by their lower decay rate after fault removal. The mode 1 oscillations are displayed for both generators over two different time periods in (c) and (d) and it can be seen that after the initial period in which both common and anti-mode oscillations are present, the controller quickly damps out the common mode and the generator oscillations settle down to the relative phase and magnitudes predicted by the mode shapes for the anti-modes. This is further verified in (e) and (f) where (e) shows the FFT of the first five seconds of the generator-2 speed signal and (f) shows the FFT of that part of the signal from 5 to 10 seconds. The presence of closely separated modes is discernible in (e) whereas in (f) the peaks are clearly due to one mode only; for mode 1 in (f) the frequency peak at 6.92 Hz is exactly that of the anti-mode frequency whereas in (e) the peak is closer to the common mode frequency of 6.74 Hz.

7.7.3 Differences in mode inertias

This section considers a difference in the mode inertias of the generators such that generator-1's mode inertias are 50% of the nominal values given in Appendix I and generator-2's are 150% of the nominal values (as in Sect 7.3). This ensures that the total inertia of each mode remains the same as for the identical units. This difference in mode inertias is not meant to represent a possible variation that could occur between nominally identical units but rather a case of dissimilar units with coincident modes; in reality if the generators were different it is not likely that there would be more than one coincident mode.

The results in Sect 7.3 showed that for this condition of unequal mode inertias, the phase difference between the mode oscillations of the

individual generators varied depending on the capacitance. The presence of large in-phase components in the anti-mode oscillations (see Fig 7.11) means that the anti-modes will be influenced by the action of the controller. This is seen to be true in Fig 7.38 which presents some of the eigenvalue loci calculated as the compensation level is varied from 20% to 100%. All modes are stable, but the controller is more effective in damping the anti-mode oscillations of mode 1 than those of modes 2 and 3.

The generator speed signals for the same three phase short circuit considered previously are presented in Fig 7.39. Small-signal analysis of the system predicts the real part of M1 at $-2.16\ s^{-1}$ and the real part of M1a at $-1.55\ s^{-1}$ so although the mode 1 common and anti-modes are both excited as in the case of unequal dampings, they are both damped out fairly quickly by the controller as evidenced in Fig 7.39. Without the controller, the real parts of M1 and M1a are $1.14\ s^{-1}$ and $-0.83\ s^{-1}$ respectively so the controller adds positive damping to both modes.

7.7.4 Differences in mode frequencies

The results of the previous section are repeated here with differences in the mode frequencies instead of the inertias. The generator-1 mode frequencies are each reduced by 0.15 Hz and those of generator-2 are each increased by 0.15 Hz so that there is a separation of 0.3 Hz between the relevant mode frequencies of the generators. Figure 7.40 presents the eigenvalue loci of the torsional modes as the compensation level is scanned from 20% to 100%. Once again both common mode and anti-mode oscillations have in-phase components (as seen in Sect 7.4) and they are thus both affected by the controller action. Without the controller, and at a compensation level of 90% (X_c = 0.9 p.u.) the real parts of M1 and M1a are $0.72\ s^{-1}$ and $-0.72\ s^{-1}$ respectively whereas with the controller in operation they are $-1.84\ s^{-1}$ and $-1.24\ s^{-1}$ showing that the controller adds positive damping to both modes; the same is true for modes 1 and 2. The generator speed signals following a 100 ms three phase short circuit at a compensation level of 90% are displayed in Fig 7.41 and they confirm the small-signal predictions that the common and anti-mode oscillations are all be damped out quickly.

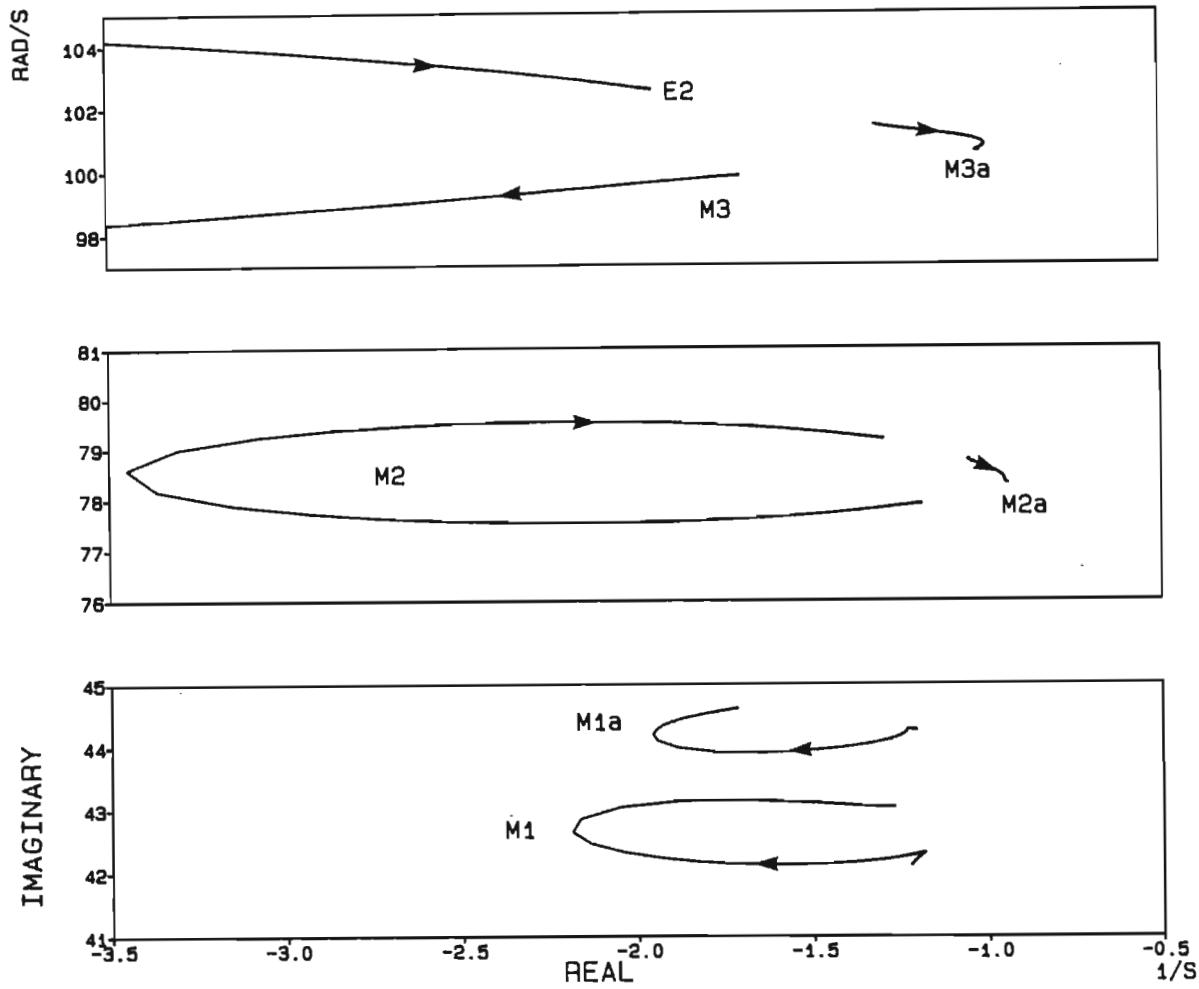

Fig 7.38 Selected eigenvalue loci for the system in Fig 7.29 with different generator mode inertias as the compensation level is varied from 20% to 100%; (Gen-1 J_{Mi}=50% of nominal values, Gen-2 J_{Mi}=150% of nominal values).

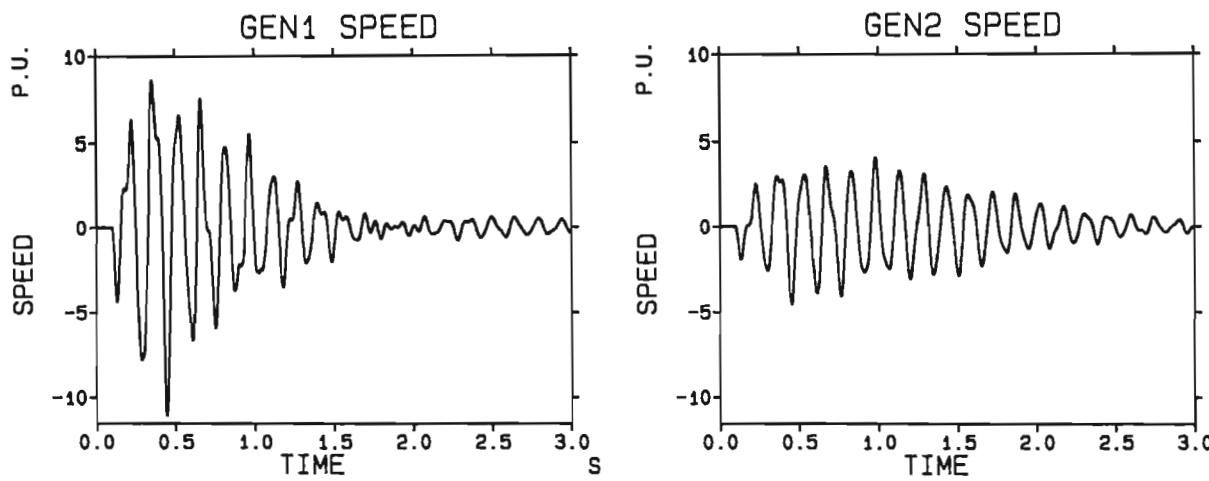

Fig 7.39 Generator speed signals following a 100 ms three-phase short circuit at the infinite bus at a compensation level of 90% when Gen-1 J_{Mi} = 50% nominal and Gen-2 J_{Mi} = 150% nominal.

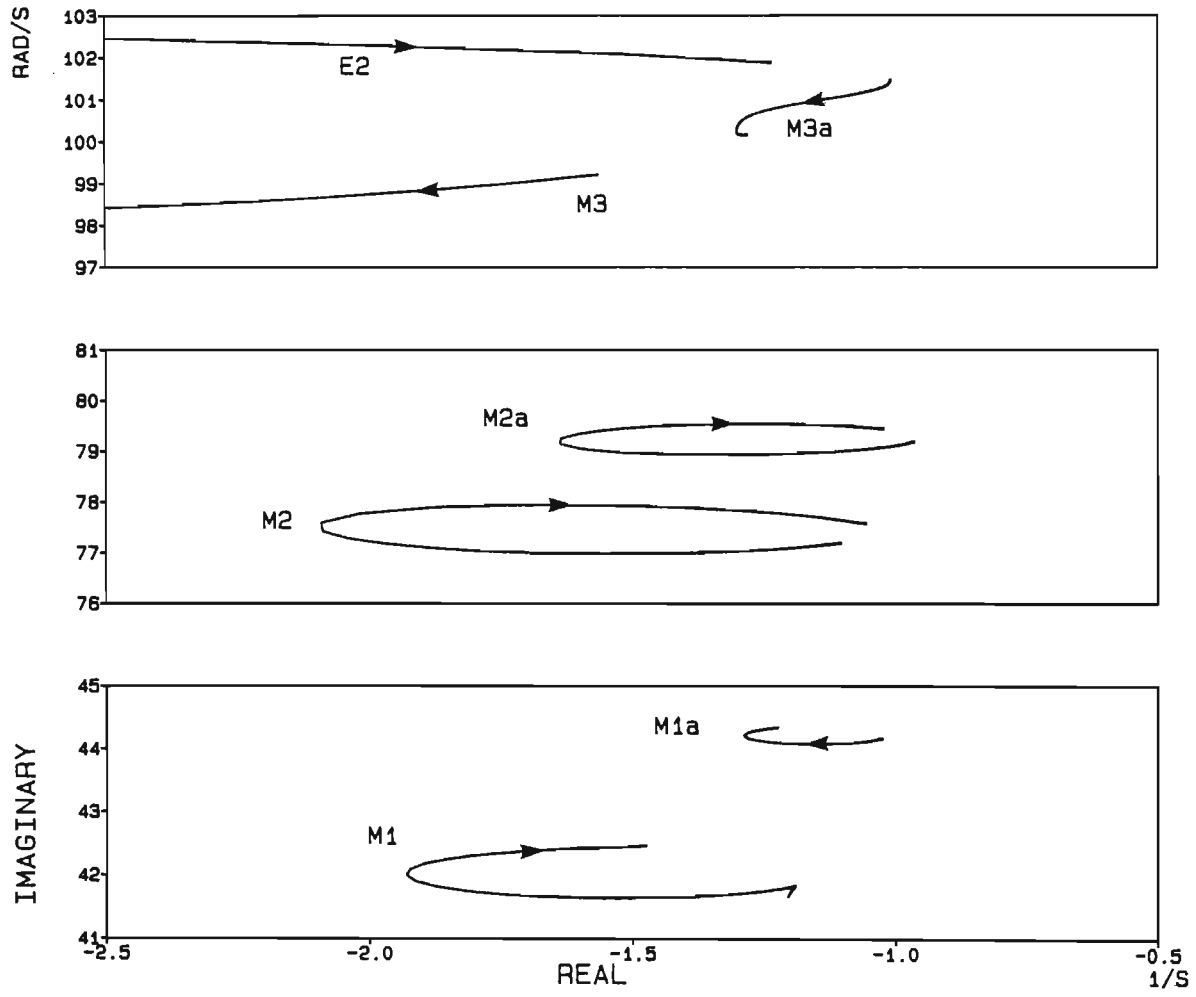

Fig 7.40 Selected eigenvalue loci for the system in Fig 7.29 with the Gen-1 mode frequencies 0.3 Hz higher than the Gen-2 mode frequencies as the compensation level is varied from 20% to 100%.

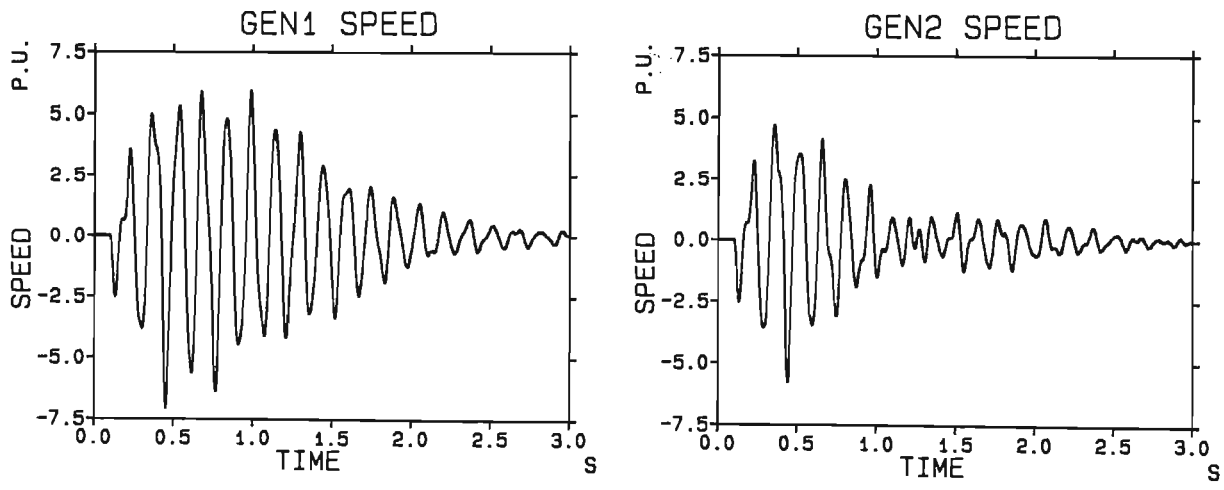

Fig 7.41 Generator speed signals following a 100 ms three-phase short circuit at the infinite bus at a compensation level of 90% when the Gen-1 mode frequencies are 0.3 Hz higher than those of Gen-2.

The results of Sect 7.7 have shown that the controller designed on the assumption of identical generating units still maintains a stable system even for large differences between the generator parameters. The out-of-phase components introduced into the generator speed signals due to differences in the generator parameters do not affect the operation of the controller. However, the in-phase components introduced into the anti-mode oscillations cause the controller to have an effect on the stability of these modes and under some conditions this results in a reduction in their stability.

7.8 Conclusions

This chapter has investigated the torsional interaction between non-identical adjacent generators at a power station. The differences considered between the generators were in mode damping, mode inertia (or excitability), mode frequency and mode shape. These differences included variations between nominally identical units as well as between largely different units with a common torsional mode. In addition, the possibility of torsional interaction between remote generators in a power system was investigated. Finally the effect of dissimilarities between the generators on the operation of a single controlled shunt reactor, which uses the sum of the generators' speeds as a control signal to damp out torsional oscillations in both generators, were investigated. From the results presented the following conclusions can be made:

(a) Differences between the parameters of two adjacent generators with common torsional modes generally results in a phase and amplitude difference between the responses of the two generators within a particular mode. This means that the idea of purely 'in-phase' and 'out-of-phase' modes is no longer valid although for a particular mode pair (common mode and anti-mode) the generator responses are generally more in-phase for one mode and out-of-phase for the other.

(b) The torsional characteristics of the non-identical generator station are very dependant, both in relative amplitude of generator responses as well their phase relationship, on the amount of series capacitance in the system. Generators with mode parameter differences may have little mutual involvement in a particular mode for some values of capacitance, but a reasonable degree of mutual involvement at other capacitance values.

(c) With specific regard to differences in the dampings of two generators, the results show that the generators do not share mechanical damping equally in a mode; the damping of the common mode is determined most strongly by the less damped generator whereas the anti-mode damping is influenced more by the higher damped generator.

(d) Remote generators with common torsional modes do not interact with each other in an uncompensated system and the mutual participation of the generators in a torsional mode is small. However, in the presence of series capacitors, there may be a strong torsional interaction between the generators.

(e) Differences between the parameters of two adjacent generators do not unduly affect the operation of the shunt reactor controller used in this chapter to damp out torsional oscillations in the two generators, even though the controller was designed assuming identical generators. (This does however depend on the particular controller used). Out-of-phase oscillations that occur in the speed signals of the two generators cancel when the speed signals are added to form the controller input; similarly the out-of-phase armature current components induced by these speed signals cancel when these currents add to form the total generator current (or transmission line current in the absence of the shunt reactor). Thus, out-of-phase speed signal components will not affect the operation of the shunt reactor controller.

CHAPTER EIGHT

CONCLUSIONS

This thesis has dealt with the modelling and analysis of turbogenerators in both single machine and multi-machine studies. In particular, the thesis addressed the problem of Subsynchronous Resonance (SSR) at the Koeberg power station in South Africa, which is connected through a 400 kV, 1400 km series capacitor compensated transmission system to a large grid. However, many of the findings in the thesis are applicable to any SSR prone power system in general.

The mathematical models used to describe the three main interacting subsystems involved in SSR, namely the transmission system, the generator electrical circuits and the turbogenerator mechanical system, were reviewed and the limitations and advantages of some of the more commonly used simplified models were considered. The results indicated that for SSR studies the most detailed models including network resonances, stator transients ($p\psi_d$ and $p\psi_q$) and shaft torsional characteristics are necessary.

The modal representation of a turbogenerator mechanical system, in which parameters are associated with each natural torsional mode of vibration of the shaft, was presented and the use of this modal model in transient and small-signal stability studies was investigated. One of the main advantages of the modal model over the conventional physical representation with parameters related to physical shaft elements, is that the mode parameters are all measurable; in the physical model the damping can be neither calculated nor measured and has mostly been estimated subject to a large degree of uncertainty. Nevertheless, errors will occur in the

measurement of mode parameters so the sensitivity of small-signal studies, in the form of Critical Compensation Level (CCL) calculations, and transient studies, in the form of torque amplification calculations, to such errors in the mode parameters was investigated.

Results have shown that CCL calculations are most sensitive to errors in the mode transfer factor (mode shape) and least sensitive to errors in the mechanical decrement factor (mode damping). However, when viewed in conjunction with the accuracy with which the mode parameters can be measured, the mode damping is likely to be the most crucial in determining the error in the predicted CCL. Transient calculations demonstrated the extent to which torque amplification predictions are affected by errors in the mode parameters. Results have shown that if the peak torque in a multi-modal response occurs only after a number of cycles and not during the initial post-fault period, then viscous forms of mechanical damping can influence the value of the peak torque experienced by the shaft.

The use of reduced order mechanical models in small-signal and transient stability studies has been investigated. The reduction in the order of the mechanical system was achieved using the modal model and neglecting certain modes, including some active subsynchronous modes which interact appreciably with the electrical system. To assist in the selection of the modes for inclusion in a particular model, the concepts of Torsional Interaction Susceptibility (TIS) and Mode Torque Susceptibility (MTS) have been introduced and these values enable comparisons to be made between different modes of a turbogenerator as well as between modes from different turbogenerators. Results have shown that the reduced order modal models are well suited to small-signal studies and a 4th order mechanical model should generally suffice for CCL calculations. However, for transient calculations the reduced order models were not as successful and the results showed that in general for transient calculations the shaft model should contain all active subsynchronous modes.

One of the main advantages of the modal shaft representation over the physical shaft representation is that the mode parameters are all

measurable. This aspect has been investigated and mode parameters have been determined from turbogenerator transient measurements. (Actual measurements on a real turbogenerator were not available so analytically generated transient curves were used to represent measured results). Due to the effects of the electrical network, especially the damping, the parameters obtained from measurements on a synchronized generator (system mode parameters) are different to those obtained from measurements on an unsynchronized generator (mechanical mode parameters). System mode parameters are easier to measure than mechanical mode parameters, but it is the latter which are required to be used in the modal model. A method has therefore been proposed to determine mechanical mode parameters from measured system mode parameters using eigenvalue-eigenvector scanning techniques and Fast Fourier Transform analysis. In addition, it has been shown that if the transmission system electrical subsynchronous mode can be identified, then it is possible to correct errors in the transmission system parameters.

The final part of this thesis has analysed the SSR behaviour of the Koeberg power station with two nominally identical generating units. Previous investigations for Koeberg had concentrated on the first phase of the project in which a single generating unit was to be commissioned, but a second nominally identical unit was commissioned at a later stage and this necessitated the extension of the earlier single machine studies to include the effects of the second unit. The SSR stability of the system with two generators has been compared to that obtained previously with only one generator and results have shown that the addition of the second generator effectively alters the transmission system characteristics. This improves one aspect of the stability in that the torsional modes are destabilized to a lesser extent with two generators and may even no longer go unstable. On the other hand, the modes that still go unstable, do so at a lower compensation level than occurs with one generator and in this respect the second generator decreases the stability of the system. For this analysis of the increased generating capacity, the two generators have been modelled as a single equivalent generator.

The modelling of the two generators separately as a multi-machine system rather than as a single equivalent generator has been investigated and results have shown that for each generator mode of the equivalent generator, the multi-machine system has two closely spaced modes called the common mode and anti-mode. For identical generators, the common modes represent in-phase oscillations of the two generators (and are identical to the equivalent generator modes), while the anti-modes represent out-of-phase oscillations; for conditions of identical generators, the anti-modes do not interact with electrical resonances in the transmission system and are thus unimportant in CCL calculations.

The investigation of two generators at Koeberg was extended to a general analysis of non-identical generating units at a power station. The differences considered between the units were in electrical operating point and mode parameters (damping, inertia, frequency and mode shape). The SSR stability of a system with non-identical generators has been compared to that for identical generators and the torsional interaction characteristics of the non-identical generators has been investigated. Results have shown that for non-identical generators the idea of purely in-phase and out-of-phase modes is no longer valid, moreover the relative amplitude and phase relationship of the generator oscillations within a particular mode is strongly dependant on the level of capacitive compensation in the system. With specific regard to damping differences between the generators, the results have shown that generators do not share torsional damping equally for a coincident mode, but the common mode damping is more strongly influenced by the lower damped generator while the anti-mode damping is more strongly influenced by the higher damped generator.

The analysis of torsional interaction between generators with coincident modes was extended to consider the possible interaction between generators which were electrically remote from each other. Results have shown that such generators do not interact with each other in an uncompensated system and respond in modes confined to their own power stations, but in the presence of series capacitors a strong interaction may exist.

Finally the effect of dissimilarities between adjacent generators on the operation of a single controlled shunt reactor, which uses the sum of the generators' speed deviations as a control signal to damp out torsional oscillations in both generators, have been investigated. Results have shown that differences between the generator parameters, (which introduce out-of-phase components in their speed signals), do not have much affect on the operation of the controller.

SUGGESTIONS FOR FURTHER WORK

(a) The practical measurement of the mode parameters of the micro-alternators in the Micro-Machines Research Laboratory using the identification technique to determine mechanical mode parameters from system mode parameters suggested in Chapter Five.

(b) The extension of the technique in Chapter Five for improving the transmission system parameters to include more complex representations of the transmission system.

(c) The practical measurement of the multi-machine behaviour of two adjacent generators using the scaled down models of the two Koeberg generators in the Micro-Machines Research Laboratory of the Department of Electrical Engineering.

(d) An investigation into using the differences in the amplitude and phase of the oscillations of adjacent non-identical generators, to determine the individual generator mode parameters from measurement taken when both generators are synchronized to the system.

(e) The practical implementation of the two-generator, single-controlled shunt-reactor-system, in the Micro-Machines Research Laboratory of the Department of Electrical Engineering.

APPENDIX A

PER-UNIT SYSTEM AND CONVENTIONS

Many different per-unit systems are available for the analysis of electrical power systems and each has its own inherent advantages and disadvantages [64]. One of the major distinctions between different per-unit systems is the choice of the base time, normally taken as either one second or the reciprocal of the nominal speed. The former is employed in this thesis as this results in the per-unit values of power and torque being numerically equal at nominal speed. This appendix presents a generalized per-unit system [11] which can be used to analyse multi-pole and multi-inertia turbogenerators.

In order for the machine equations to be independent of the number of pole pairs in a per-unit system, a multi-pole machine is converted to an equivalent two-pole machine of the same power. This effectively requires two sets of base values, one for electrical parameters and another for mechanical parameters.

A.1 Sign Conventions

δ is positive for a generator

$p\delta$ is positive for supersynchronous speeds

$p^2\delta$ is positive for acceleration

P_m is negative for power input to the turbine

P_e is positive for power output from the generator

T_e is positive for generator action

Quantities in the ABC reference frame are transformed into the dq0 reference frame via the Park's transformation matrix [11] which is given by

$$[P_\theta] = 2/3 \begin{bmatrix} \cos\theta & \cos(\theta-2\pi/3) & \cos(\theta+2\pi/3) \\ \sin\theta & \sin(\theta-2\pi/3) & \sin(\theta+2\pi/3) \\ 1/2 & 1/2 & 1/2 \end{bmatrix} \quad (A.1)$$

The angle θ is defined for the rotor reference frame of the generator as the angle between the stator phase 'A' axis and the positive d-axis of the rotor:

$$\theta = \omega_o t + \delta \quad (A.2)$$

where δ is the generator load angle.

A.2 Derivation of Per-Unit System

For this per-unit system four base values are chosen independently, namely the base armature power P_a^b, the base armature voltage V_a^b, the base time t^b and the base electrical angle θ_e^b. The rest of the base values are calculated from these four. The base field power is fixed by the particular Park's transform used while the base field current is chosen by forcing X_{md} and X_{fd} to be equal in per-unit [11].

Electrical base values

Base armature power	P_a^b	= total three phase rating
Base armature voltage	V_a^b	= rated voltage per phase
Base armature current	I_a^b	= $P_a^b/(3V_a^b)$
Base armature impedance	Z_a^b	= V_a^b/I_a^b
Base field power	P_f^b	= $1.5(P_a^b/3)$
Base field current	I_f^b	= $I_a^b X_{md}/X_{fd}$

Base field voltage	$V_f^b = P_f^b/I_f^b$
Base field impedance	$Z_f^b = V_f^b/I_f^b$
Base time	$t^b = 1$ s
Base electrical angle	$\theta_e^b = 1$ electrical radian (rad^e)
Base electrical speed	$\omega_e^b = \theta_e^b/t^b$ (rad^e/s)
Base electrical acceleration	$\alpha_e^b = \omega_e^b/t^b$ (rad^e/s^2)

Base electrical torque is defined as that torque which produces base power at nominal electrical speed ω_{en}.

Base electrical torque $T_e^b = P_a^b/\omega_{en} = P_a^b/\omega_o$

where ω_o is the system synchronous speed expressed in electrical rad/s.

The per-unit value of torque in the two-axis theory is calculated from the per-unit values of d- and q-axis currents and flux linkages as follows:

In physical units

$$T_e = \psi_d i_q - \psi_q i_d$$

Normalizing this equation (and using the superscript 'u' to indicate that a parameter is being expressed as a per-unit value) yields

$$T^u = T_e/T_e^b = (\psi_d i_q - \psi_q i_d)/T_e^b$$

$$= \omega_o(\psi_d i_q - \psi_q i_d)/P_a^b$$

Since $P_a^b = 3V_a^b I_a^b$, $I_d^b = 1.5I_a^b$ and $V_d^b = V_a^b$

$$T^u = \omega_o(\psi_d i_q - \psi_q i_d)/(2V_d^b I_d^b)$$

$$= \omega_o(\psi_d^u i_q^u - \psi_q^u i_d^u)/2$$

In order for the mechanical angles, speed, acceleration and torque to be equal to the corresponding electrical quantities when expressed as per-unit values (for an equivalent two-pole machine) the following mechanical base values are chosen with 'n' as the number of pole pairs and ω_{mn} as the mechanical nominal speed:

Mechanical base values

Base mechanical angle	$\theta_m^b = \theta_e^b/n$	in mechanical radians (rad^m)
Base mechanical speed	$\omega_m^b = \omega_e^b/n$	(rad^m/s)
Base mechanical acceleration	$\alpha_m^b = \alpha_e^b/n$	(rad^m/s^2)
Base mechanical torque	$T_m^b = P_a^b/\omega_{mn} = nP_a^b/\omega_o$	
Thus	$T_m^b = nT_e^b$	

In physical units the mechanical and electrical parameters are related as follows:

$$\theta_e = n\theta_m, \qquad \omega_e = n\omega_m, \qquad \alpha_e = n\alpha_m$$

and since the electrical power P_e and the mechanical power P_m must be equal at steady state:

$$T_e\omega_e = T_m\omega_m$$

and thus

$$nT_e = T_m$$

The mechanical parameters of inertia and shaft stiffness in physical units are normalized into per-unit values by considering the second order differential equation of motion in physical units as follows:

$$T_m = J_m\alpha_m + K_m\theta_m$$

or $$nT_e = J_m\alpha_e/n + K_m\theta_e/n$$

and normalizing it yields (in per-unit):

$$T^u = \frac{T_e}{T_e^b} = \frac{J_m \alpha_e}{n^2 T_e^b} + \frac{K_m \theta_e}{n^2 T_e^b}$$

$$= \frac{J_m}{n^2 T_e^b/\alpha_e^b} \frac{\alpha_e}{\alpha_e^b} + \frac{K_m}{n^2 T_e^b/\theta_e^b} \frac{\theta_e}{\theta_e^b}$$

$$= J^u \alpha^u + K^u \theta^u$$

where

Base inertia $\quad J_b = n^2 T_e^b/\alpha_e^b = T_m^b/\alpha_m^b$

Base stiffness $\quad K_b = n^2 T_e^b/\theta_e^b = T_m^b/\theta_m^b$

The machine's inertia is often expressed in terms of the inertia constant H in seconds so it is useful to find the per-unit value of J in terms of H.

By definition

$$H = \frac{\text{Stored kinetic energy at synchronous speed [W-sec]}}{\text{Turbogenerator rated power [VA]}}$$

$$= J_m \omega_{mn}^2/(2P_a^b)$$

Now $\quad J^b = n^2 T_e^b/\alpha_e^b = n^2 P_a^b/(\alpha_e^b \omega_o)$

Thus

$$H = \frac{J_m(\omega_o/n)^2}{2P_a^b} \frac{n^2 \alpha_e^b}{n^2 \alpha_e^b}$$

$$= J_m \frac{\alpha_e^b \omega_o}{n^2 P_a^b} \frac{\omega_o}{2\alpha_e^b}$$

$$= J^u \omega_o/(2\alpha_e^b)$$

Thus $J^u = 2H\alpha_e^b/\omega_o$

$= 2H/\omega_o$

where H and ω_o are in per-unit (or in seconds and electrical rad/s respectively since the base time and base electrical speed are both numerically equal to one). The equation of motion in per-unit is then given by

$$T^u = (2H/\omega_o)\alpha^u + K^u\theta^u$$

A.3 System Base Values

The base values calculated as described in the previous section for a single 1072 MVA Koeberg turbogenerator and a 2144 MVA equivalent turbogenerator representing two single units are as follows:

	Single Generator	Equivalent Generator	
Electrical base values			
Base time	1	1	s
Base armature power	1072	2144	MVA
Base armature voltage	$24/\sqrt{3}$	$24/\sqrt{3}$	kV
Base armature current	25.79	51.58	kA
Base armature impedance	0.537	0.269	ohm
Base field power	536	1072	MVA
Base field voltage	188	188	kV
Base field current	2.85	5.70	kA
Base field impedance	65.94	37.97	ohm
Base electrical angle	1	1	rad^e
Base electrical speed	1	1	rad^e/s
Base electrical acceleration	1	1	rad^e/s^2
Base electrical torque	3.412×10^6	6.825×10^6	$N\text{-}m/rad^e$

Mechanical base values

Base mechanical angle	0.5	0.5	rad^m
Base mechanical speed	0.5	0.5	rad^m/s
Base mechanical acceleration	0.5	0.5	rad^m/s^2
Base mechanical torque	6.825×10^6	1.365×10^7	$N-m/rad^m$
Base inertia	1.365×10^7	2.730×10^7	$kgm^2/(rad^m)^2$
Base stiffness	1.365×10^7	2.730×10^7	$N-m/(rad^m)^2$

APPENDIX B

SUBTRANSIENT AND TRANSIENT MODELS

B.1 Derivation of Expressions for $\omega_o\psi_d$ and $\omega_o\psi_q$

For the 'voltage behind subtransient reactance' and 'voltage behind transient reactance' models (Model 2 and Model 3 respectively in Chapter Two) the transformer voltages $p\psi_d$ and $p\psi_q$ are neglected and the voltage equations for the d- and q-axis stator coils are given by:

$$v_d = R_a i_d + \omega\psi_q \tag{B.1}$$

$$v_q = R_a i_q - \omega\psi_d \tag{B.2}$$

In the state-space representation of the transient and subtransient models, the rotor flux linkages are customarily chosen as the state variables. Hence in eqns (B.1) and (B.2) it is necessary to obtain expressions for $\omega\psi_d$ and $\omega\psi_q$ in terms of rotor flux linkages. The flux linkages are related to the axis coil currents by the following equation:

$$\begin{bmatrix} \psi_d \\ \psi_{fd} \\ \psi_{kd} \\ \psi_q \\ \psi_{kq1} \\ \psi_{kq2} \end{bmatrix} = \left[\begin{array}{ccc|ccc} L_d & L_{md} & L_{md} & & & \\ L_{md} & L_{ffd} & L_{md} & & [0] & \\ L_{md} & L_{md} & L_{kkd} & & & \\ \hline & & & L_q & L_{mq} & L_{mq} \\ & [0] & & L_{mq} & L_{kkq1} & L_{mq} \\ & & & L_{mq} & L_{mq} & L_{kkq2} \end{array}\right] \begin{bmatrix} i_d \\ i_{fd} \\ i_{kd} \\ i_q \\ i_{kq1} \\ i_{kq2} \end{bmatrix} \tag{B.3}$$

By manipulating eqn (B.3) the following equations can be obtained for rotor currents in terms of rotor flux linkages and stator currents:

$$L_{md}i_f = \frac{\frac{L_{md}^2}{L_{ffd}}\psi_{kd} - \frac{L_{md}L_{kkd}}{L_{ffd}}\psi_f + \frac{(L_{kkd} - L_{md})L_{md}^2}{L_{ffd}} i_d}{\frac{L_{md}^2}{L_{ffd}} - L_{kkd}} \tag{B.4}$$

$$L_{md}i_{kd} = \frac{\frac{L_{md}^2}{L_{ffd}}\psi_f - L_{md}\psi_{kd} + \frac{(L_{ffd} - L_{md})L_{md}^2}{L_{ffd}} i_d}{\frac{L_{md}^2}{L_{ffd}} - L_{kkd}} \tag{B.5}$$

$$L_{mq}i_{kq1} = \frac{\frac{L_{mq}^2}{L_{kkq1}}\psi_{kq2} - \frac{L_{mq}L_{kkq2}}{L_{kkq1}}\psi_{kq1} + \frac{(L_{kkq2} - L_{mq})L_{mq}^2}{L_{kkq1}} i_q}{\frac{L_{mq}^2}{L_{kkq1}} - L_{kkq2}} \tag{B.6}$$

$$L_{mq}i_{kq2} = \frac{\frac{L_{mq}^2}{L_{kkq1}}\psi_{kq1} - L_{mq}\psi_{kq2} + \frac{(L_{kkq1} - L_{mq})L_{mq}^2}{L_{kkq1}} i_q}{\frac{L_{mq}^2}{L_{kkq1}} - L_{kkq2}} \tag{B.7}$$

Eqns (B.4) to (B.7) can be substituted into the expressions for ψ_d and ψ_q from eqn (B.3) to obtain expressions for ψ_d and ψ_q as:

$$\psi_d = \left[L_d - \frac{L_{md}^2}{L_{ffd}}\right] i_d + \frac{L_{md}}{L_{ffd}}\psi_f + \left[L_{md} - \frac{L_{md}^2}{L_{ffd}}\right]\left[\frac{\psi_{kd} - \frac{L_{md}}{L_{ffd}}\psi_f - \left[L_{md} - \frac{L_{md}^2}{L_{ffd}}\right] i_d}{L_{kkd} - \frac{L_{md}^2}{L_{ffd}}}\right] \tag{B.8}$$

$$\psi_q = \left[L_q - \frac{L_{mq}^2}{L_{kkq1}}\right] i_q + \frac{L_{mq}}{L_{kkq1}} \psi_{kq1} + \left[L_{mq} - \frac{L_{mq}^2}{L_{kkq1}}\right] \left[\frac{\psi_{kq2} - \frac{L_{mq}}{L_{kkq1}} \psi_{kq1} - \left[L_{mq} - \frac{L_{mq}^2}{L_{kkq1}}\right] i_q}{L_{kkq2} - \frac{L_{mq}^2}{L_{kkq1}}}\right] \qquad (B.9)$$

Using the following identities (which can be derived from the definitions of transient and subtransient parameters given in Appendix B.2):

$$X'_d = \omega_o(L_d - L_{md}^2/L_{ffd})$$

$$X'_q = \omega_o(L_q - L_{mq}^2/L_{kkq1})$$

$$X'_d - X_a = \omega_o(L_{md} - L_{md}^2/L_{ffd})$$

$$X'_q - X_a = \omega_o(L_{mq} - L_{mq}^2/L_{kkq1})$$

$$X_{kd}(X'_d - X_a)/(X''_d - X_a) = \omega_o(L_{kkd} - L_{md}^2/L_{ffd})$$

$$X_{kq2}(X'_q - X_a)/(X''_q - X_a) = \omega_o(L_{kkq2} - L_{mq}^2/L_{kkq1})$$

$$L_{md}/L_{ffd} = (X'_d - X_a)/X_{fd}$$

$$L_{mq}/L_{kkq1} = (X'_q - X_a)/X_{kq1}$$

eqns (B.8) and (B.9) can be simplified and rewritten as:

$$\omega_o\psi_d = X''_d i_d + \omega_o(X''_d - X_a)(\psi_f/X_{fd} + \psi_{kd}/X_{kd}) \qquad (B.10)$$

$$\omega_o\psi_q = X''_q i_q + \omega_o(X''_q - X_a)(\psi_{kq1}/X_{kq1} + \psi_{kq2}/X_{kq2}) \qquad (B.11)$$

B.2 Subtransient and Transient Constants

The subtransient and transient models derived in Chapter Two and Appendix B.1 describe the generator in terms of reactances and time constants related to the d- and q-axes and not in terms of the reactances and resistances given in Appendix I describing each axis coil. In terms of these axes coil parameters the transient and subtransient reactances are defined as:

$$X'_d = X_a + X_{md}X_{fd}/(X_{md} + X_{fd}) \tag{B.12}$$

$$X''_d = X_a + X_{md}X_{fd}X_{kd}/(X_{md}X_{fd} + X_{md}X_{kd} + X_{fd}X_{kd}) \tag{B.13}$$

$$X'_q = X_a + X_{mq}X_{kq1}/(X_{mq} + X_{kq1}) \tag{B.14}$$

$$X''_q = X_a + X_{mq}X_{kq1}X_{kq2}/(X_{mq}X_{kq1} + X_{mq}X_{kq2} + X_{kq1}X_{kq2}) \tag{B.15}$$

while the transient and subtransient open-circuit time constants are defined as:

$$T'_{do} = (X_{fd} + X_{md})/\omega_o R_{fd} \tag{B.16}$$

$$T''_{do} = [X_{kd} + X_{md}X_{fd}/(X_{md} + X_{fd})]/\omega_o R_{kd} \tag{B.17}$$

$$T'_{qo} = (X_{kq1} + X_{mq})/\omega_o R_{kq1} \tag{B.18}$$

$$T''_{qo} = [X_{kq2} + X_{mq}X_{kq1}/(X_{mq} + X_{kq1})]/\omega_o R_{kq2} \tag{B.19}$$

Implicit in the above definitions are the assumptions [10,65] that

(i) the mutual inductance between the d-axis rotor and stator circuits are equal;

(ii) the transient and subtransient phenomena can be separated and attributed to particular coils (i.e. during the transient period $R_{kd} = R_{kq2} = \infty$ and during the subtransient period $R_{fd} = R_{kq1} = 0$).

B.3 Modification of Parameters for Zero Saliency

In conventional stability programs it is customary to neglect saliency so as to be able to represent the generator as a network component. The value of generator reactance (transient or subtransient) used in the network model is normally taken as the d-axis value since for many generators the q-axis parameters are either unknown or are known with less certainty than those of the d-axis. In Chapter Two the assumption of zero transient (or subtransient) saliency is achieved by modifying the q-axis parameters in such a way that the q-axis transient and subtransient short circuit time constants, defined as:

$$T'_q = [X_{kq1} + X_{mq}X_a/(X_{mq} + X_a)]/\omega_o R_{kq1} \tag{B.20}$$

$$T''_q = [X_{kq2} + X_{mq}X_aX_{kq1}/(X_{mq}X_a + X_{mq}X_{kq1} + X_aX_{kq1})]/\omega_o R_{kq2} \tag{B.21}$$

remain the same for the modified machine.

For zero transient saliency

Set $X'_q = X' = X'_d$ and calculate X_{kq1} and R_{kq1} from eqns (B.14) and (B.20) as

$$X_{kq1} = X_{mq}(X'_q - X_a)/(X_{mq} - X'_q + X_a) \tag{B.22}$$

$$R_{kq1} = [X_{kq1} + X_{mq}X_a/(X_{mq} + X_a)]/\omega_o T'_q \tag{B.23}$$

Finally calculate T'_{qo} from eqn (B.18).

For zero subtransient saliency

Set $X''_q = X'' = X''_d$ and calculate X_{kq2} and R_{kq2} from eqns (B.15) and (B.21) as

$$X_{kq2} = X_{mq}X_{kq1}(X''_q - X_a)/[X_{mq}X_{kq1} - (X''_q - X_a)(X_{mq} - X_{kq1})] \tag{B.24}$$

$$R_{kq2} = [X_{kq2} + X_{mq}X_aX_{kq1}/(X_{mq}X_a + X_{mq}X_{kq1} + X_aX_{kq1})]/\omega_o T''_q \tag{B.25}$$

Finally calculate T''_{qo} from eqn (B.19).

APPENDIX C

SINGLE GENERATOR SYSTEM EQUATIONS

This appendix presents the non-linear and linearized equations that describe a single generator connected via a radial transmission line to an infinite busbar as shown in Fig C.1. The mechanical system of the generator is represented by the conventional physical representation of lumped inertias interconnected by torsionally flexible shafts as shown in Fig C.2. The system equations for a modal representation of the shaft are given in Appendix D.

C.1 Generator Electrical Equations

The state-space equations describing the electrical behaviour of a generator with two q-axis damper circuits and one d-axis damper circuit as shown in Fig C.3 can be written in per-unit matrix form with currents as state variables (see eqn (2.12)) as:

$$p\underline{i} = [L]^{-1}\{\underline{v} - ([R] + \omega[G])\underline{i}\} \qquad (C.1)$$

where the vectors of axis coil currents $\underline{i}$ and axis coil voltages $\underline{v}$ are given by:

$$\underline{i} = [i_d, i_{fd}, i_{kd}, i_q, i_{kq1}, i_{kq2}]^T \qquad (C.2)$$

$$\underline{v} = [v_d, v_{fd}, 0, v_q, 0, 0]^T \qquad (C.3)$$

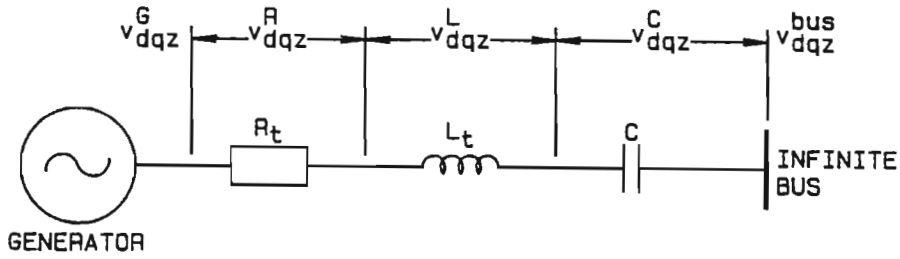

Fig C.1 Single generator connected to an infinite busbar.

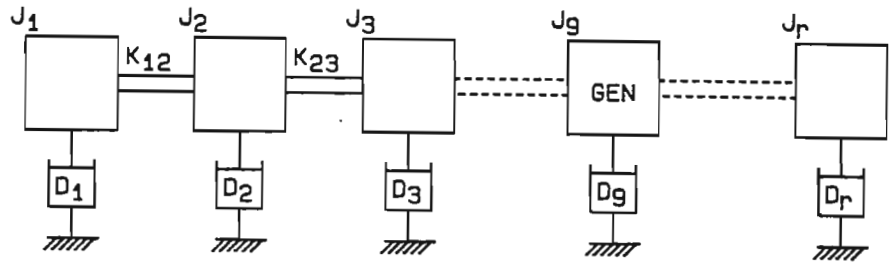

Fig C.2 Conventional physical representation of a turbogenerator multi-inertia shaft.

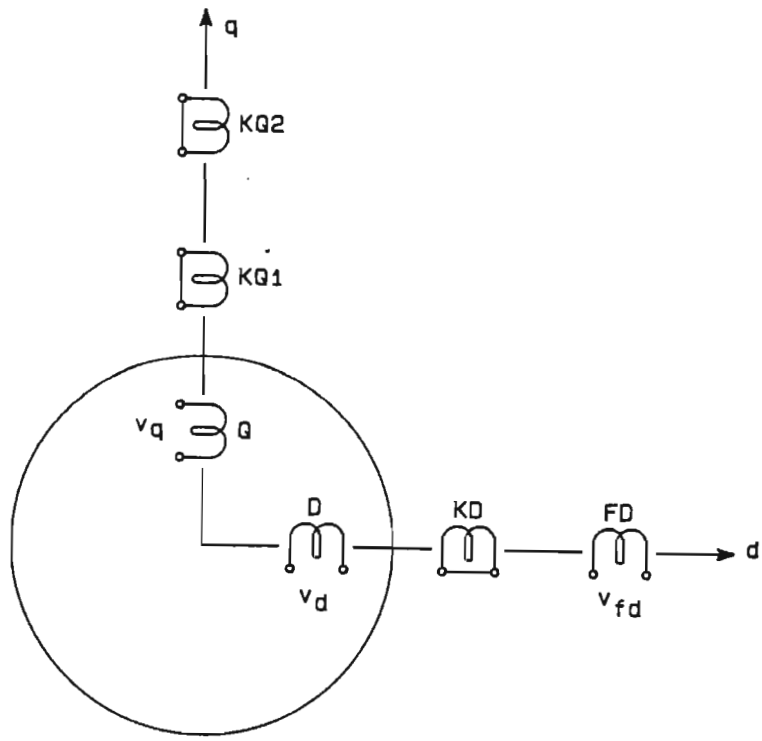

Fig C.3 Two-axis representation of a three phase synchronous machine.

and the matrices [R], [G] and [L] are defined as:

$$[R] = \text{diag.}\,[R_a,\ R_{fd},\ R_{kd},\ R_a,\ R_{kq1},\ R_{kq2}] \tag{C.4}$$

$$[G] = \begin{bmatrix} 0 & 0 & 0 & L_q & L_{mq} & L_{mq} \\ 0 & 0 & 0 & 0 & 0 & 0 \\ 0 & 0 & 0 & 0 & 0 & 0 \\ -L_d & -L_{md} & -L_{md} & 0 & 0 & 0 \\ 0 & 0 & 0 & 0 & 0 & 0 \\ 0 & 0 & 0 & 0 & 0 & 0 \end{bmatrix} \tag{C.5}$$

$$[L] = \left[\begin{array}{ccc|ccc} L_d & L_{md} & L_{md} & & & \\ L_{md} & L_{ffd} & L_{md} & & [0] & \\ L_{md} & L_{md} & L_{kkd} & & & \\ \hline & & & L_q & L_{mq} & L_{mq} \\ & [0] & & L_{mq} & L_{kkq1} & L_{mq} \\ & & & L_{mq} & L_{mq} & L_{kkq2} \end{array}\right] \tag{C.6}$$

with

$$L_d = L_a + L_{md}$$
$$L_q = L_a + L_{mq}$$

The electrical torque can be expressed in terms of axis coil currents only as:

$$T_e = \underline{i}^T[G]\underline{i}\omega_o/2 \tag{C.7}$$

For small-signal stability studies eqn (C.1) is linearized around some nominal operating point [66] to become

$$\Delta p\underline{i} = [L]^{-1}\{\Delta\underline{v} - ([R] + \omega_o[G])\Delta\underline{i} - [G]\underline{i}_o\Delta\omega\} \qquad (C.8)$$

where Δ indicates a small change in a variable. Linearization of the electrical torque in eqn (C.7) leads to

$$\Delta T_e = -(\omega_o/2)\underline{i}_o^T([G]^T + [G])\Delta\underline{i} \qquad (C.9)$$

C.2 Transmission System Equations

For a single generator connected to an infinite busbar, the transmission system is assumed to consist of a lumped series combination of resistance, inductance and capacitance in each of the stator phases as shown in Fig C.1. For such a system the two-axis (d,q,z) voltage vector at the generator terminals is given by:

$$\underline{v}_{dqz}^G = \underline{v}_{dqz}^{bus} - \underline{v}_{dqz}^C - \underline{v}_{dqz}^L - \underline{v}_{dqz}^R \qquad (C.10)$$

where the terms on the right hand side of eqn (C.10) are the infinite bus voltage and the voltage drops across the capacitance, inductance and resistance given by eqns (C.11), (C.12) and (C.13) respectively (for the balanced conditions considered in this thesis the zero sequence components of voltage are all zero):

$$\begin{aligned} pv_d^C &= i_d/C - \omega v_q^C \\ pv_q^C &= i_q/C + \omega v_d^C \end{aligned} \qquad (C.11)$$

$$\begin{aligned} v_d^L &= Lpi_d + \omega Li_q \\ v_q^L &= Lpi_q - \omega Li_d \end{aligned} \qquad (C.12)$$

$$\begin{aligned} v_d^R &= Ri_d \\ v_q^R &= Ri_q \end{aligned} \qquad (C.13)$$

where ω is the instantaneous rotor speed in electrical rad/s.

The d,q-axis components of the infinite busbar voltage of eqn (C.10) in the rotor reference frame are obtained by applying the Park's transform $[P_\theta]$ (stated in Appendix A.1) to the three-phase infinite busbar voltages which are assumed to have the following form:

$$\begin{aligned} v_a^b &= \sqrt{2}V_b\cos(\omega_o t) \\ v_b^b &= \sqrt{2}V_b\cos(\omega_o t - 2\pi/3) \\ v_c^b &= \sqrt{2}V_b\cos(\omega_o t + 2\pi/3) \end{aligned} \qquad (C.14)$$

where V_b is the RMS value of the infinite busbar voltage. Thus

$$\begin{aligned} v_d^b &= \sqrt{2}V_b\sin\delta \\ v_q^b &= -\sqrt{2}V_b\cos\delta \end{aligned} \qquad (C.15)$$

The linearized transmission system equations required for small-signal stability analysis are as follows:

$$\begin{aligned} \Delta p v_d^C &= \Delta i_d/C - \omega_o \Delta v_q^C - v_{qo}^C \Delta\omega \\ \Delta p v_q^C &= \Delta i_q/C + \omega_o \Delta v_d^C + v_{do}^C \Delta\omega \end{aligned} \qquad (C.16)$$

$$\begin{aligned} \Delta v_d^L &= L\Delta p i_d + \omega_o L\Delta i_q + Li_{qo}\Delta\omega \\ \Delta v_q^L &= L\Delta p i_q - \omega_o L\Delta i_d - Li_{do}\Delta\omega \end{aligned} \qquad (C.17)$$

$$\begin{aligned} \Delta v_d^R &= R\Delta i_d \\ \Delta v_q^R &= R\Delta i_q \end{aligned} \qquad (C.18)$$

$$\begin{aligned} \Delta v_d^b &= \sqrt{2}V_b\cos\delta_o\Delta\delta = -v_{qo}^b\Delta\delta \\ \Delta v_q^b &= \sqrt{2}V_b\sin\delta_o\Delta\delta = v_{do}^b\Delta\delta \end{aligned} \qquad (C.19)$$

C.3 Mechanical System Equations

This section presents the equations which describe a generalized turbogenerator multi-inertia mechanical system as shown in Fig C.2 with 'r' inertias and 'r-1' interconnecting torsionally flexible shafts. The generator rotor is assumed to be located at inertia 'g'.

The dynamics of the multi-inertia system are described by the following set of second-order differential equations:

$$[J]p^2\underline{\delta} + [D]p\underline{\delta} + [K]\underline{\delta} + \underline{T}_e + \underline{T}_m = \underline{0} \tag{C.20}$$

where

$$[J] = \text{diag. } [J_1, \ldots\ldots, J_r] \tag{C.21}$$

$$[D] = \text{diag. } [D_1, \ldots\ldots, D_r] \tag{C.22}$$

$$[K] = \begin{bmatrix} K_{12} & -K_{12} & & & 0 \\ -K_{12} & (K_{12}+K_{23}) & \cdot & & \\ & \cdot & \cdot & \cdot & \\ & & \cdot & \cdot & -K_{r-1,r} \\ 0 & & & -K_{r-1,r} & K_{r-1,r} \end{bmatrix} \tag{C.23}$$

$\underline{\delta}$ = rotor angular position vector

$$\underline{T}_e = [0, \ldots\ldots, 0, T_e, 0, \ldots\ldots, 0] \tag{C.24}$$

$$\underline{T}_m = \underline{F}_m P_m \tag{C.25}$$

P_m = total output power to the shaft from all turbine stages

$$\underline{F}_m = \omega_o[a_1/\omega_1, \ldots\ldots\ldots, a_r/\omega_r] \tag{C.26}$$

a_i = fraction of input power contributed by stage 'i'

ω_i = rotational speed of stage 'i'

ω_o = system synchronous speed

All mechanical parameters are in electrical per-unit (i.e. equivalent two-pole machine). For generator action the electrical torque T_e has a positive numerical value while P_m has a negative numerical value (as explained in Appendix A.1).

Eqn (C.20) can be written in state-space form by applying a change of variable to obtain the following set of '2r' first-order differential equations:

$$\begin{bmatrix} -[J] & [0] \\ [0] & [I] \end{bmatrix} p \begin{bmatrix} p\underline{\delta} \\ \underline{\delta} \end{bmatrix} = \begin{bmatrix} [D] & [K] \\ [I] & [0] \end{bmatrix} \begin{bmatrix} p\underline{\delta} \\ \underline{\delta} \end{bmatrix} + \begin{bmatrix} \underline{T_e} \\ \underline{0} \end{bmatrix} + \begin{bmatrix} \underline{F_m} \\ \underline{0} \end{bmatrix} P_m \qquad \text{(C.27)}$$

For a single lumped inertia mechanical system (see eqns (2.53) and (2.54)) eqn (C.27) takes the following form:

$$\begin{aligned} -Jpx_{m1} &= Dx_{m2} + T_e + P_m\omega_o/\omega \\ px_{m2} &= x_{m1} \end{aligned} \qquad \text{(C.28)}$$

where $x_{m1} = p\delta$ and $x_{m2} = \delta$. Linearization of eqn (C.27) yields

$$\begin{bmatrix} -[J] & [0] \\ [0] & [I] \end{bmatrix} \Delta p \begin{bmatrix} p\underline{\delta} \\ \underline{\delta} \end{bmatrix} = \begin{bmatrix} [D]+[F_e] & [K] \\ [I] & [0] \end{bmatrix} \Delta \begin{bmatrix} p\underline{\delta} \\ \underline{\delta} \end{bmatrix} + \begin{bmatrix} \Delta\underline{T_e} \\ \underline{0} \end{bmatrix} \qquad \text{(C.29)}$$

where $[F_e] = \text{diag.}[-a_i P_m/\omega_o]$ (C.30)

and P_m is assumed to be constant (no governor action).

APPENDIX D

SINGLE GENERATOR SYSTEM EQUATIONS IN MODAL FORM

This appendix presents the single generator system equations in terms of the mode variables described in Chapter Three instead of the conventional representation in physical variables as presented in Appendix C.

D.1 Mechanical System Equations

The motion of the mechanical system of a turbogenerator can be described in modal form (Sect 3.2) by the following second order matrix equation where the torsional characteristics of the shaft are represented by 'r' modes and the relative displacement of each mode is defined at 'n' locations along the shaft:

$$[J_M]p^2\underline{q} + [D_M]p\underline{q} + [K_M]\underline{q} + [Q]^T(\underline{T}_e + \underline{T}_m) = \underline{0} \qquad (D.1)$$

where

$$[J_M] = \text{diag.}[J_{MO}, \ldots\ldots, J_{M(r-1)}] \qquad (D.2)$$

$$[D_M] = \text{diag.}[D_{MO}, \ldots\ldots, D_{M(r-1)}] \qquad (D.3)$$

$$[K_M] = \text{diag.}[0, K_{M1}, \ldots., K_{M(r-1)}] \qquad (D.4)$$

$$[Q] = [\underline{Q}_0, \ldots\ldots\ldots, \underline{Q}_{(r-1)}] \qquad (D.5)$$

$\underline{q}$ = mode angle position vector

$$\underline{T}_e = [0, \ldots\ldots, 0, T_e, 0, \ldots\ldots, 0]^T \qquad (D.6)$$

$$\underline{T}_m = \underline{G}_m P_m \qquad (D.7)$$

P_m = total output power on shaft from all turbine stages

$$\underline{G}_m = [G_{m1}, \ldots\ldots, G_{mr}]^T \tag{D.8}$$

$$G_{mi} = \omega_o a_i/(\omega_o + \underline{Q}_i' p\underline{q}) \tag{D.9}$$

a_i = fraction of input power from location 'i'

ω_o = system synchronous frequency

$\underline{Q}_i'$ is row 'i' of the mode shape matrix and contains the relative mode deflections at physical location 'i'. For generator action the electrical torque T_e has positive numerical value while P_m has a negative numerical value as explained in Appendix A.1. Eqn (D.1) can be written in state-space form by applying a change of variable to obtain the following set of '2r' first-order differential equations:

$$\begin{bmatrix} -[J_M] & [0] \\ [0] & [I] \end{bmatrix} p \begin{bmatrix} p\underline{q} \\ \underline{q} \end{bmatrix} = \begin{bmatrix} [D_M] & [K_M] \\ [I] & [0] \end{bmatrix} \begin{bmatrix} p\underline{q} \\ \underline{q} \end{bmatrix} + \begin{bmatrix} [Q]^T \underline{T}_e \\ \underline{0} \end{bmatrix} + \begin{bmatrix} [Q]^T \underline{G}_m \\ \underline{0} \end{bmatrix} P_m \tag{D.10}$$

Linearization of eqn (D.10) leads to

$$\begin{bmatrix} -[J_M] & [0] \\ [0] & [I] \end{bmatrix} \Delta p \begin{bmatrix} p\underline{q} \\ \underline{q} \end{bmatrix} = \begin{bmatrix} [D_M]+[G_e] & [K_M] \\ [I] & [0] \end{bmatrix} \Delta \begin{bmatrix} p\underline{q} \\ \underline{q} \end{bmatrix} + \begin{bmatrix} [Q]^T \Delta \underline{T}_e \\ \underline{0} \end{bmatrix} \tag{D.11}$$

where $[G_e] = [Q]^T [F_e][Q]$ (D.12)

$[F_e]$ is defined by eqn (C.30) and P_m is assumed to be constant (no governor action).

D.2 Generator Electrical Equations

The state-space equations for the generator axis currents in terms of mode variables can be written in per-unit matrix form as:

$$p\underline{i} = [L]^{-1}\{\underline{v} - ([R] + \omega_o[G])\underline{i} - [G]\underline{i}\underline{Q}_g' p\underline{q}\} \tag{D.13}$$

where the subscript 'g' refers to the position of the generator within a mode shape vector. The matrices [L], [R] and [G] and the vectors of axis currents and voltages $\underline{i}$ and $\underline{v}$ are defined in Appendix C.1. The non-linear and linear equations for the electrical torque are the same as those for the physical representation of the shaft given by eqns (C.7) and (C.9) respectively. The linearized equation for the generator axis currents is obtained from eqn (D.13) as

$$\Delta p\underline{i} = [L]^{-1}\{\Delta\underline{v} - ([R] + \omega_o[G])\Delta\underline{i} - [G]\underline{i}_o\underline{Q}'_g\Delta p\underline{q}\} \qquad (D.14)$$

D.3 Transmission System Equations

The d,q-axis equations describing the transmission system in terms of physical rotor variables are given in Appendix C.2. The voltage drop across the resistance given by eqn (C.13) is the same in physical and modal co-ordinates. However, the capacitive and inductive voltage drops (eqns (C.11) and (C.12) respectively) and the infinite busbar voltage axis equations (C.15) need to be redefined in terms of modal components as

$$\begin{aligned} pv_d^C &= i_d/C - \omega_o v_q^C - \underline{Q}'_g p\underline{q} v_q^C \\ pv_q^C &= i_q/C + \omega_o v_d^C + \underline{Q}'_g p\underline{q} v_d^C \end{aligned} \qquad (D.15)$$

$$\begin{aligned} v_d^L &= Lpi_d + \omega_o Li_q + L\underline{Q}'_g p\underline{q} i_q \\ v_q^L &= Lpi_q - \omega_o Li_d - L\underline{Q}'_g p\underline{q} i_d \end{aligned} \qquad (D.16)$$

$$\begin{aligned} v_d^b &= \sqrt{2}V_b \sin(\underline{Q}'_g\underline{q}) \\ v_q^b &= -\sqrt{2}V_b \cos(\underline{Q}'_g\underline{q}) \end{aligned} \qquad (D.17)$$

For small-signal stability calculations eqns (D.15) to (D.17) are linearized to become:

$$\begin{aligned} \Delta pv_d^C &= \Delta i_d/C - \omega_o \Delta v_q^C - v_{qo}^C \underline{Q}'_g \Delta p\underline{q} \\ \Delta pv_q^C &= \Delta i_q/C + \omega_o \Delta v_d^C + v_{do}^C \underline{Q}'_g \Delta p\underline{q} \end{aligned} \qquad (D.18)$$

$$\begin{aligned} \Delta v_d^L &= L\Delta pi_d + \omega_o L\Delta i_q + Li_{qo}\underline{Q'_g}\Delta p\underline{q} \\ \Delta v_q^L &= L\Delta pi_q - \omega_o L\Delta i_d - Li_{do}\underline{Q'_g}\Delta p\underline{q} \end{aligned} \qquad (D.19)$$

$$\begin{aligned} \Delta v_d^b &= \sqrt{2}V_b\cos(\underline{Q'_g q_o})\underline{Q'_g}\ \underline{q} = -v_{qo}^b\underline{Q'_g}\Delta\underline{q} \\ \Delta v_q^b &= \sqrt{2}V_b\sin(\underline{Q'_g q_o})\underline{Q'_g}\ \underline{q} = v_{do}^b\underline{Q'_g}\Delta\underline{q} \end{aligned} \qquad (D.20)$$

APPENDIX E

MODE PARAMETER DETERMINATION FROM TRANSIENT DATA

This Appendix briefly describes how mode parameters are extracted from transient response data. This description considers systems with proportional damping; a more general analysis including non-proportional damping is contained in Refs [46,67].

The linear equations of motion of an n-degree of freedom system in matrix form (of which the rotational shaft system in Fig 2.5 is an example) can be written in generalized co-ordinates $b_1(t) \ldots b_n(t)$ as:

$$[J]p^2\underline{b}(t) + [D]p\underline{b}(t) + [K]\underline{b}(t) = \underline{f}(t) \qquad (E.1)$$

where p is the derivative operator d/dt. In order to determine the steady-state response due to sinusoidal excitation, let $\underline{f}(t) = \underline{F}e^{j\omega t}$ and seek a solution of the form:

$$\underline{b}(t) = \underline{B}e^{j\omega t}$$
$$p\underline{b}(t) = j\omega\underline{B}e^{j\omega t}$$
$$p^2\underline{b}(t) = -\omega^2\underline{B}e^{j\omega t}$$

where $\underline{F} = [F_1, \ldots, F_n]^T$ and $\underline{B} = [B_1, \ldots, B_n]^T$

Substituting these equations into eqn (E.1) yields

$$-\omega^2[J]\underline{B} + j\omega[D]\underline{B} + [K]\underline{B} = \underline{F} \qquad (E.2)$$

First consider the homogeneous undamped system described by

$$-\omega^2[J]\underline{B} + [K]\underline{B} = \underline{0} \tag{E.3}$$

This set of equations only has a solution if the determinant of the coefficient matrix is zero;

$$\det\{[K] - \omega^2[J]\} = 0$$

There is a set of 'n' eigenvalues (natural frequencies) $\nu_1^2, \ldots \nu_n^2$ (ν_i is used for the eigenvalues instead of ω_i in order to be consistent with the variable for mode frequency in Chapter Three) which yield a zero determinant. Associated with each eigenvalue ν_r^2 there is an eigenvector $\underline{Q}_r$ which is a solution to eqn (E.3). These eigenvectors have important orthogonality conditions which are shown in Sect 3.2 for proportional damping ($[D] = \alpha[J] + \beta[K]$) and are restated here for convenience:

$$\underline{Q}_j^T[J]\underline{Q}_i = \begin{cases} 0 & i \neq j \\ J_{Mi} & i = j \end{cases}$$

$$\underline{Q}_j^T[D]\underline{Q}_i = \begin{cases} 0 & i \neq j \\ D_{Mi} & i = j \end{cases} \tag{E.4}$$

$$\underline{Q}_j^T[K]\underline{Q}_i = \begin{cases} 0 & i \neq j \\ K_{Mi} & i = j \end{cases}$$

The 'n' eigenvectors form a linearly independent set of vectors in n-space and any vector in n-space can be expressed as a linear combination of these vectors. In particular, the solution $\underline{B}$ of the non-homogeneous equation (E.2) can be written as:

$$\underline{B} = \sum_{r=1}^{n} q_r \underline{Q}_r \tag{E.5}$$

Substituting eqn (E.5) into eqn (E.2) gives

$$-\omega^2[J]\sum_{r=1}^{n} q_r\underline{Q}_r + j\omega[D]\sum_{r=1}^{n} q_r\underline{Q}_r + [K]\sum_{r=1}^{n} q_r\underline{Q}_r = \underline{F} \qquad \text{(E.6)}$$

In order to determine a particular coefficient q_s, multiply eqn (E.6) by $\underline{Q}_s^T$ and use the orthogonality conditions in eqn (E.4) to obtain:

$$-\omega^2 q_s J_{Ms} + j\omega q_s D_{Ms} + q_s K_{Ms} = \underline{Q}_s^T\underline{F}$$

thus

$$q_s = \frac{\underline{Q}_s^T\underline{F}}{-\omega^2 J_{Ms} + j\omega D_{Ms} + K_{Ms}} \qquad \text{(E.7)}$$

Substituting eqn (E.7) into eqn (E.5) gives:

$$\underline{B} = \sum_{r=1}^{n} \frac{\underline{Q}_r^T\underline{F}\underline{Q}_r}{-\omega^2 J_{Mr} + j\omega D_{Mr} + K_{Mr}}$$

or writing the transfer function for one excitation point 'k' and one response point 'i'

$$H_{ik} = \frac{B_i}{F_k} = \sum_{r=1}^{n} \frac{Q_r^i Q_r^k}{J_{Mr}(-\omega^2 + j2\xi_r\nu_r\omega + \nu_r^2)} \qquad \text{(E.8)}$$

where $\nu_r^2 = K_{Mr}/J_{Mr}$ and $2\xi_r\nu_r = D_{Mr}/J_{Mr} = 2\sigma_r$

Now the complex representation of the transfer function can be derived as:

$$H_{ik} = \sum_{r=1}^{n} \frac{A_{ik}^r}{(s-s_r)} + \frac{A_{ik}^{r\,*}}{(s-s_r^*)} \qquad \text{(E.9)}$$

With $s = j\omega$ and $s_r = -\xi_r\nu_r + j\nu_r\sqrt{1-\xi_r^2}$ and noting that $A^* + A = 0$, (for a real mode the residues are imaginary), eqn (E.9) can be rewritten as

$$H_{ik} = \sum_{r=1}^{n} \frac{2|A_{ik}^{r}|\nu_r\sqrt{1-\xi_r^2}}{(-\omega^2 + j2\xi_r\nu_r\omega + \nu_r^2)} \qquad (E.10)$$

The process of mode parameter extraction thus involves taking a measured transfer function between a response signal 'i' (such as rotor angle) and a forcing function 'k' (such as a torque acting on the shaft) and curve fitting the transfer function to an equation such as eqn (E.9). (In the actual curve fitting process an 'inertial term' and 'residual flexibility' term are included to take into account the effect of modes which may be present outside the frequency band of interest [46]). This curve fitting process identifies for mode 'r', the complex pole s_r from which ν_r and ξ_r (and thus σ_r) are obtained and the complex residue A_{ik}^{r}. The mode shape $\underline{Q}_r$ is determined by the relative sizes of the residues of transfer functions from different response locations. (In actual fact, the mode shapes can be determined from the relative amplitudes of the residues of any row or column of the transfer function matrix [46]). The mode inertia (or mass) J_{Mr} is obtained from the magnitude of the residue as seen by comparing eqns (E.8) and (E.10):

$$J_{Mr} = \frac{Q_r^i Q_r^k}{2|A_{ik}^{r}|\nu_r\sqrt{1-\xi_r^2}} \qquad (E.11)$$

Equation (E.11) holds true for a displacement/force (or angle/torque) transfer function. It can be shown that for a speed/force (or speed/torque) and acceleration/force (or acceleration/torque) transfer function the mode inertia is given by eqns (E.12) and (E.13) respectively:

$$J_{Mr} = \frac{Q_r^i Q_r^k}{2|A_{ik}^{r}|\sqrt{1-\xi_r^2}} \qquad (E.12)$$

$$J_{Mr} = \frac{Q_r^i Q_r^k \nu_r}{2|A_{ik}^{r}|\sqrt{1-\xi_r^2}} \qquad (E.13)$$

This then shows how mode parameters can be obtained from transfer function data. It should be noted that only one set of parameters ξ_r (or σ_r), ν_r and A_{ik}^r can exist for a particular mode but the mode inertia, damping and stiffness are dependent on the scaling of the mode shape.

APPENDIX F

CORRECTION OF TRANSMISSION SYSTEM PARAMETER ERRORS

This appendix presents the equations used in Chapter Five to update the transmission system parameters. The process involves using the differences between calculated and measured values of system mode 0 frequency f_{s0}, electrical subsynchronous mode damping σ_s and electrical subsynchronous mode frequency f_s to correct errors in the transmission line parameters for a turbogenerator connected through a single transmission line to an infinite bus. The transmission line parameters are updated according to the equation:

$$\begin{bmatrix} \Delta\sigma_s \\ \Delta f_s \\ \Delta f_{s0} \end{bmatrix} = \begin{bmatrix} \partial\sigma_s/\partial R_e & \partial\sigma_s/\partial X_e & \partial\sigma_s/\partial X_c \\ \partial f_s/\partial R_e & \partial f_s/\partial X_e & \partial f_s/\partial X_c \\ \partial f_{s0}/\partial R_e & \partial f_{s0}/\partial X_e & \partial f_{s0}/\partial X_c \end{bmatrix} \begin{bmatrix} \Delta R_e \\ \Delta X_e \\ \Delta X_c \end{bmatrix} \qquad (F.1)$$

or

$$\Delta\underline{E} = [P]\Delta\underline{Z} \qquad (F.2)$$

where R_e is the total external circuit resistance (given by $R_1 + R_2$ in Fig 2.1) and X_e is the total external inductive reactance (given by $X_1 + X_2$ in Fig 2.1). The partial derivatives in [P] are obtained from equations which approximate the values σ_s, f_s, f_{s0} as described below and these approximations give acceptable results for this simple transmission system. For a more complex network configuration, the actual eigenvalue sensitivities [68,69] could be calculated.

σ_s - Electrical subsynchronous mode damping

The components of matrix [P] related to σ_s are derived from the expression for the real part of the eigenvalues of an RLC system:

$$\sigma_s = -R/(2L) = -\frac{\omega_o(R_e + R_a)}{2(X_e + X''_d)}$$

Partial differentiation of this equation yields for σ_s:

$$\frac{\partial\sigma_s}{\partial R_e} = -\frac{\omega_o}{2(X_e + X''_d)} \qquad (F.3)$$

$$\frac{\partial\sigma_s}{\partial X_e} = \frac{\omega_o(R_e + R_a)}{2(X_e + X''_d)^2} \qquad (F.4)$$

$$\frac{\partial\sigma_s}{\partial X_c} = 0 \qquad (F.5)$$

f_s - Electrical subsynchronous frequency

The components of matrix [P] related to f_s are determined by assuming that $f_s = 50 - f_r$ Hz where f_r is the resonant frequency of an RLC system given by:

$$f_r = \frac{\omega_o}{2\pi}\sqrt{\frac{X_c}{X_L} - \frac{R_L^2}{4X_L^2}}$$

where $R_L = R_e + R_a$ and $X_L = X_e + X''_d$

Partial differentiation of this equation leads to the following for f_s:

$$\frac{\partial f_s}{\partial R_e} = -\frac{\omega_o R_L}{4\pi X_L\sqrt{4X_L X_c - R_L^2}} \qquad (F.6)$$

$$\frac{\partial f_s}{\partial X_e} = -\frac{\omega_o(R_L^2 - 2X_L X_c)}{4\pi X_L^2\sqrt{4X_L X_c - R_L^2}} \tag{F.7}$$

$$\frac{\partial f_s}{\partial X_c} = \frac{\omega_o}{2\pi\sqrt{4X_L X_c - R_L^2}} \tag{F.8}$$

f_{s0} - System mode 0 frequency

Consider a modified generator where the generator terminals are 'extended' to the infinite bus; the modified machine parameters X_d, X_q and X_a are then related to the original parameters X_d^*, X_q^* and X_a^* by

$$X_d = X_d^* + X_e - X_c, \quad X_q = X_q^* + X_e - X_c, \quad X_a = X_a^* + X_e - X_c$$

The system mode 0 frequency is given by [11]

$$f_{s0} = (1/2\pi)\sqrt{K/J} \tag{F.9}$$

where J is the total inertia of the shaft and K is the synchronizing torque coefficient. If resistance is neglected then K can be defined [11] as the real part of $\partial T_e/\partial\delta$ such that:

$$K = \mathrm{Re}\left\{\frac{UU_o\cos\delta}{X_d} + U^2\cos^2\delta\left[\frac{1}{X_q(j\omega)} - \frac{1}{X_d}\right] + U^2\sin^2\delta\left[\frac{1}{X_d(j\omega)} - \frac{1}{X_q}\right]\right\} \tag{F.10}$$

where U is the infinite busbar voltage, U_o is the generator internal voltage and $X_d(j\omega)$, $X_q(j\omega)$ are the d- and q-axis operational inductive reactances defined below:

$$X_d(j\omega) = \frac{(1 + j\omega T_d')(1 + j\omega T_d'')}{(1 + j\omega T_{do}')(1 + j\omega T_{do}'')} X_d \tag{F.11}$$

$$X_q(j\omega) = \frac{(1 + j\omega T_q')(1 + j\omega T_q'')}{(1 + j\omega T_{qo}')(1 + j\omega T_{qo}'')} X_q \tag{F.12}$$

The real parts of the complex components of eqn (F.10) can be derived from eqns (F.11) and (F.12) as:

$$\mathrm{Re}\{1/(X_d(j\omega)\} = R_d/X_d \qquad \text{and} \qquad \mathrm{Re}\{1/(X_q(j\omega)\} = R_q/X_q$$

where

$$R_d = \frac{\mathrm{NUMd}}{\mathrm{DENd}} = \frac{(1 - \omega^2 T'_{do} T''_{do})(1 - \omega^2 T'_d T''_d) + \omega^2 (T'_{do} + T''_{do})(T'_d + T''_d)}{(1 + \omega^2 T'^2_d)(1 + \omega^2 T''^2_d)}$$

$$R_q = \frac{\mathrm{NUMq}}{\mathrm{DENq}} = \frac{(1 - \omega^2 T'_{qo} T''_{qo})(1 - \omega^2 T'_q T''_q) + \omega^2 (T'_{qo} + T''_{qo})(T'_q + T''_q)}{(1 + \omega^2 T'^2_q)(1 + \omega^2 T''^2_q)}$$

The elements of [P] related to f_{s0} can now be derived in terms of the equations given above. Since resistance effects on f_{s0} have been neglected:

$$\frac{\partial f_{s0}}{\partial R_e} = 0 \qquad \text{(F.13)}$$

Now for the X_e term:

$$\frac{\partial f_{s0}}{\partial X_e} = \frac{\partial f_{s0}}{\partial K} \frac{\partial K}{\partial X_e} \qquad \text{(F.14)}$$

where (from eqn (F.9))

$$\frac{\partial f_{s0}}{\partial K} = \frac{1}{4\pi\sqrt{JK}} \qquad \text{(F.15)}$$

and $\partial K/\partial X_e$ is derived from eqn (F.10) noting that

$$\frac{\partial X_d}{\partial X_e} = \frac{\partial X_q}{\partial X_e} = \frac{\partial X_a}{\partial X_e} = 1$$

Hence

$$\frac{\partial K}{\partial X_e} = \frac{\partial K}{\partial X_d} + \frac{\partial K}{\partial X_q} + \frac{\partial K}{\partial R_d}\frac{\partial R_d}{\partial T'_d}\frac{\partial T'_d}{\partial X_a} + \frac{\partial K}{\partial R_d}\frac{\partial R_d}{\partial T''_d}\frac{\partial T''_d}{\partial X_a} + \frac{\partial K}{\partial R_q}\frac{\partial R_q}{\partial T'_q}\frac{\partial T'_q}{\partial X_a}$$
$$+ \frac{\partial K}{\partial R_q}\frac{\partial R_q}{\partial T''_q}\frac{\partial T''_q}{\partial X_a} + \frac{\partial K}{\partial \delta}\frac{\partial \delta}{\partial X_q} + \frac{\partial K}{\partial U_o}\frac{\partial U_o}{\partial U_d}\frac{\partial U_d}{\partial X_q} + \frac{\partial K}{\partial U_o}\frac{\partial U_o}{\partial U_q}\frac{\partial U_q}{\partial X_d}$$
$$+ \frac{\partial K}{\partial U_o}\frac{\partial U_o}{\partial U_d}\frac{\partial U_d}{\partial \delta}\frac{\partial \delta}{\partial X_q} + \frac{\partial K}{\partial U_o}\frac{\partial U_o}{\partial U_q}\frac{\partial U_q}{\partial \delta}\frac{\partial \delta}{\partial X_q} \qquad \text{(F.16)}$$

The various components of eqn (F.16) are:

$$\frac{\partial K}{\partial X_d} = \frac{-UU_o\cos\delta + U^2\cos^2\delta - U^2\sin^2\delta R_d}{X_d^2} \qquad \text{(F.17)}$$

$$\frac{\partial K}{\partial X_q} = \frac{U^2\sin^2\delta - U^2\cos^2\delta R_q}{X_q^2} \qquad \text{(F.18)}$$

$$\partial K/\partial R_d = (U^2\sin^2\delta)/X_d \qquad \text{(F.19)}$$

$$\partial K/\partial R_q = (U^2\cos^2\delta)/X_q \qquad \text{(F.20)}$$

$$\frac{\partial R_d}{\partial T'_d} = \omega^2\frac{(-T''_d + \omega^2 T'_{do}T''_{do}T''_d + T'_{do} + T''_{do})DENd - NUMd(1 + \omega^2 T''^2_d)T'^2_d}{(DENd)^2} \qquad \text{(F.21)}$$

$$\frac{\partial R_d}{\partial T''_d} = \omega^2\frac{(-T'_d + \omega^2 T'_{do}T''_{do}T'_d + T'_{do} + T''_{do})DENd - NUMd(1 + \omega^2 T'^2_d)T''^2_d}{(DENd)^2} \qquad \text{(F.22)}$$

$$\frac{\partial R_q}{\partial T'_q} = \omega^2\frac{(-T''_q + \omega^2 T'_{qo}T''_{qo}T''_q + T'_{qo} + T''_{qo})DENq - NUMq(1 + \omega^2 T''^2_q)T'^2_q}{(DENq)^2} \qquad \text{(F.23)}$$

$$\frac{\partial R_q}{\partial T''_q} = \omega^2\frac{(-T'_q + \omega^2 T'_{qo}T''_{qo}T'_q + T'_{qo} + T''_{qo})DENq - NUMq(1 + \omega^2 T'^2_q)T''^2_q}{(DENq)^2} \qquad \text{(F.24)}$$

$$\frac{\partial T'_d}{\partial X_a} = \frac{(X'_d/X_a - 1)^2}{\omega_o R_f} \qquad (F.25)$$

$$\frac{\partial T'_q}{\partial X_a} = \frac{(X'_q/X_a - 1)^2}{\omega_o R_{kq1}} \qquad (F.26)$$

$$\frac{\partial T''_d}{\partial X_a} = \frac{(X''_d/X_a - 1)^2}{\omega_o R_{kd}} \qquad (F.27)$$

$$\frac{\partial T''_q}{\partial X_a} = \frac{(X''_q/X_a - 1)^2}{\omega_o R_{kq2}} \qquad (F.28)$$

$$\frac{\partial K}{\partial \delta} = -\frac{UU_o \sin\delta}{X_d} + U^2 \sin 2\delta \left[\frac{1 + R_d}{X_d} - \frac{1 + R_q}{X_q}\right] \qquad (F.29)$$

$$\partial K/\partial U_o = (U\cos\delta)/X_d \qquad (F.30)$$

The terms involving partial derivatives of the generator internal voltage U_o and the load angle δ are determined from the equations describing the steady-state phasor diagram of the generator. Neglecting resistance, the load angle can be derived from the steady-state phasor diagram as:

$$\delta = \arctan\{I_a X_q \cos\varphi/(U + I_a X_q \sin\varphi)\}$$

where φ is the angle between the infinite busbar voltage and the armature current. Also from the steady-state phasor diagram:

$$U_d = U\sin\delta - I_a X_q \cos(\delta+\varphi)$$

$$U_q = U\cos\delta + I_a X_d \sin(\delta+\varphi)$$

where $U_o^2 = U_d^2 + U_q^2$

Hence the rest of the terms in eqn (F.16) are as follows:

$$\frac{\partial\delta}{\partial X_q} = \frac{1}{1+\tan^2\delta}\left[\frac{UI_a\cos\varphi - I_a^2X_q\sin 2\varphi}{(U + I_aX_q\sin\varphi)^2}\right] \tag{F.31}$$

$$\partial U_o/\partial U_d = U_d/U_o \tag{F.32}$$

$$\partial U_o/\partial U_q = U_q/U_o \tag{F.33}$$

$$\partial U_d/\partial X_q = -I_a\cos(\delta+\varphi) = I_q \tag{F.34}$$

$$\partial U_q/\partial X_d = I_a\sin(\delta+\varphi) = -I_d \tag{F.35}$$

$$\partial U_d/\partial\delta = U\cos\delta - I_dX_q \tag{F.36}$$

$$\partial U_q/\partial\delta = -U\sin\delta - I_qX_d \tag{F.37}$$

The expression for $\partial f_{s0}/\partial X_e$ is thus obtained by combining eqns (F.14) through (F.37). Since partial derivatives involving X_e are related to those involving X_c by:

$$\frac{\partial X_d}{\partial X_c} = \frac{\partial X_q}{\partial X_c} = \frac{\partial X_a}{\partial X_c} = -1 = -\frac{\partial X_d}{\partial X_e} = -\frac{\partial X_q}{\partial X_e} = -\frac{\partial X_a}{\partial X_e}$$

it follows from an inspection of eqn (F.14) and (F.16) that

$$\partial f_{s0}/\partial X_c = -\partial f_{s0}/\partial X_e \tag{F.38}$$

The elements of matrix [P] in eqn (F.2) are now all defined and the change in the transmission system parameters can be obtained as:

$$\Delta\underline{Z} = [P]^{-1}\Delta\underline{E} \tag{F.39}$$

APPENDIX G

THE MULTI-GENERATOR SYSTEM EQUATIONS

This appendix presents the equations describing the multi-machine systems of Chapters Six and Seven. The method of analysis is based on an earlier [70] scheme which allowed the systematic modelling of generator dynamics as well as line transients and which was later extended [20,61,62] to include induction motors and to allow small-signal stability studies of the system to be performed. This multi-machine package [20] is further extended here to allow the modal representation of generator shaft dynamics as well as the inclusion of Shunt Reactor Stabilizers. Only the generator related equations are presented here since they are the ones affected by the modifications to the model and since induction motors are not dealt with in this thesis. The reader is referred to Refs [20] and [62] for detail concerning the induction motor modelling.

G.1 The Multi-Machine Form of the Mechanical Equations

To maintain the flexibility of the multi-machine program it is desirable to be able to represent any generator mechanical system in either physical or modal form. This means that the overall system would consist of a mixture of shaft representations and this is only possible if a single set of equations describing the mechanical system exists that holds for both modal and physical co-ordinates. This is attained by eqn (G.1) below (cf

eqn (C.27) for the physical representation and eqn (D.10) for the modal representation) which describes the motion of the mechanical system of a single generator having either a physical shaft representation with 'r' inertias or a modal shaft representation with 'r' modes defined at 'n' locations along the shaft:

$$\begin{bmatrix} -[A] & [0] \\ [0] & [I] \end{bmatrix} p \begin{bmatrix} p\underline{m} \\ \underline{m} \end{bmatrix} = \begin{bmatrix} [B] & [C] \\ [I] & [0] \end{bmatrix} \begin{bmatrix} p\underline{m} \\ \underline{m} \end{bmatrix} + \begin{bmatrix} [V]^T \underline{T}_e \\ \underline{0} \end{bmatrix} + \begin{bmatrix} [V]^T \underline{H}_m \\ \underline{0} \end{bmatrix} P_m \qquad (G.1)$$

where

$$\underline{H}_m = [H_{m1}, \ldots\ldots, H_{mn}]^T \qquad (G.2)$$

$$H_{mi} = \omega_o a_i / (\omega_o + \underline{V}_i p\underline{m}) \qquad (G.3)$$

$$\underline{T}_e = [0, \ldots, 0, T_e, 0, \ldots, 0]^T \qquad (G.4)$$

$\underline{m}$ = vector of mechanical angles (mode or physical)

P_m = total output power on shaft from all turbine stages

a_i = fraction of input power from location (inertia) 'i'

ω_o = system supply frequency

and $\underline{V}_i$ is row 'i' of matrix [V] defined below. For generator action the electrical torque T_e has positive numerical value while P_m has negative numerical value (as explained in Appendix A.1). The rest of the terms in eqn (G.1) are given below for a physical shaft representation as:

$[A] = [J]$ (see eqn (C.21))

$[B] = [D]$ (see eqn (C.22))

$[C] = [K]$ (see eqn (C.23))

$[V] = [I]$ (identity matrix)

$\underline{m} = \underline{\delta}$

and for a modal shaft representation as:

$$[A] = [J_M] \quad \text{(see eqn (D.2))}$$

$$[B] = [D_M] \quad \text{(see eqn (D.3))}$$

$$[C] = [K_M] \quad \text{(see eqn (D.4))}$$

$$[V] = [Q] \quad \text{(see eqn (D.5))}$$

$$\underline{m} = \underline{q}$$

The mechanical motion of each generator in the system is thus represented by a single equation regardless of its shaft representation. This equation (eqn (G.1)) can be expressed in a more compact form as

$$[M_A]p\underline{f}_m = [M_B]\underline{f}_m + \underline{M}_C + \underline{M}_D P_m \qquad \text{(G.5)}$$

where the matrices $[M_A]$, $[M_B]$ and the vectors $\underline{M}_C$, $\underline{M}_D$ and $\underline{f}_m$ are easily determined by comparison with eqn (G.1).

G.2 The Multi-Machine Form of the Generator Electrical Equations

G.2.1 Definition of generator vectors and matrices

The electrical vectors and matrices of the multi-machine model of the generator have been defined previously [20] and are repeated here for the sake of completeness. The generator model allows z-1 rotor circuit coils on each axis (d,q) and together with the stator circuit coils this results in 'z' coils on each axis.

The vectors of rotor flux linkages are defined as:

$$\underline{\psi}_{dr} = [\psi_{d2}, \psi_{d3}, \ldots\ldots, \psi_{dz}]^T$$

$$\underline{\psi}_{qr} = [\psi_{q2}, \psi_{q3}, \ldots\ldots, \psi_{qz}]^T$$

The vectors of rotor currents are defined as:

$$\underline{i}_{dr} = [i_{d2}, i_{d3}, \ldots\ldots, i_{dz}]^T$$
$$\underline{i}_{qr} = [i_{q2}, i_{q3}, \ldots\ldots, i_{qz}]^T$$

The inductance matrices and vectors:

$$\underline{M}_d = [L_{md}, \ldots\ldots, L_{md}]^T \qquad z-1 \text{ in number}$$
$$\underline{M}_q = [L_{mq}, \ldots\ldots, L_{mq}]^T \qquad z-1 \text{ in number}$$

$$[L_{dr}] = \begin{bmatrix} L_{22d} & L_{md} & \ldots\ldots & L_{md} \\ L_{md} & L_{33d} & \ldots\ldots & \cdot \\ \cdot & \cdot & & \cdot \\ \cdot & \cdot & & \cdot \\ L_{md} & L_{md} & \ldots\ldots & L_{zzd} \end{bmatrix}$$

where $L_{22d}, \ldots\ldots, L_{zzd}$ = total self inductance of d-axis winding
$= L_{jd} + L_{md}$ for $j = 2, \ldots\ldots, z$

L_{jd} = leakage inductance of the j'th d-axis winding

$$[L_{qr}] = \begin{bmatrix} L_{22q} & L_{mq} & \ldots\ldots & L_{mq} \\ L_{mq} & L_{33q} & \ldots\ldots & \cdot \\ \cdot & \cdot & & \cdot \\ \cdot & \cdot & & \cdot \\ L_{mq} & L_{mq} & \ldots\ldots & L_{zzq} \end{bmatrix}$$

where $L_{22q}, \ldots\ldots, L_{zzq}$ = total self inductance of d-axis winding
$= L_{jq} + L_{mq}$ for $j = 2, \ldots\ldots, z$

L_{jq} = leakage inductance of the j'th q-axis winding

L_d, L_q are the total self inductance of the stator windings

$$[R_{dr}] = \text{diag.}[R_{d2}, \ldots\ldots, R_{dz}]$$
$$[R_{qr}] = \text{diag.}[R_{q2}, \ldots\ldots, R_{qz}]$$

$$\underline{v}_{dr} = [v_{fd}, 0, \ldots\ldots, 0]^T$$

if the field winding is taken as the first of the rotor circuits.

G.2.2 The generator transient equivalent circuit

Based on the sign convention and per-unit system of Ref [11] (explained in Appendix A) the d,q axis stator flux linkages are given by the following equations:

$$\begin{aligned} \psi_d &= L_d i_d + \underline{M}_d^T \underline{i}_{dr} \\ \psi_q &= L_q i_q + \underline{M}_q^T \underline{i}_{qr} \end{aligned} \qquad \text{(G.6)}$$

and the d,q axis rotor flux linkages are given by:

$$\begin{aligned} \underline{\psi}_{dr} &= \underline{M}_d i_d + [L_{dr}]\underline{i}_{dr} \\ \underline{\psi}_{qr} &= \underline{M}_q i_q + [L_{qr}]\underline{i}_{qr} \end{aligned} \qquad \text{(G.7)}$$

The stator and rotor voltage equations in terms of the generator's own rotor reference frame are given by:

$$\begin{bmatrix} v_d \\ v_q \end{bmatrix} = p\begin{bmatrix} \psi_d \\ \psi_q \end{bmatrix} + R_a\begin{bmatrix} i_d \\ i_q \end{bmatrix} + (\omega_o + \underline{V}'_g p\underline{m})\begin{bmatrix} \psi_q \\ -\psi_d \end{bmatrix} \qquad \text{(G.8)}$$

$$\begin{bmatrix} \underline{v}_{dr} \\ \underline{0} \end{bmatrix} = p\begin{bmatrix} \underline{\psi}_{dr} \\ \underline{\psi}_{qr} \end{bmatrix} + \begin{bmatrix} [R_{dr}] & [0] \\ [0] & [R_{qr}] \end{bmatrix}\begin{bmatrix} \underline{i}_{dr} \\ \underline{i}_{qr} \end{bmatrix} \qquad \text{(G.9)}$$

where ω_o = system synchronous frequency
$\underline{m}$ = vector of mechanical angles (mode or physical)
$\underline{V}'_g$ = row 'g' of matrix [V] (defined in Appendix G.1)

Following minor manipulations to eqns (G.6) to (G.9) the d,q axis components of the generator terminal voltage may be obtained as follows:

$$\begin{bmatrix} v_d \\ v_q \end{bmatrix} = \begin{bmatrix} L_d^* & 0 \\ 0 & L_q^* \end{bmatrix} p \begin{bmatrix} i_d \\ i_q \end{bmatrix} + (\omega_o + \underline{V'_g pm}) \begin{bmatrix} 0 & L_q^* \\ -L_d^* & 0 \end{bmatrix} \begin{bmatrix} i_d \\ i_q \end{bmatrix} + R_a \begin{bmatrix} i_d \\ i_q \end{bmatrix} + \begin{bmatrix} b_d \\ b_q \end{bmatrix} \qquad (G.10)$$

where

$$\begin{aligned} L_d^* &= L_d - \underline{M}_d^T [L_{dr}]^{-1} \underline{M}_d \\ L_q^* &= L_q - \underline{M}_q^T [L_{qr}]^{-1} \underline{M}_q \end{aligned} \qquad (G.11)$$

$$\begin{bmatrix} b_d \\ b_q \end{bmatrix} = \begin{bmatrix} \underline{M}_d^T [L_{dr}]^{-1} & 0 \\ 0 & \underline{M}_q^T [L_{qr}]^{-1} \end{bmatrix} p \begin{bmatrix} \underline{\psi}_{dr} \\ \underline{\psi}_{qr} \end{bmatrix} + (\omega_o + \underline{V'_g pm}) \begin{bmatrix} 0 & \underline{M}_q^T [L_{qr}]^{-1} \\ -\underline{M}_d^T [L_{dr}]^{-1} & 0 \end{bmatrix} \begin{bmatrix} \underline{\psi}_{dr} \\ \underline{\psi}_{qr} \end{bmatrix} \qquad (G.12)$$

If a synchronously rotating reference frame (D,Q) is chosen for the network, the transformation of a generator's variables from its rotor reference frame (d,q) to the synchronous reference frame is carried out by the matrix [T] given by:

$$[T] = \begin{bmatrix} \cos(\underline{V'_g m}) & \sin(\underline{V'_g m}) \\ -\sin(\underline{V'_g m}) & \cos(\underline{V'_g m}) \end{bmatrix} \qquad (G.13)$$

Variables can similarly be transformed from the synchronous frame (D,Q) to the rotor frame (d,q) by the inverse transformation $[T]^{-1}$ which is easily obtained from eqn (G.13). Transforming the generator stator currents and their derivatives as well as the terminal voltage to the synchronous reference frame via eqn (G.13) result in eqns (G.10) to (G.12) becoming:

$$\begin{bmatrix} v_D \\ v_Q \end{bmatrix} = L_g^* p \begin{bmatrix} i_D \\ i_Q \end{bmatrix} + \omega_o L_g^* \begin{bmatrix} 0 & 1 \\ -1 & 0 \end{bmatrix} \begin{bmatrix} i_D \\ i_Q \end{bmatrix} + R_a \begin{bmatrix} i_D \\ i_Q \end{bmatrix} + \begin{bmatrix} b_D \\ b_Q \end{bmatrix} \qquad (G.14)$$

where

$$\begin{bmatrix} b_D \\ b_Q \end{bmatrix} = [T]\begin{bmatrix} b_d \\ b_q \end{bmatrix} + (L_d^*-L_q^*)/2\begin{bmatrix} \cos(2\underline{V'_g m}) & -\sin(2\underline{V'_g m}) \\ -\sin(2\underline{V'_g m}) & -\cos(2\underline{V'_g m}) \end{bmatrix} p\begin{bmatrix} i_D \\ i_Q \end{bmatrix}$$

$$+ (L_d^*-L_q^*)(\omega_o + 2\underline{V'_g p m})/2\begin{bmatrix} \sin(2\underline{V'_g m}) & \cos(2\underline{V'_g m}) \\ \cos(2\underline{V'_g m}) & -\sin(2\underline{V'_g m}) \end{bmatrix}\begin{bmatrix} i_D \\ i_Q \end{bmatrix} \qquad (G.15)$$

$$L_g^* = (L_d^* + L_q^*)/2$$

If i_D, i_Q, v_D, v_Q, b_D and b_Q are converted by the appropriate inverse Park's transform into instantaneous phase A quantities i_G, v_G and b as follows:

$$\begin{aligned} i_G &= i_D\cos\omega_o t + i_Q\sin\omega_o t \\ v_G &= v_D\cos\omega_o t + v_Q\sin\omega_o t \\ b &= b_D\cos\omega_o t + b_Q\sin\omega_o t \end{aligned} \qquad (G.16)$$

then the generator can be represented as an equivalent non-linear voltage source b in series with the stator phase resistance R_a and an equivalent inductance L_g^* as elements in an AC network (see Fig 6.3).

The electrical state variables of the generator are chosen as:

$$i_D,\ i_Q,\ \underline{\psi}_{dr},\ \underline{\psi}_{qr}$$

but i_D and i_Q are also states of the transmission network in a synchronously rotating reference frame as explained in Appendix G.3. The equations describing the rotor state variables $\underline{\psi}_{dr}$, $\underline{\psi}_{qr}$ are:

$$p\begin{bmatrix} \underline{\psi}_{dr} \\ \underline{\psi}_{qr} \end{bmatrix} = \begin{bmatrix} \underline{v}_{dr} \\ \underline{0} \end{bmatrix} - \begin{bmatrix} [R_{dr}][L_{dr}]^{-1} & [0] \\ [0] & [R_{qr}][L_{qr}]^{-1} \end{bmatrix}\begin{bmatrix} \underline{\psi}_{dr} \\ \underline{\psi}_{qr} \end{bmatrix}$$

$$+ \begin{bmatrix} [R_{dr}][L_{dr}]^{-1}\underline{M}_d & \underline{0} \\ \underline{0} & [R_{qr}][L_{qr}]^{-1}\underline{M}_q \end{bmatrix}[T]^{-1}\begin{bmatrix} i_D \\ i_Q \end{bmatrix} \qquad (G.17)$$

The electrical torque of the generator in terms of synchronous reference frame variables is given by:

$$T_e = \omega_o\{(L_d^* - L_q^*)(2i_D i_Q \cos(2\underline{V'_g m}) + (i_D^2 - i_Q^2)\sin(2\underline{V'_g m}))/2 + \underline{M}_d^T[L_{dr}]^{-1}\underline{\psi}_{dr}(i_D \sin(\underline{V'_g m}) + i_Q \cos(\underline{V'_g m})) - \underline{M}_q^T[L_{qr}]^{-1}\underline{\psi}_{qr}(i_D \cos(\underline{V'_g m}) - i_Q \sin(\underline{V'_g m}))\}/2 \qquad (G.18)$$

G.3 The Transmission Network

Methods of forming the state equations of linear time-invariant R-L-C networks in terms of ABC variables are well known and the terminology used here is that which normally applies to graph theory. Only balanced networks with fully transposed lines are considered so only a positive sequence representation of the network is necessary; furthermore, shunt capacitance of the line is neglected.

The generators are represented by their equivalent non-linear voltage sources b, in series with their stator phase resistances R_a and their equivalent inductances L_g^*, and are treated as part of the AC transmission network which can be represented by using graph theory [71,72]. A single infinite busbar is assumed to exist somewhere in the system and is represented as a voltage source.

The first stage in the development of the network state equations is the selection of a proper tree [20,71] such that all voltage sources (infinite busbar and generator b) and as many capacitors as possible are twig elements, and all controlled shunt reactances and as many other inductances as possible are link elements. The branch numbering order for the proper tree is as follows:

TWIGS	LINKS
1 Voltage sources	5 Capacitor links (excess)
2 Capacitor twigs	6 Resistor links
3 Resistor twigs	7 Inductor links
4 Inductor twigs (excess)	8 Controlled shunt reactors

The link cut-set submatrix [20,71] then has the following form:

$$[Q_l] = \begin{bmatrix} 0 & Q_{ER} & Q_{EL} & Q_{ES} \\ Q_{CC} & Q_{CR} & Q_{CL} & Q_{CS} \\ 0 & Q_{RR} & Q_{RL} & Q_{RS} \\ 0 & 0 & Q_{LL} & Q_{LS} \end{bmatrix} \tag{G.19}$$

The derivation of the state equations then follows the form in Ref [72] with the states of the system being the voltages across the twig capacitors, $\underline{v}_{Ct}$, the currents through the link inductors, $\underline{i}_{Ll}$ and the controlled shunt reactor currents $\underline{i}_S$. The result is:

$$\begin{bmatrix} [C] & 0 & 0 \\ 0 & [L] & [L_S] \\ 0 & [S_L] & [S] \end{bmatrix} p \begin{bmatrix} \underline{v}_{Ct} \\ \underline{i}_{Ll} \\ \underline{i}_S \end{bmatrix} = \begin{bmatrix} [Y] & [H_L] & [H_S] \\ [G_L] & [Z_L] & [L_Z] \\ [G_S] & [S_Z] & [Z_S] \end{bmatrix} \begin{bmatrix} \underline{v}_{Ct} \\ \underline{i}_{Ll} \\ \underline{i}_S \end{bmatrix} + \begin{bmatrix} [\hat{Y}] \\ [\hat{G}_L] \\ [\hat{G}_S] \end{bmatrix} \underline{v}_E$$

$$- \begin{bmatrix} 0 & 0 & 0 \\ 0 & 0 & 0 \\ 0 & 0 & p[L_s] \end{bmatrix} \begin{bmatrix} \underline{v}_{Ct} \\ \underline{i}_{Ll} \\ \underline{i}_S \end{bmatrix} \tag{G.20}$$

where

$$[C] = [C_t] + [Q_{CC}][C_l][Q_{CC}]^T$$

$$[L] = [L_l] + [Q_{LL}]^T[L_t][Q_{LL}]$$

$$[S] = [L_s] + [Q_{LS}]^T[L_t][Q_{LS}]$$

$$[L_S] = [S_L]^T = [Q_{LL}]^T[L_t][Q_{LS}]$$

$$[Y] = -[Q_{CR}][\tilde{R}]^{-1}[Q_{CR}]^T$$

$$[H_L] = -[Q_{CL}] + [Q_{CR}][\tilde{R}]^{-1}[Q_{RR}]^T[R_t][Q_{RL}]$$

$$[H_S] = -[Q_{CS}] + [Q_{CR}][\tilde{R}]^{-1}[Q_{RR}]^T[R_t][Q_{RS}]$$

$$[G_L] = -[H_L]^T$$

$$[G_S] = -[H_S]^T$$

$$[Z_L] = -[Q_{RL}]^T[\tilde{G}]^{-1}[Q_{RL}]$$
$$[Z_S] = -[Q_{RS}]^T[\tilde{G}]^{-1}[Q_{RS}]$$
$$[L_Z] = [S_Z]^T = -[Q_{RL}]^T[\tilde{G}]^{-1}[Q_{RS}]$$
$$[\hat{Y}] = -[Q_{CR}][\tilde{R}]^{-1}[Q_{ER}]^T$$
$$[\hat{G}_L] = [Q_{EL}]^T - [Q_{RL}]^T[\tilde{G}]^{-1}[Q_{RR}][G_1][Q_{ER}]^T$$
$$[\hat{G}_S] = [Q_{ES}]^T - [Q_{RS}]^T[\tilde{G}]^{-1}[Q_{RR}][G_1][Q_{ES}]^T$$

and

$$[\tilde{R}] = [R_1] + [Q_{RR}]^T[R_t][Q_{RR}]$$
$$[\tilde{G}] = [G_t] + [Q_{RR}][G_1][Q_{RR}]^T$$
$$[G_1] = [R_1]^{-1}$$
$$[G_t] = [R_t]^{-1}$$

The following components are diagonal with the relative twig or link components on the diagonal:

$$[R_1], [L_1], [C_1], [R_t], [L_t], [C_t]$$

$[L_s]$ is a diagonal matrix of controlled shunt reactor inductances and $p[L_s]$ is given by eqn (G.33). On application of the Park's transformation to the network equations and defining the following vectors:

$$\underline{v}_{ED} = [v_{bD}, \underline{b}_D^T]^T$$
$$\underline{v}_{EQ} = [v_{bQ}, \underline{b}_Q^T]^T$$
$$\underline{i}_{L1D} = [\underline{i}_{ED}^T, \underline{i}_D^T]^T$$
$$\underline{i}_{L1Q} = [\underline{i}_{EQ}^T, \underline{i}_Q^T]^T$$

where v_{bD}, v_{bQ} are the D,Q axis components of the infinite busbar voltage, $\underline{b}_D$, $\underline{b}_Q$, $\underline{i}_D$, $\underline{i}_Q$ are vectors of generator axis voltages and currents (defined in Appendix G.5), and $\underline{i}_{ED}$, $\underline{i}_{EQ}$ are non-generator link inductor currents, eqn (G.20) becomes for the d,q axis components of the network states:

$$
\begin{aligned}
[C]p\underline{v}_{CtD} &= [Y]\underline{v}_{CtD} + [H_L]\underline{i}_{L1D} + [H_S]\underline{i}_{SD} - \omega_o[C]\underline{v}_{CtQ} + [\hat{Y}]\underline{v}_{ED} \\
[C]p\underline{v}_{CtQ} &= [Y]\underline{v}_{CtQ} + [H_L]\underline{i}_{L1Q} + [H_S]\underline{i}_{SQ} + \omega_o[C]\underline{v}_{CtD} + [\hat{Y}]\underline{v}_{EQ}
\end{aligned} \tag{G.21}
$$

$$
\begin{aligned}
[L]p\underline{i}_{L1D} + [L_S]p\underline{i}_{SD} &= [G_L]\underline{v}_{CtD} + [Z_L]\underline{i}_{L1D} + [L_Z]\underline{i}_{SD} + [\hat{G}_L]\underline{v}_{ED} \\
&\quad - \omega_o[L]\underline{i}_{L1Q} - \omega_o[L_S]\underline{i}_{SQ} \\
[L]p\underline{i}_{L1Q} + [L_S]p\underline{i}_{SQ} &= [G_L]\underline{v}_{CtQ} + [Z_L]\underline{i}_{L1Q} + [L_Z]\underline{i}_{SQ} + [\hat{G}_L]\underline{v}_{EQ} \\
&\quad + \omega_o[L]\underline{i}_{L1D} + \omega_o[L_S]\underline{i}_{SD}
\end{aligned} \tag{G.22}
$$

$$
\begin{aligned}
[S_L]p\underline{i}_{L1D} + [S]p\underline{i}_{SD} &= [G_S]\underline{v}_{CtD} + [S_Z]\underline{i}_{L1D} + [Z_S]\underline{i}_{SD} + [\hat{G}_S]\underline{v}_{ED} \\
&\quad - \omega_o[S_L]\underline{i}_{L1Q} - \omega_o[S]\underline{i}_{SQ} - p[L_s]\underline{i}_{SD} \\
[S_L]p\underline{i}_{L1Q} + [S]p\underline{i}_{SQ} &= [G_S]\underline{v}_{CtQ} + [S_Z]\underline{i}_{L1Q} + [Z_S]\underline{i}_{SQ} + [\hat{G}_S]\underline{v}_{EQ} \\
&\quad + \omega_o[S_L]\underline{i}_{L1D} + \omega_o[S]\underline{i}_{SD} - p[L_s]\underline{i}_{SQ}
\end{aligned} \tag{G.23}
$$

G.4 The Shunt Reactor Controller

The modulated inductance L_s of a controlled shunt reactor in the network (shown as X_3 in Fig 7.29 in the main text) is assumed to be given by [20,53]:

$$L_s = L_{sn}(1 + U_L) \tag{G.24}$$

where L_{sn} is the nominal value of the shunt inductance and U_L is the output of the shunt reactor controller. Each shunt reactor can have a controller of order 'k' and the input to each controller can be the sum of 'u' generator speed signals. This facilitates the modelling of a single controlled shunt reactor at a power station which damps out SSR oscillations in multiple adjacent units. The state space representation of the controller is as follows:

$$
\begin{aligned}
p\underline{z} &= [A_c]\underline{z} + [B_c]\underline{u}_c \\
U_L &= \underline{C}_c^T\underline{z} + \underline{D}_c^T\underline{u}_c
\end{aligned} \tag{G.25}
$$

where the input vector $\underline{u}_c$ of generator speeds is given by

$$\underline{u}_c = [w]\underline{F}_m \tag{G.26}$$

$\underline{F}_m$ is a composite vector of all mechanical states (see Appendix G.1) and [w] is a matrix which selects the relevant generator mechanical states as inputs to the controller. Row 'i' of [w] is zero except at the column locations corresponding to the mechanical speeds (mode or physical) of the generator whose speed signal constitutes u_i; at these positions $\underline{V}'_g$ for the relevant generator appears.

According to eqns (G.24) to (G.26) the modulated value of a shunt inductance is obtained as

$$L_s = L_{sn}(1 + \underline{C}_c^T\underline{z} + \underline{D}_c^T[w]\underline{F}_m) \tag{G.27}$$

An equation describing the time rate of change of the inductance is required for the network equations and this is obtained from eqn (G.27) as

$$pL_s = L_{sn}(\underline{C}_c^T p\underline{z} + \underline{D}_c^T[w]p\underline{F}_m) \tag{G.28}$$

G.5 Full Network Equations

Appendices G.1 and G.2 described the multi-machine form of the mechanical and electrical equations for a single generator, while Appendix G.4 described the equations for a single controlled shunt reactor; this section describes the full network equations for a system with one infinite busbar, 'm' generators and 's' controlled shunt reactors.

Mechanical equations

Define the following set of composite vectors in terms of previously defined symbols (Appendix G.1) where the added subscript represents the generator number:

$$[F_A] = \text{block diag.}\{ [M_{Ak}] \} \qquad k = 1, \ldots\ldots, m$$

$$[F_B] = \text{block diag.}\{ [M_{Bk}] \} \qquad k = 1, \ldots\ldots, m$$

$$\underline{F}_C = [\, \underline{M}_{C1}^T, \ldots\ldots, \underline{M}_{Cm}^T \,]^T$$

$$[F_D] = \text{block diag.}\{ \underline{M}_{Dk} \} \qquad k = 1, \ldots\ldots, m$$

$$\underline{F}_m = [\, \underline{f}_{m1}^T, \ldots\ldots, \underline{f}_{mm}^T \,]^T$$

$$\underline{P}_m = [P_{m1}, \ldots\ldots, P_{mm}]^T$$

where block diag. { X } is a partitioned matrix with elements X (either matrices or vectors). Using the above definitions eqn (G.5) can be expressed for a system of 'm' generators as:

$$[F_A]p\underline{F}_m = [F_B]\underline{F}_m + \underline{F}_C + [F_D]\underline{P}_m \qquad \text{(G.29)}$$

where the representation of generator shaft dynamics in physical or modal form is arbitrarily mixed.

Generator electrical equations

The following set of composite vectors is defined in terms of previously defined symbols (Appendix G.2) where the added subscript represents the generator number:

$$[p\underline{\psi}_{dr}] = [p\underline{\psi}_{dr1}^T, \ldots\ldots, p\underline{\psi}_{drm}^T]^T$$

$$[p\underline{\psi}_{qr}] = [p\underline{\psi}_{qr1}^T, \ldots\ldots, p\underline{\psi}_{qrm}^T]^T$$

$$[\underline{\psi}_{dr}] = [\underline{\psi}_{dr1}^T, \ldots\ldots, \underline{\psi}_{drm}^T]^T$$

$$[\underline{\psi}_{qr}] = [\underline{\psi}_{qr1}^T, \ldots\ldots, \underline{\psi}_{qrm}^T]^T$$

$$\underline{i}_D = [i_{D1}, \ldots\ldots, i_{Dm}]^T$$

$$\underline{i}_Q = [i_{Q1}, \ldots\ldots, i_{Qm}]^T$$

$$\underline{b}_D = [b_{D1}, \ldots\ldots, b_{Dm}]^T$$

$$\underline{b}_Q = [b_{Q1}, \ldots\ldots, b_{Qm}]^T$$

The following set of partitioned matrices is defined:

$$[S_A] = \text{block diag.}\{\ [R_{drk}][L_{drk}]^{-1}\ \} \qquad k=1,\ \ldots,\ m$$

$$[S_B] = \text{block diag.}\{\ [R_{drk}][L_{drk}]^{-1}\underline{M}_{dk}\cos(\underline{V}'_{gk}\underline{m}_k)\ \}$$

$$[S_C] = \text{block diag.}\{\ [R_{drk}][L_{drk}]^{-1}\underline{M}_{dk}\sin(\underline{V}'_{gk}\underline{m}_k)\ \}$$

$$[S_D] = \text{block diag.}\{\ [R_{qrk}][L_{qrk}]^{-1}\ \}$$

$$[S_E] = \text{block diag.}\{\ [R_{qrk}][L_{qrk}]^{-1}\underline{M}_{qk}\cos(\underline{V}'_{gk}\underline{m}_k)\ \}$$

$$[S_F] = \text{block diag.}\{\ [R_{qrk}][L_{qrk}]^{-1}\underline{M}_{qk}\sin(\underline{V}'_{gk}\underline{m}_k)\ \}$$

where $\underline{V}'_{gk}\underline{m}_k$ is the load angle of generator 'k'. Using the above definitions and placing the rotor state equations in multi-machine form, eqn (G.17) becomes:

$$\begin{aligned}[p\underline{\psi}_{dr}] &= -[S_A][\underline{\psi}_{dr}] + [S_B]\underline{i}_D - [S_C]\underline{i}_Q + [N][\underline{v}_{dr}] \\ [p\underline{\psi}_{qr}] &= -[S_D][\underline{\psi}_{qr}] + [S_E]\underline{i}_D + [S_F]\underline{i}_Q\end{aligned} \qquad \text{(G.30)}$$

where

$$[\underline{v}_{dr}] = [\ \underline{v}^T_{dr1},\ \ldots\ldots,\ \underline{v}^T_{drm}\ ]^T$$

= voltage inputs to rotor d-axis

$$[N] = \begin{bmatrix} 1,\ 0,\ \ldots\ldots,\ 0 & & \\ & \ddots & \\ & & 1,\ 0,\ \ldots\ldots,\ 0 \end{bmatrix}$$

The equivalent circuit voltage sources of the generators, given by eqn (G.15) are retained as elements of the input vector $\underline{v}_E$ in eqns (G.21) to (G.23) and are recalculated at each integration step. The generator stator currents are obtained from the network state equations.

Network equations

The network equations for the complete system are given by eqns (G.21) to (G.23).

Shunt reactor controller equations

Define the following matrices and vectors in terms of previously defined variables (Appendix G.4) where the added subscript refers to shunt reactor number:

$$\underline{Z} = [\ \underline{z}_1^T, \ldots\ldots, \underline{z}_s^T\ ]^T$$

$$[L_s] = \text{diag.}[L_{si}] \qquad i = 1, \ldots, s$$

$$[L_{sn}] = \text{diag.}[L_{sni}] \qquad i = 1, \ldots, s$$

$$[E_A] = \text{block diag.}\{\ [A_{ci}]\ \} \qquad i = 1, \ldots, s$$

$$[E_B] = \text{block diag.}\{\ [B_{ci}]\ \} \qquad i = 1, \ldots, s$$

$$[E_C] = \text{block diag.}\{\ \underline{C}_{ci}^T\ \} \qquad i = 1, \ldots, s$$

$$[E_D] = \text{block diag.}\{\ \underline{D}_{ci}^T\ \} \qquad i = 1, \ldots, s$$

$$[W] = \{\ [w_1]^T, \ldots\ldots, [w_s]^T\ \}^T$$

In terms of the above definitions, eqn (G.25) for the shunt reactor controller states, eqn (G.27) for the modulated shunt inductance and eqn (G.28) for the rate of change of inductance become:

$$p\underline{Z} = [E_A]\underline{Z} + [E_B][W]\underline{F}_m \qquad \text{(G.31)}$$

$$[L_s] = [L_{sn}]\{[I] + [E_C]\underline{Z} + [D_C][W]\underline{F}_m\} \qquad \text{(G.32)}$$

$$p[L_s] = [L_{sn}]\{[E_C]p\underline{Z} + [D_C][W]p\underline{F}_m\} \qquad \text{(G.33)}$$

The complete state equations of the power system can now be assembled from eqns (G.21) to (G.23) and eqns (G.29) to (G.33).

APPENDIX H

THE LINEARIZED MULTI-GENERATOR SYSTEM EQUATIONS

This appendix presents the linearized form of the multi-machine system equations used to carry out the small-signal stability studies in Chapters Six and Seven. The subscript 'o' denotes the steady-state value of a variable.

H.1 The Mechanical Equations

The motion of the multi-inertia mechanical system of a single generator is described by eqn (G.1) where the mechanical system can be modelled in either physical or modal co-ordinates. Linearization of this equation leads to:

$$\begin{bmatrix} -[A] & [0] \\ [0] & [I] \end{bmatrix} \Delta p \begin{bmatrix} \underline{pm} \\ \underline{m} \end{bmatrix} = \begin{bmatrix} [B]+[H_e] & [C] \\ [I] & [0] \end{bmatrix} \Delta \begin{bmatrix} \underline{pm} \\ \underline{m} \end{bmatrix} + \begin{bmatrix} [V]^T \Delta \underline{T}_e \\ \underline{0} \end{bmatrix} \qquad (H.1)$$

where $[H_e] = [V]^T[F_e][V]$ (H.2)

$[F_e]$ is defined by eqn (C.30) and P_m is assumed to be constant (no governor action).

The linearized electrical torque of a single generator is obtained from eqn (G.18) as:

$$\begin{aligned}\Delta T_e = \{&((i_{Do}^2 - i_{Qo}^2)(L_d^* - L_q^*)\cos(2\underline{V'm}_o) - 2i_{Do}i_{Qo}(L_d^* - L_q^*)\sin(2\underline{V'm}_o) + \\ &\underline{M}_d^T[L_{dr}]^{-1}\underline{\psi}_{dro}(i_{Do}\cos(\underline{V'm}_o) - i_{Qo}\sin(\underline{V'm}_o)) + \\ &\underline{M}_q^T[L_{qr}]^{-1}\underline{\psi}_{qro}(i_{Do}\sin(\underline{V'm}_o) + i_{Qo}\cos(\underline{V'm}_o)))\underline{V'}_g\underline{\Delta m} \\ + &(i_{Do}(L_d^* - L_q^*)\sin(2\underline{V'm}_o) + i_{Qo}(L_d^* - L_q^*)\cos(2\underline{V'm}_o) + \\ &\underline{M}_d^T[L_{dr}]^{-1}\underline{\psi}_{dro}\sin(\underline{V'm}_o) - \underline{M}_q^T[L_{qr}]^{-1}\underline{\psi}_{qro}\cos(\underline{V'm}_o))\,\Delta i_D \\ + &(-i_{Qo}(L_d^* - L_q^*)\sin(2\underline{V'm}_o) + i_{Do}(L_d^* - L_q^*)\cos(2\underline{V'm}_o) + \\ &\underline{M}_d^T[L_{dr}]^{-1}\underline{\psi}_{dro}\cos(\underline{V'm}_o) + \underline{M}_q^T[L_{qr}]^{-1}\underline{\psi}_{qro}\sin(\underline{V'm}_o))\,\Delta i_Q \\ + &\underline{M}_d^T[L_{dr}]^{-1}(i_{Do}\sin(\underline{V'm}_o) + i_{Qo}\cos(\underline{V'm}_o))\,\Delta\underline{\psi}_{dr} \\ - &\underline{M}_q^T[L_{qr}]^{-1}(i_{Do}\cos(\underline{V'm}_o) - i_{Qo}\sin(\underline{V'm}_o))\,\Delta\underline{\psi}_{qr} \end{aligned} \qquad \text{(H.3)}$$

The multi-machine form of the linearized mechanical equations can now be constructed by following the same procedures as in Appendix G.

H.2 The Generator Electrical Equations

The rotor flux linkages are state variables of the system and are described for a single generator by eqn (G.17). Linearization of this equation leads to:

$$\begin{aligned}\Delta p\underline{\psi}_{dr} = -[R_{dr}][L_{dr}]^{-1}\{&\Delta\underline{\psi}_{dr} - \underline{M}_d\cos(\underline{V'm}_o)\Delta i_D + \underline{M}_d\sin(\underline{V'm}_o)\Delta i_Q \\ &+ (\underline{M}_d i_{Do}\sin(\underline{V'm}_o) + \underline{M}_d i_{Qo}\cos(\underline{V'm}_o))\underline{V'}_g\underline{\Delta m}\} + \Delta\underline{v}_{dr} \\ \Delta p\underline{\psi}_{qr} = -[R_{qr}][L_{qr}]^{-1}\{&\Delta\underline{\psi}_{qr} - \underline{M}_q\sin(\underline{V'm}_o)\Delta i_D - \underline{M}_q\cos(\underline{V'm}_o)\Delta i_Q \\ &- (\underline{M}_q i_{Do}\cos(\underline{V'm}_o) - \underline{M}_q i_{Qo}\sin(\underline{V'm}_o))\underline{V'}_g\underline{\Delta m}\}\end{aligned} \qquad \text{(H.4)}$$

The multi-machine form of the linearized rotor flux linkage equations can be written as:

$$\begin{aligned}\Delta[p\underline{\psi}_{dr}] &= -[S_A]\Delta[\underline{\psi}_{dr}] + [S_{Bo}]\Delta\underline{i}_D - [S_{Co}]\Delta\underline{i}_Q + [S_{Go}][\tilde{V}]\Delta\underline{F}_m \\ &\quad + [N]\Delta[\underline{v}_{dr}] \\ \Delta[p\underline{\psi}_{qr}] &= -[S_D]\Delta[\underline{\psi}_{qr}] + [S_{Eo}]\Delta\underline{i}_D + [S_{Fo}]\Delta\underline{i}_Q + [S_{Ho}][\tilde{V}]\Delta\underline{F}_m\end{aligned} \tag{H.5}$$

where

$$[S_{Go}] = \text{block diag.}\{[R_{drk}][L_{drk}]^{-1}\underline{M}_{drk}(-i_{Dko}\sin(\underline{V}'_{gk}\underline{m}_{ko}) - i_{Qko}\cos(\underline{V}'_{gk}\underline{m}_{ko}))\}$$

$$[S_{Ho}] = \text{block diag.}\{[R_{qrk}][L_{qrk}]^{-1}\underline{M}_{qrk}(i_{Dko}\cos(\underline{V}'_{gk}\underline{m}_{ko}) - i_{Qko}\sin(\underline{V}'_{gk}\underline{m}_{ko}))\}$$

$$[\tilde{V}] = \text{block diag.}\{\ [\underline{V}'_{gk},\ \underline{0}^T]\ \}$$

and $k=1, \ldots\ldots, m$

The generator d,q axis stator currents are also state variables but they are included as states of the transmission network.

H.3 The Transmission Network

The two-axis equations of the transmission network are stated in eqns (G.21) to (G.23). Eqn (G.23) is non-linear due to the presence of the variable inductance matrices [S] and $[L_s]$ while all three equations contain the non-linear generator equivalent voltage sources $\underline{b}_D$ and $\underline{b}_Q$ as elements of the input vectors $\underline{v}_{ED}$ and $\underline{v}_{EQ}$ respectively. The linearized form of eqn (G.23) is obtained as:

$$\begin{aligned}[S_L]\Delta p\underline{i}_{L1D} + [S_o]\Delta p\underline{i}_{SD} &= [G_S]\Delta\underline{v}_{CtD} + [S_Z]\Delta\underline{i}_{L1D} + [Z_S]\Delta\underline{i}_{SD} \\ &\quad + [\hat{G}_S]\Delta\underline{v}_{ED} - \omega_o[S_L]\Delta\underline{i}_{L1Q} - \omega_o[S_o]\Delta\underline{i}_{SQ} \\ &\quad - \omega_o\underline{i}_{SQo}\Delta[L_s] - \underline{i}_{SDo}\Delta p[L_s] \\ [S_L]\Delta p\underline{i}_{L1Q} + [S_o]\Delta p\underline{i}_{SQ} &= [G_S]\Delta\underline{v}_{CtQ} + [S_Z]\Delta\underline{i}_{L1Q} + [Z_S]\Delta\underline{i}_{SQ} \\ &\quad + [\hat{G}_S]\Delta\underline{v}_{EQ} + \omega_o[S_L]\Delta\underline{i}_{L1D} + \omega_o[S_o]\Delta\underline{i}_{SD} \\ &\quad + \omega_o\underline{i}_{SDo}\Delta[L_s] - \underline{i}_{SQo}\Delta p[L_s]\end{aligned} \tag{H.6}$$

where $\Delta[L_s]$ and $\Delta p[L_s]$ are given by eqns (H.10) and (H.11) respectively.

All that is required to complete the linearized network equations is the linearized form of the generator voltages $\underline{b}_D$ and $\underline{b}_Q$. These are obtained for a single generator from the linearization of eqns (G.12), (G.13) and (G.15) as:

$$\begin{aligned}
\Delta b_D = {} & \underline{M}_d^T[L_{dr}]^{-1}\cos(\underline{V'm}_o)\Delta p\underline{\psi}_{dr} + \underline{M}_q^T[L_{qr}]^{-1}\sin(\underline{V'm}_o)\Delta p\underline{\psi}_{qr} \\
& + \underline{M}_q^T[L_{qr}]^{-1}\omega_o\cos(\underline{V'm}_o)\Delta\underline{\psi}_{qr} - \underline{M}_d^T[L_{dr}]^{-1}\omega_o\sin(\underline{V'm}_o)\Delta\underline{\psi}_{dr} \\
& + L_y^*\cos(2\underline{V'm}_o)\Delta pi_D - L_y^*\sin(2\underline{V'm}_o)\Delta pi_Q \\
& - L_y^*\omega_o\sin(2\underline{V'm}_o)\Delta i_D - L_y^*\omega_o\cos(2\underline{V'm}_o)\Delta i_Q \\
& - \{\underline{M}_q^T[L_{qr}]^{-1}\omega_o\sin(\underline{V'm}_o)\underline{\psi}_{qro} + \underline{M}_d^T[L_{dr}]^{-1}\omega_o\cos(\underline{V'm}_o)\underline{\psi}_{dro} + \\
& \quad 2L_y^*\omega_o\cos(2\underline{V'm}_o)i_{Do} - 2L_y^*\omega_o\sin(2\underline{V'm}_o)i_{Qo}\}\underline{V'}_g\Delta\underline{m} \\
& + \{\underline{M}_q^T[L_{qr}]^{-1}\cos(\underline{V'm}_o)\underline{\psi}_{qro} - \underline{M}_d^T[L_{dr}]^{-1}\sin(\underline{V'm}_o)\underline{\psi}_{dro} - \\
& \quad 2L_y^*\sin(2\underline{V'm}_o)i_{Do} - 2L_y^*\cos(2\underline{V'm}_o)i_{Qo}\}\underline{V'}_g\Delta p\underline{m}
\end{aligned} \tag{H.7}$$

$$\begin{aligned}
\Delta b_Q = {} & -\underline{M}_d^T[L_{dr}]^{-1}\sin(\underline{V'm}_o)\Delta p\underline{\psi}_{dr} + \underline{M}_q^T[L_{qr}]^{-1}\cos(\underline{V'm}_o)\Delta p\underline{\psi}_{qr} \\
& - \underline{M}_q^T[L_{qr}]^{-1}\omega_o\sin(\underline{V'm}_o)\Delta\underline{\psi}_{qr} - \underline{M}_d^T[L_{dr}]^{-1}\omega_o\cos(\underline{V'm}_o)\Delta\underline{\psi}_{dr} \\
& - L_y^*\sin(2\underline{V'm}_o)\Delta pi_D - L_y^*\cos(2\underline{V'm}_o)\Delta pi_Q \\
& - L_y^*\omega_o\cos(2\underline{V'm}_o)\Delta i_D + L_y^*\omega_o\sin(2\underline{V'm}_o)\Delta i_Q \\
& - \{\underline{M}_q^T[L_{qr}]^{-1}\omega_o\cos(\underline{V'm}_o)\underline{\psi}_{qro} - \underline{M}_d^T[L_{dr}]^{-1}\omega_o\sin(\underline{V'm}_o)\underline{\psi}_{dro} - \\
& \quad 2L_y^*\omega_o\sin(2\underline{V'm}_o)i_{Do} - 2L_y^*\omega_o\cos(2\underline{V'm}_o)i_{Qo}\}\underline{V'}_g\Delta\underline{m} \\
& - \{\underline{M}_q^T[L_{qr}]^{-1}\sin(\underline{V'm}_o)\underline{\psi}_{qro} + \underline{M}_d^T[L_{dr}]^{-1}\cos(\underline{V'm}_o)\underline{\psi}_{dro} + \\
& \quad 2L_y^*\cos(2\underline{V'm}_o)i_{Do} - 2L_y^*\sin(2\underline{V'm}_o)i_{Qo}\}\underline{V'}_g\Delta p\underline{m}
\end{aligned} \tag{H.8}$$

where

$$L_y^* = (L_d^* - L_q^*)/2$$

The multi-machine form of eqns (H.7) and (H.8) can now be assembled to give $\underline{b}_D$ and $\underline{b}_Q$.

H.4 The Shunt Reactor Controller

The multi-machine form of the shunt reactor controller equation is given by eqn (G.31) while the modulation of the shunt inductances is described by eqns (G.32) and (G.33). Linearization of these equations leads to the following:

$$\Delta p\underline{Z} = [E_A]\Delta\underline{Z} + [E_B][W]\Delta\underline{F}_m \tag{H.9}$$

$$\Delta[L_s] = [L_{sn}]\{[E_C]\Delta\underline{Z} + [D_C][W]\Delta\underline{F}_m\} \tag{H.10}$$

$$\Delta p[L_s] = [L_{sn}]\{[E_C]\Delta p\underline{Z} + [D_C][W]\Delta p\underline{F}_m\} \tag{H.11}$$

These equations complete the linearized description of the complete power system and the full linearized system equations can now be assembled in the form:

$$[P']\Delta p\underline{x} = [E']\Delta\underline{x} + [S']\Delta\underline{u} \tag{H.12}$$

The eigenvalues of the system are then determined from the system dynamic matrix $[P']^{-1}[E']$.

APPENDIX I

SYSTEM DATA

This appendix contains the relevant data for all case studies in this thesis. All the parameters are in per-unit (unless otherwise specified) with reference to a 1072 MVA base power. The reader is referred to Appendix A for a description of the per-unit system.

Generator Electrical Parameters

Generator	Koeberg	Grootvlei
Rated Power	1072 MVA	1110 MVA
X_d	2.466	1.806
X_q	2.28	1.758
X_a	0.22	0.073
R_a	0.003	0.0048
X_{fd}	0.19	0.119
R_{fd}	0.000984	0.00069
X_{kd}	0.13	0.0714
R_{kd}	0.015	0.0097
X_{kq1}	0.59	0.885
R_{kq1}	0.00545	0.00978
X_{kq2}	0.06	0.053
R_{kq2}	0.011	0.05

Koeberg Mechanical System Data in Physical Form

Inertia	Type	H	D	K	T dist %
1	HP	0.158	0.158E-2	10.63	33.7
2	LP1	1.598	1.598E-2	25.34	21.6
3	LP2	1.593	1.593E-2	23.41	18.8
4	LP3	1.625	1.625E-2	26.92	25.9
5	GEN	0.674	0.674E-2	70.53	0.0
6	EXC	0.034	0.034E-2		0.0

Koeberg Mechanical System Data in Modal Form

The elements of the transformation matrix [Q] derived from the physical parameters presented above are as follows:

	Mode					
	0	1	2	3	4	5
Inertia						
HP	1.000	-1.000	1.000	-.520	1.000	.000
LP1	1.000	-.834	.430	-.035	-.139	-.000
LP2	1.000	-.174	-.853	.307	.056	.000
LP3	1.000	.672	-.009	-.639	-.027	-.000
GEN	1.000	.954	.746	.969	.027	.052
EXC	1.000	.959	.760	1.000	.028	-1.000

The transformation matrix is normalized so that the sign of the deflection at the generator rotor is positive for each mode shape and the maximum element in each mode shape has an absolute magnitude of 1.

The following are the mode parameters determined from the physical parameters:

Mode	f_{mi} (Hz	σ_{mi} (s^{-1})	ξ (%)	J_{Mi} (p.u.)
0	0.0	0.785	-	3.617E-2
1	6.681	0.785	1.87	1.716E-2
2	12.373	0.785	1.01	1.277E-2
3	15.836	0.785	0.789	9.713E-3
4	17.493	0.785	0.714	1.241E-3
5	92.590	0.785	0.135	2.309E-4

Grootvlei Mechanical System Data in Physical Form

Inertia	Type	H	D	K	T dist %
1	HP	0.404	0.404E-2	125.84	74.45
2	LP	1.098	1.098E-2	90.85	25.55
3	GEN	1.025	1.025E-2		0.0

Grootvlei Mechanical System Data in Modal Form

The elements of the transformation matrix [Q] derived from the physical parameters presented above are as follows:

	Mode 0	1	2
Inertia			
HP	1.000	-1.000	1.000
LP	1.000	-.556	-.474
GEN	1.000	.989	.113

The following are the mode parameters determined from the physical parameters:

Mode	f_{mi} (Hz)	σ_{mi} (s^{-1})	ξ (%)	J_{Mi} (p.u.)
0	0.0	0.785	-	1.609E-2
1	23.468	0.785	0.533	1.112E-2
2	42.738	0.785	0.292	4.225E-3

Network data for chapter two

The network considered is that shown in Fig 2.1 in the main text and the parameters are:

$R_1 = 0.001$ $X_1 = 0.15$ $R_2 = 0.0845$

$X_2 = 0.6897$ when there is no series compensation

$X_2 = 1.0097$ when $X_c = 0.32$ or 0.66

Network data for chapters three and four

The network considered is that shown in Fig 2.1 in the main text and the parameters are:

$R_1 = 0.001$ $X_1 = 0.15$ $R_2 = 0.0845$ $X_2 = 1.0097$

Network data for chapter five

The network considered is that shown in Fig 2.1 in the main text and the parameters are:

$R_1 + R_2 = R_e = 0.0845$ $X_1 + X_2 = X_e = 1.0097$

Network data for chapters six and seven

The parameters for the network in Fig 6.1 in the main text are:

$R_1 = R_2 = 0.001$ $\quad X_1 = X_2 = 0.15$

$R = 0.0845$ $\quad X_L = 1.0097$ $\quad X_c = 0.746$

The parameters for the network in Fig 6.2 in the main text are:

	Single Generator	Equivalent Generator (2144 MVA base)
R_1	0.001	0.001
X_1	0.15	0.15
R	0.0845	0.169
X_L	1.0097	2.0194
X_c	0.746	1.492

The parameters for the network in Fig 6.7 in the main text are:

Line section	Single Generator			Equivalent Generator (2144 MVA base)		
	R	X_L	X_c	R	X_L	X_c
1-2	0.008	0.087	0.0	0.016	0.174	0.0
2-3-4	0.043	0.462	0.277	0.086	0.924	0.554
4-5-7	0.059	0.746	0.448	0.118	1.492	0.896
4-6-7	0.17	2.037	1.222	0.34	4.074	2.444
7-8	0.001	0.15	0.0	0.001	0.15	0.0

The parameters for the network in Fig 7.23 in the main text are:

Line section	R	X_L	X_c
1-2	0.008	0.087	0.0
2-3-4	0.0845	1.0097	0.746
4-5	0.001	0.15	0.0
2-6	0.001	0.15	0.0

The parameters for the network in Fig 7.29 in the main text are:

$$R_1 = R_2 = 0.001 \qquad X_1 = X_2 = 0.13 \qquad X_L = 1.003 \qquad R_L = 0.092$$

$$R_3 = 0.0052 \qquad X_3 = 3.64$$

Shunt Reactor Controller Parameters

The shunt reactor controller parameters, defined by $[A_c]$, $[B_c]$, $\underline{C}_c$ and $\underline{D}_c$ in eqn (G.25), for the controller in Fig 7.29 are [40]:

$$[A_c] = \begin{bmatrix} -52.5 & 0 \\ -5706 & -600 \end{bmatrix} \qquad [B_c] = \begin{bmatrix} 1 & 1 \\ 384 & 384 \end{bmatrix}$$

$$\underline{C}_c = \begin{bmatrix} 9.6 \\ 2 \end{bmatrix} \qquad \underline{D}_c = \begin{bmatrix} -0.64 \\ -0.64 \end{bmatrix}$$

REFERENCES

[1] Harley R G, Jennings G D, Lahoud M A and Hadingham M F: "Level of Mathematical Model Required to Predict the Response of a Turbogenerator System With and Without Series Capacitors", Transactions SAIEE, Vol 75, Part 3, Dec 1984, pp 28-39.

[2] Harley R G, Jennings G D and Levy D C: "Modal Analysis Representation of Multi-Inertia Turbogenerators", Electric Power Systems Research Journal (EPSR), Elsevier, Switzerland, Vol 8, No 1, March 1985, pp 53-58.

[3] Jennings G D, Harley R G and Levy D C : "Sensitivity of Sub-synchronous Resonance Predictions to Turbo-Generator Modal Parameter Values and to Omitting Certain Active Subsynchronous Modes", IEEE PES 1986 Summer Meeting, Mexico City, Mexico, July 20-25, 1986, Paper 86SM482-2.

[4] Jennings G D, Harley R G and Levy D C: "Subsynchronous Resonance of Two Neighbouring Generating Units", Electric Power Systems Research Journal (EPSR), Elsevier, Switzerland, Vol 10, No 2, 1986, pp 175-188.

[5] Jennings G D, Harley R G and Levy D C: "Subsynchronous Resonance of a Power Station With Two Identical Generating Units", Proceedings IEE, Vol 133, Part C, No 1, Jan 1986, pp 33-43.

[6] Crary S B: "Power System Stability, Vol II", Chapman and Hall, London, 1947.

[7] Concordia C: "Steady State Stability of Synchronous Machines as Affected by Voltage Regulator Characteristics', Transactions AIEE, Vol 63, 1944, pp 215-220.

[8] Miles J G: "Analysis of Overall Stability of Multi-Machine Power Systems", Proceedings IEE, Vol 109A, 1962, pp 203-211.

[9] Park R H: "Two-Reaction Theory of Synchronous Machines: Generalized Method of Analysis - Part I", Transactions AIEE, Vol 48, 1929, p 716.

[10] Kundur P and Dandeno P L: "Implementation of Synchronous Machine Models into Power System Stability Programs", IEEE PES Winter Meeting, Symposium on Synchronous Machine Modeling for Power System Studies, 83TH0101-6-PWR, pp 49-50.

[11] Adkins B and Harley R G: "The General Theory of Alternating Current Machines: Applications to Practical Problems", Chapman and Hall, London, ISBN 0-412-15560-5, 1975.

[12] Umans S D: "Equivalent Circuit Modeling of Synchronous Machines", IEEE PES 1983 Winter Meeting, Symposium on Synchronous Machine Modeling for Power System Studies, 83TH0101-6-PWR, pp 5-11.

[13] Kundur P and Dandeno P L: "Implementation of Advanced Generator Models into Power System Stability Programs", IEEE Transactions on Power Apparatus and Systems, Vol PAS-102, July 1983, pp 2047-2054.

[14] Dandeno P L, Kundur P, Poray A T and Coultes M: "Validation of Turbogenerator Stability Models by Comparison with Power System Tests", IEEE Transactions on Power Apparatus and Systems, Vol PAS-100, April 1981, pp 1637-1645.

[15] Limebeer D J N, Harley R G and Schuck S M: "Subsynchronous Resonance of the Koeberg Turbogenerators and of a Laboratory Micro-Alternator System", Transactions SAIEE, Vol 70, Part 11, Nov 1979, pp 278-297.

[16] de Mello P F: "Power System Dynamics - Overview", IEEE PES 1975 Winter Meeting, Symposium on 'Adequacy and Philosophy of Modelling: Dynamic System Performance', 75 CH0970-4-PWR, pp 5-15.

[17] Harley R G, Limebeer D J N and Chirricozzi E: "Comparative Study of Saturation Methods in Synchronous Machine Models", Proceedings IEE, Vol 127, Part B, 1980, pp 1-7.

[18] Harley R G and Adkins B: "Calculation of the Angular Back Swing Following a Short Circuit of a Loaded Alternator", Proceedings IEE, Vol 117, No 2, Feb 1970, pp 377-386.

[19] IEEE Joint Working Group on Determination and Application of Synchronous Machine Models for Stability Studies: "Current Usage and Suggested Practices in Power System Stability Simulations for Synchronous Machines", IEEE Transactions on Energy Conversion, Vol EC-1, March 1986, pp 77-93.

[20] Lahoud M A: "The Analysis and Control of Synchronous and Asynchronous Machines in Power Systems", Ph D thesis, University of Natal, 1982.

[21] Badr M A and El-Serafi A M: "Effect of Synchronous Generator Regulation on the Subsynchronous Resonance Phenomenon in Power Systems", IEEE Transactions on Power Apparatus and Systems, Vol PAS-95, March/April 1976, pp 461-468.

[22] IEEE Subsynchronous Resonance Working Group : "Terms, Definitions and Symbols for Subsynchronous Oscillations", IEEE Transactions on Power Apparatus and Systems, Vol PAS-104, June 1985, pp 1326-1334.

[23] Subsynchronous Resonance Task Force : "Analysis and Control of Subsynchronous Resonance", IEEE PES Special Publication 76CH1066-0-PWR, 1976.

[24] Lahoud M A and Harley R G : "Multi-Machine Subsynchronous Resonance : Part I - Line Representation", Transactions SAIEE, Vol 75, Part 2, Sept 1984, pp 3-13.

[25] Lahoud M A and Harley R G : "Multi-Machine Subsynchronous Resonance : Part II - Load Representation", Transactions SAIEE, Vol 75, Part 2, Sept 1984, pp 14-27.

[26] Concordia C, Tice J B and Bowler C E J : "Subsynchronous Torques on Generating Units Feeding Series Capacitor Compensated Lines", Proceedings of the American Power Conference, Vol 35, 1973, pp 1129-1136.

[27] Smith J R, Mykura J F and Cudworth C J : "The Effect of Hysteretic Damping on Turbogenerator Shaft Torsional Oscillations", IEEE Transactions on Energy Conversion, Vol EC-1, March 1986, pp 152-160.

[28] Walker D N, Bowler C E J, Jackson R L and Hodges D A : "Results of Subsynchronous Resonance Test at Mohave", IEEE Transactions on Power Apparatus and Systems, Vol PAS-94, Sept/Oct 1975, pp 1878-1889.

[29] Walker D N, Adams S L and Plaeck R J : "Torsional Vibration and Fatigue of Turbine Generator Shafts", IEEE Transactions on Power Apparatus and Systems, Vol PAS-100, Nov 1981, pp 4373-4380.

[30] Joyce J S and Lambrecht D : "Status of Evaluating the Fatigue of Large Steam Turbine Generators Caused by Electrical Disturbances", IEEE Transactions on Power Apparatus and Systems, Vol PAS-99, Jan/Feb 1980, pp 111-119.

[31] Lambrecht D and Kulig T : "Torsional Performance of Turbine Generator Shafts Especially Under Resonant Excitation", IEEE Transactions on Power Apparatus and Systems, Vol PAS-101, Oct 1982, pp 3689-3702.

[32] Fouad A A and Khu K T : "Subsynchronous Resonance Zones in the IEEE 'Bench Mark' Power System", IEEE Transactions on Power Apparatus and Systems, Vol PAS-97, May/June 1978, pp 754-762.

[33] Bowler C E J : "Understanding Subsynchronous Resonance", IEEE PES Special Publication 76 CH 1066-0-PWR, pp 59-65.

[34] Timoshenko S, Young D H and Weaver W Jr : "Vibration Problems in Engineering", John Wiley and Sons, New York, ISBN 0-471-87315-2, 1974.

[35] Kilgore L A, Ramey D G and Hall M C : "Simplified Transmission and Generation System Analysis Procedures for Subsynchronous Resonance Problems", IEEE Transactions on Power Apparatus and Systems, Vol PAS-96, Nov/Dec 1977, pp 1840-1846.

[36] Walker D E and Schwalb A L: "Results of Subsynchronous Resonance Test at Navajo", IEEE PES Special Publication 76CH1066-0-PWR, pp 37-45.

[37] Ramey D G, Harold P F, Maddox H A, Starnes R B and Knickerbocker J L: "Measurements of Torsional Dynamic Characteristics of The San Juan No 2 Turbine-Generator", Transactions of The American Society of Mechanical Engineers, Engineering for Power, Vol 99, No 3, July 1977, pp 378-384.

[38] Canay I M, Roher H J and Schnirel K E : "Effect of Electrical Disturbances, Grid Recovery Voltage and Generator Inertia on Maximization of Mechanical Torques in Large Turbogenerator Sets", IEEE Transactions on Power Apparatus and Systems, Vol PAS-99, July/August 1980, pp 1357-1370.

[39] IEEE Joint Working Group on Determination and Application of Synchronous Machine Models for Stability Studies : "Current Usage and Suggested Practices in Power System Stability Simulations for Synchronous Machines", IEEE Transactions on Energy Conversion, Vol EC-1, March 1986, pp 77-93.

[40] Balda J C : "Subsynchronous Resonance of Turbogenerators with Particular Reference to a Few Selected Countermeasures", Ph D Thesis, University of Natal, 1985.

[41] Balda J C, Eitelberg E and Harley R G : "Optimal Output Feedback Design of a Shunt Reactor Controller for Damping Torsional Oscillations", Electric Power Systems Research Journal (EPSR), Elsevier, Switzerland, Vol 10, No 1, January 1986, pp 25-34.

[42] Balda J C, Harley R G and Eitelberg E : "Damping of Torsional Shaft Oscillations in Two Interacting Neighbouring Turbogenerators", IEEE PES 1986 Winter Meeting, New York, Febuary 2-7, Paper 86WM207-5.

[43] Hammons T J and Canay I M : "Effect of Damper Modelling and the Fault Clearing Process on Response Torque and Stressing of Turbine-Generator Shafts", IEEE Transactions on Energy Conversion, Vol EC-1, March 1986, pp 113-121.

[44] Chow J H, Javid S H, Sanchez-Gasca J J, Bowler C E J and Edmonds J S: "Torsional Model Identification for Turbine-Generators", IEEE Transactions on Energy Conversion, Vol EC-1, Dec 1986, pp 83-90.

[45] Bigret R, Coetzee C J, Levy D C and Harley R G: "Measuring the Torsional Modal Frequencies of a 900 MW Turbogenerator", IEEE Transactions on Energy Conversion, Vol EC-1, Dec 1986, pp 99-107.

[46] Hewlett Packard: "Modal Analysis Operating and Services Manual", 05451-90294, May 1975.

[47] Ramey D G, Demeko J A, Farmer R G and Agrawal B L: "Subsynchronous Resonance Tests and Torsional Monitoring System Verification at the Cholla Station", IEEE Transaction on Power Apparatus and Systems, Vol PAS-99, Sept-Oct 1980, pp 1900-1907.

[48] Stein J and Fick H: "The Torsional Stress Analyser for Continuously Monitoring Turbine Generators", IEEE Transactions on Power Apparatus and Systems, Vol PAS-99, March-April 1980, pp 703-710.

[49] Limebeer D J N, Harley R G and Lahoud M A: "Suppressing Sub-synchronous Resonance with Static Filters", Proceedings IEE, Vol 128, Part C, 1981, pp 33-44.

[50] Lahoud M A and Harley R G: "An Optimal Controller for the Suppression of Subsynchronous Resonance", Electric Power Systems Research Journal (EPSR), Elsevier, Switzerland, Vol 6, No 3, 1983, pp 203-216.

[51] Limebeer D J N, Harley R G and Lahoud M A: "The Suppression of Subsynchronous Resonance with the Aid of an Auxillary Excitation Control Signal", Transactions SAIEE, Vol 74, Part 8, pp 198-209.

[52] Harley R G and Balda J C: "Subsynchronous Resonance Damping by Specially Controlling a Parallel HVDC Link", Proceedings IEE, Vol 132, Part C, 1985, pp 154-160.

[53] Lahoud M A and Harley R G: "Theoretical Study of a Shunt Reactor SSR Stabilizer for a Nuclear Powered Generator", Electric Power Systems Research Journal (EPSR), Elsevier, Switzerland, Vol 8, No 3, 1985, pp 261-274.

[54] Kimbark E W: "Power System Stability", Vol 1, John Wiley and Sons, New York, 1967.

[55] Huang T S and Parker R R: "Network Theory: An Introductory Course", Addison-Wesley, Reading, 1971.

[56] Agrawal B L and Farmer R G: "Use of Frequency Scanning Techniques for Subsynchronous Resonance", IEEE Transactions on Power Apparatus and Systems, Vol PAS-98, March/April 1979, pp 341-348.

[57] Alden R T H, Nolan P J and Bayne J P: "Shaft Dynamics in Closely Coupled Identical Generators", IEEE Transactions on Power Apparatus and Systems, Vol PAS-96, May/June 1977, pp 721-728.

[58] Walker D N, Bowler C E J and Baker D H: "Torsional Dynamics of Closely Coupled Turbine-Generators", IEEE Transactions on Power Apparatus and Systems, Vol PAS-97, July/August 1978, pp 1458-1466.

[59] IEEE Subsynchronous Resonance Working Group: "Second Benchmark Model for Computer Simulation of Subsynchronous Resonance", IEEE Transactions on Power Apparatus and Systems, Vol PAS-104, May 1985, pp 1057-1066.

[60] General Electric Company: "HVDC System Control for Damping of Subsynchronous Oscillations", EPRI EL-2708, Project 1425-1, Final Report, October 1982, Appendix C and D.

[61] Lahoud M A and Harley R G: "Analysis Techniques for the Dynamic Behavior of a Multigenerator System", Transactions SAIEE, Vol 74, Part 4, April 1983, pp 53-63.

[62] Lahoud M A, Harley R G and Balda J C: "Induction Motor Modelling for Short-Term Transient Studies in a Multigenerator-Multimotor Power System", Electric Power Systems Research Journal (EPSR), Elsevier, Switzerland, Vol 7, 1984, pp 53-63.

[63] Limebeer D J N, Harley R G and Erasmus S J: "An Investigation of Subsynchronous Resonance by Fourier Transformation", Electric Power Systems Research Journal (EPSR), Elsevier, Switzerland, Vol 2, No 2, 1979, pp 133-143.

[64] Harris M R, Lawrenson P J and Stephenson J M: "Per-Unit Systems: With Special Reference to Electrical Machines", Cambridge University Press, London, SBN 521-07857-1, 1970.

[65] IEEE Joint Working Group on Determination of Synchronous Machine Stability Constants: "Supplementary Definitions and Associated Test Methods for Obtaining Parameters for Synchronous Machines Stability Study Simulations", IEEE Transactions on Power Apparatus and Systems, Vol PAS-99, July/August 1980, pp 1625-1633.

[66] Ogata K : "Modern Control Engineering", Prentice-Hall, Englewood Cliffs, ISBN 13-590232-0, 1970.

[67] Klosterman A: "On the Experimental Determination and Use of Modal Representations of Dynamic Characteristics", Ph D thesis, University of Cincinnati, 1971.

[68] Nolan P J, Sinha N K and Alden R T H: "Eigenvlaue Sensitivities of Power Systems Including Network and Shaft Dynamics", IEEE Transactions on Power Apparatus and Systems, Vol PAS-95, July/August 1976, pp 1318-1324.

[69] Porter B and Crossley T R: "Modal Control: Theory and Applications", Taylor and Francis, London, ISBN 0 85066 057 2, 1972, Chapter 3.

[70] Jaleeli-Parschi N, Vaahedi E and MacDonald D C: "Multi-Machine System Transient Behaviour", IEEE 1974 PICA Conference, Toronto, Ontaria, Canada, pp 51-58.

[71] Balabanian B and Bickart T A: "Electrical Network Theory", John Wiley and Sons Inc, 1971.

[72] Comer D J: "Computer Analysis of Circuits", International Text Book Company, 1971.